CONSTRUCTION MATERIALS CONSULTANTS, INC.

Laboratory Analyses of Clay Bricks & Masonry Mortars From Early to Mid-20th Century – A Case Study

Langford Building, Guilford County
325 East Russell Avenue
High Point, NC 27260

March 30, 2020
CMC 0220106

TABLE OF CONTENTS

LABORATORY STUDIES OF CLAY BRICKS AND MASONRY MORTARS FROM EARLY TO MID-20TH CENTURY – A CASE STUDY

EXECUTIVE SUMMARY

Located in an industrial section at 325 Russell Avenue in Guilford County, High Point, North Carolina, the Langford Building was originally constructed in 1916 and has since received multiple episodes of additions and renovations. As a result, a variety of brick and masonry mortar samples were provided, spanning almost five decades of construction periods from the original 1916 vintage through 1950s to late 1960s, to determine compositions of bricks and mortars used during those periods. The samples were examined to determine the types of bricks and mortars present, materials and mix proportions of mortars, evidence of any physical or chemical deterioration of bricks and mortars during service, and recommendations for appropriate pointing mortar to be used in renovations. Bricks were tested for compressive strengths by using the methods of ASTM C 67 and petrography by ASTM C 856, whereas, mortars were studied by following the petrographic, chemical, and other ancillary methods of ASTM C 1324.

A total of four sets of bricks (2 bricks/set/location) and five masonry mortar samples were provided from: (1) 1916 period (Bricks 3A/3B and 4A/4B, and Mortars M3 and M4), (2) 1950s period (Bricks 1A/1B and 2A/2B, and Mortars M1 and M2), and (3) late 1960s period (no Brick, only Mortar M5). Some subtle differences in appearances and properties of bricks and mortars from three periods were obvious when samples were received. For example, bricks 3A and 3B from 1916 era are medium gray, soft, highly absorptive, appeared to have very low strengths (and subsequently confirmed 1010 psi and 790 psi strengths for 3A and 3B, respectively). These bricks are severely disintegrated and contained numerous elongated separations or lineation due to their manufacturing by hand-pressing methods. Bricks 4A and 4B from 1916 vintage are reddish-brown, relatively denser, harder, and have strengths from as low as 970 psi for disintegrated one (4A) to 3220 psi for the better one (4B) as opposed to relatively denser reddish-brown bricks from 1950s and 1960s. Bricks 1A and 1B from 1950s era are the best in appearance (no chipping), reddish brown, and gave the highest strength of 3210 psi and 2980 psi, whereas companion Bricks 2A and 2B from 1950s are disintegrated (chipped, cracked), reddish-brown and gave strength results of 1510 psi and 1870 psi, respectively. Therefore, strength results of bricks even from the same age varied from sample-to-sample as their appearance and properties. Of all the bricks, the ones marked as 3A and 3B from 1916 are noticeably grayer in color tone as opposed to reddish-brown tones of other bricks, and are the worst of all, e.g., provided the lowest strengths.

Similar to bricks, masonry mortars from three periods are also found to be different. For example, M3 and M4 from the earliest 1916 era are found to be cement-lime mortars made using coarsely-ground Portland cement, lime, and silica sand. By contrast, M1 and M2 from 1950s are found to contain natural cement, lime, and silica sand where natural cement was manufactured by calcining impure dolomitic limestone raw feed containing siliceous and argillaceous impurities. Mortar M5 from late 1960s is a masonry cement mortar made using major amount of hydrated lime, limestone fines, and subordinate amount of Portland cement (cement is well-hydrated), and silica sand. Therefore, the binder component of mortars have changed from coarsely ground Portland cement and lime in the 1916 mortars to natural cement and lime in 1950s samples to finely ground masonry cement (which is a mixture of lime, limestone fines, and Portland cement) in late 1960s samples.

Mortar samples were analyzed by comprehensive laboratory examinations following various industry standards, e.g., ASTM C 1324 and RILEM methods (Middendorf et al. 2004, 2005) starting with visual examinations, extensive optical microscopy, scanning electron microscopy and energy-dispersive X-ray microanalyses (SEM-EDS), followed by wet chemical analyses, X-ray diffraction (XRD), X-ray fluorescence (XRF), thermal analyses (TGA, DTG, DSC), and ion chromatography.

Optical microscopy and scanning electron microscopy with X-ray microanalyses distinguished three different types of mortars from three different periods of constructions:

a. A cement-lime mortar from 1916 construction, where Portland cement was mixed with lime putty and silica sand. Portland cement was coarsely ground, consistent with the grinding technologies of early 20th century, hence left many coarse (some close to sand size) residual cement particles with dense hydration rims around many such particles. Most residual cement particles show characteristic microstructures of Portland cements in

having subhedral alite or pseudomorphs of alite and skeletal interstitial dark brown ferrite phases, and, spherical belite with interstitial dark ferrite phases.

b. A natural cement-based mortar from 1950s construction, where natural cement was mixed with lime for aided workability. Natural cement was manufactured from calcination of impure dolomitic limestones having a large range of clay and silica impurities. Due to variations in the original compositions of impure (argillaceous) dolomitic limestone feeds, compositions of natural cements produced were diverse and so were the resultant pastes of those mortars.

c. Finally, a masonry cement mortar from late 1960s construction, where masonry cement was manufactured with a mixture of fine-grained hydrated lime, coarser grained limestone fines, and subordinate amount of Portland cement where cement was added at a low amount to be detected from residual cement and was well-hydrated leaving only pseudomorphs of alite and skeletal remains of dark interstitial ferrite phases. Silica sand was added to the lime-limestone-cement mix to prepare the proprietary blend of masonry cement.

Each mortar type left its own characteristic microstructure and microchemistry to be detected from optical and electron microscopy and microanalyses. For example, natural cement mortar showed the following characteristic microstructures to readily identify such mortar from thin section microscopy:

a. Residual calcined products of impure dolomitic limestone feeds as residual natural cement particles that are readily distinguished in the paste from the characteristic birefringence of carbonate rocks in crossed polarized light mode in a petrographic microscope.

b. Characteristic texture of such particles readily observed in plane or crossed polarized-light modes showing subhedral to euhedral rhombic crystals of dolomite grains in a finer-grained matrix of calcite, quartz, and interstitial phases. Such textures are more prominent in particles that have lost their original textures during the calcination process.

c. The typical texture of dolomitic limestone become obliterated with increased calcination turning an original birefringent particle to become near-isotropic due to lime-silica-alumina-iron reactions between dolomite, calcite, and interstitial clay-silica impurities which eventually form various calcium-aluminum-silicate phases (e.g., gehlenite, mullite) and an amorphous calcium aluminosilicate phase. This amorphous reaction product from calcination provides the main hydraulicity of natural cement. With increasing degree of calcination, this amorphous phase becomes the dominant phase in the matrix, which may contain skeletal remains or pseudomorphs of dolomite rhombs.

d. Calcination process rearranges original elemental distribution in dolomite rhombs, sometimes causing diffusion of iron and magnesia within the dolomitic rhombs creating a darker brown rim enriched in iron within dolomite rhombs, which may become distinct and best visible in plane polarized light in a petrographic microscope.

e. Increasing temperatures during calcination brings polymorphic transition of silica impurities at 575°C in the original impure dolomitic limestone feeds, thus forming tridymite or cristobalite phases or sometimes melt reaction rims around some silica particles within residual cement particles, which are usually confirmed from SEM-EDS and subsequent X-ray diffraction studies. Paste fraction separated from sand in a natural cement mortar showed such polymorphs of silica in the XRD studies, which is shown later.

f. The startling chemical signature of natural cement mortar is revealed from SEM-EDS studies, where paste shows noticeably higher magnesia contents than all other mortar types. Also noticed are high silica and large range of paste-CIs due to large variability of original impure dolomitic limestone feeds having large range of clay-silica impurities.

Portland cement-based mortars are readily identified by residual Portland cement particles, where depending on the degree of hydration of cement, grain size of original cement particles, and degree of carbonation during service, many residual cement particles preserve original microstructures of cements, e.g., subhedral to euhedral alite and spherical belite grains with dark interstitial ferrite phases. Depending on the lime content mixed with the cement, and the type of lime added (e.g., non-hydraulic high-calcium lime as lime putty, or hydrated lime in powder form) many cement-lime mortars may show lumps of unmixed lime or less calcined (or even unburnt) limestone particles in lime. Depending on the degree of carbonation during service, paste in cement-lime mortars show variable degrees of carbonation converting

the original calcium-silica-hydrate and calcium hydroxide component of cement hydration to finely crystalline calcium carbonate.

Finally, masonry cement mortar is identified by its proprietary mix composition, incorporating not only Portland cement and lime but also limestone fines, which is a common ingredient of masonry cement often added for enhanced workability where limestone fine particles found in the present mortar M5 are coarser than lime and provide an overall granular appearance best seen in backscatter electron image.

SEM-EDS studies of pastes *per se* in all mortars showed overall enrichment of silica in siliceous sand grains and enrichment of lime in the interstitial lime-based pastes that are well-reflected in the elemental (Ca-Si-Al-Mg-etc.) maps. Additionally, paste compositions showed high magnesia due to use of dolomitic lime in natural cement or cement-lime mortars. Natural cement mortars showed highest magnesia contents in pastes, which is the characteristic feature of natural cement pastes. Alumina contents in pastes of natural cement mortars are also higher than that in cement-lime or masonry cement mortars due to contribution of alumina from natural cements. Cementation indices of pastes (paste-CI after Eckel 1922) show wide range within and between the mortars which is not unexpected considering large compactional variations of natural cements used during 1950s era, and proprietary mix composition of masonry mortars during 1960s eras, as well as variable degrees of mixing of cement, and lime in the cement-lime mortar from 1916 era. A systematic trend in compositional plots of silica and lime contents of pastes against paste-CI from SEM-EDS studies of individual mortars demonstrated their respective natural cement or Portland cement and lime-based compositions of original binders.

Thermal analyses of mortars showed very similar thermograms of two natural cement mortars from 1950s vintage from a minimal loss of free water (<0.5%) and water from hydrated salts (<0.5-0.7%) at up to 200ºC followed by a measurable loss (2.1 to 2.2%) of hydrate water from 200ºC to 600ºC. Degrees of carbonation are higher in M2 mortar (5.38%) than 3.82% found in M1 mortar. Quartz contents are around 45 percent in M1 and 70% in M2 determined from polymorphic transition of quartz around 575ºC. Two cement-lime mortars, M3 and M4, from 1916 also showed similar thermograms from a minimal loss of free water (<0.6%) and water from hydrated salts (<1%) at up to 200ºC followed by a measurable loss (3%) of hydrate water from 200ºC to 600ºC. Degrees of carbonation are lower in M3 mortar (5.5%) than 7% found in M4 mortar. Quartz contents are around 44.7 percent in M3 and 41.2% in M4 determined from polymorphic transition of quartz around 575ºC. Compared to these four mortars, the masonry cement mortar M5 from late 1960s vintage showed the simplest thermogram from a minimal loss of free water (<0.5%) and water from hydrated salts (<6%) at up to 200ºC followed by a measurable loss (2.1%) of hydrate water from 200ºC to 600ºC. Degrees of carbonation are highest of all mortars in M5, 7.38%, due to the presence of limestone fine particles along with carbonated lime in the mortar. Quartz content is 60% as determined from polymorphic transition of quartz around 575ºC. A comparison of thermograms of natural cement mortars M1 and M2 with cement-lime mortars M3 and M4 showed some similarities in having: (a) endotherms from loss of free water and water from hydrate salts, following by (b) peaks from losses of structural/hydrate water around 350 to 460ºC range, followed by (c) decomposition of carbonates around 750 to 800ºC. By contrast, masonry cement mortar M5 shows (a) smallest endotherm of all mortars for loss of water from hydrate salts at 120ºC, (b) lack of any endotherm from losses of hydrate water, and (c) largest endotherm from decomposition of calcite from limestone fines and fine-grained carbonated paste at 775ºC. Loss of structural water is highest (around 3% loss in 200 to 600ºC range) in the two cement-lime mortars, M3 and M4, due to higher amount of calcium-silicate-hydrate and calcium hydroxide components of Portland cement hydration than the corresponding natural cement mortars, M1 and M2 (which show 2.1 to 2.2% loss at 200 to 600ºC range).

FTIR studies of all four mortars showed the simple inorganic phases (e.g., quartz, calcite) that are detected in microscopy and XRD studies and lack of any polymer component in the mortars.

Ion chromatography (IC) of water-soluble salts showed detectable water-soluble chloride and sulfate contents in all mortars, which are highest in mortars M2 (natural cement) and M4 (cement-lime), intermediate in masonry cement mortar M5, and negligible in M1 and M3. Water-soluble chloride contents are 0.009%, 0.014%, 0.013%, 0.017%, and 0.023% percent by mass of mortars in samples M1 through M5, respectively. Water-soluble sulfate contents are 0.036%, 0.745%, 0.062%, 0.768%, and 0.405% percent by mass of mortars in samples M1 through M5, respectively. Results are indicative of lack of any chloride ingress or chloride-induced distress, and, sulfate contents anticipated from contributions from binders' ingredients with no external sulfate ingress. Variations in chloride and sulfate contents as well as of other water-soluble anions are due to leaching and moisture migration through the mortars during service that have disturbed the original concentrations of these anions.

Information obtained from: (a) petrographic examinations to determine the sand compositions, binder types, as well as overall mortar types, and (b) chemical analyses of mortars to determine the soluble silica contents, water contents, and

insoluble residue contents are used to calculate the volumetric proportions of mortars' ingredients. Mix calculations of mortars showed: (a) **1-part natural cement to 1/2 part hydrated lime to 10-part siliceous sand mix (6 1/2 times sand to sum of separate volumes of natural cement and lime) for the natural cement mortars from 1950s construction**, (b) **1-part Portland cement to 1-part lime to 7-part siliceous sand (3 1/2 times sand to sum of separate volumes of Portland cement and lime) for cement-lime mortar from 1916 construction**, and (c) **1-part ASTM C 91 Type S masonry cement to 2 3/4-part siliceous sand for late 1960s masonry cement mortar**.

Based on the determined natural cement-lime-siliceous sand compositions of 1950s mortars, and the determined 1-part natural cement to 1/2 part hydrated lime to 10-part siliceous sand mix (6 1/2 times sand to sum of separate volumes of natural cement and lime) volumetric proportions, a possible tuck-pointing mortar for both locations of 1950s mortars could be a modern-day Rosendale cement manufactured by Edison Coatings Inc., e.g., Rosendale 10C cement, or prepackaged Rosendale 10M cement-sand mix, but preferably the 10C type mixed with siliceous sand used in the original mortars, where the natural cement should be in conformance to the specifications of ASTM C 10 and sand should correspond to the specification of masonry sand *a la* ASTM C 144. The final choice of binder and sand ingredients would depend on the match in appearance, compositions, and properties with the original mortars. Design and formulation of an appropriate tuck-pointing mortar should be based on trial and error on small test areas by the project engineer/architect.

Based on the determined Portland cement-lime-siliceous sand compositions of 1916 mortars, and the determined 1-part Portland cement to 1-part hydrated lime to 7-part siliceous sand mix (3 1/2 times sand to sum of separate volumes of natural cement and lime) volumetric proportions, a possible tuck-pointing mortar for both locations of 1916 mortars could be 1-part Portland or blended cement (conforming ASTM C 150 or C 595, respectively) to 1/4 to 1 1/2 part dolomitic lime (conforming ASTM C 207) to not less than 2 1/4 and not more than 3 times sand to the sum of the separate volumes of cement and lime by volume. The final choice of binder and sand ingredients would depend on the match in appearance, compositions, and properties with these pointing mortars, or if these mortars are to be entirely replaced then to the original mortar. The chosen mortar should bond well to the brick, as well as to the existing jointing mortars and preferably be softer than the present mortars without introducing any undue stress from any compositional or proportional mismatch to the existing mortars or mismatch to the brick masonries.

Based on determined masonry cement and siliceous sand composition of late 1960s masonry cement mortar, and the determined 1-part masonry cement to 2 3/4-part siliceous sand volumetric proportions, a possible tuck-pointing mortar can be: (a) an ASTM C 270 Type S masonry/mortar cement and silica sand mortar (e.g., prepared by mixing 1-part ASTM C 91/C 1329 Type S masonry/mortar cement to 2 1/4 to 3 part ASTM C 144 masonry sand, by volume), or, (b) an air-entrained Type N or S cement-lime mortar (e.g., prepared by mixing 1-part ASTM C 150 Portland cement, 1/2 to 1 1/2 part ASTM C 207 Type N or S hydrated lime or ASTM C 1489 lime putty, and 2 1/4 to 3 part ASTM C 144 masonry sand, by volume). However, finding a match to the examined mortar may not be beneficial for overall performance of masonry if the mortar examined is inappropriate for the adjacent masonry units and intended applications. The final choice should be verified by preparing mock-up mortar batches applied over small test areas to see the match not only in the appearance and properties with the existing mortar, but also in providing overall improvement in performance and durability of the masonry wall, e.g., without incorporating any undue stresses from mismatch between the mortar and masonry units.

Due to the overall low compressive strengths of bricks, especially for the ones from 1916 (e.g., 790 psi, 970 psi, 1010 psi strengths), replacement of those bricks with ones in conformance to the ASTM C 216 specified facing bricks are recommended.

INTRODUCTION

Located in an industrial section at 325 Russell Avenue in Guilford County, High Point, North Carolina, the Langford Building was originally constructed in 1916 and since received multiple episodes of additions and renovations. As a result, a variety of brick and masonry mortar samples were provided, spanning almost five decades of construction periods from the original 1916 vintage through 1950s to late 1960s, to determine the compositions of bricks and mortars used during those periods. The samples were examined to determine the types of bricks and mortars present, materials and mix proportions of mortars, evidence of any physical or chemical deterioration of bricks and mortars during service, and recommendations for appropriate pointing mortars to be used in renovations.

Figure 1: Langford Building, Guilford County, High Point, North Carolina.

SAMPLES RECEIVED

Figures 2 through 7 show the brick and mortar samples received. Table 1 documents weights, dimensions, appearance, integrity and figures of bricks and mortars.

Period	Sample	Weight (grams) and Largest Piece Dimensions (mm)	Appearance, Integrity, Figure	Figure
1950s	Brick 1A	2040g; 195 mm × 90 mm × 60 mm	Reddish-brown, dense, hard, intact	2
	Brick 1B	2174g; 200 mm × 90 mm × 60 mm	Reddish-brown, dense, hard, intact	2
	Brick 2A	1741g; 200 mm × 90 mm × 60 mm	Reddish-brown, chipped, cracked	3
	Brick 2B	1308g; 110 mm × 95 mm × 60 mm	Reddish-brown, chipped, cracked	3
	Mortar 1	202g; 90 mm × 64 mm × 11 mm	Soft, dusty, beige/tan, multiple pieces	2
	Mortar 2	205g; 94 mm × 70 mm × 10 mm	Dense, hard, beige/gray, multiple pieces	3
1916	Brick 3A	2016g; 200 mm × 100 mm × 60 mm	Gray, chipped, cracked	4
	Brick 3B	1237g; 120 mm × 100 mm × 60 mm	Gray, chipped, cracked	4
	Brick 4A	1290g; 115 mm × 100 mm × 60 mm	Reddish-brown, chipped, cracked	5
	Brick 4B	2170g; 195 mm × 100 mm × 60 mm	Reddish-brown, chipped, cracked	5
	Mortar 3	402g; 125 mm × 52 mm × 11 mm	Dense, hard, gray, two pieces	4
	Mortar 4	364g; 120 mm × 110 mm × 16 mm	Dense, hard, gray, one intact piece	5
Late 1960s	Brick 5	Not received	Figure 6 shows bricks in the field	6
	Mortar 5	120g; 50 mm × 40 mm × 10 mm	Soft, dusty, beige, multiple pieces	6

Table 1: Brick and mortar samples received from three periods of constructions.

METHODOLOGIES

Bricks were tested for (a) compressive strengths by using the methods of ASTM C 67, and, (b) compositions by petrographic examinations according to the procedures of ASTM C 856. Petrographic examinations of bricks include optical and scanning electron microscopical examinations for mineralogies and microstructures of bricks, X-ray fluorescence for bulk compositions, and X-ray diffraction for non-plastic (mineral) components of bricks. Masonry mortars were studied by following the petrographic, chemical, and other ancillary methods of ASTM C 1324. Details of various analytical techniques for mortar analyses are provided in Appendix A. Also, visit www.cmc-concrete.com for analytical facilities for laboratory examinations of bricks and masonry mortars.

Figure 2: Bricks 1A, 1B, and Mortar M1 from 1950s vintage, as received. Also shown is the location on the masonry wall from where samples were retrieved. Both Bricks (1A and 1B) are intact, sound, and of best condition of all the brick samples received. By contrast, adjacent mortar M1 shows beige color, soft, friable, dusty nature, and received in multiple pieces.

Figure 3: Bricks 2A, 2B, and Mortar M2 from 1950s vintage, as received. Also shown is the location on the masonry wall from where brick and mortar samples were retrieved. Notice chipped nature of Brick 2A as well as some surface cracks in Brick 2B, some of which are marked with arrows. Bed joint surface of one mortar piece also shows some craze cracks. Closed polygonal-shaped surface cracks on Brick 2B are remnants of drying processes during manufacturing process that have extended to depths of 15 to 20 mm from the bedding surfaces.

Compared to Mortar M1, this Mortar M2 from the same vintage (1950s) is noticeably denser and harder. Binders in both M1 and M2 mortars are found to be natural cement, where significant leaching of paste fraction of mortar in M1 has resulted in a soft, friable and dusty nature, whereas interstitial spaces between sand particles in the M2 mortar shows a relatively denser paste with lesser evidence of leaching by moisture migration. Hence, this M2 mortar is denser and more intact than the M1 mortar.

Figure 4: Bricks 3A, 3B, and Mortar M3 from 1916 vintage, as received. Also shown is the location on the masonry wall from where brick and mortar samples were retrieved. Notice some surface cracks and chipped nature of Brick 3A and broken (half) piece of Brick 3B, both of which are noticeably darker (gray) colored as opposed to reddish-brown bricks from all other locations. Two mortar pieces were received, which are noticeably denser, harder, and darker gray than M1 and M2 mortars of 1950s vintage.

Figure 5: Bricks 4A, 4B, and Mortar M4 from 1916 vintage, as received. Also shown is the location on the masonry wall from where brick and mortar samples were retrieved. Brick 4A was received as a half brick, and Brick 4B shows chipped nature. One mortar piece was received, which is dense, hard, gray with adhered remains of brick. Mortar M4 is as dense and hard as M3, and both are found to be cement-lime based where Portland cement was used as opposed to natural cement found in 1950s vintage in M1 and M2. Use of Portland cement has resulted in unnecessarily (and detrimentally) stronger mortars in 1916 vintages than the natural cement based ones found in M1 and M2.

Figure 6: Mortar M5 from late 1960s vintage, as received. Also shown is the location on the masonry wall from where sample was retrieved. Mortar shows beige color, soft, friable, dusty nature, and was received in multiple pieces. Along with M1, this mortar is amongst the softest and most disintegrated of all mortars received.

Figure 7: Shown are all mortar samples received from 1916 to late 1960s constructions. As mentioned before, Mortar M1 from 1950s vintage is soft and dusty with beige appearance. Mortar M5 from late 1960s vintage is also very soft and tan colored. Mortars M2, M3, and M4 are noticeably denser, harder, and gray in color. Mortars M1 and M2 are found to be made using natural cement. Mortars M3 and M4 are made using coarsely ground Portland cement and lime, Mortar M5 was made using masonry cement, consisting of lime, limestone fines, and subordinate Portland cement where Portland cement particles are well-hydrated. The denser and harder mortars M3 and M4 are found to be Portland cement-based. The soft, dusty nature of Mortar M1 is found to be due to leaching of a natural cement mortar. Mortar M2 is also natural cement-based, which, however, is present in denser and harder condition due to lack of leaching of lime as found in Mortar M1 from the same 1950s vintage.

For each mortar sample, there is no mixing of different mortar types from later pointing events. Pieces within a single mortar are uniform in appearance and composition, hence representative of the mortar of interest. Representative pieces from each mortar were selected for preparation of light-transmitted blue dye-mixed epoxy-impregnated thin sections for (i) optical microscopy, and, (ii) scanning electron microscopy and X-ray microanalyses. Subsequent pieces were lightly ground in a mortar and pestle and subsequently digested in hydrochloric acid for separation of siliceous (acid-insoluble) components to conduct (iii) sieve analyses of siliceous sand components of mortars. Portions of remaining pieces were finely ground (less than 44-micron in size) for (iv) wet chemical (gravimetry), (v) X-ray fluorescence, (vi) X-ray diffraction, (vii) thermal analyses, (viii) Fourier Transform Infrared spectroscopy, and (ix) ion chromatographic studies.

RESULTS

Lapped Cross Sections of Bricks & Mortars

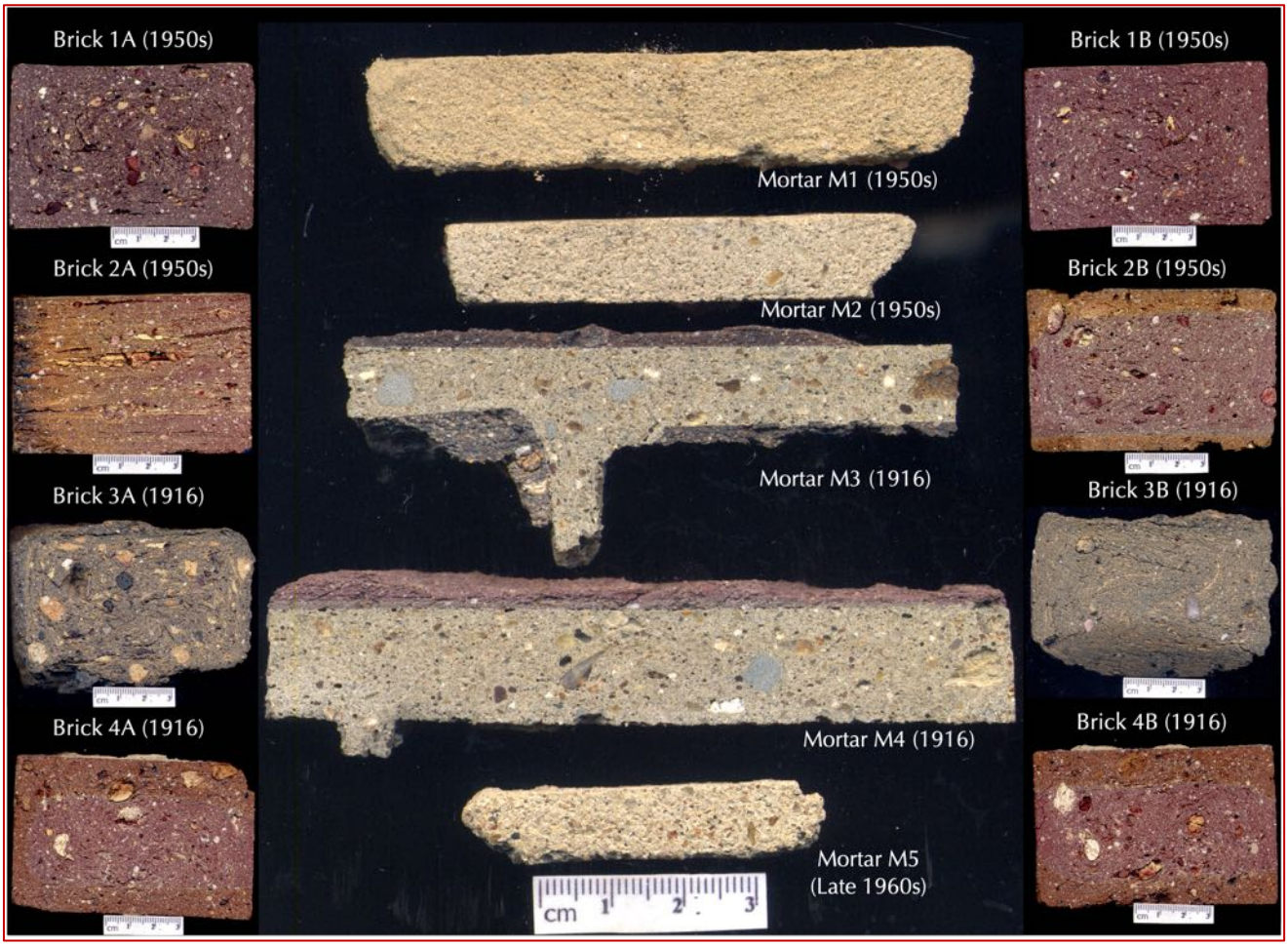

Figure 8: Lapped cross sections of brick and mortar samples showing dark reddish-brown color of Brick 1A and 1B from 1950s vintage, and lighter reddish-brown color of brick 2A and 2B from 1950s vintage, where Brick 2A showed many elongated voids in the interior and a lighter colored oxidation zone of 5 to 10 mm thickness at the exposed ends (which is found in both Brick 2A and 2B, where color of brick has changed from reddish-brown in the interior to yellowish brown at the exposed ends due to atmospheric oxidation and alterations during interaction with the adjacent masonry mortars and environmental elements, e.g., moisture during service). Bricks 3A and 3B from 1916 showed a gray color tone, which is not only different in color tone from the rest reddish-brown bricks, but also appears to be softer, most absorptive, and has many lineation all of which are the result of use of a different clay mix (having very low carbonate content), different firing conditions, and different manufacturing processes (e.g., hand-pressing the bricks) than the other bricks.

Lapped cross sections of bricks and mortars in Figures 8 to 10 show: (i) variations in color tones of bricks and mortars, (ii) uniformity in interior compositions of each brick and mortar sample, (iii) reddish-brown glassy aluminosilicate matrix (plastic component) in bricks 1A/B, 2A/B, and 4A/B but noticeably grayish tone of bricks 3A/B, (iv) tempered quartz, and previously fired grog particles amongst the non-plastic components in bricks, (v) overall porous natures of bricks from abundance of characteristic elongated voids in bricks from drying occurred before and during the baking processes, (vi) clear light brown to gray silica sand particles in mortars, (vii)

beige/tan color tone of mortars M1 and M2 from 1950s vintage, whereas noticeably grayish color tone of M3 and M4 mortar from 1916, but again beige/tan color tone of M5 from late 1960s vintage.

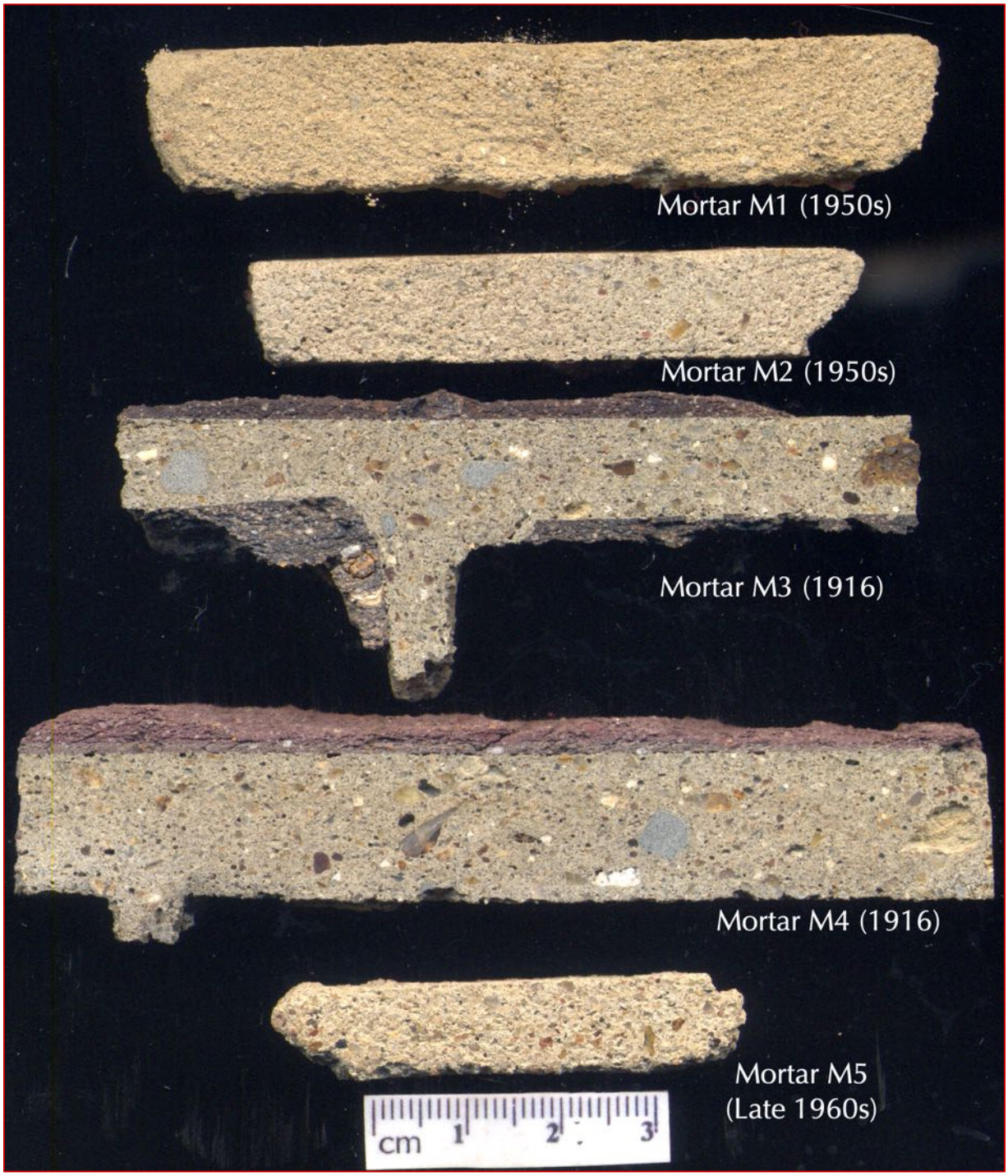

Figure 9: Lapped cross sections of masonry mortars from 1950s, 1916, and late 1960s vintages showing typical beige color tone and soft, dusty nature of Mortar M1 from 1950s vintage but relatively harder, denser and tan color tone of Mortar M2 from 1950s vintage, much denser, harder and gray color tone of Mortars M3 and M4 from 1916 vintage, and soft, dusty beige color tone of Mortar M5 from late 1960s vintage. Such color variations are found to be due to use of different binders in the mortars from natural cement-based binder in Mortars M1 and M2 to cement-lime based binders in Mortars M3 and M4 to masonry cement based binder in Mortar M5.

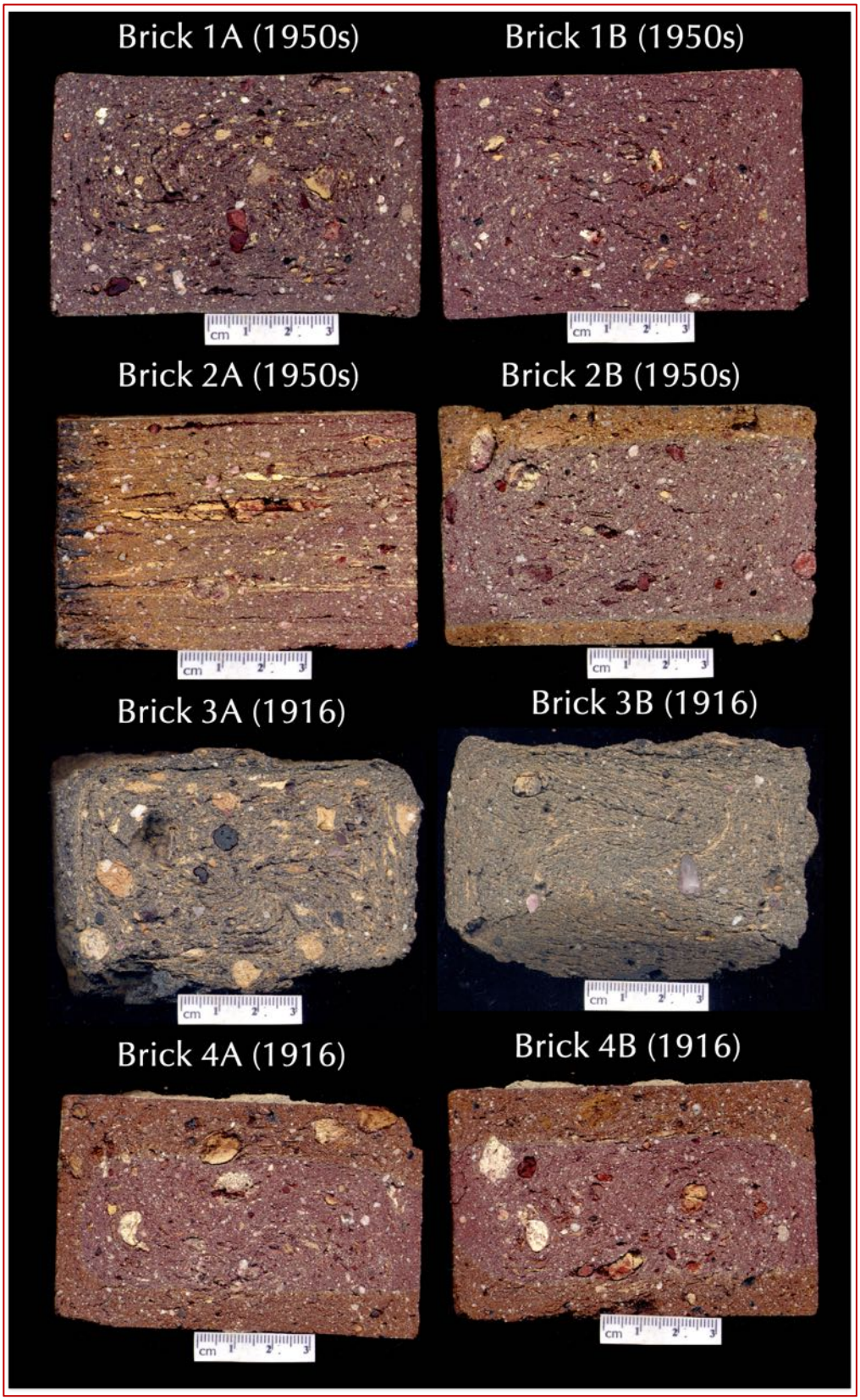

Figure 10: Lapped cross sections of bricks showing reddish-brown color tones of Bricks 1A/B, 2A/B, and 4A/B, but gray color tone of Bricks 3A/B indicating a very different composition of clay, firing conditions, and manufacturing processes of Brick 3 than the other ones.

Micrographs of Lapped Cross Sections of Bricks & Mortars

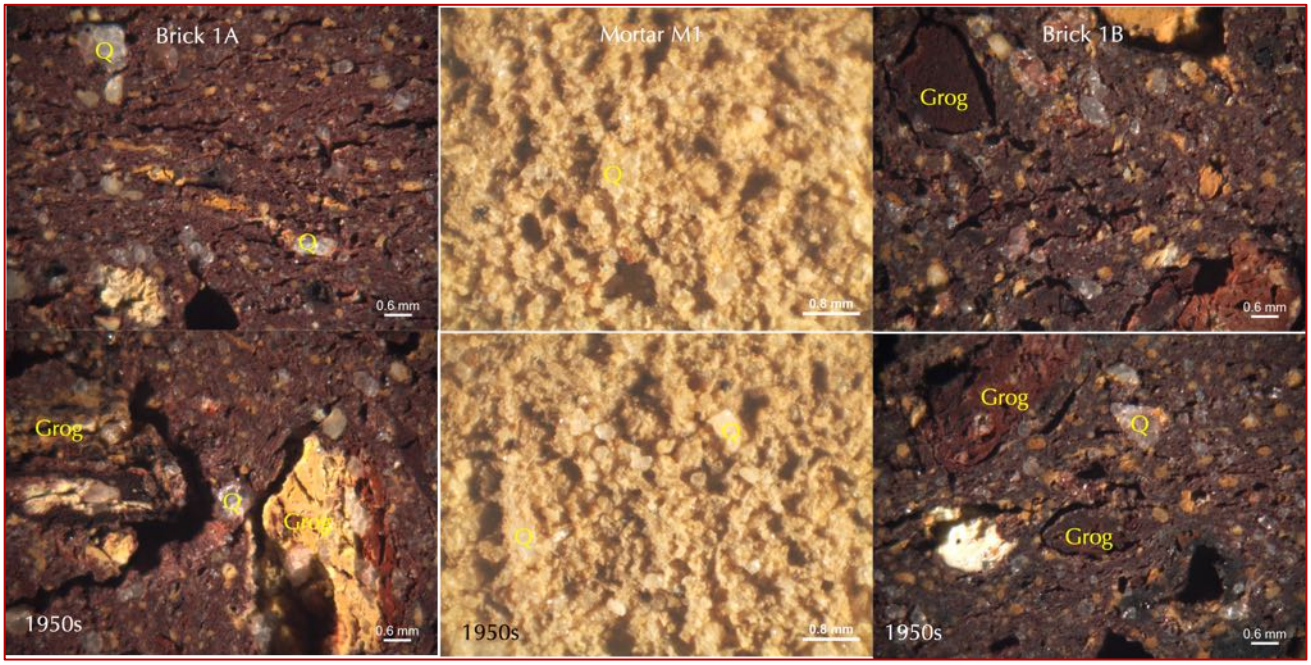

Figure 11: Micrographs of lapped cross sections of bricks (1A/B) and mortar (M1) from 1950s vintage showing: (a) tempered additives (quartz, Q, and previously fired grog particles) in non-plastic components and reddish-brown iron oxide-based vitrified aluminosilicate matrix of bricks having many elongated voids, and, (b) fine clear to light brown silica sand, soft beige paste, and non-air-entrained nature of the mortar.

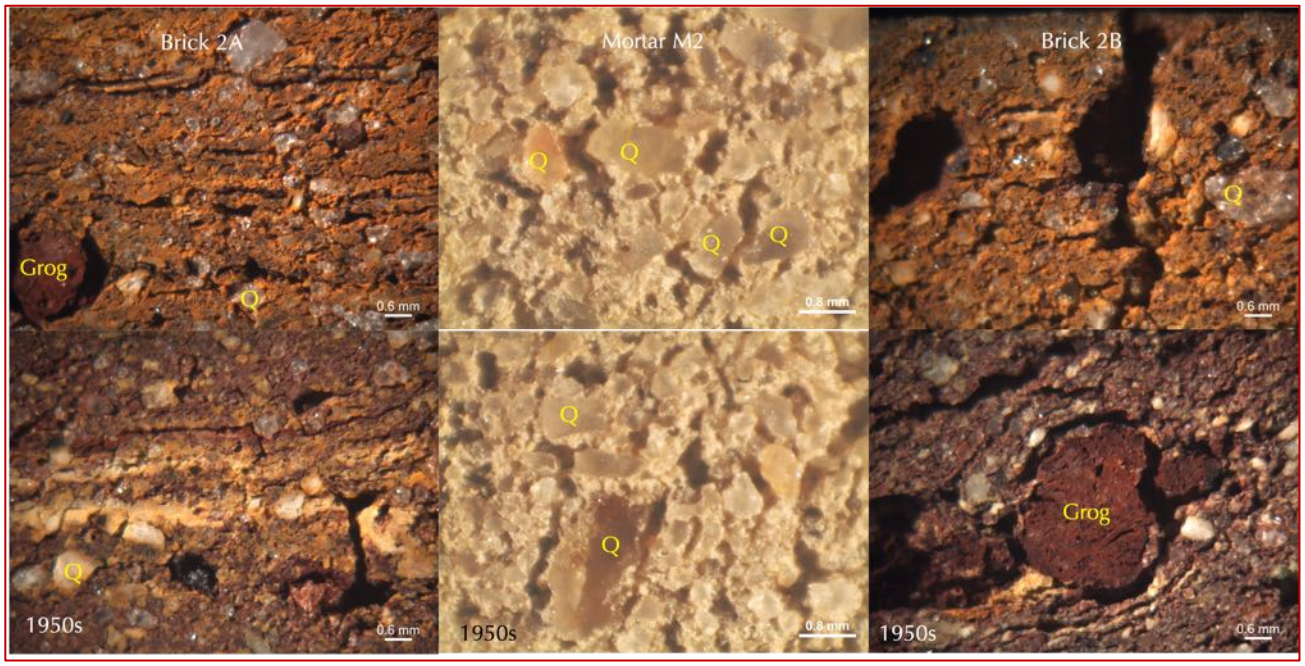

Figure 12: Micrographs of lapped cross sections of bricks (2A/B) and mortar (M2) from 1950s vintage showing: (a) tempered additives (quartz, Q, and previously fired grog particles) in non-plastic components and reddish-brown iron oxide based vitrified aluminosilicate matrix of bricks having many elongated voids, and, (b) fine clear to light brown silica sand, soft beige paste, and non-air-entrained nature of the mortar.

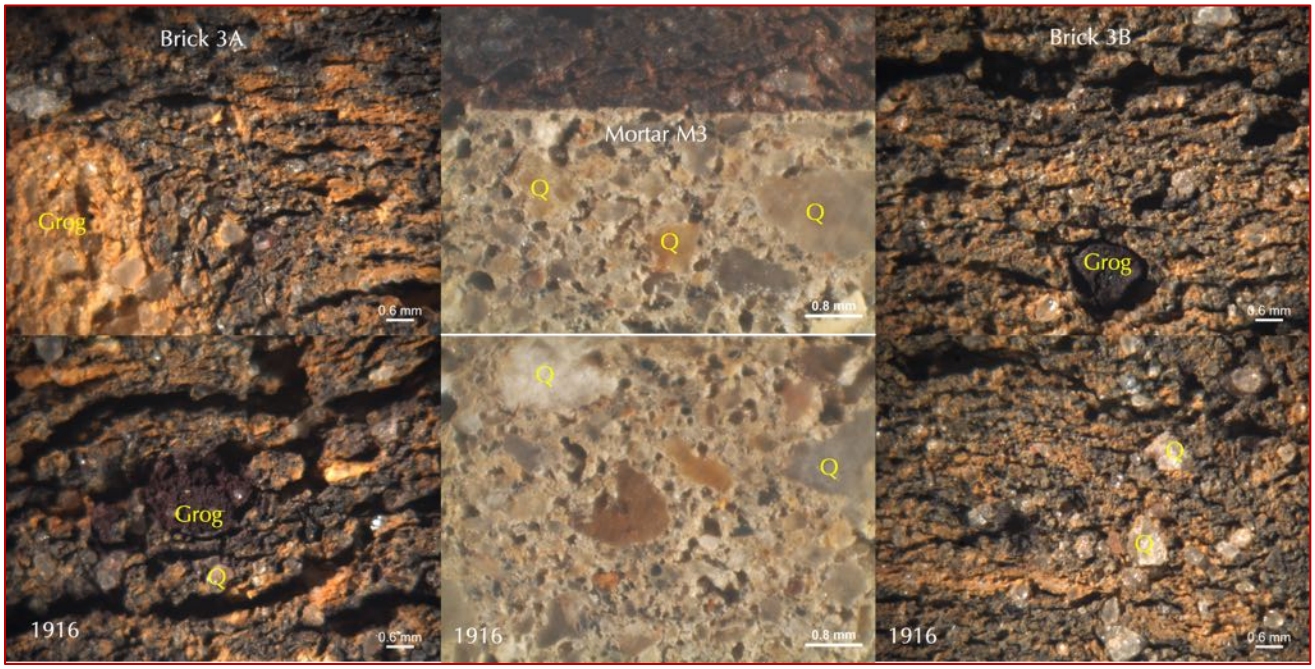

Figure 13: Micrographs of lapped cross sections of bricks (3A/B) and mortar (M3) from 1916 vintage showing: (a) tempered additives (quartz, Q, and previously fired grog particles) in non-plastic components and gray vitrified aluminosilicate matrix of bricks having many parallel, elongated voids, and, (b) fine clear to light brown silica sand, soft beige paste, and non-air-entrained nature of the mortar.

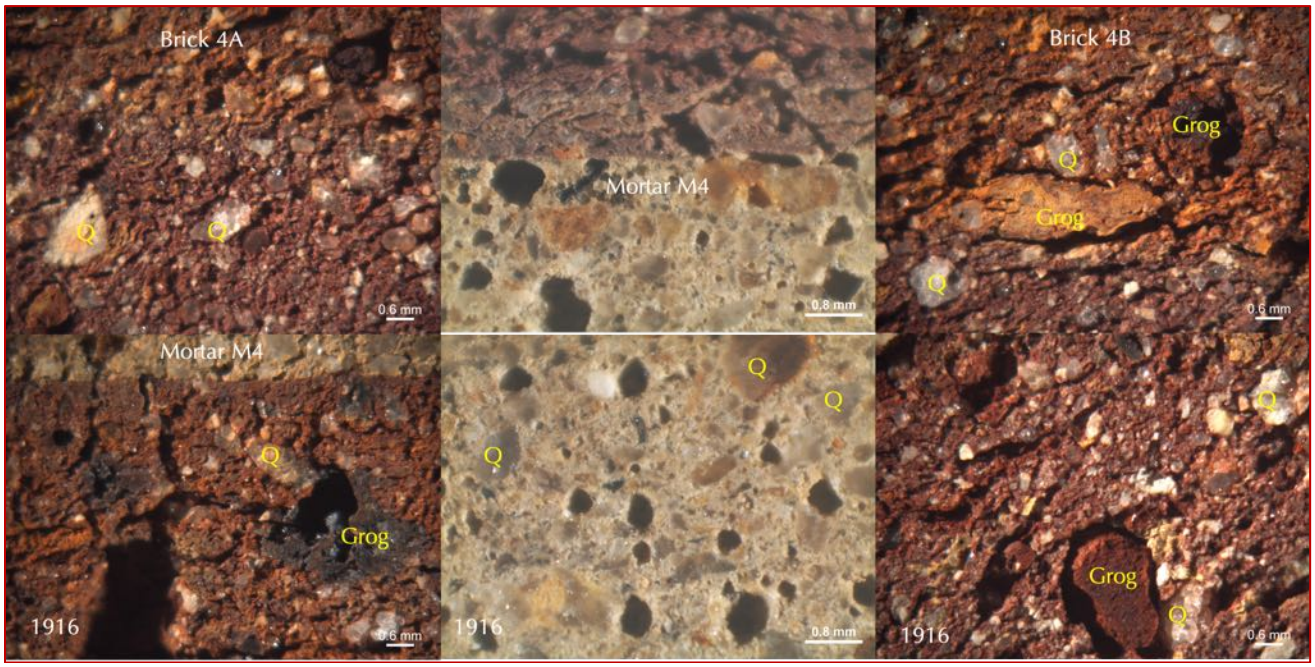

Figure 14: Micrographs of lapped cross sections of bricks (4A/B) and mortar (M4) from 1916 vintage showing: (a) tempered additives (quartz, Q, and grog particles) in non-plastic components and reddish-brown vitrified aluminosilicate matrix of bricks having many parallel, elongated voids, and, (b) fine clear to light brown silica sand, soft beige paste, and non-air-entrained nature of the mortar containing many coarse spherical voids.

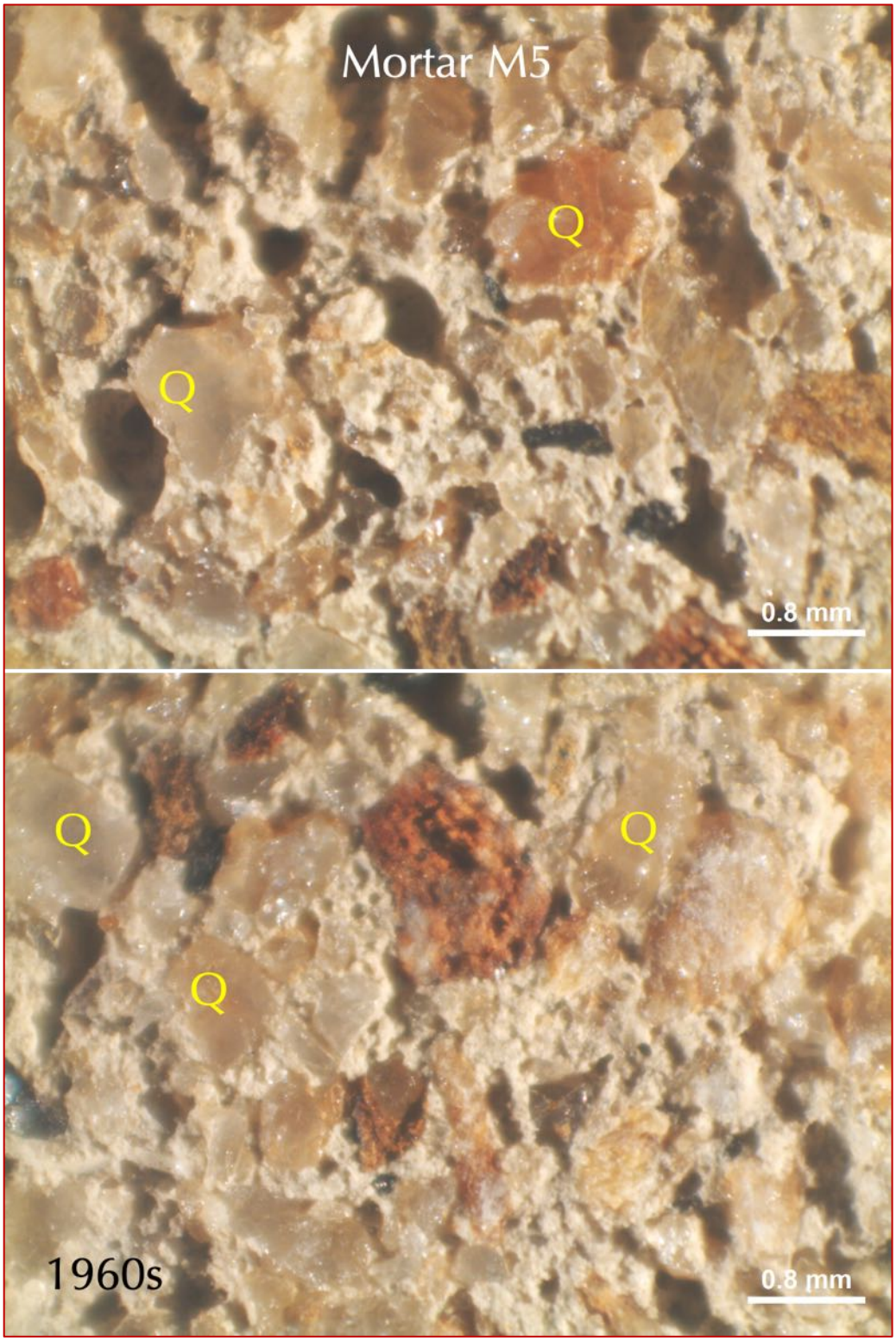

Figure 15: Micrographs of lapped cross section mortar from late 1960s vintage (M5) showing fine clear to light brown silica sand, a few brick dusts, soft beige paste, and non-air-entrained nature of the mortar containing many coarse spherical voids.

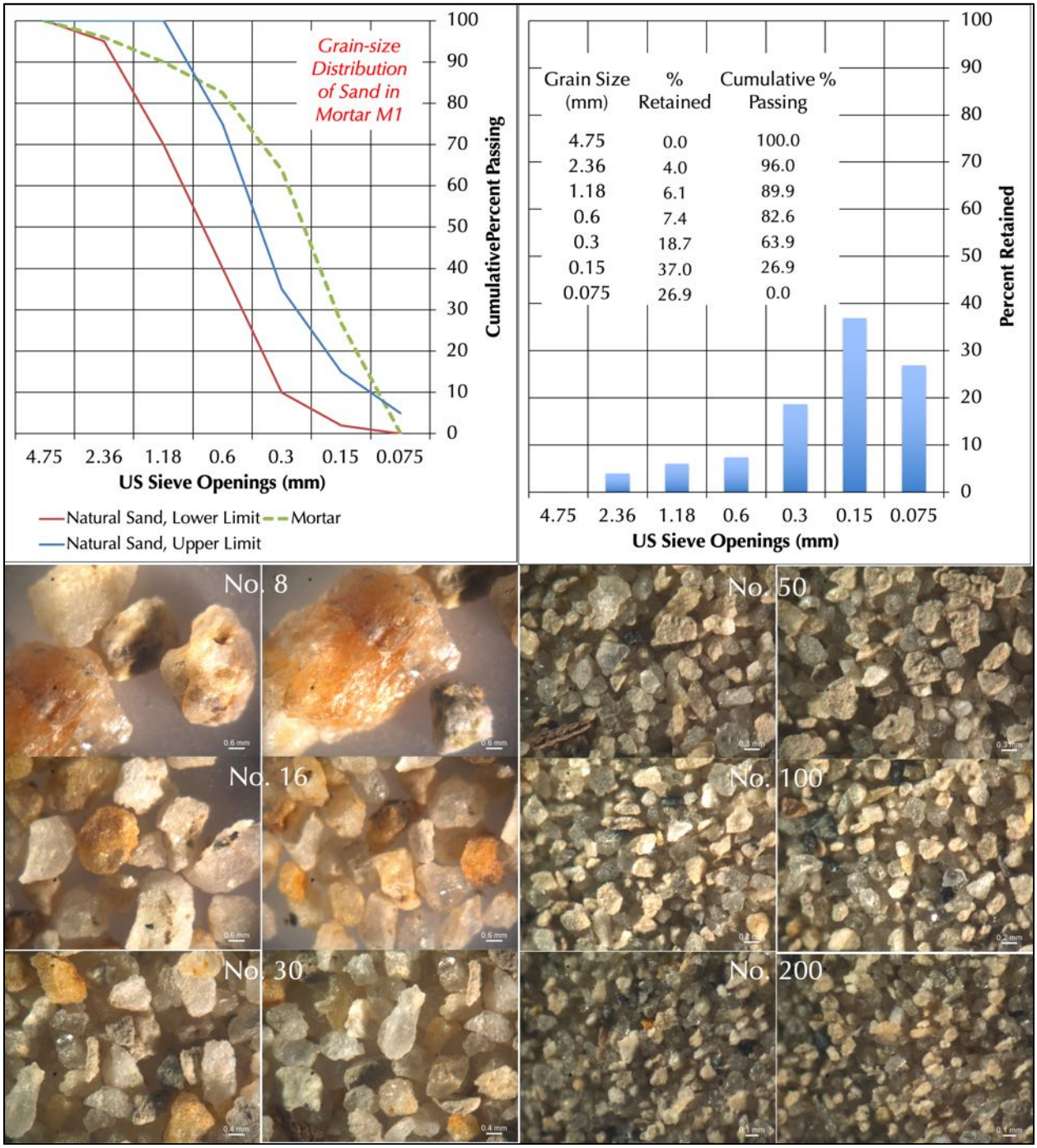

Figure 16: Grain-size distribution of sand extracted from Mortar M1 (1950s vintage) after acid digestion. In the top left plot, size distribution of sand is compared with upper and lower limits of natural sand in ASTM C 144 (blue and red lines, respectively). The top right 'percent retained' histogram plot shows enrichment of fines compared to a 'normal' size distribution of sand. Bottom photos show stereo-micrographs of sand particles retained on various sieves, including size, shape, angularity, and color variations of sand particles. Note noticeably clear to light brown to off-white color tone of majority of sand particles. Subsequent optical microscopical examinations of sand determined its siliceous composition, and lack of any calcareous components. Therefore, sand extracted from acid digestion is determined to be the entire amount of sand without leaving any component and hence results provided here are a close representation of the bulk sand used.

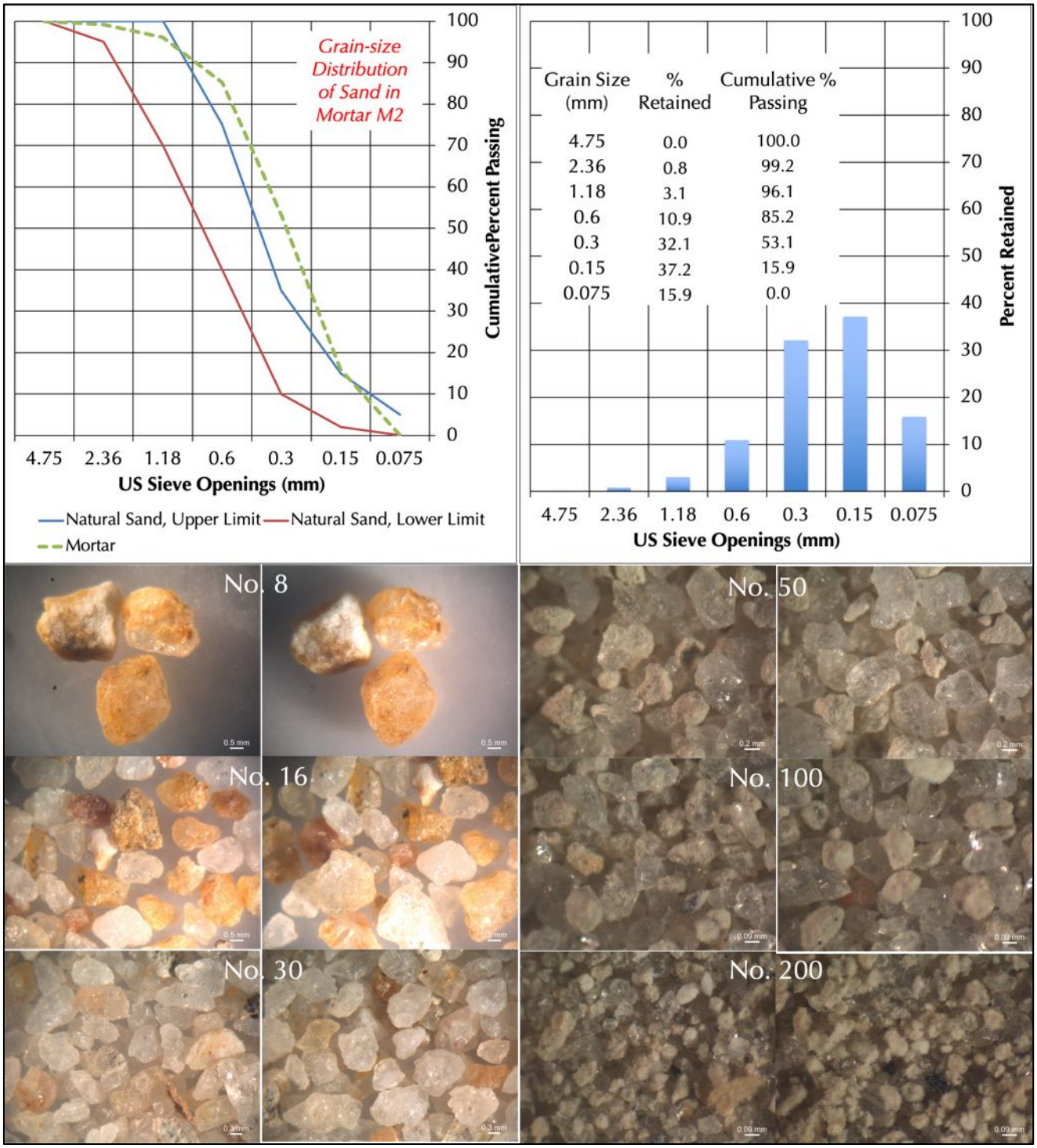

Figure 17: Grain-size distribution of sand extracted from Mortar M2 (1950s vintage) after acid digestion. In the top left plot, size distribution of sand is compared with upper and lower limits of natural sand in ASTM C 144 (blue and red lines, respectively). The top right 'percent retained' histogram plot shows enrichment of fines compared to a 'normal' size distribution of sand. Bottom photos show stereo-micrographs of sand particles retained on various sieves, including size, shape, angularity, and color variations of sand particles. Note noticeably clear to light brown to off-white color tone of majority of sand particles. Subsequent optical microscopical examinations of sand determined its **siliceous composition**, and lack of any calcareous components. Therefore, sand extracted from acid digestion is determined to be the entire amount of sand without leaving any component and hence results provided here are a close representation of the bulk sand used.

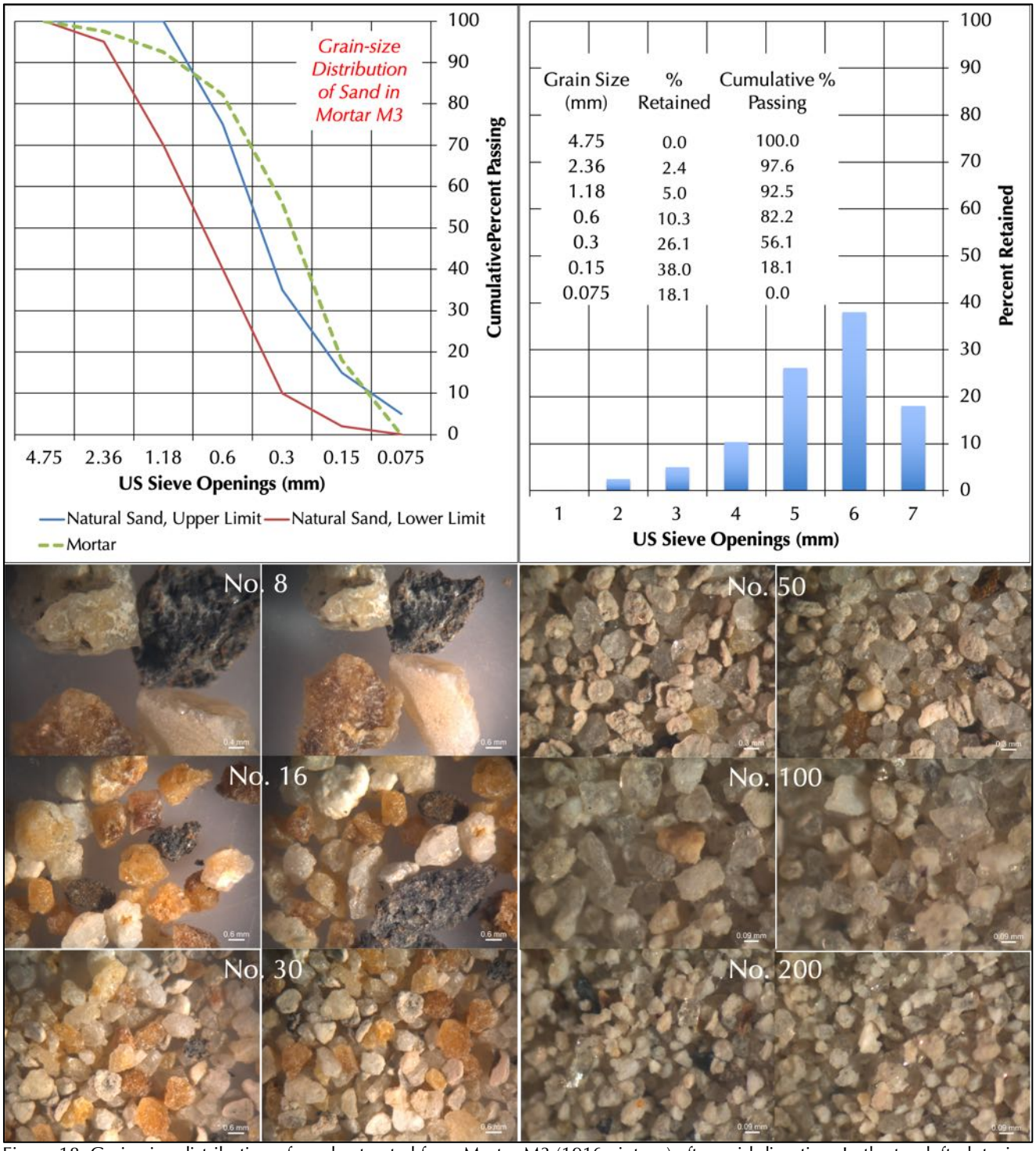

Figure 18: Grain-size distribution of sand extracted from Mortar M3 (1916 vintage) after acid digestion. In the top left plot, size distribution of sand is compared with upper and lower limits of natural sand in ASTM C 144 (blue and red lines, respectively). The top right 'percent retained' histogram plot shows enrichment of fines compared to a 'normal' size distribution of sand. Bottom photos show stereo-micrographs of sand particles retained on various sieves, including size, shape, angularity, and color variations of sand particles. Note noticeably clear to light brown to off-white color tone of majority of sand particles. Subsequent optical microscopical examinations of sand determined its **siliceous composition**, and lack of any calcareous components. Therefore, sand extracted from acid digestion is determined to be the entire amount of sand without leaving any component and hence results provided here are a close representation of the bulk sand used.

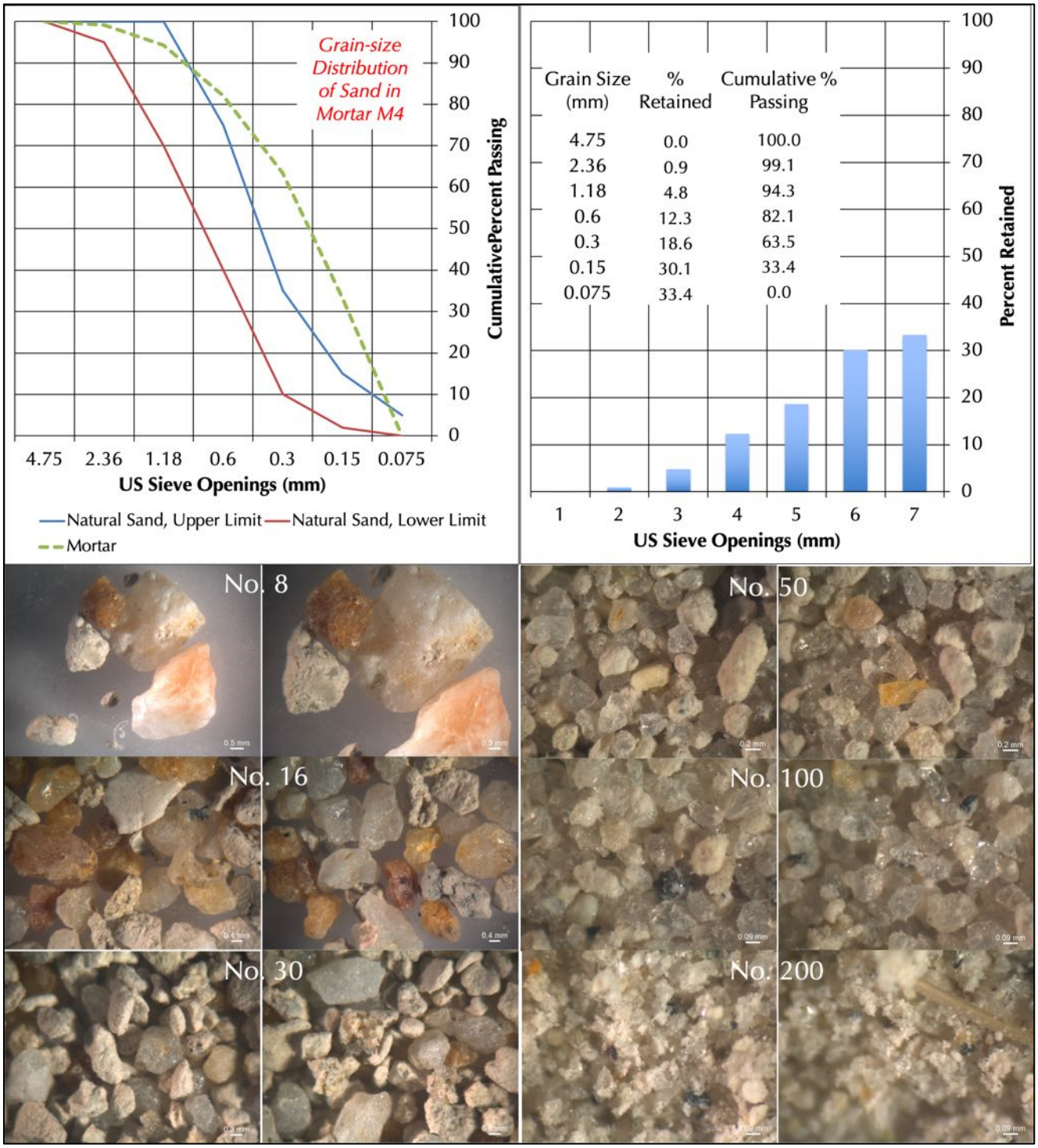

Figure 19: Grain-size distribution of sand extracted from Mortar M4 (1916 vintage) after acid digestion. In the top left plot, size distribution of sand is compared with upper and lower limits of natural sand in ASTM C 144 (blue and red lines, respectively). The top right 'percent retained' histogram plot shows enrichment of fines compared to a 'normal' size distribution of sand. Bottom photos show stereo-photomicrographs of sand particles retained on various sieves, including size, shape, angularity, and color variations of sand particles. Note noticeably clear to light brown to off-white color tone of majority of sand particles. Subsequent optical microscopical examinations of sand determined its **siliceous composition**, and lack of any calcareous components. Therefore, sand extracted from acid digestion is determined to be the entire amount of sand without leaving any component and hence results provided here are a close representation of the bulk sand used.

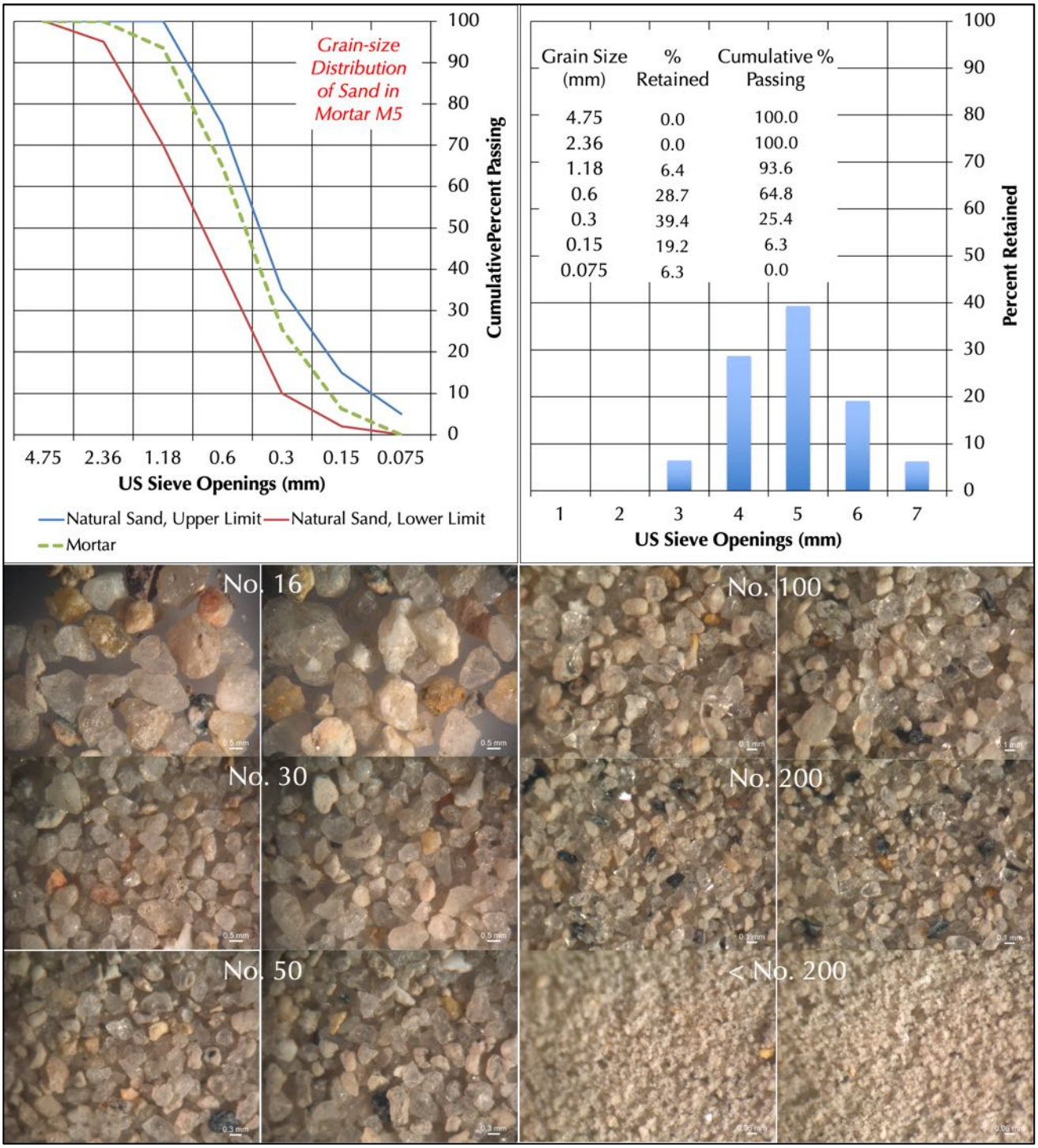

Figure 20: Grain-size distribution of sand extracted from Mortar M5 (late 1960s vintage) after acid digestion. In the top left plot, size distribution of sand is compared with upper and lower limits of natural sand in ASTM C 144 (blue and red lines, respectively). The top right 'percent retained' histogram plot shows more or less 'normal' size distribution of sand without any enrichment of fines. Bottom photos show stereo-micrographs of sand particles retained on various sieves, including size, shape, angularity, and color variations of sand particles. Note noticeably clear to light brown to off-white color tone of majority of sand particles. Subsequent optical microscopical examinations of sand determined its **siliceous composition**, and lack of any calcareous components. Therefore, sand extracted from acid digestion is determined to be the entire amount of sand without leaving any component and hence results provided here are a close representation of the bulk sand used. Of all the mortars, this sample shows size distribution that is most consistent with the specifications of ASTM C 144 sand as seen in the top left plot.

Optical Microscopy of Natural Cement Mortars M1 and M2 From 1950s

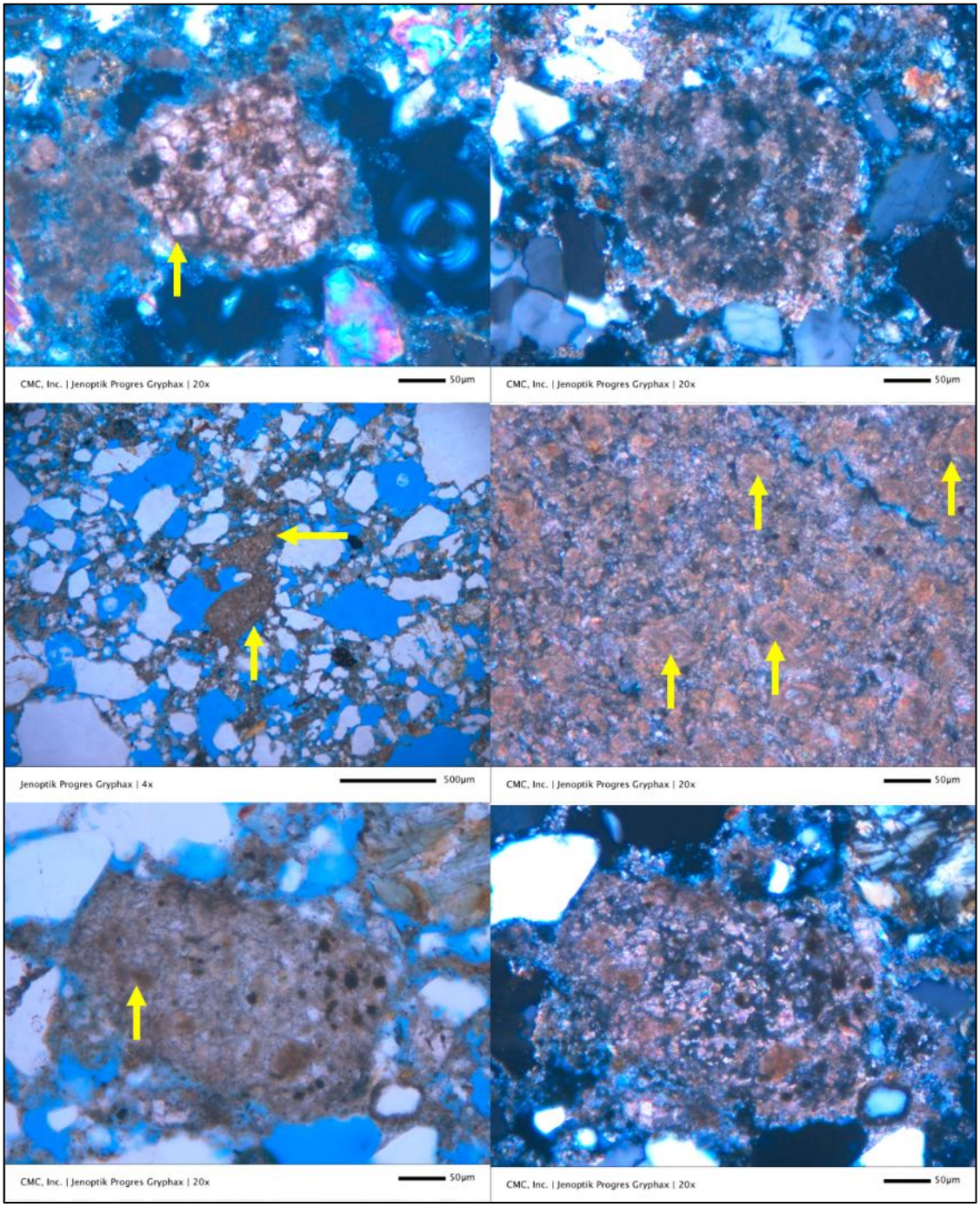

Figure 21: Optical micrographs of natural cement mortar M1 (circa 1950s) showing residual calcined impure dolomitic limestone feed containing dolomite rhombs with interstitial anhedral calcite, silica, and clay matrix of variable degrees of calcination, e.g., from a less calcined particle in the top left to more advanced calcination resulting in amorphous matrix within the particle in the top right. Middle left photo shows sand size of many such residual natural cement particles (shown with arrows). Middle right photo shows internal texture and mineralogy of one residual dolomitic limestone feed of natural cement containing dolomite rhombs (arrows) and interstitial silica and calcined clay matrix. Bottom row shows plane (left) and crossed (right) polarized light view of a residual natural cement particle showing advanced calcination and subsequent hydration of natural cement leaving some dolomite pseudomorphs, amorphous matrix, and granular calcite. Mortar contains siliceous sand and overall carbonated matrix of hydration products of natural cement and carbonated lime. See Appendix B (Figures B2 through B7) for more micrographs.

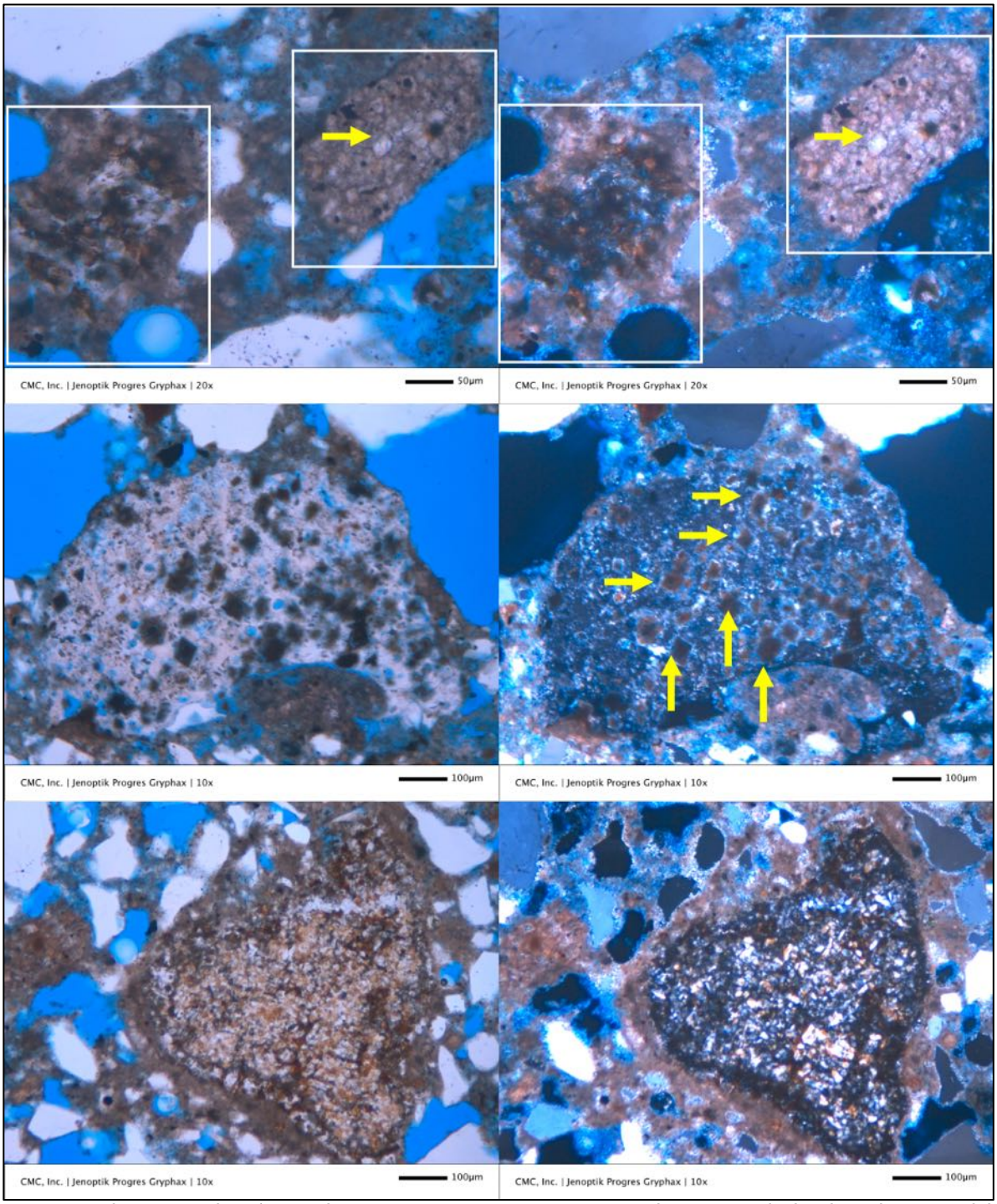

Figure 22: Optical micrographs of natural cement mortar M2 (circa 1950s) showing residual calcined impure dolomitic limestone feed containing dolomite rhombs with interstitial anhedral calcite, silica, and clay matrix of variable degrees of calcination, e.g., from a less calcined particle to more advanced calcination resulting in amorphous matrix within the particle. Top row shows plane (left) and crossed (right) polarized light views of two residual natural cement particles, one at left showing advanced calcination resulting in amorphous matrix, and one at right showing less calcination where pristine mineralogy and texture of dolomitic limestone is still preserved. Middle row shows internal texture and mineralogy of one residual dolomitic limestone feed of natural cement that has an overall amorphous matrix with dolomite pseudomorphs from advanced calcination. Bottom row shows a residual cement particle having coarsely crystalline calcium aluminate silicate phases developed from calcination of dolomitic limestone; the particle is surrounded by a dense, less carbonated paste of hydration products. Mortar contains siliceous sand and overall carbonated matrix of hydration products of natural cement and carbonated lime. See Appendix B (Figures B8 through B19) for more micrographs.

Optical Microscopy of Cement-Lime Mortars M3 and M4 From 1916

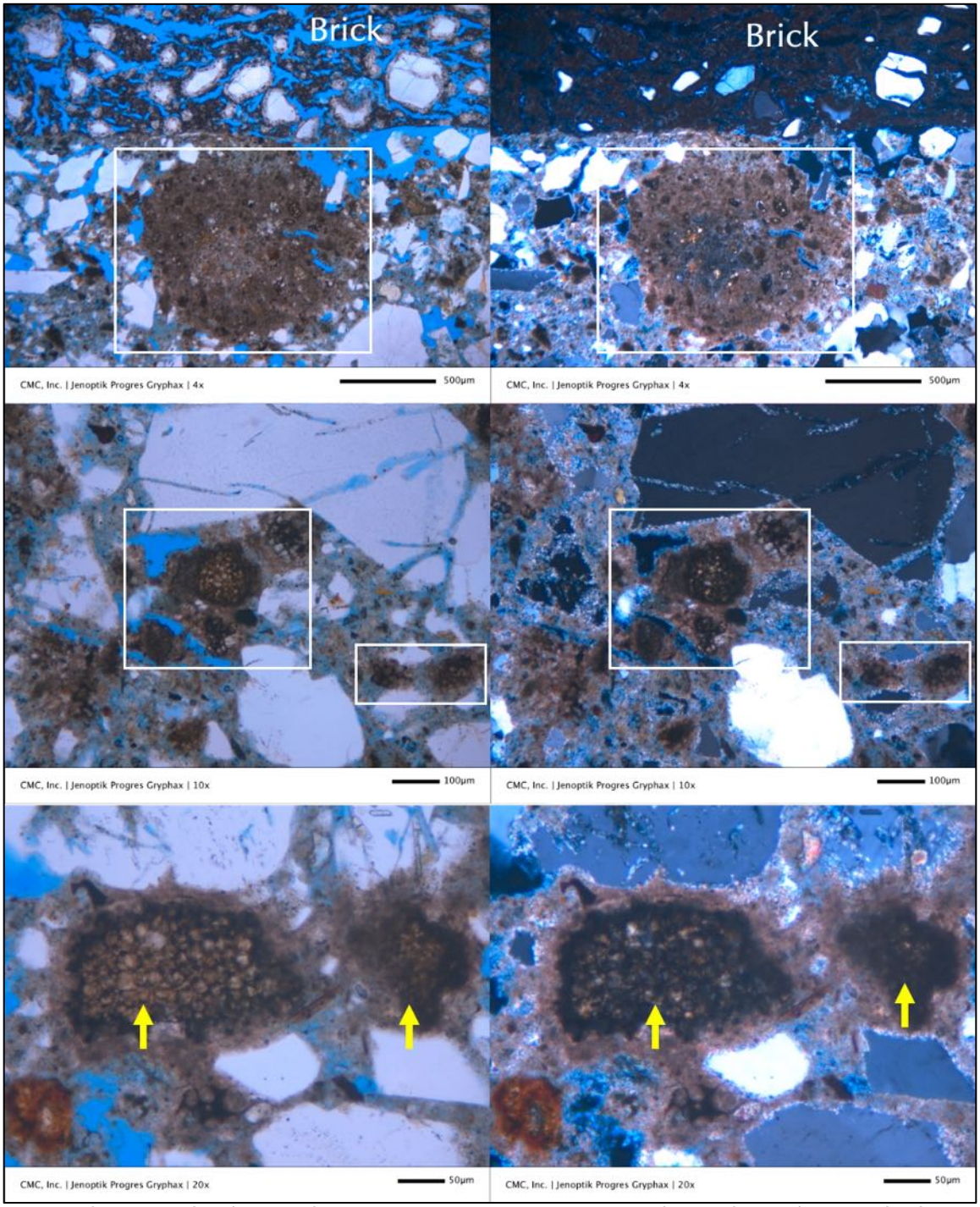

Figure 23: Optical micrographs of cement-lime mortar M3 (circa 1916). Top row shows a lump of neat Portland cement paste (boxed) containing many residual Portland cement particles scattered in a dense, less carbonated paste than paste elsewhere outside the lump. Mortar contains natural siliceous sand and carbonated cement-lime paste. Adhered to the mortar in the top row is a fired clay brick containing tempered quartz additive in a reddish-brown aluminosilicate glass matrix, and abundant parallel elongated voids creating a highly porous nature of the brick. Middle row shows many residual Portland cement particles (boxed) with rims of dense paste of hydration products scattered in a more carbonated and porous paste. Sand contains major amount of quartz and subordinate amounts of feldspar and quartzite. Bottom row shows belite clusters with dark interstitial ferrite phases in two residual Portland cement particles. See Appendix B (Figures B20 through B27) for more micrographs. Paste microstructure is very different from what is found in the natural cement mortars in M1 and M2.

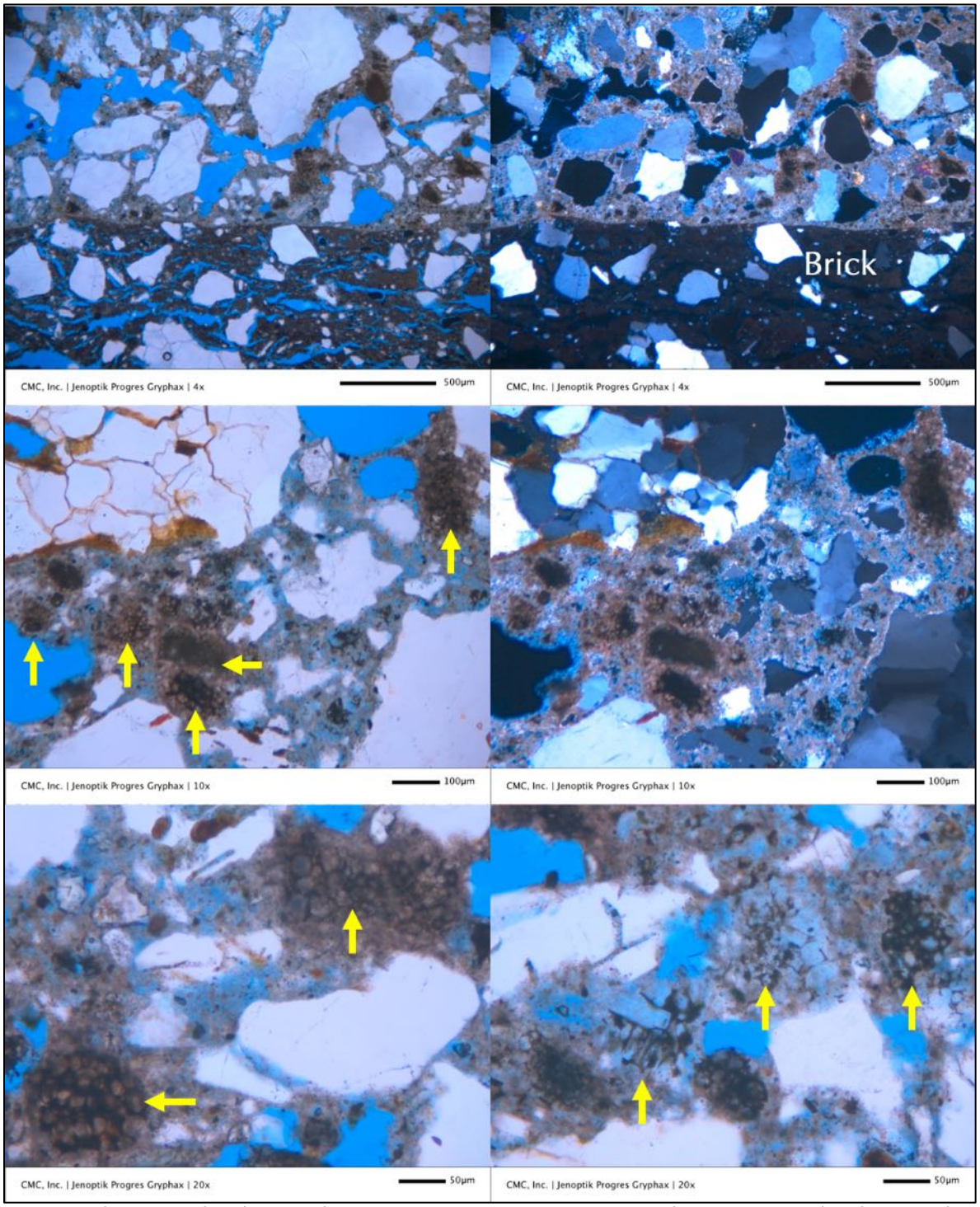

Figure 24: Optical micrographs of cement-lime mortar M4 (circa 1916). Top row shows intact interface between the mortar and adhered fired clay brick. Mortar contains natural siliceous sand and carbonated cement-lime paste containing scattered residual Portland cement particles. Fired clay brick contains tempered quartz additive in a reddish-brown aluminosilicate glass matrix, and abundant parallel elongated voids creating a highly porous nature of the brick. Middle row shows many residual Portland cement particles (arrows) with rims of dense paste of hydration products scattered in a more carbonated and porous paste. Sand contains major amount of quartz and subordinate amounts of feldspar and quartzite. Bottom left photo shows belite clusters with dark interstitial ferrite phases in two residual Portland cement particles. Bottom right photo shows some residual cement particles where pseudomorphs of euhedral alite phase is seen that are hydrated leaving euhedral shape and interstitial dark ferrite phase. See Appendix B (Figures B28 through B33) for more micrographs. Paste microstructure is similar to that found in M3 but very different from what is found in the natural cement mortars in M1 and M2.

Optical Microscopy of Masonry Cement Mortar M5 From Late 1960s

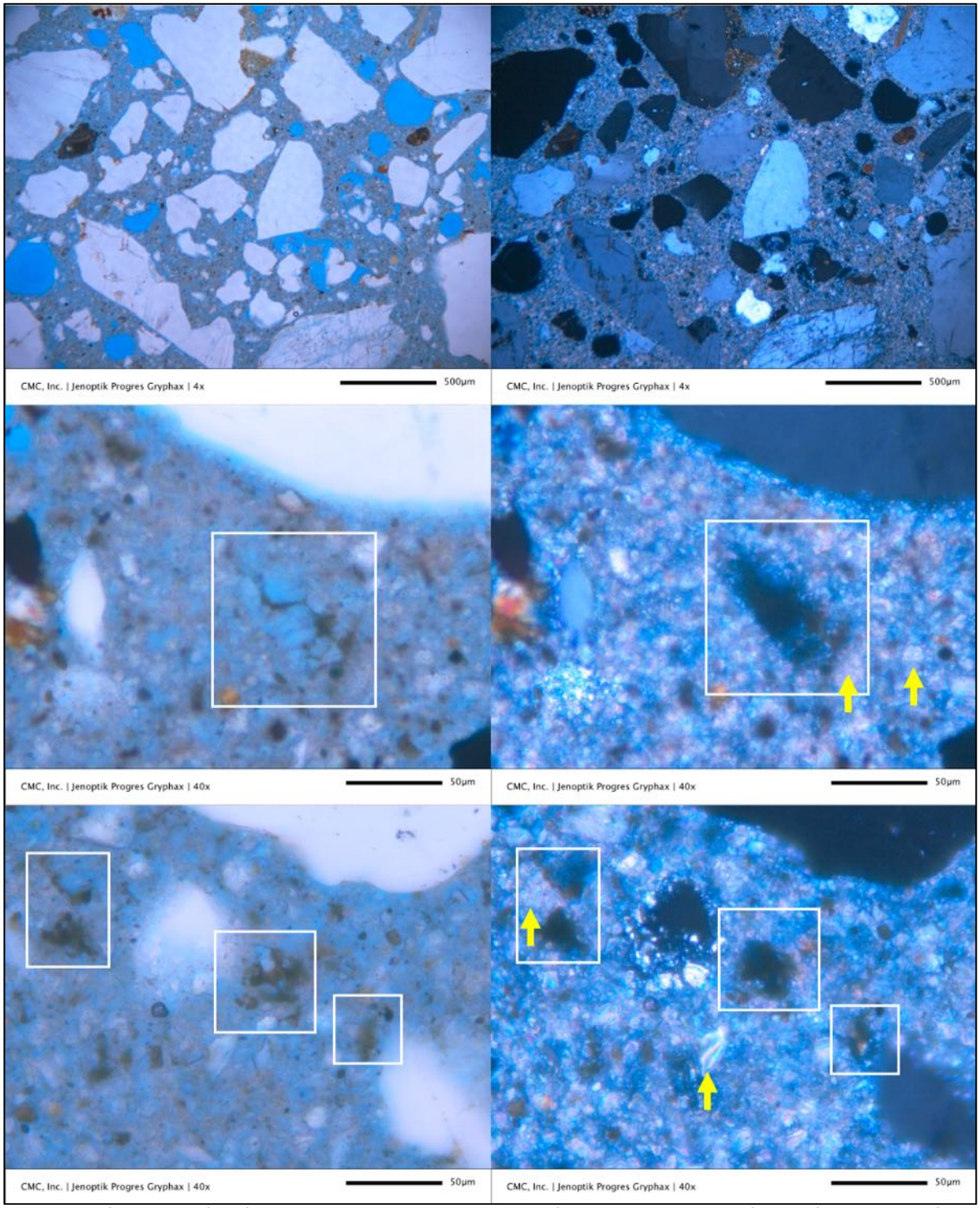

Figure 25: Optical micrographs of masonry cement mortar M5 (circa late 1960s). Top row shows siliceous natural sand and highly carbonated paste that is typical of many masonry cements. The mortar, however, is non-air-entrained. Middle row shows the paste at high magnification, where a residual Portland cement particle is boxed that contains pseudomorphs of subhedral alite and skeletal dark interstitial ferrite. Paste shows carbonation and many carbonated lime and limestone fine particles giving an overall granular appearance of paste. Bottom row shows many residual Portland cement particles (boxed) that are well-hydrated leaving mostly skeletal ferrite remains and an overall carbonated paste. See Appendix B (Figures B34 through B36) for more micrographs. Paste microstructure is very different from all other mortars.

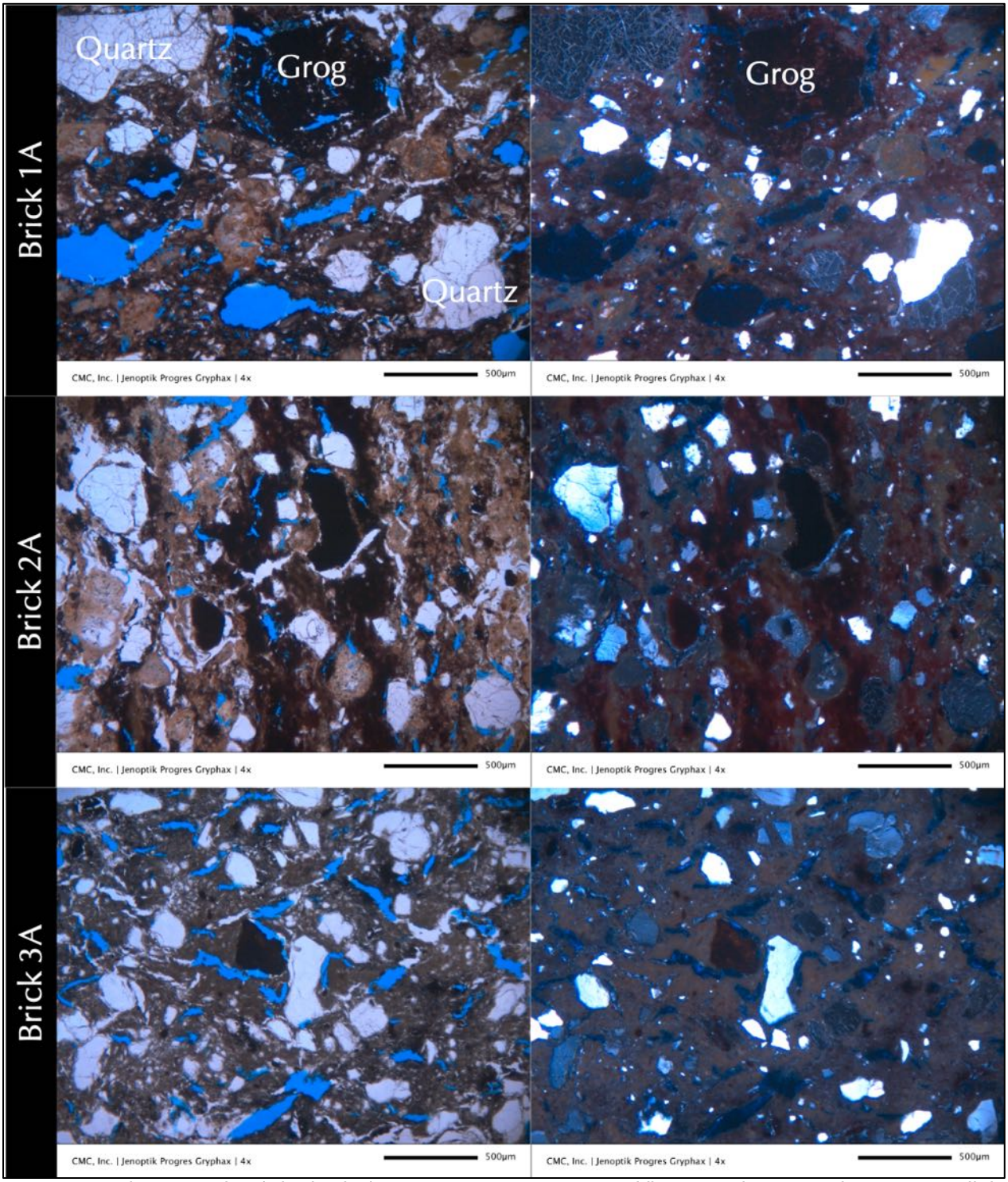

Figure 26: Optical micrographs of clay bricks from 1950s (1A top row, 2A middle row) and 1916 (3A, bottom row). All three bricks show: (a) tempered quartz additions as main non-plastic component, where quartz particles are well sorted and of one population, abundant elongated parallel voids creating highly porous microstructure, a few grog particles of previously fired clay, and (b) the plastic component constituting aluminosilicate glass matrix from firing of clay. Overall reddish-brown color of brick in 1A and 2A are from iron oxide component of clay and due to firing in an oxidizng condition in kiln, as opposed to the gray color tone of brick 3A which is found to be due to low carbonate content of clay and firing in a reducing condition in the kiln. See Appendix B (Figures B38 through B49) for more micrographs.

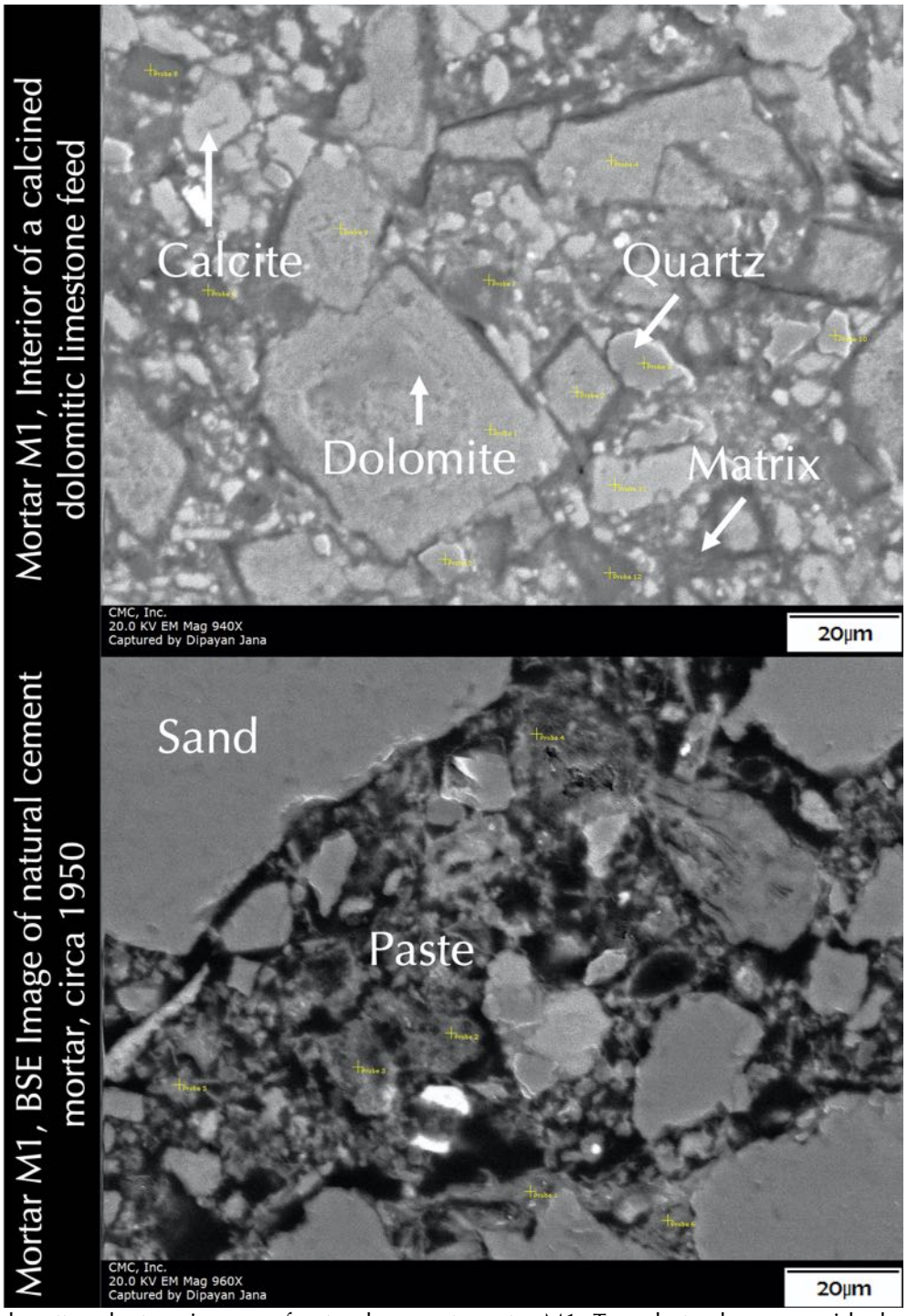

Figure 27: Backscatter electron images of natural cement mortar M1. Top photo shows a residual natural cement particle having the characteristic microstructure of subhedral dolomitc rhombs and interstitial anhedral calcite, quartz, and aluminsilicate matrix phases where, depending on the degree of calcination, the interstitial aluminosilicate phase becomes amorphous from lime-magnesia-silica-alumnina reactions between dolomite, calcite, quartz, and clay phases of impure dolomitic limestone feed, which is responsible for the hydraulicity of natural cement. Bottom photo shows the overall microstructure of mortar consisitng of sand grains and interstitial

phase. Various areas of both images were subseqeuntly analyzed in SEM-EDS for compositional analyses, which are provided (along with numerous other images of this mortar) in Appendix C.

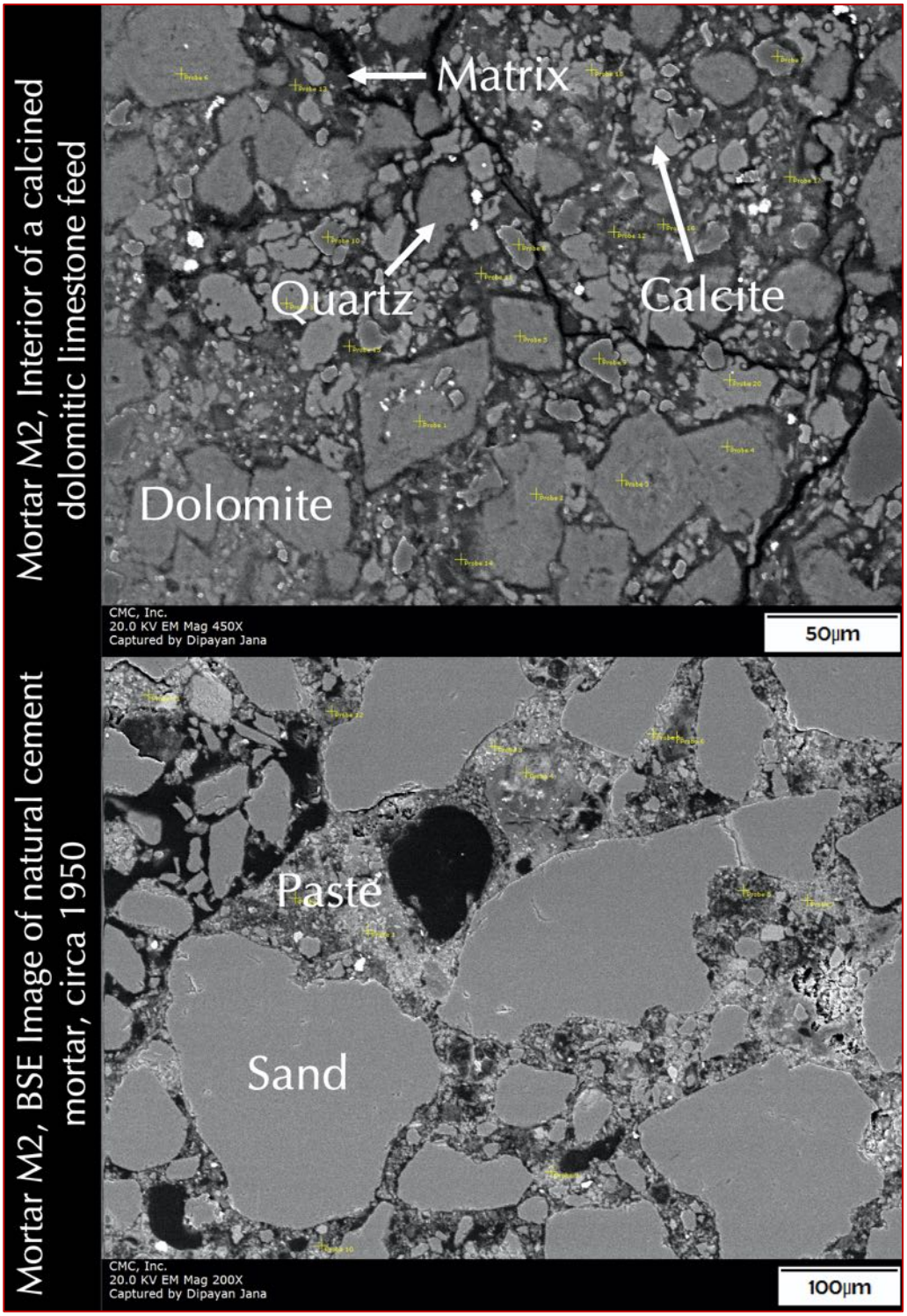

Figure 28: Backscatter electron images of natural cement mortar M2. Top photo shows a residual natural cement particle having the characteristic microstructure of subhedral dolomitc rhombs and interstitial anhedral calcite, quartz, and aluminsilicate matrix phases where, depending on the degree of calcination, the interstitial aluminosilicate phase becomes amorphous from lime-magnesia-silica-alumnina reactions between dolomite, calcite, quartz, and clay phases of impure dolomitic limestone feed, which is responsible for the hydraulicity of

natural cement. Bottom photo shows the overall microstructure of mortar consisitng of sand grains and interstitial phase. Various areas of both images were subseqeuntly analyzed in SEM-EDS for compositional analyses, which are provided (along with numerous other images of this mortar) in Appendix C.

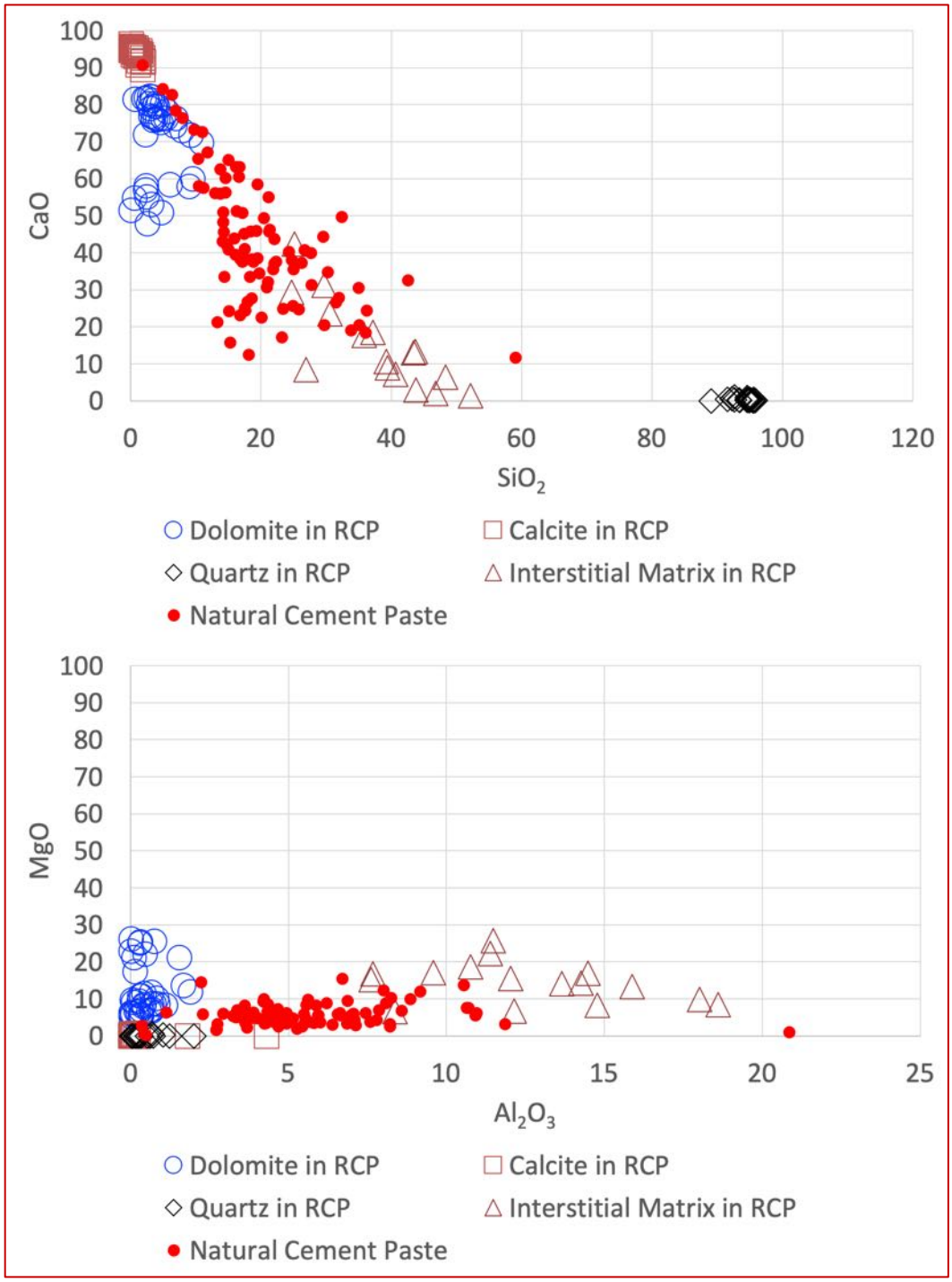

Figure 29: SEM-EDS oxide compositional variations of residual natural cement particles and pastes in mortar M1 and M2 from 1950s vintage showing: (i) variations in lime versus silica (top) and (ii) magnesia versus alumina (bottom) contents in the residual cement particles, and, in bulk pastes. In both plots, the solid red dots show compositional variations in natural cement pastes, which are superposed on the oxide compositional variations in dolomite rhombs, and anhedral calcite, quartz, and interstitial matrix phases of residual cements. Notice the compositional ranges of residual cement particles (shown in open circles, squares, diamonds, and triangles for

dolomite, calcite, quartz, and interstitial phases, respectively) where oxide compositional variations of paste fall between the compositional spaces of dolomite and calcite phases at one end and interstitial matrix phase of cements at the other, indicating the major role of interstitial phases of cement in hydraiton and formation of cement paste.

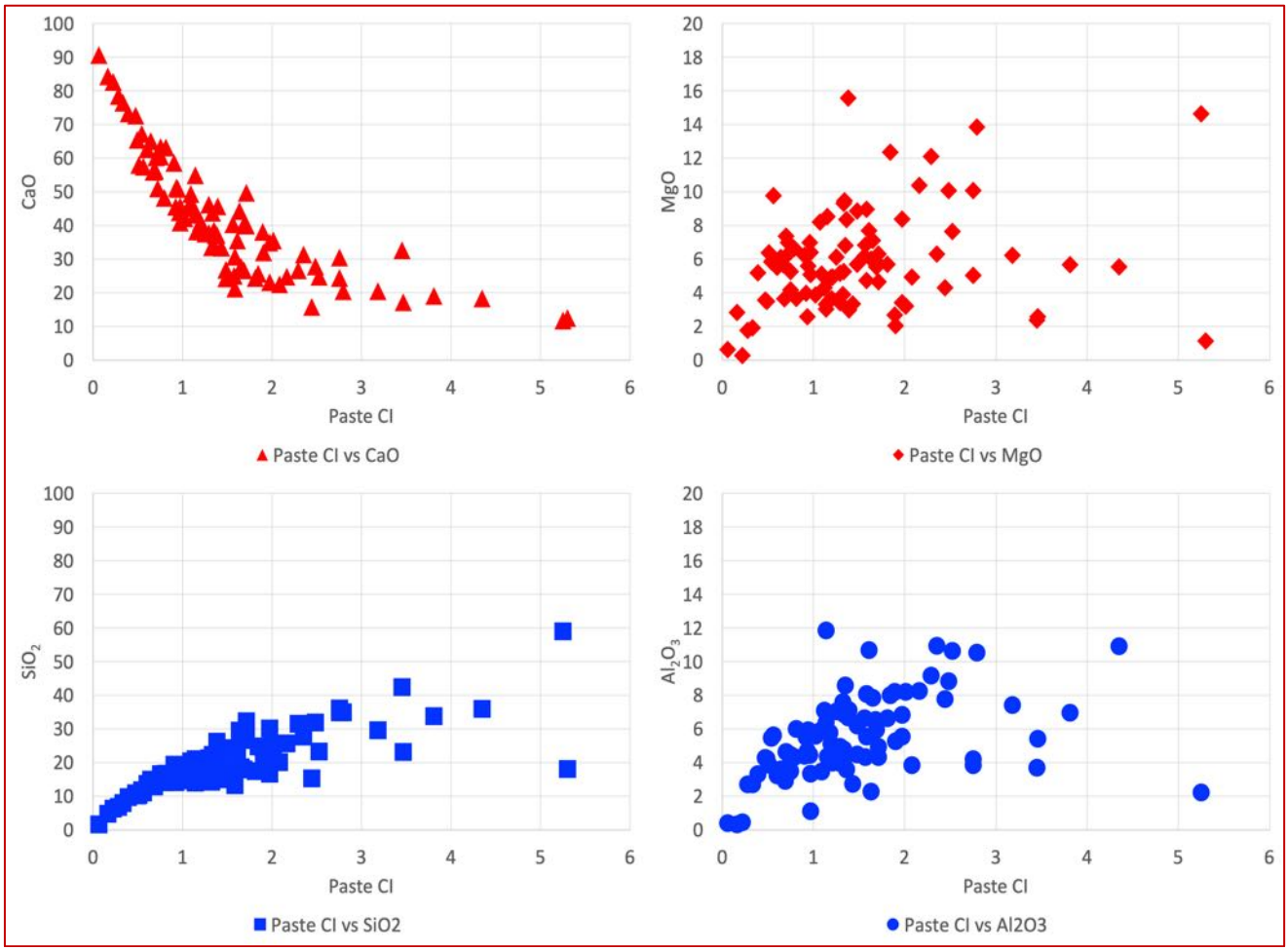

Figure 30: SEM-EDS oxide compositional variations of pastes in natural cement mortars M1 and M2 from 1950s vintage showing variations in lime (top left), magnesia (top right), silica (bottom left), and alumina (bottom right) contents of pastes plotted against cementation indices of paste, Paste CI, after Eckel 1922 where Paste CI = $[(2.8\times SiO_2)+(1.1\times Al_2O_3)+(0.7\times Fe_2O_3)]/[(CaO)+(1.4\times MgO)]$. Paste CI is a characteristic index of hydraulicites of pastes where lime-based pastes show very low CIs as opposed to Portland cement-based pastes. A range in paste CIs is usually obtained from the paste component in a mortar depending on the proportions and degree of mixing/homogenizations of various binder (lime and cement) components in the mortar, along with subsequent alterations (leaching, carbonation) of paste during service. The compositional trend of lime versus paste CI in the top left photo is very typical not only of many natural cement mortars but also in many cement-lime mortars from historic to modern constructions, which is representative of contributions of lime and cement components where former reduces the paste CI to the left but the latter increases the paste CI to the right thus forming the trend. Compared to lime and silica trends against paste CIs, trends for magenia and alumina are more scattered due to their lesser abundance in the binder phases than lime and silica.

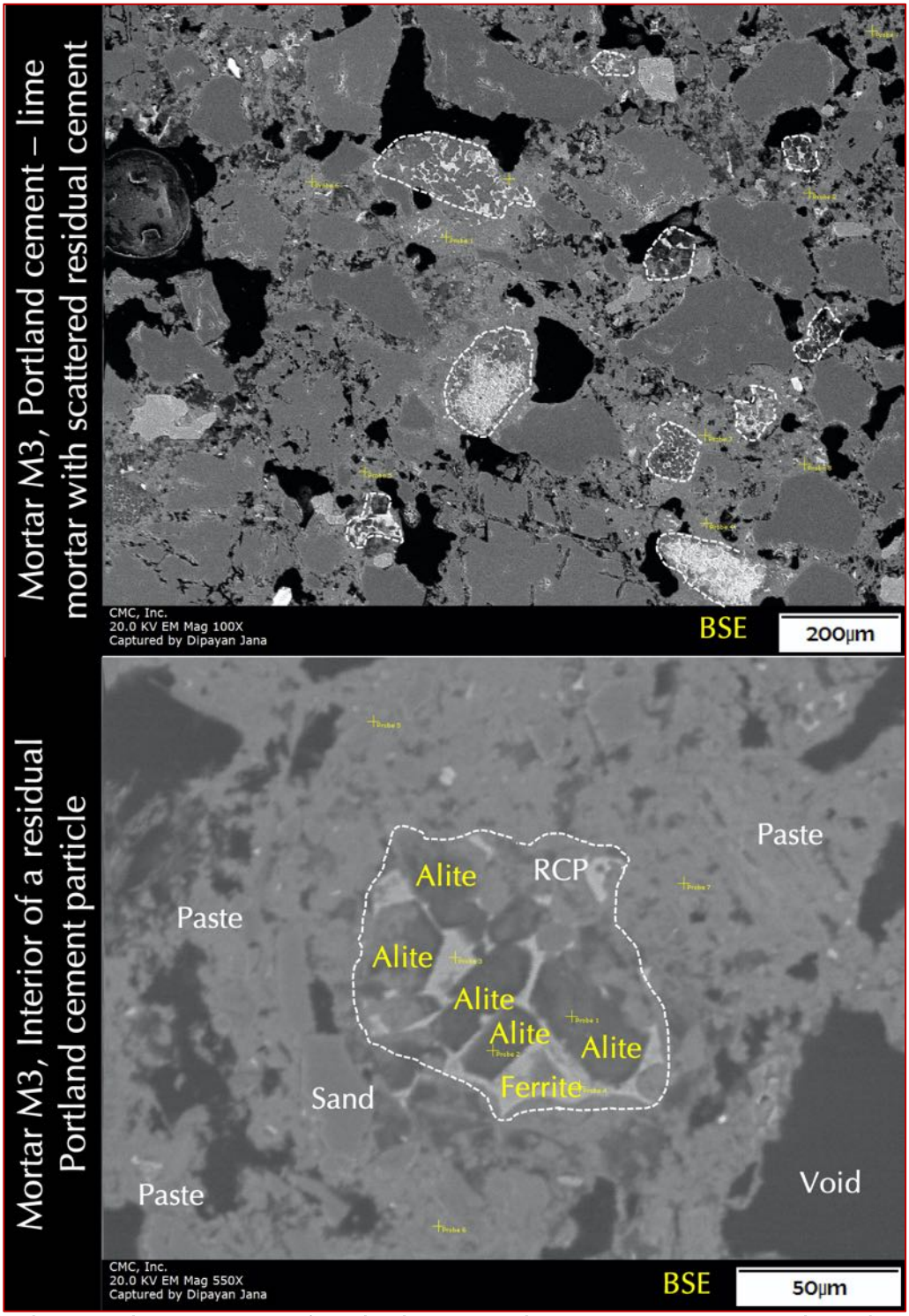

Figure 31: Backscatter electron images of Portland cement – lime mortar M3. Bottom photo shows a residual Portland cement particle (RCP, marked in white dashed line) having the characteristic microstructure of subhedral alite and interstitial ferrite phases in cement. Top photo shows the overall microstructure of mortar consisting of sand grains and interstitial phase having scattered residual Portland cement particles (marked in white dashed lines). Various areas of both images were subseqeuntly analyzed in SEM-EDS for compositional analyses, which are provided (along with numerous other images of this mortar) in Appendix C.

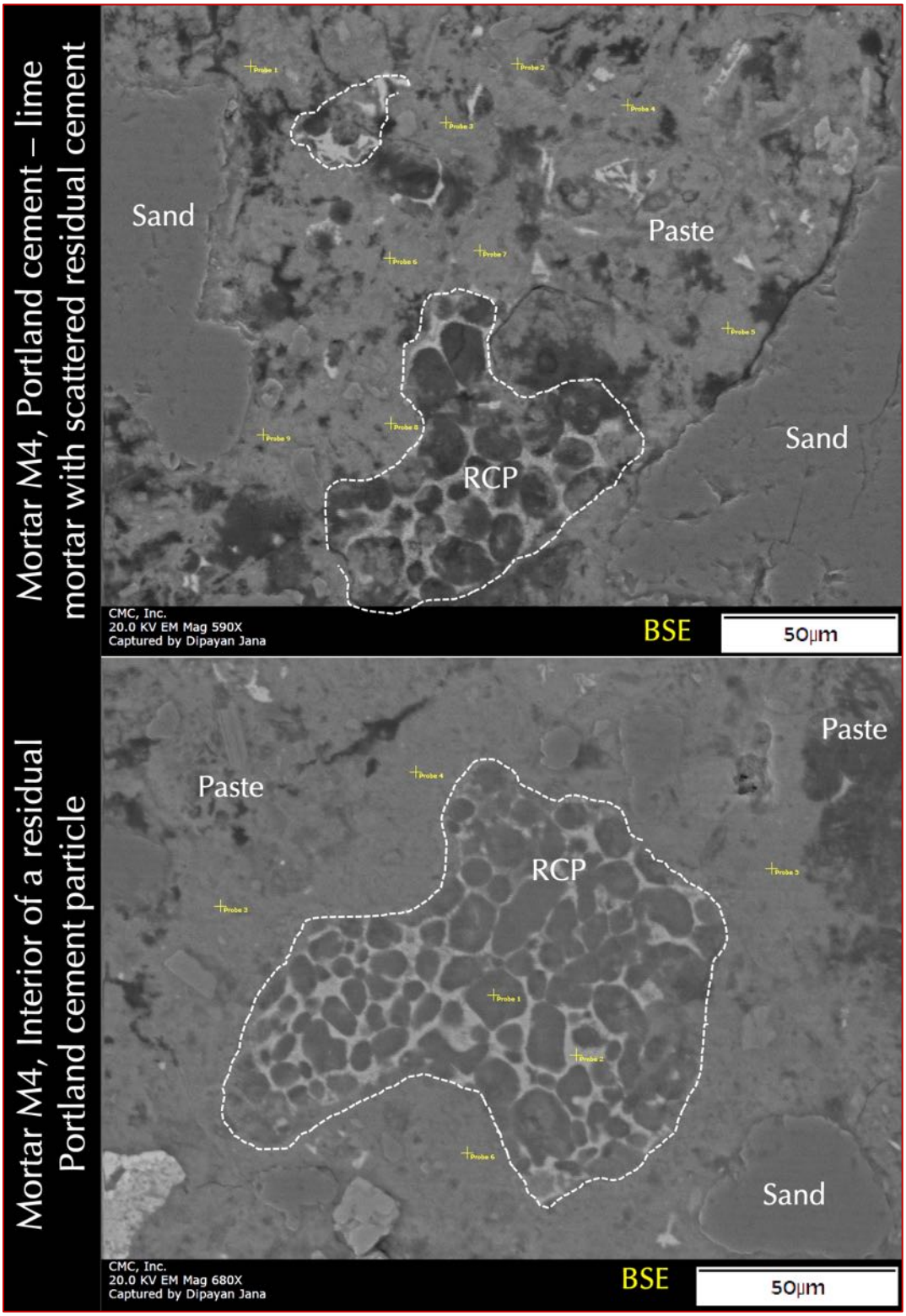

Figure 32: Backscatter electron images of Portland cement – lime mortar M4. Both photos show residual Portland cement particles (RCPs, marked in white dashed lines) having the characteristic microstructure of subhedral alite, anhedral belite, and interstitial ferrite phases in cement. Also shown are the overall microstructure of mortar consisting of sand grains and interstitial phase having scattered residual Portland cement particles. Various areas of both images were subseqeuntly analyzed in SEM-EDS for compositional analyses, which are provided (along with numerous other images of this mortar) in Appendix C.

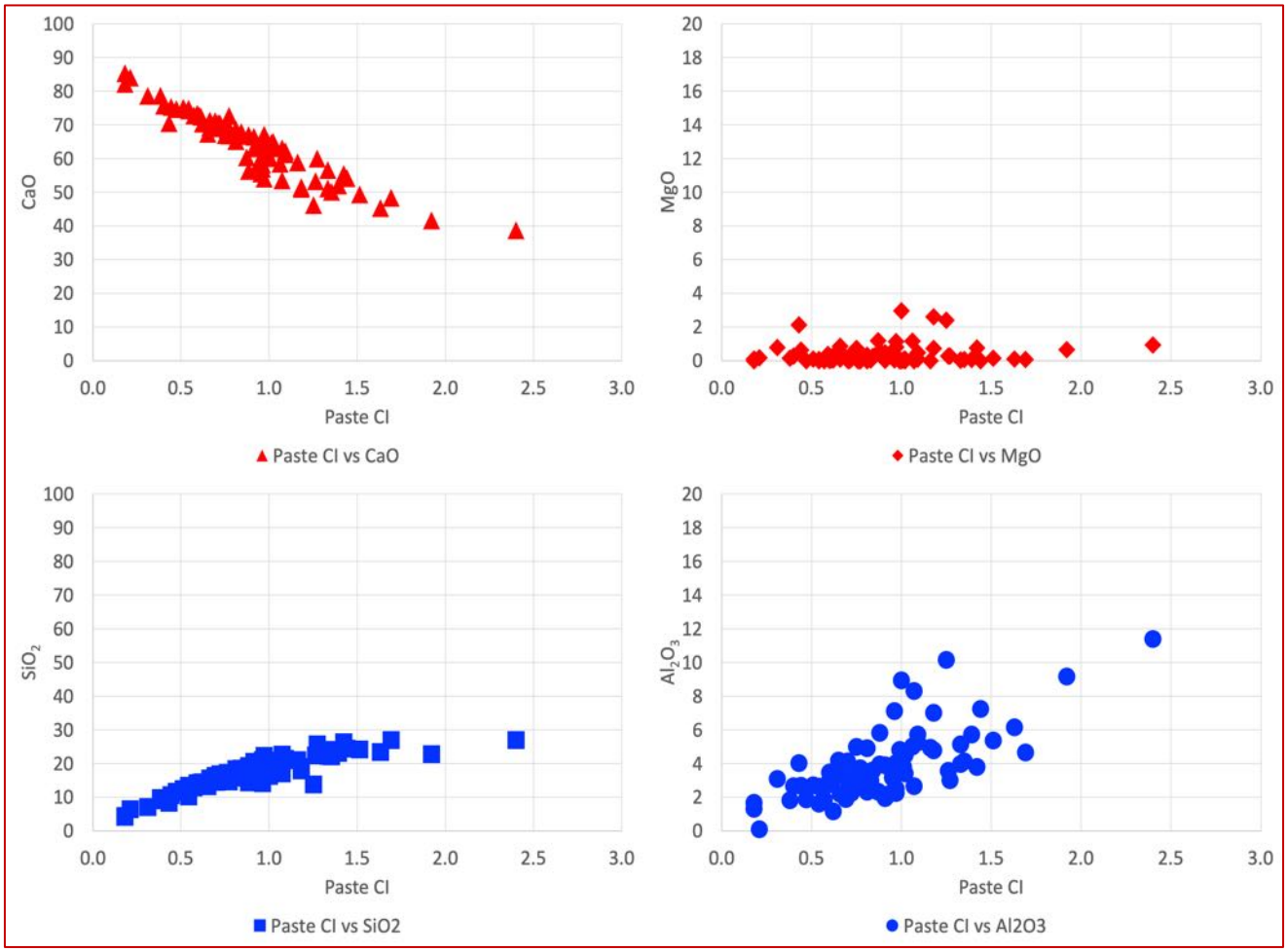

Figure 33: SEM-EDS oxide compositional variations of pastes in cement-lime mortars M3 and M4 from 1916 vintage showing variations in lime (top left), magnesia (top right), silica (bottom left), and alumina (bottom right) contents of pastes plotted against cementation indices of paste, Paste CI, after Eckel 1922 where Paste CI = $[(2.8\times SiO_2)+(1.1\times Al_2O_3)+(0.7\times Fe_2O_3)]/[(CaO)+(1.4\times MgO)]$. Paste CI is a characteristic index of hydraulicites of pastes where lime-based pastes show very low CIs as opposed to Portland cement-based pastes. A range in paste CIs is usually obtained from the paste component in a mortar depending on the proportions and degree of mixing/homogenizations of various binder (lime and cement) components in the mortar, along with subsequent alterations (leaching, carbonation) of paste during service. The compositional trend of lime versus paste CI in the top left plot is very typical not only of many cement-lime mortars but also in many natural cement-lime mortars from historic to modern constructions, as found in M1 and M2, which is representative of contributions of lime and cement components where former reduces the paste CI to the left but the latter increases the paste CI to the right thus forming the trend. Compared to lime and silica trends against paste CIs, trends for magenia and alumina are more scattered due to their lesser abundance in the binder phases than lime and silica. Notice the overall lower magnesia contents in the pastes compared to the natural cement mortars in M1 and M2, which is the characteristic compositional (high-magnisa) signature of natural cement mortars.

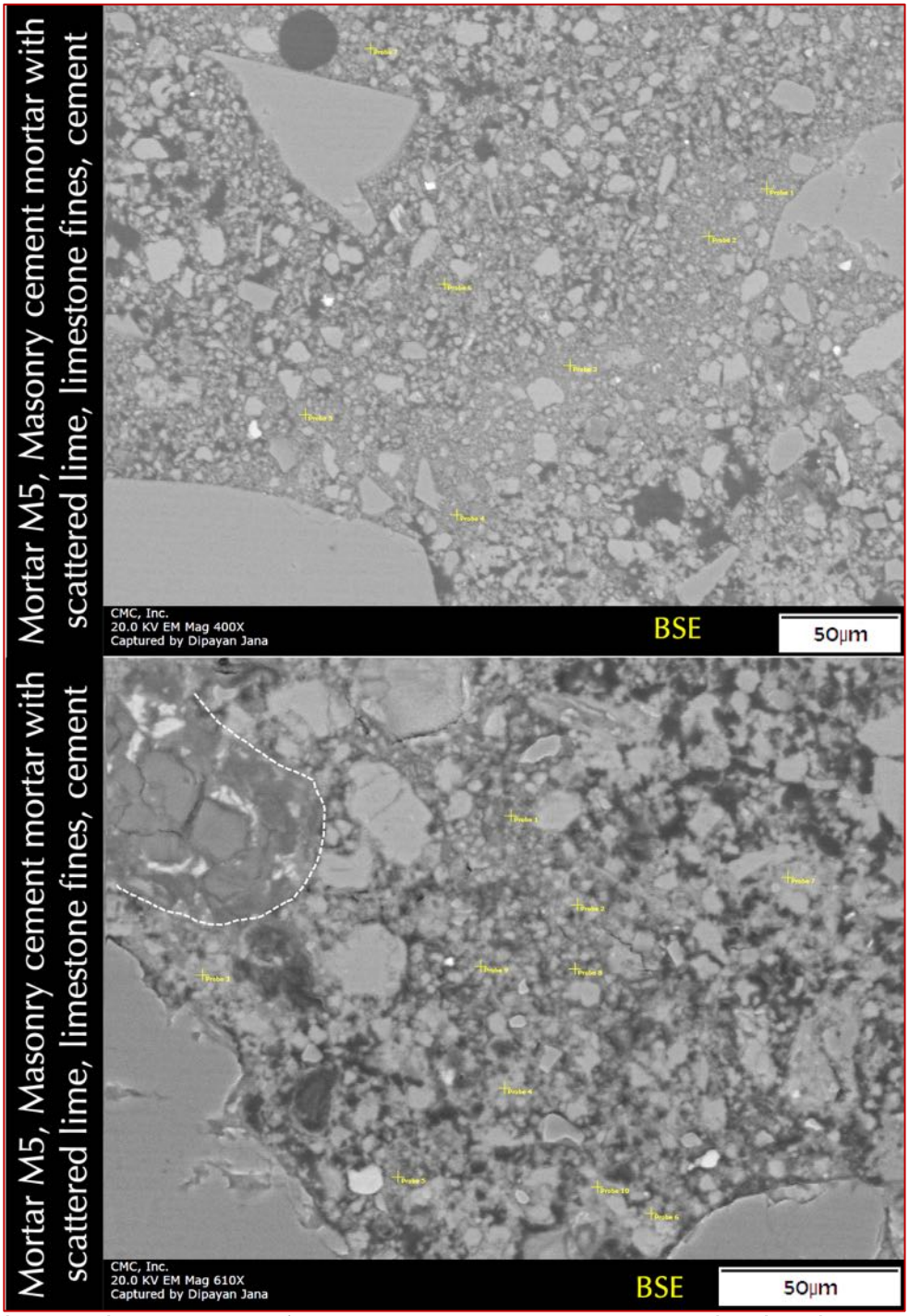

Figure 34: Backscatter electron images of masonry cement mortar M5. Compared to the other mortars, notice the overall granular appearance of the mortar, which is due to the abundance of fine-grained carbonated lime, and limestone fine particles in the mortar. Both photos show the overall microstructure of the mortar consisting of silica sand and interstitial severely carbonated paste of dominantly hydrated lime and limestone fines and subordinate well-hydrated Portland cement. Bottom photo shows a residual Portland cement particle in the top left corner (marked with white dashed line). Various areas of both images were subseqeuntly analyzed in SEM-EDS for compositional analyses, which are provided (along with numerous other images of this mortar) in Appendix C.

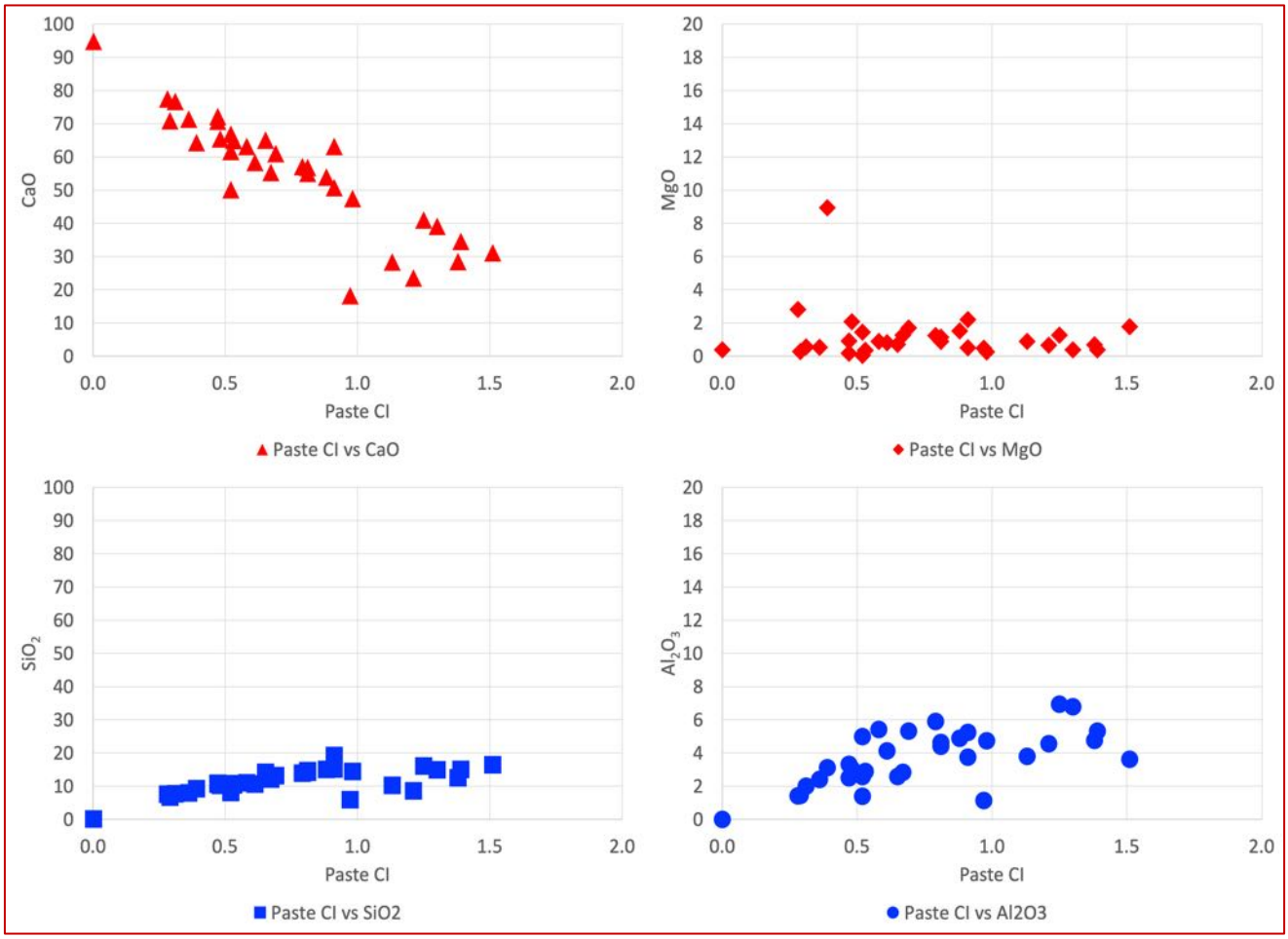

Figure 35: SEM-EDS oxide compositional variations of paste in masonry cement mortar M5 from late 1960s construction showing variations in lime (top left), magnesia (top right), silica (bottom left), and alumina (bottom right) contents of paste plotted against cementation indices of paste, Paste CI, after Eckel 1922 where Paste CI = $[(2.8\times SiO_2)+(1.1\times Al_2O_3)+(0.7\times Fe_2O_3)]/[(CaO)+(1.4\times MgO)]$. Paste CI is a characteristic index of hydraulicites of pastes where lime-based pastes show very low CIs as opposed to Portland cement-based pastes. A range in paste CIs is usually obtained from the paste component in a mortar depending on the proportions and degree of mixing/homogenizations of various binder (lime and cement) components in the mortar, along with subsequent alterations (leaching, carbonation) of paste during service. The compositional trend of lime versus paste CI in the top left plot is very typical not only of many masonry cement mortars but also in many natural cement-lime or Portland cement-lime mortars from historic to modern constructions, as found in the other four mortars, which is representative of contributions of lime and cement components where former (along with limestone fine particles in masonry cement mortar) reduces the paste CI to the left, but the latter increases the paste CI to the right thus forming the trend. Compared to lime and silica trends against paste CIs, trends for magenia and alumina are more scattered due to their lesser abundance in the binder phases than lime and silica. Notice the overall lower magnesia contents in the paste compared to the natural cement mortars in M1 and M2, which is the characteristic compositional (high-magnisa) signature of natural cement mortars.

SEM-EDS Compositional Variations of Pastes Between Natural Cement, Portland Cement-Lime, and Masonry Cement Mortars

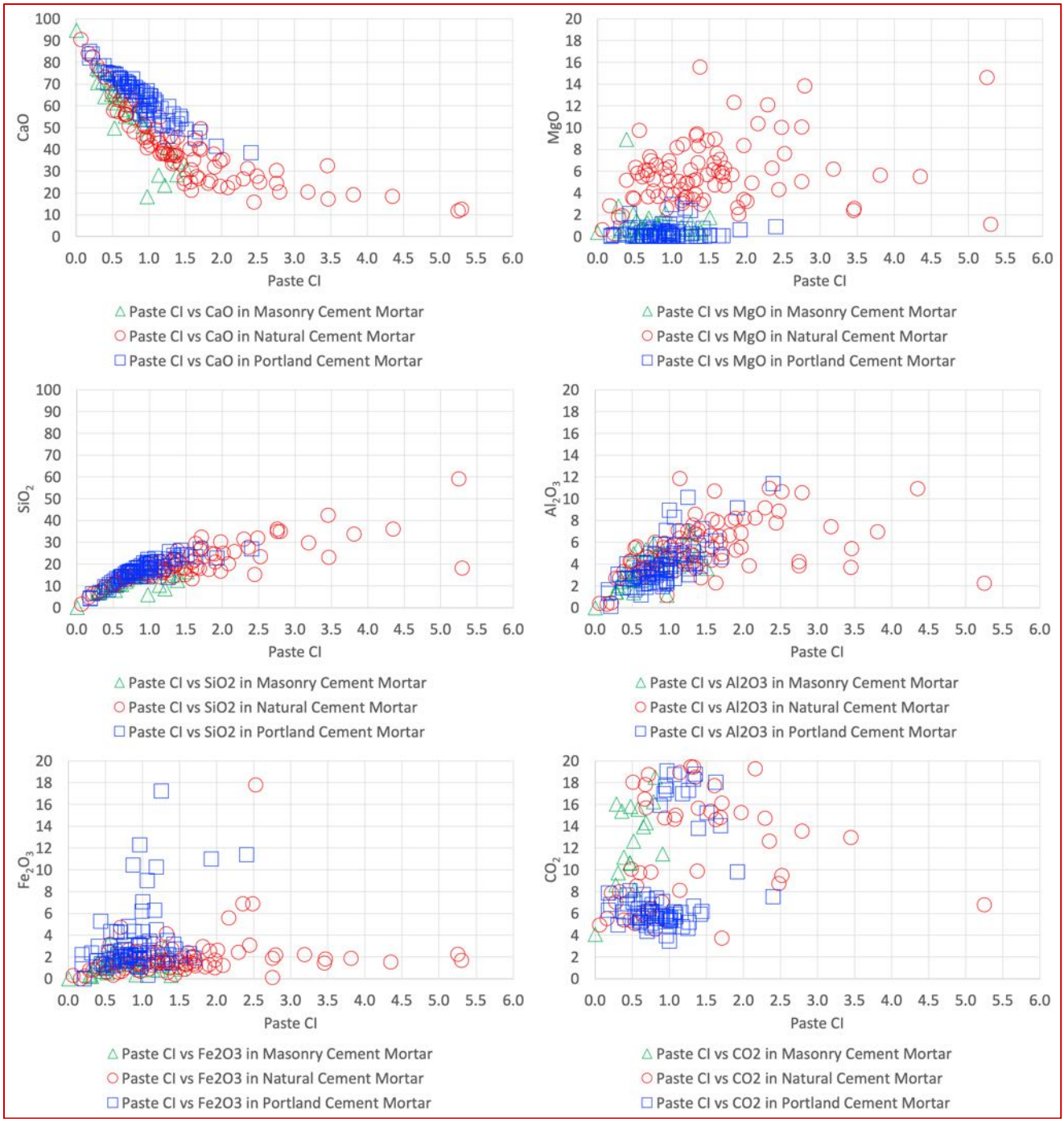

Figure 36: SEM-EDS oxide compositional variations of pastes between natural cement mortars (M1 and M2 from 1950s, in red circles), cement-lime mortars (M3 and M4 from 1916, in blue squares), and masonry cement mortar (M5 from late 1960s, in green triangle) showing some characteristic trends, e.g., (i) high-magnesia content in natural cement paste in top right plot, (ii) high silica content in natural cement paste in middle left plot, (iii) near-linear trends of lime and silica against paste-CI in all mortars showing progressive systematic decrease of paste-CaO and increase of paste-SiO_2 with increasing paste-CIs, (iv) absence of such linearities of oxides other than silica and lime against paste-CI due to their lesser contributions on paste-CI than lime and silica, (v) large range of

paste-CIs for natural cement paste compared to cement-lime or masonry cement mortars, (vi) generally lower paste-CIs for masonry cement paste than other mortars due to high-lime and limestone content of masonry cement mortar in M5,making binder in M5 less hydraulic than the natural cement binder in M1 and M2 or cement-binder in M3 and M4.

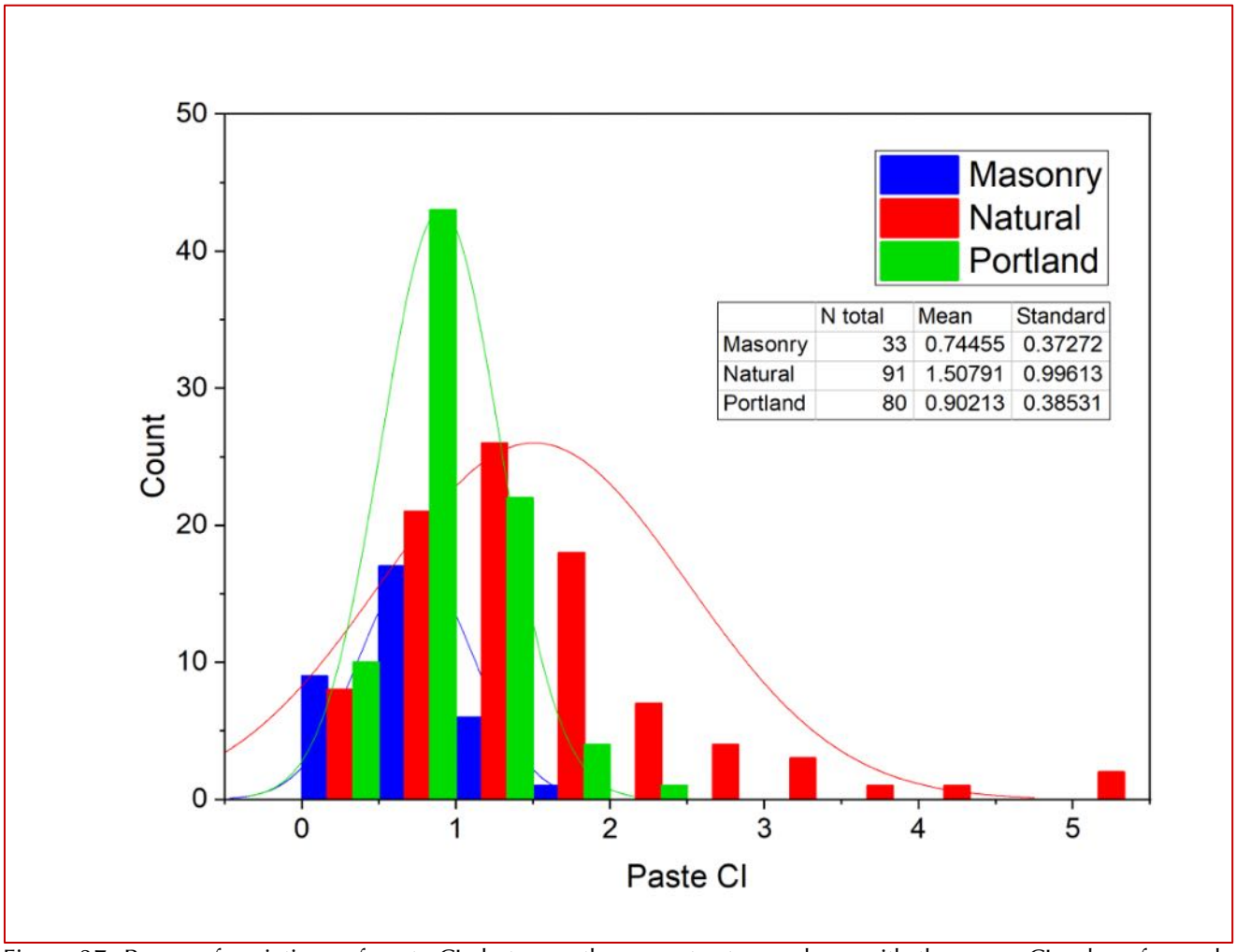

Figure 37: Range of variations of paste-CIs between three mortar types along with the mean-CI values for each showing an overall larger range and higher mean-CI for natural cement mortar than other two types, where the mean-CI for masonry cement mortar is slightly less (with a lesser spread) than the mean-CI for cement-lime mortar. Large range of paste-CIs for natural cement mortar is consistent with wide compositional range of natural cements (e.g., Eckel 1922) due to less restriction on its composition than the well-restricted composition of Portland cements, or of lime. Such large range of paste-CIs in natural cement mortars is a testment of large range of clay and silica impurities in the original dolomitic limestone raw feeds used in the production of natural cements in the US (which are commonly manufactured using dolomitic limestone feeds compared to impure calcitic limestones used in production of Roman cements, which are the Europan equivalents of American natural cements).

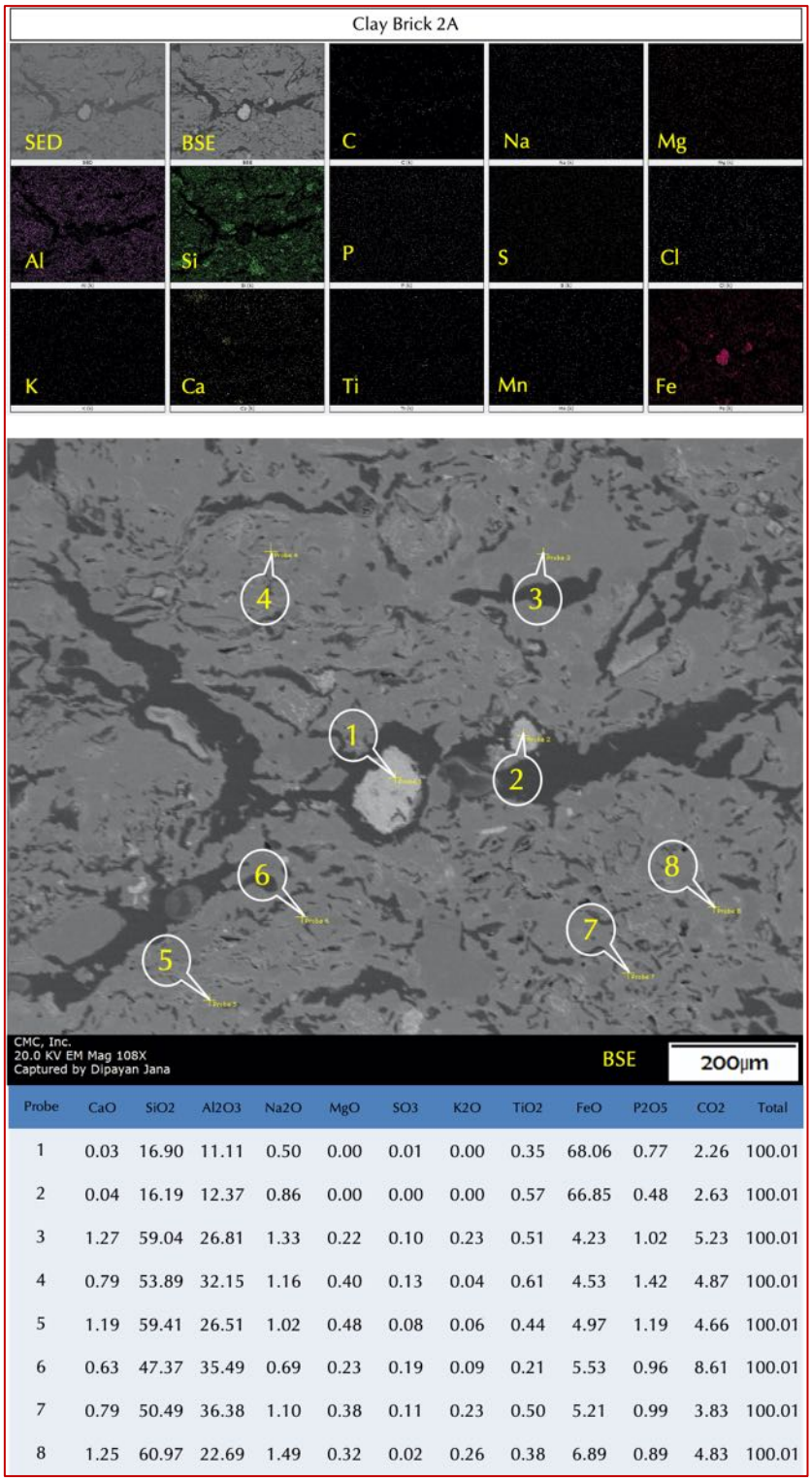

Probe	CaO	SiO2	Al2O3	Na2O	MgO	SO3	K2O	TiO2	FeO	P2O5	CO2	Total
1	0.03	16.90	11.11	0.50	0.00	0.01	0.00	0.35	68.06	0.77	2.26	100.01
2	0.04	16.19	12.37	0.86	0.00	0.00	0.00	0.57	66.85	0.48	2.63	100.01
3	1.27	59.04	26.81	1.33	0.22	0.10	0.23	0.51	4.23	1.02	5.23	100.01
4	0.79	53.89	32.15	1.16	0.40	0.13	0.04	0.61	4.53	1.42	4.87	100.01
5	1.19	59.41	26.51	1.02	0.48	0.08	0.06	0.44	4.97	1.19	4.66	100.01
6	0.63	47.37	35.49	0.69	0.23	0.19	0.09	0.21	5.53	0.96	8.61	100.01
7	0.79	50.49	36.38	1.10	0.38	0.11	0.23	0.50	5.21	0.99	3.83	100.01
8	1.25	60.97	22.69	1.49	0.32	0.02	0.26	0.38	6.89	0.89	4.83	100.01

Figure 38: X-ray elemental maps (top), backscatter electron image (BSE, middle), and X-ray elemental compositions at the tips of callouts shown in the backscatter electron image of a fired clay brick from 1950s vintage (2A) showing: (i) typical aluminosilicate composition of plastic component (glassy matrix) of brick as seen in silica and alumina elemental maps, and in corresponding oxide composition Table for Probe #3 through 8. Probe #1 and 2 are from two iron oxide grains in bricks that are responsible for imparting the typical reddish-brown color tone of brick.

Similar microstructural and compositional features are found for other brick samples which are a testament of using tempered quartz grains with raw clay mix in the kiln. Gray color tones of bricks from 1916 in Samples 3A/B and 4A/B are found to be due to low lime (carbonate) content of bricks from XRF studies compared to all other reddish-brown bricks.

Mortar Types from Optical & Electron Microscopy

Optical microscopy and scanning electron microscopy with X-ray microanalyses clearly distinguished three different types of mortars from three different periods of construction:

a. A cement-lime mortar from 1916 construction, where Portland cement was mixed with lime putty and silica sand. Portland cement was coarsely ground, consistent with the grinding technologies of early 20th century, henceforth left many coarse (some close to sand size) residual cement particles with dense hydration rims around many such particles. Most residual cement particles show characteristic microstructures of Portland cements in having subhedral alite or pseudomorphs of alite and skeletal interstitial dark brown ferrite phases, and, spherical belite with interstitial dark ferrite phases.
b. A natural cement-based mortar from 1950s construction, where natural cement was mixed with lime for aided workability. Natural cement was manufactured from calcination of impure dolomitic limestones having a large range of clay and silica impurities. Due to variations in the original compositions of impure (argillaceous) dolomitic limestone feeds, compositions of natural cements produced were diverse and so were the resultant pastes of those mortars.
c. Finally, a masonry cement mortar from late 1960s construction, where masonry cement was manufactured with a mixture of fine-grained hydrated lime, coarser grained limestone fines, and subordinate amount of Portland cement where cement was added at a low amount to be detected from residual cement and was well-hydrated leaving only pseudomorphs of alite and skeletal remains of dark interstitial ferrite phases. Silica sand was added to the lime-limestone-cement mix to prepare the proprietary blend of masonry cement.

Each mortar type left its own characteristic microstructure and microchemistry to be detected from optical and electron microscopy and microanalyses. For example, natural cement mortar showed the following characteristic microstructures to readily identify such mortar from thin section microscopy:

a. Residual calcined products of impure dolomitic limestone feeds as residual natural cement particles that are readily distinguished in the paste from the characteristic birefringence of carbonate rocks in crossed polarized light mode in a petrographic microscope.
b. Characteristic texture of such particles readily observed in plane or crossed polarized-light modes showing subhedral to euhedral rhombic crystals of dolomite grains in a finer-grained matrix of calcite, quartz, and interstitial phases. Such textures are more prominent in particles that have lost their original textures during the calcination process.
c. The typical texture of dolomitic limestone become obliterated with increased calcination turning an original birefringent particle to become near-isotropic due to lime-silica-alumina-iron reactions between dolomite, calcite, and interstitial clay-silica impurities, which eventually form various calcium-aluminum-silicate phases (e.g., gehlenite, mullite) and an amorphous calcium aluminosilicate phase. This

amorphous reaction product from calcination provides the main hydraulicity of natural cement. With increasing degree of calcination, this amorphous phase becomes the dominant phase in the matrix, which may contain skeletal remains or pseudomorphs of dolomite rhombs.

d. Calcination process rearranges original elemental distribution in dolomite rhombs sometimes causing diffusion of iron and magnesia within the dolomitic rhombs creating a darker brown rim enriched in iron within dolomite rhombs, which may become distinct and is best visible in plane polarized light in a petrographic microscope.
e. Increasing temperatures during calcination brings polymorphic transition of silica impurities at 575°C in the original impure dolomitic limestone feeds, thus forming tridymite or cristobalite phases or sometimes melt reaction rims around some silica particles within residual cement particles, which are usually confirmed from SEM-EDS and subsequent X-ray diffraction studies. Paste fraction separated from sand in a natural cement mortar showed such polymorphs of silica in the XRD studies, which is shown later.
f. The startling chemical signature of natural cement mortar is revealed from SEM-EDS studies, where paste shows noticeably higher magnesia contents than all other mortar types. Also noticed are high silica and large range of paste-CIs due to large variability of original impure dolomitic limestone feeds having large range of clay-silica impurities.

Portland cement-based mortars are readily identified by residual Portland cement particles, where depending on the degree of hydration of cement, grain size of original cement particles, and degree of carbonation during service, many residual cement particles preserve original microstructures of cements, e.g., subhedral to euhedral alite and spherical belite grains with dark interstitial ferrite phases. Depending on the lime content mixed with the cement, and the type of lime added (e.g., non-hydraulic high-calcium lime as lime putty, or hydrated lime in powder form) many cement-lime mortar may show lumps of unmixed lime or less calcined (or even unburnt) limestone particles in lime. Depending on the degree of carbonation during service, paste in cement-lime mortar show variable degrees of carbonation converting the original calcium silica hydrate and calcium hydroxide component of cement hydration to finely crystalline calcium carbonate.

Finally, masonry cement mortar is identified from its proprietary mix composition, incorporating not only Portland cement and lime but also limestone fines, which is a common ingredient of masonry cement often added for enhanced workability where limestone fine particles found in the present M5 mortar are coarser than lime and provide an overall granular appearance best seen in backscatter electron image.

Mineralogical Compositions of Mortars from X-Ray Diffraction (XRD)

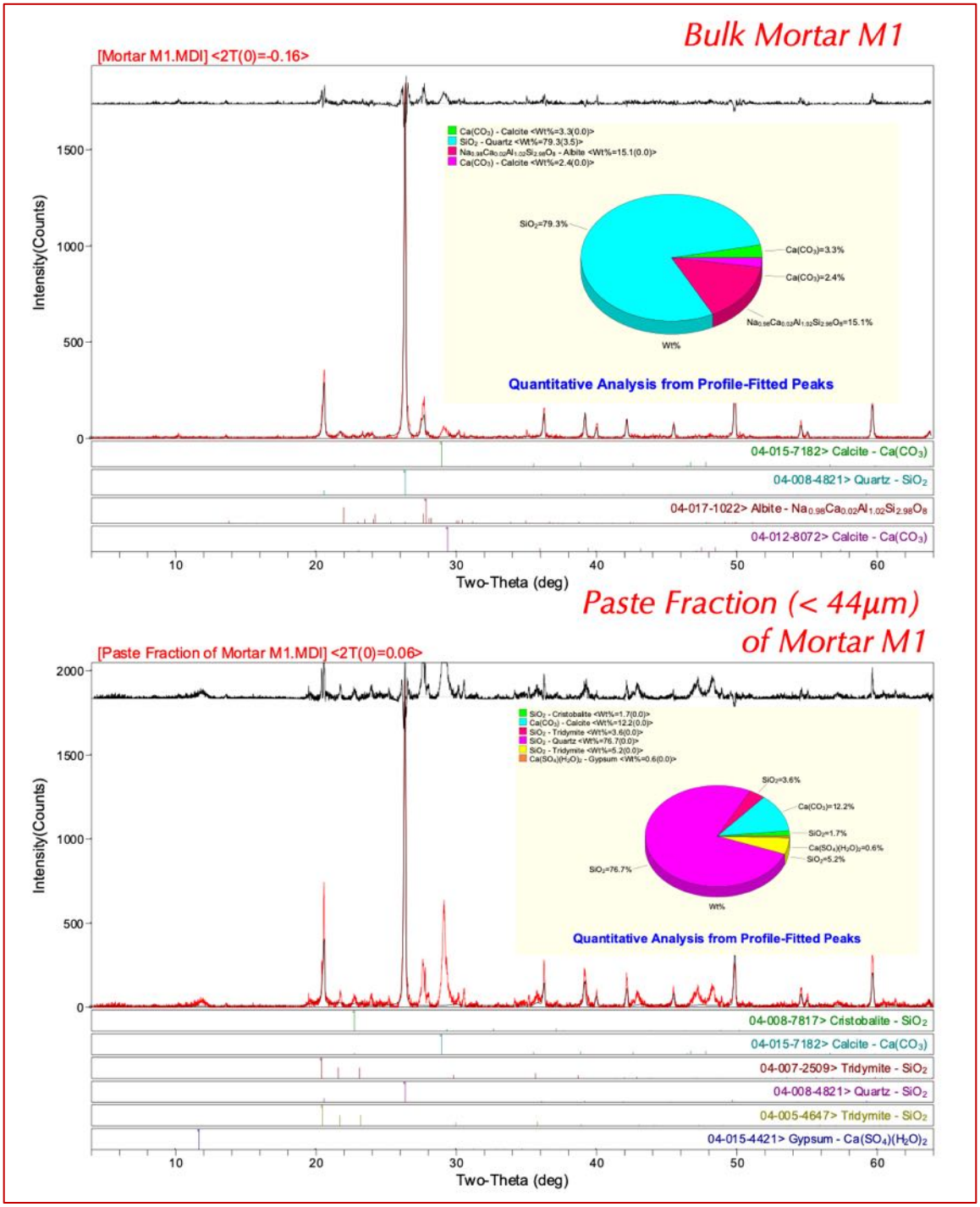

Figure 39: X-ray diffraction patterns of bulk mortar M1 from 1950s vintage (top), and, paste fraction of mortar after screening pulverized mortar through US 325 sieve (44-micron openings) to separate coarser sand fractions (bottom) showing the overall mineralogies of bulk mortar in the top and specific mineralogies of fine fraction in the bottom. Bulk mineralogy shows the dominance of quartz in quartz sand, subordinate feldspar (albite) in the sand, and calcite from carboated paste and lime. Fine fraction in the bottom XRD shows cristoblite and tridymite, which are two silica polymorphs found in natural cement pastes formed during polymorphic transition of quartz grains in argillaceous limestone feed during the calcination process of natural cement production. Also detected is a trace amount of gypsum in the paste, which was not detected in optical microscopy.

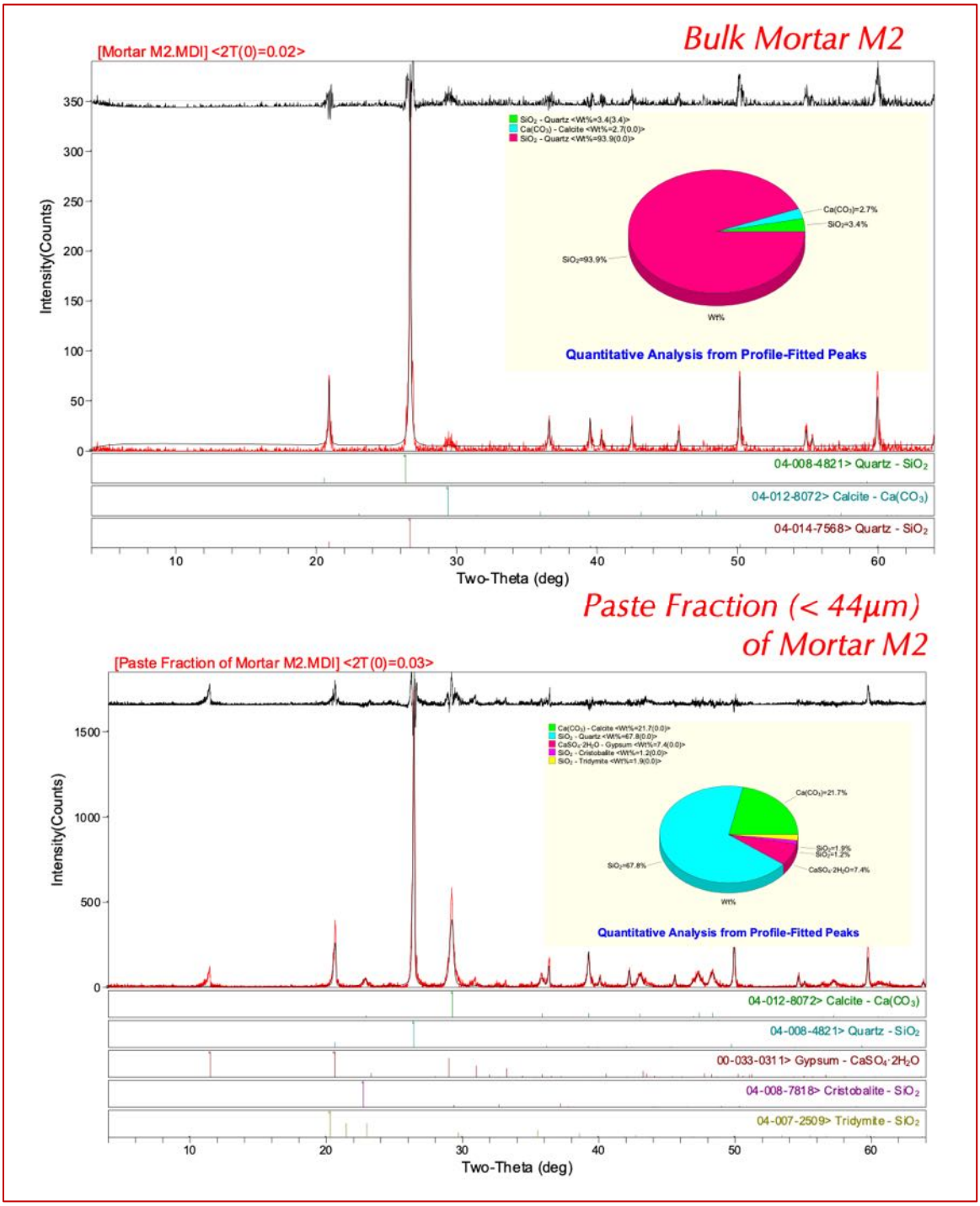

Figure 40: X-ray diffraction patterns of bulk mortar M2 from 1950s vintage (top), and, paste fraction of mortar after screening pulverized mortar through US 325 sieve (44-micron openings) to separate coarser sand fractions (bottom) showing the overall mineralogies of bulk mortar in the top and specific mineralogies of fine fraction in the bottom. Bulk mineralogy shows the dominance of quartz in quartz sand, subordinate feldspar (albite) in the sand, and calcite from carboated paste and lime. Fine fraction in the bottom XRD shows cristoblite and tridymite, which are two silica polymorphs found in natural cement pastes formed during polymorphic transition of quartz grains in argillaceous limestone feed during the calcination process of natural cement production. Also detected is a trace amount of gypsum in the paste (slightly higher than that detected in M1), which was not detected in optical microscopy. Notice the similarities in overall mineralogies of bulk and fine fractions of two natural cement mortars from 1950s vintage.

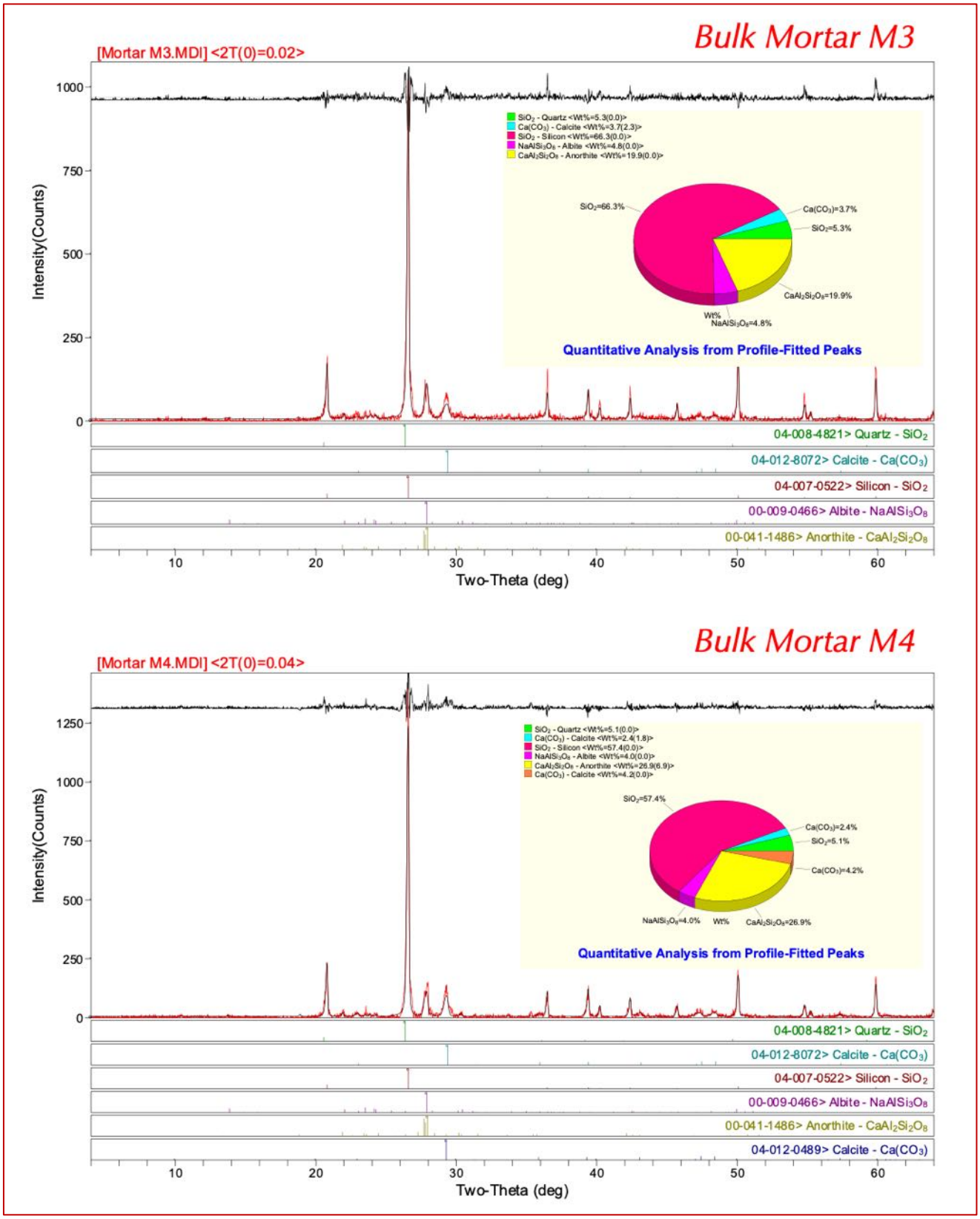

Figure 41: X-ray diffraction patterns of cement-lime mortars from 1916 vinatge – M3 at the top, and M4 at the bottom showing similarities in overall mineralogies of both mortars, e.g., dominance of quartz from quartz sand, subordinate feldspar (e.g., albite) in sand, and calcite in carbonated paste and lime.

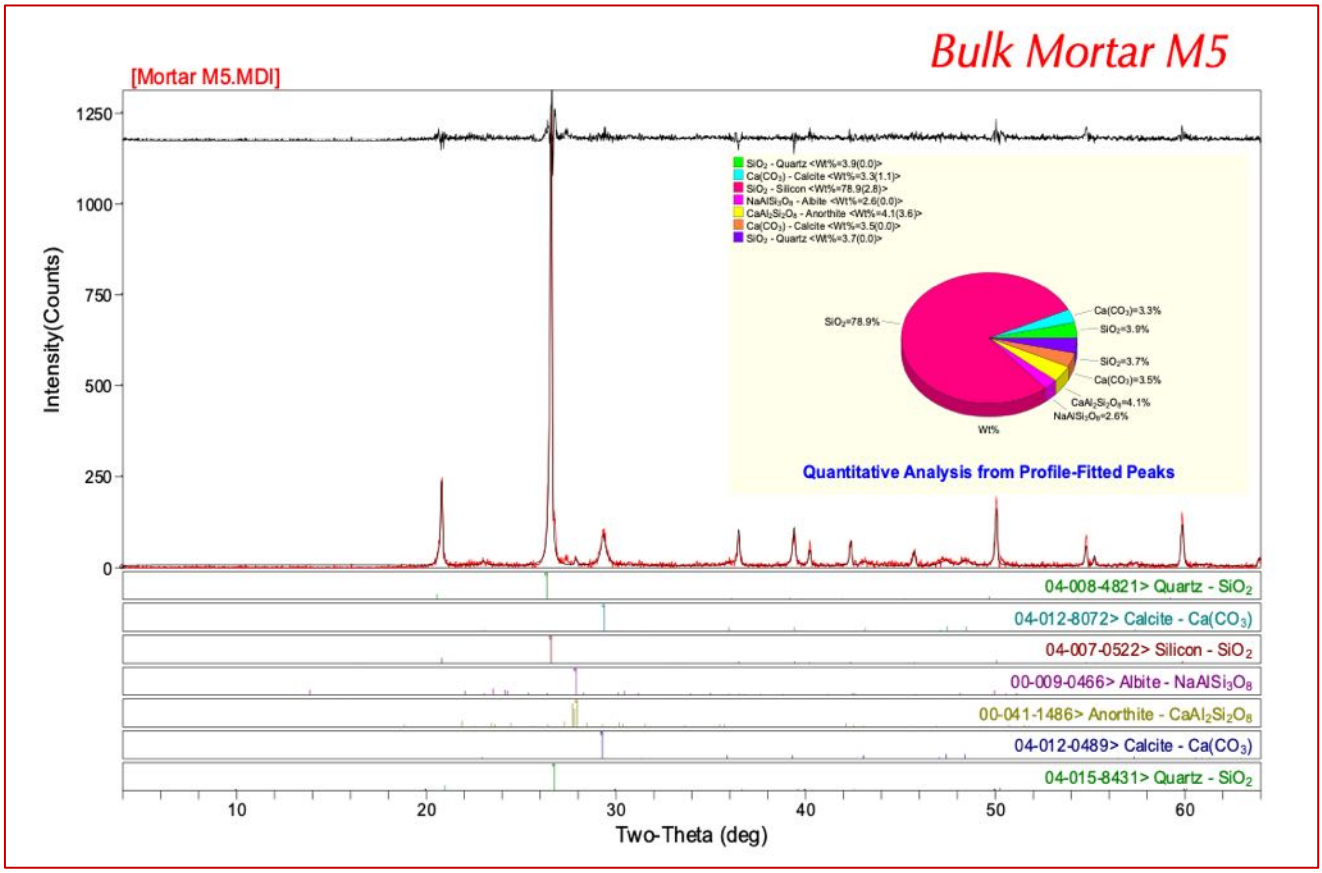

Figure 42: X-ray diffraction pattern of masonry cement mortar M5 from 1960s construction showing abundant quartz from use of siliceous sand, feldspar (e.g., albite) in sand, and calcite from carbonated paste.

Semi-quantitative estimates of various minerals detected in XRD studies and shown in pie graph insets in each XRD pattern are summarized in Table 2.

Period	Mortar	Major mineralogies of bulk mortar
1950s	M1	Quartz – 79.3%, Albite – 15.1%, Calcite – 5.7%
	M2	Quartz – 97.3%, Calcite – 2.7%
1916	M3	Quartz – 71.8%, Albite – 4.8%, Anorthite -19.9%, Calcite – 3.7%
	M4	Quartz – 62.5%, Albite – 4.0%, Anorthite -26.9%, Calcite – 6.6%
1960s	M5	Quartz – 86.5%, Albite – 2.6%, Anorthite -4.1%, Calcite – 6.8%

Table 2: Mineralogical compositions of mortars from XRD studies. Quartz is the dominant mineral in all mortars from quartz-based siliceous sand used in the mortars.

Mineralogical Compositions of Fired Clay Bricks from X-Ray Diffraction (XRD)

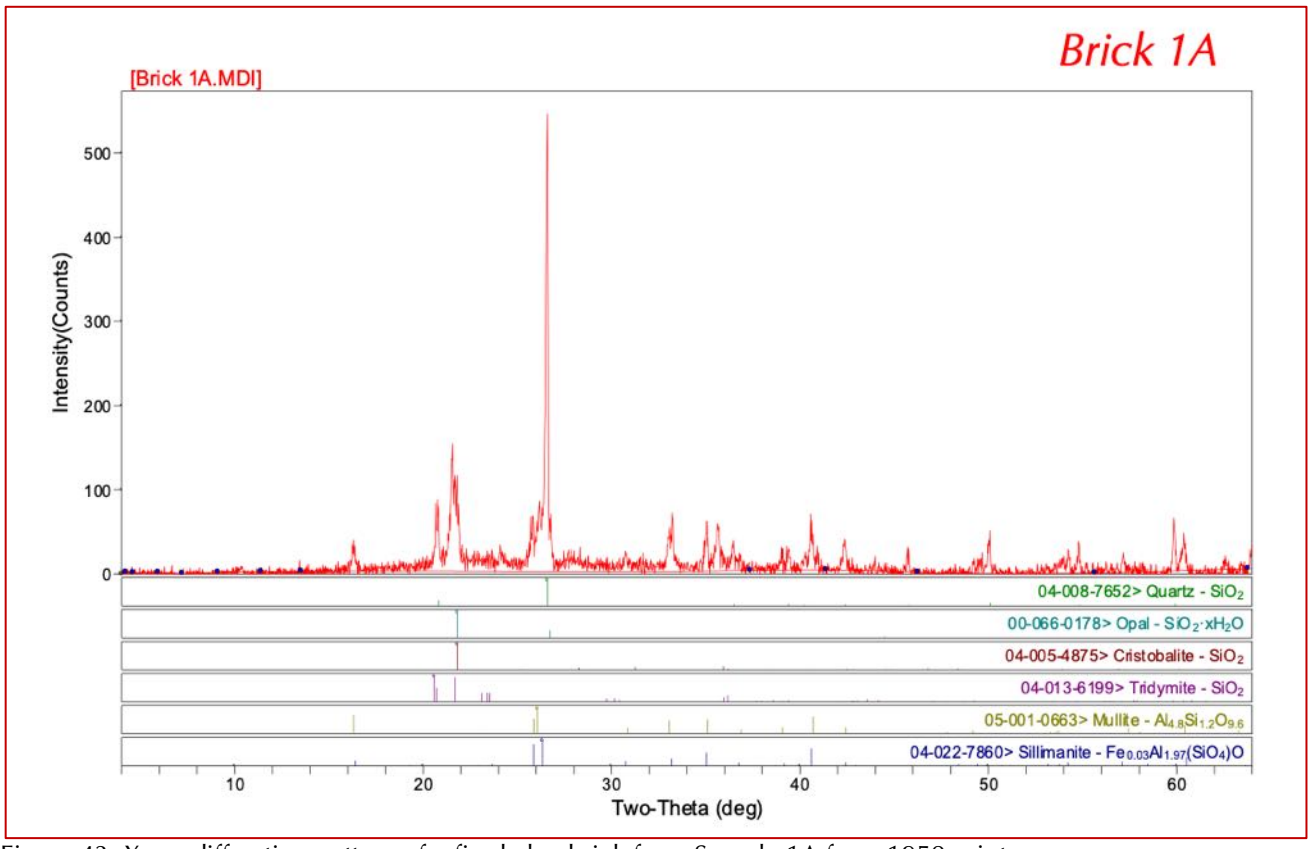

Figure 43: X-ray diffraction pattern of a fired clay brick from Sample 1A from 1950s vintage.

Figure 43 shows X-ray diffraction pattern of a pulverized fired clay brick (Sample 1A) from 1950s vintage. The pattern shows typical mineralogical compositions of bricks, where most of the portion of brick is glassy (amorphous) aluminosilicate composition hence not detected in XRD. Diffraction peaks are from minor amount of crystalline phases that have not been fused and hence detected as:

(a) Quartz from tempered quartz additive in the clay along with original quartz grains in the clay,

(b) Two high-temperature polymorphs of quartz (tridymite and cristobalite that are commonly found in bricks due to polymorphic transition of quartz at 575°C), and,

(c) Some aluminosilicate phases (e.g., mullite and sillimanite).

Most fired clay bricks share these typical mineralogies.

Chemical Compositions of Fired Clay Bricks from X-Ray Fluorescence (XRF)

After bulk mineralogies of fired clay bricks from XRD, Table 3 shows bulk chemical compositions of four fired clay bricks 1A through 4A spanning 1916 to 1950s vintages all showing typical aluminosilicate compositions of bricks. Brick 3A shows very low lime compared to other bricks due to low carbonate content of original clay, which is also responsible for the gray color tone of this brick. Other differences of Brick 3A from the rest, e.g., low alkalis, low magnesia, high titanium oxide, etc. are due to inherent variations in the compositions of clay used in this brick compared to the clay used in other ones. Brick 4A from 1916 vintage is more similar in oxide compositions (as well as in overall color tone) to the bricks from 1950s vintage than its companion one, 3A).

Bulk Chemical Compositions of Bricks From XRF												
Bricks	SiO_2	Al_2O_3	Fe_2O_3	CaO	MgO	Na_2O	K_2O	TiO_2	P_2O_3	SO_3	Balance (LOI)	Total
1A Circa 1950	60.4	15.9	7.91	1.48	0.988	1.27	0.194	0.624	ND	ND	11.6	100
2A Circa 1950	57.1	14.7	6.71	1.13	0.781	1.68	0.181	0.552	ND	ND	17.6	100
3A Circa 1916	68.3	12.1	6.97	0.153	0.702	ND	0.0835	0.937	0.005	ND	11.0	100
4A Circa 1916	66.1	13.2	5.28	1.22	0.830	1.37	0.173	0.578	ND	ND	11.6	100

Table 3: Oxide compositions of bricks determined from X-ray fluorescence spectroscopy. Balance represents loss on ignition parts of bricks.

Mineralogical (from XRD) and chemical (from XRF) compositions of fired clay bricks are consistent with overall amorphous fused aluminosilicate glass composition of the plastic component of bricks in which tempered quartz additives are responsible for the dominant quartz peak found in the XRD as well as contributed to the bulk silica content of bricks in XRF. Tempered quartz additive is found in all bricks studied (e.g., see Figure 26, and Appendix B38 to B49). Alumina, iron oxide, lime, magnesia, alkalis, and titanium oxide contents are inherent from the fused clay mass whereas sulfate content may show a contribution from external salts, which is not found in any of the four bricks studied in XRF.

Compressive Strengths of Fired Clay Bricks

For compressive strength testing, the bricks were sectioned in half, prepared according to ASTM C 67, and tested for compression in their air-dry conditions. Individual bricks from 1916 era are noticeably lower than the ASTM C 216-recommended minimum values of 2500 psi and 3000 psi for individual brick's strength and average of 5-brick strengths, respectively, indicating poor strengths of brick units (which are also consistent with the overall porous natures of bricks found during microscopical examinations and hence anticipated high water absorption values.

Brick#	Construction Era	Area (sq.-in.)	Failure Load (lbs.)	Compressive Strength (psi.)
1A	1950s	13.79	44265	3210
1B		14.96	44610	2980
2A	1950s	14.86	22510	1510
2B		14.93	27960	1870
3A	1916	13.37	13480	1010
3B		15.29	12115	790
4A	1916	16.03	15535	970
4B		8.70	28025	3220

Table 4: Compressive strengths of bricks from 1950s and 1916 constructions showing noticeably lower strengths for most of the bricks (except 1A and 1B from 1950s era) compared to the minimum 2500 psi strength requirement of ASTM C 216 facing bricks in a severe weather environment.

Strength results of most of the bricks, e.g., from 2A through 4A are very low and consistent with the porous nature of these bricks as determined from optical microscopy.

Chemical Compositions of Mortars from Gravimetry

Table 5 shows loss on ignition and acid-insoluble residue contents of above four mortars:

Volatiles & Acid-Insoluble Residue Contents of Mortars From Gravimetry				
Mortars	**LOI at 110°C**	**LOI at 550°C**	**LOI at 950°C**	**Acid-Insoluble Residue**
Natural cement mortar, M1, 1950s	0.50	2.90	4.30	82.96
Natural cement mortar, M2, 1950s	0.70	3.00	6.00	79.02
Cement-lime mortar, M3, 1916	0.50	3.40	7.60	70.88
Cement-lime mortar, M4, 1916	0.40	4.00	8.20	70.83
Masonry mortar, M5, late 1960s	0.30	2.60	8.80	72.81

Table 5: Loss on ignition and acid-insoluble residue contents of mortars.

Oxide compositions of Portland cement-only pointing mortars show consistent silica contents from 1920s and 1940s construction (47.3 and 47.8 percent, respectively) which is indicative of use of similar pointing mortar at both upper and lower levels during a later pointing event probably after both upper and lower level constructions were done. Lime contents of both mortars are also similar (32.9 and 28.9 percent, respectively) except a slight variation, which could be from some alterations during service. Silica content of slag-lime mortar from 1920s vintage is highest of four tested, which is consistent with the presence of ground slag, the main source of silica in

the mortar after silica sand. Sulfate content in the slag-lime mortar is below the detection limit whereas other three mortars gave detectable sulfates (as SO_3) from 0.79 to 0.99 percent.

Sand contents are determined from acid-insoluble residue contents since sands in all mortars are siliceous, which are insoluble in acid. Natural cement mortars from 1950s have higher sand contents than cement-lime mortars from 1916 or masonry cement mortar from late 1960s. Loss on ignition values at 110°C, 550°C, and 950°C show good correlations to losses determined from thermogravimetric studies (discussed later)..

Chemical Compositions of Mortars from X-Ray Fluorescence (XRF)

Bulk Chemical Compositions of Mortars From XRF

Mortars	SiO_2	Al_2O_3	Fe_2O_3	CaO	MgO	Na_2O	K_2O	TiO_2	P_2O_3	SO_3	Balance (LOI)	Total
Natural cement mortar, M1, 1950s	70.6	6.45	3.09	6.50	1.580	1.7100	0.397	0.263	0.0353	ND	9.63	100
Natural cement mortar, M2, 1950s	79.8	1.51	1.41	7.16	1.940	ND	0.234	0.282	0.0413	0.7450	6.91	100
Cement-lime mortar, M3, 1916	67.3	5.07	3.03	12.00	0.770	1.3300	0.237	0.289	0.0514	0.0224	9.93	100
Cement-lime mortar, M4, 1916	61.6	5.19	3.14	13.40	0.874	1.4300	0.314	0.480	0.0571	1.0400	12.40	100
Masonry mortar, M5, late 1960s	70.0	2.96	2.67	11.10	0.942	0.2900	0.909	0.383	0.0554	0.3150	10.30	100

Mortar Types	Samples & Binder Types	Characteristic Chemical Compositions
Type I Mortar	Natural cement Mortar, M1	High MgO, Al_2O_3, Fe_2O_3, Na_2O
Type II Mortar	Natural cement Mortar, M2	High MgO, SiO_2
Type III Mortar	Cement-Lime Mortar, M3 and M5	High CaO, Al_2O_3, Fe_2O_3, Na_2O
Type IV Mortar	Masonry cement Mortar, M5	High CaO
Type V Mortar	High-sulfate Mortars, M2 and M4	High SO_3

Table 6: Oxide compositions of mortars determined from X-ray fluorescence spectroscopy. Balance represents loss on ignition parts of mortars. Based on the determined compositions, mortars are classified into five types that are describe in the Table.

Table 6 shows chemical compositions of all five mortars determined from X-ray fluorescence spectroscopy, as well as classifications of mortars based on their characteristic chemical compositions. Values in red are characteristic compositions used in classification of mortars into various types.

Thermal Analyses

Milligrams of mortars were subjected to controlled heating experiments in a Mettler-Toledo TGA/DSC simultaneous thermogravimetric and differential scanning calorimetry unit to detect the presence of various hydrous, sulfate, and carbonate phases in these mortars and their relative abundance. Figures 44 to 48 show TGA (in bold black), DSC (in dotted red), and DTG (in dashed blue) curves of mortars showing losses in weights due to decompositions (loss of water and carbon dioxide) of various phases during controlled heating in a Mettler-Toledo's simultaneous TGA/DSC 1 unit from 30ºC to 1000ºC in a ceramic crucible (alumina 70µl, no lid) at a heating rate of 10ºC/min in a nitrogen purge at a rate of 75 mL/min. Dehydration and decarbonation reactions are marked as endothermic peaks in the DTG curve, whereas alpha to beta-form polymorphic transition of quartz is marked at the characteristic temperature of 575 ºC in the DSC curve.

In the DTG curve, successive losses in weights are detected at (i) up to 120ºC from losses of free and combined water, (ii) from 120ºC to 200ºC for water from hydrated salts, (iii) from 200ºC to 600ºC for dihydroxylation of structural/hydrate water in various hydraulic components, and (iv) from 600ºC to 950ºC for decomposition of carbonate phases from limestone fines and fine-grained calcite in carbonated pastes. DSC curve shows polymorphic transition from alpha to beta form of quartz around 575ºC from silica (quartz) sand.

Figure 44 shows very similar thermograms of two natural cement mortars M1 and M2 from 1950s vintages showing a minimal loss of free water (<0.5%) and water from hydrated salts (<0.5-0.7%) at up to 200ºC followed by a measurable loss (2.1 to 2.2%) of hydrate water from 200ºC to 600ºC. Degrees of carbonation are higher in the M2 mortar (5.38%) than 3.82% found in M1 mortar. Quartz contents are around 45 percent in M1 and 70% in M2 determined from polymorphic transition of quartz around 575ºC.

Figure 45 shows very similar thermograms of two cement-lime mortars M3 and M4 from 1916 showing a minimal loss of free water (<0.6%) and water from hydrated salts (<1%) at up to 200ºC followed by a measurable loss (3%) of hydrate water from 200ºC to 600ºC. Degrees of carbonation are lower in the M3 mortar (5.5%) than 7% found in M4 mortar. Quartz contents are around 44.7 percent in M3 and 41.2% in M4 determined from polymorphic transition of quartz around 575ºC.

Figure 46 shows a relatively simple thermogram of masonry cement mortar M5 from late 1960s vintage showing a minimal loss of free water (<0.5%) and water from hydrated salts (<6%) at up to 200ºC followed by a measurable loss (2.1%) of hydrate water from 200ºC to 600ºC. Degrees of carbonation are highest of all mortars, 7.38%, due to the presence of limestone fine particles along with carbonated lime in the mortar. Quartz content is 60% as determined from polymorphic transition of quartz around 575ºC.

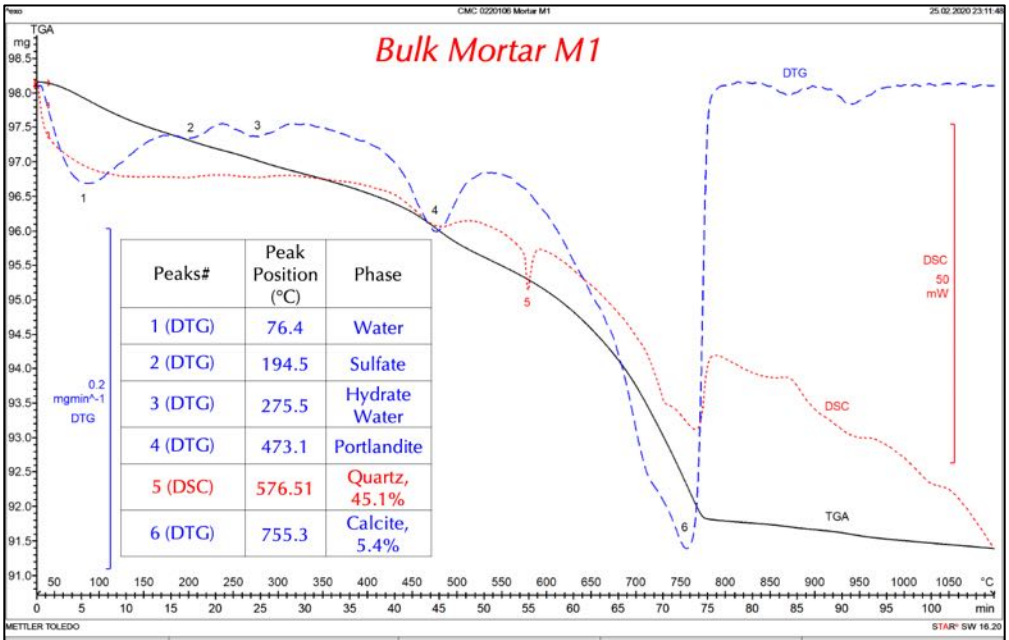

T(°C)	Up to 120°C	120°C to 200°C	200°C to 600°C	> 600°C
Phases	Hygroscopic Water	Water from Hydrated Salts	Structural Water From Hydraulic Components	CO_2 from decomposition of carbonates
Mass Loss (%) from TGA	0.42	0.37	2.22	3.82

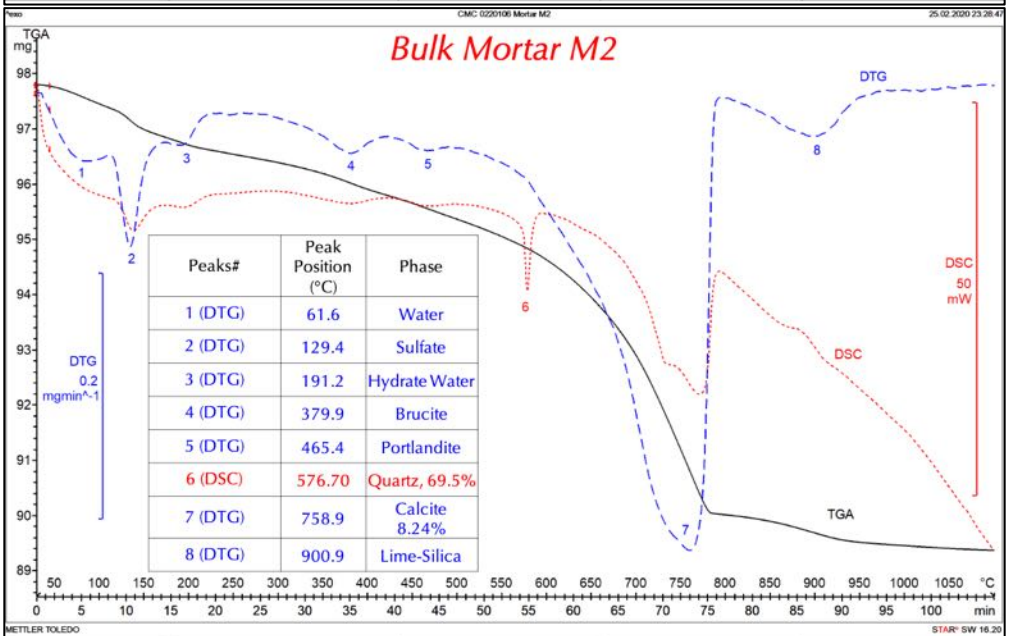

T(°C)	Up to 120°C	120°C to 200°C	200°C to 600°C	> 600°C
Phases	Hygroscopic Water	Water from Hydrated Salts	Structural Water From Hydraulic Components	CO_2 from decomposition of carbonates
Mass Loss (%) from TGA	0.41	0.70	2.10	5.38

Figure 44: TGA (bold black), DSC (dotted red), and DTG (dashed blue) curves of two natural cement mortars from 1950s construction showing losses in weight due to various decompositions (loss of water and carbon dioxide) during controlled heating in a Mettler-Toledo's simultaneous TGA/DSC 1 unit from 30ºC to 1000ºC in a ceramic crucible (alumina 70µl, no lid) at a heating rate of 10ºC/min in a nitrogen purge at a rate of 75 mL/min.

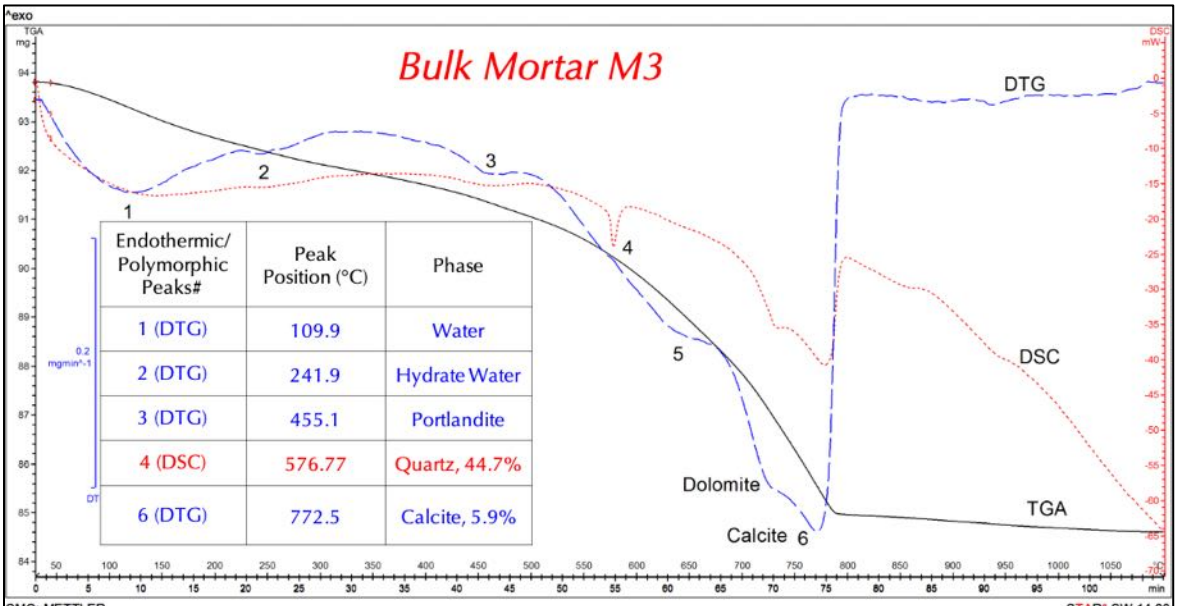

T(°C)	Up to 120°C	120°C to 200°C	200°C to 600°C	> 600°C
Phases	Hygroscopic Water	Water from Hydrated Salts	Structural Water From Hydraulic Components	CO_2 from decomposition of carbonates
Mass Loss (%) from TGA	0.56	0.65	2.97	5.57

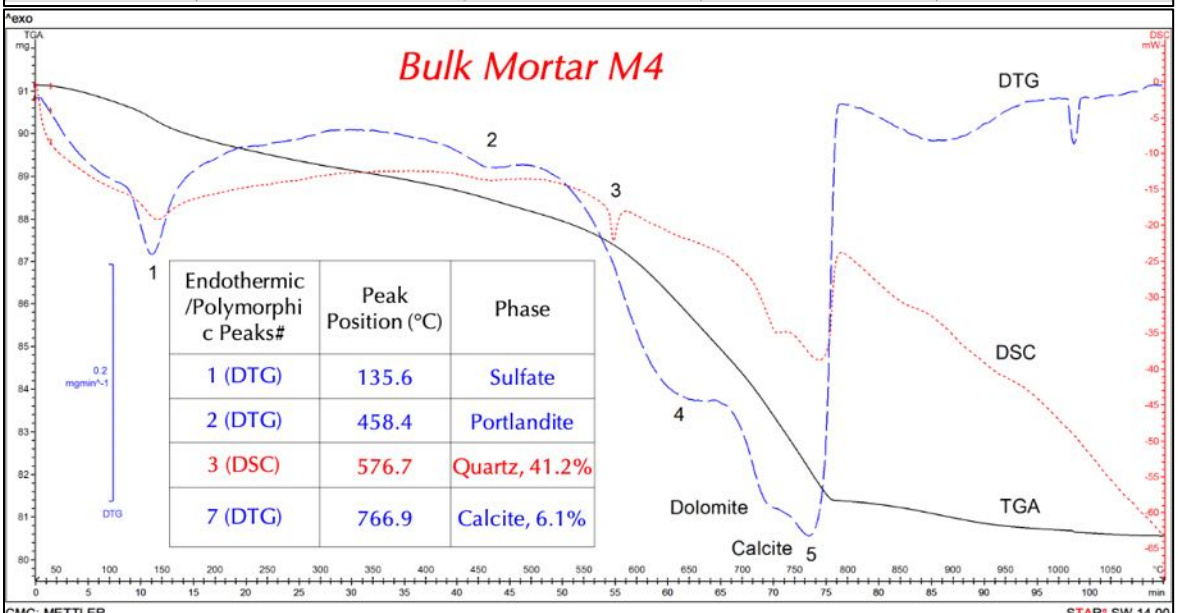

T(°C)	Up to 120°C	120°C to 200°C	200°C to 600°C	> 600°C
Phases	Hygroscopic Water	Water from Hydrated Salts	Structural Water From Hydraulic Components	CO_2 from decomposition of carbonates
Mass Loss (%) from TGA	0.57	0.90	3.06	7.07

Figure 45: TGA (bold black), DSC (dotted red), and DTG (dashed blue) curves of two cement-lime mortars from 1916 construction showing losses in weight due to various decompositions (loss of water and carbon dioxide) during controlled heating in a Mettler-Toledo's simultaneous TGA/DSC 1 unit from 30ºC to 1000ºC in a ceramic crucible (alumina 70µl, no lid) at a heating rate of 10ºC/min in a nitrogen purge at a rate of 75 mL/min.

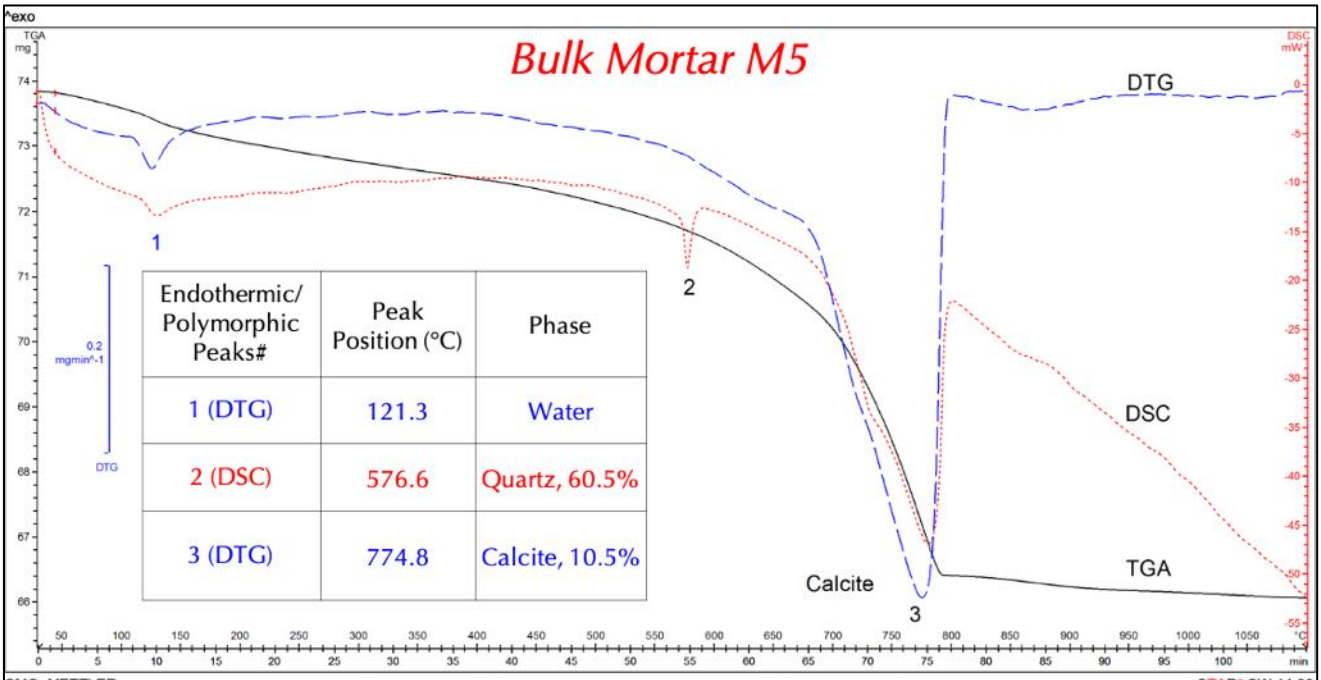

T(°C)	Up to 120°C	120°C to 200°C	200°C to 600°C	> 600°C
Phases	Hygroscopic Water	Water from Hydrated Salts	Structural Water From Hydraulic Components	CO_2 from decomposition of carbonates
Mass Loss (%) from TGA	0.48	0.55	2.09	7.38

Figure 46: TGA (bold black), DSC (dotted red), and DTG (dashed blue) curves of masonry cement mortar from late 1960s construction showing losses in weight due to various decompositions (loss of water and carbon dioxide) during controlled heating in a Mettler-Toledo's simultaneous TGA/DSC 1 unit from 30ºC to 1000ºC in a ceramic crucible (alumina 70µl, no lid) at a heating rate of 10ºC/min in a nitrogen purge at a rate of 75 mL/min.

A comparison of thermograms of natural cement mortars M1 and M2 with cement-lime mortars M3 and M4 show some similarities in having: (a) endotherms from loss of free water and water from hydrate salts, followed by (b) peaks from losses of structural/hydrate water around 350 to 460ºC range, followed by (c) decomposition of carbonates around 750 to 800ºC.

By contrast, masonry cement mortar M5 shows (a) smallest endotherm of all mortars for loss of water from hydrate salts at 120ºC, (b) lack of any endotherm from losses of hydrate water, and (c) largest endotherm from decomposition of calcite from limestone fines and fine-grained carbonated paste at 775ºC.

Loss of structural water is highest (around 3% loss in 200 to 600ºC range) in the two cement-lime mortars M3 and M4 due to higher amount of calcium silicate hydrate and calcium hydroxide components of Portland cement hydrations than the corresponding natural cement mortars M1 and M2 (which show 2.1 to 2.2% loss at 200 to 600ºC range).

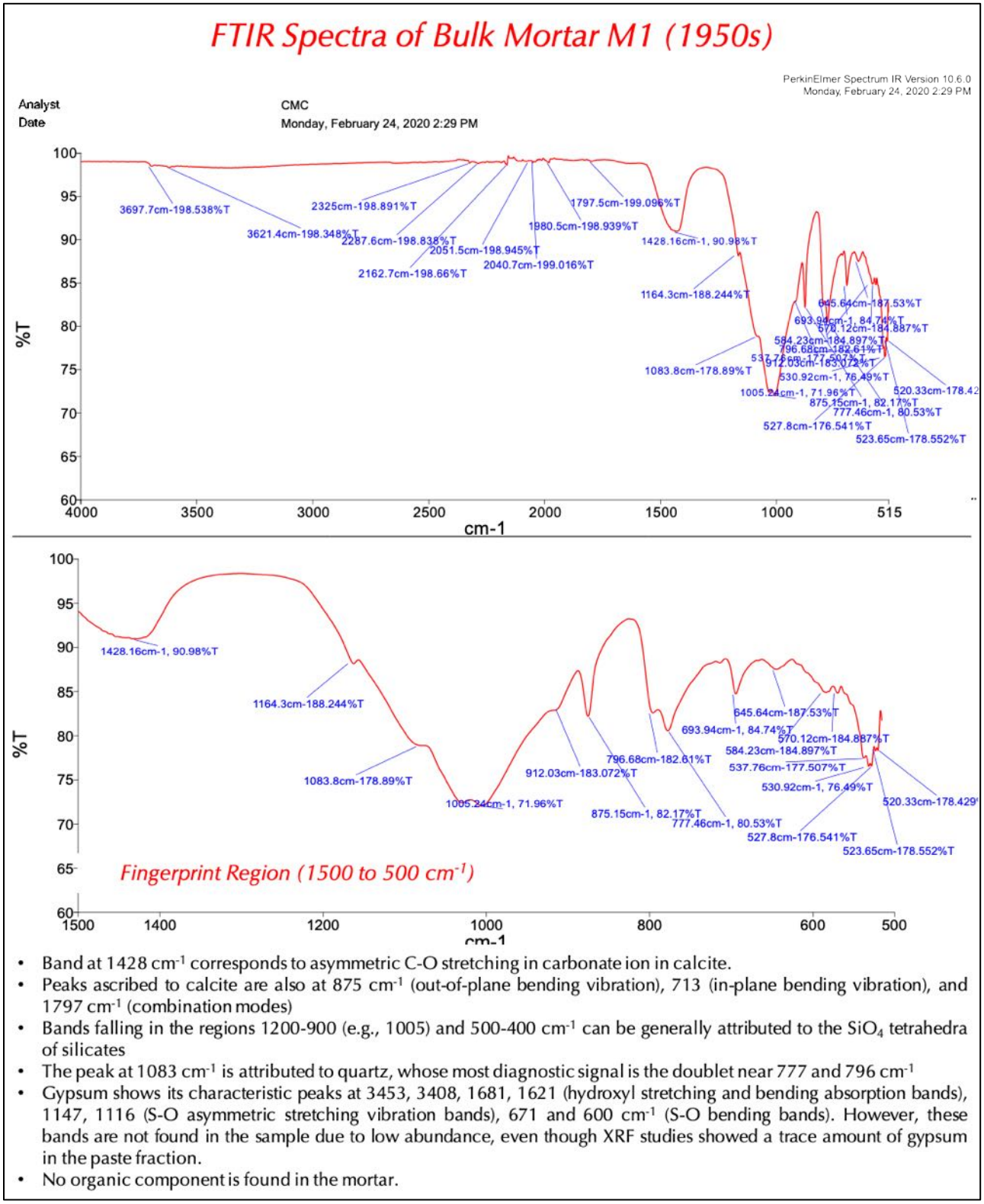

- Band at 1428 cm^{-1} corresponds to asymmetric C-O stretching in carbonate ion in calcite.
- Peaks ascribed to calcite are also at 875 cm^{-1} (out-of-plane bending vibration), 713 (in-plane bending vibration), and 1797 cm^{-1} (combination modes)
- Bands falling in the regions 1200-900 (e.g., 1005) and 500-400 cm^{-1} can be generally attributed to the SiO_4 tetrahedra of silicates
- The peak at 1083 cm^{-1} is attributed to quartz, whose most diagnostic signal is the doublet near 777 and 796 cm^{-1}
- Gypsum shows its characteristic peaks at 3453, 3408, 1681, 1621 (hydroxyl stretching and bending absorption bands), 1147, 1116 (S-O asymmetric stretching vibration bands), 671 and 600 cm^{-1} (S-O bending bands). However, these bands are not found in the sample due to low abundance, even though XRF studies showed a trace amount of gypsum in the paste fraction.
- No organic component is found in the mortar.

Figure 47: FTIR spectra of pulverized mortar M1 from 1960s construction showing characteristic absorbance bands from calcite in the binder and quartz in the sand. No organic component is detected in this mortar from the lack of any characteristic functional group.

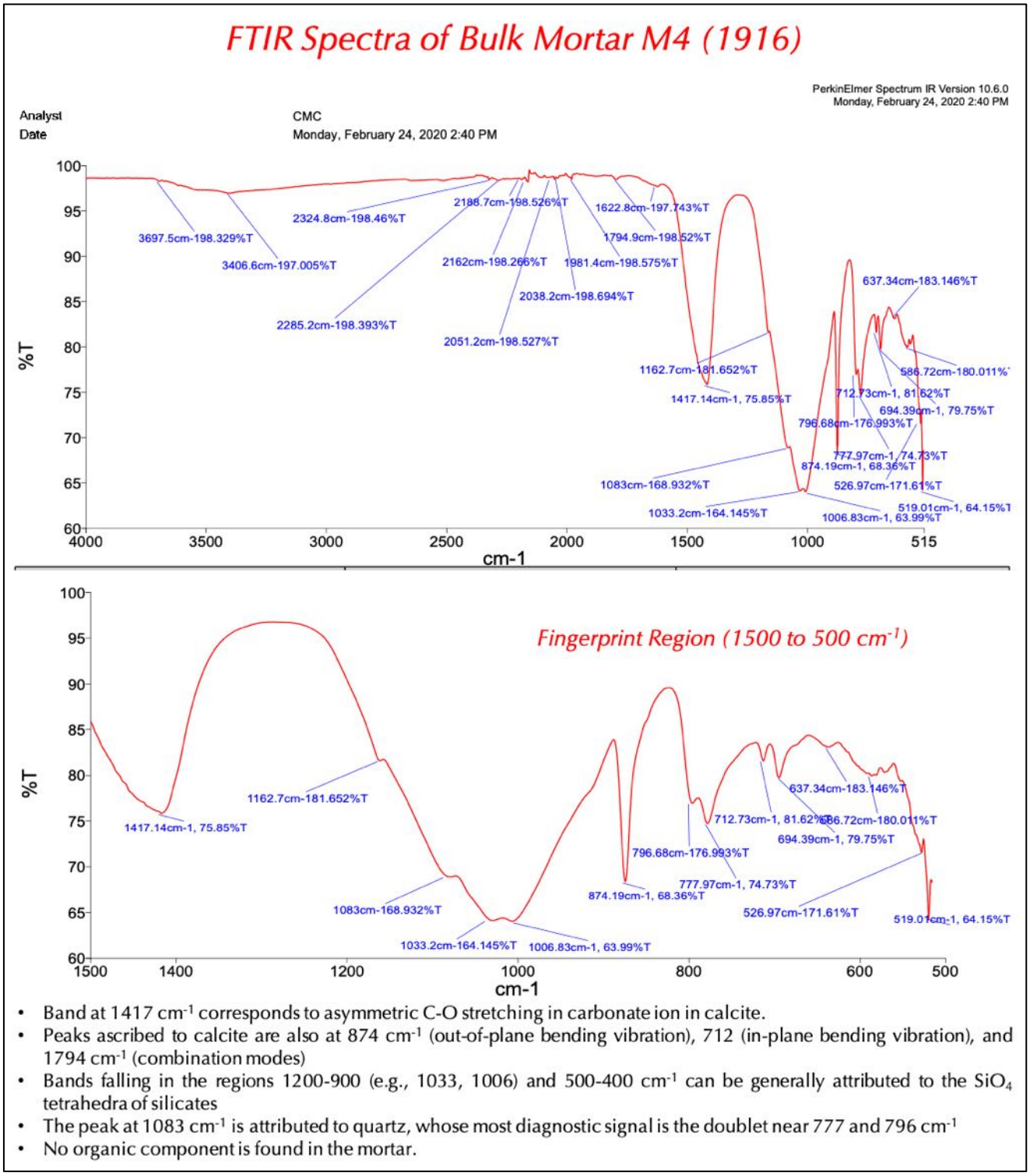

Figure 48: FTIR spectra of pulverized mortar M4 from 1916 construction showing characteristic absorbance bands from calcite in the binder and quartz in the sand. No organic component is detected in this mortar from the lack of any characteristic functional group.

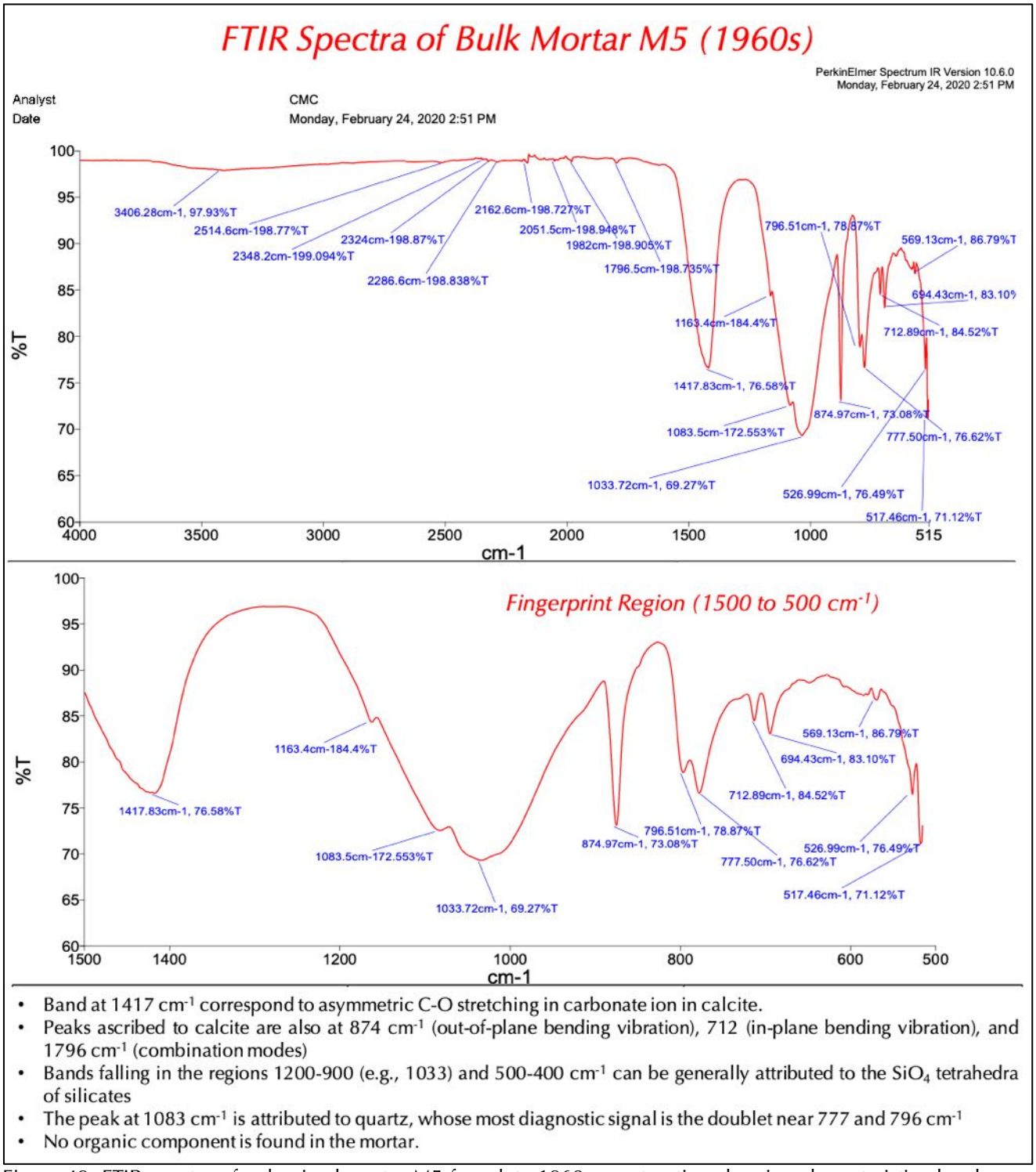

- Band at 1417 cm^{-1} correspond to asymmetric C-O stretching in carbonate ion in calcite.
- Peaks ascribed to calcite are also at 874 cm^{-1} (out-of-plane bending vibration), 712 (in-plane bending vibration), and 1796 cm^{-1} (combination modes)
- Bands falling in the regions 1200-900 (e.g., 1033) and 500-400 cm^{-1} can be generally attributed to the SiO_4 tetrahedra of silicates
- The peak at 1083 cm^{-1} is attributed to quartz, whose most diagnostic signal is the doublet near 777 and 796 cm^{-1}
- No organic component is found in the mortar.

Figure 49: FTIR spectra of pulverized mortar M5 from late 1960s construction showing characteristic absorbance bands from calcite in the binder and quartz in the sand. No organic component is detected in this mortar from the lack of any characteristic functional group.

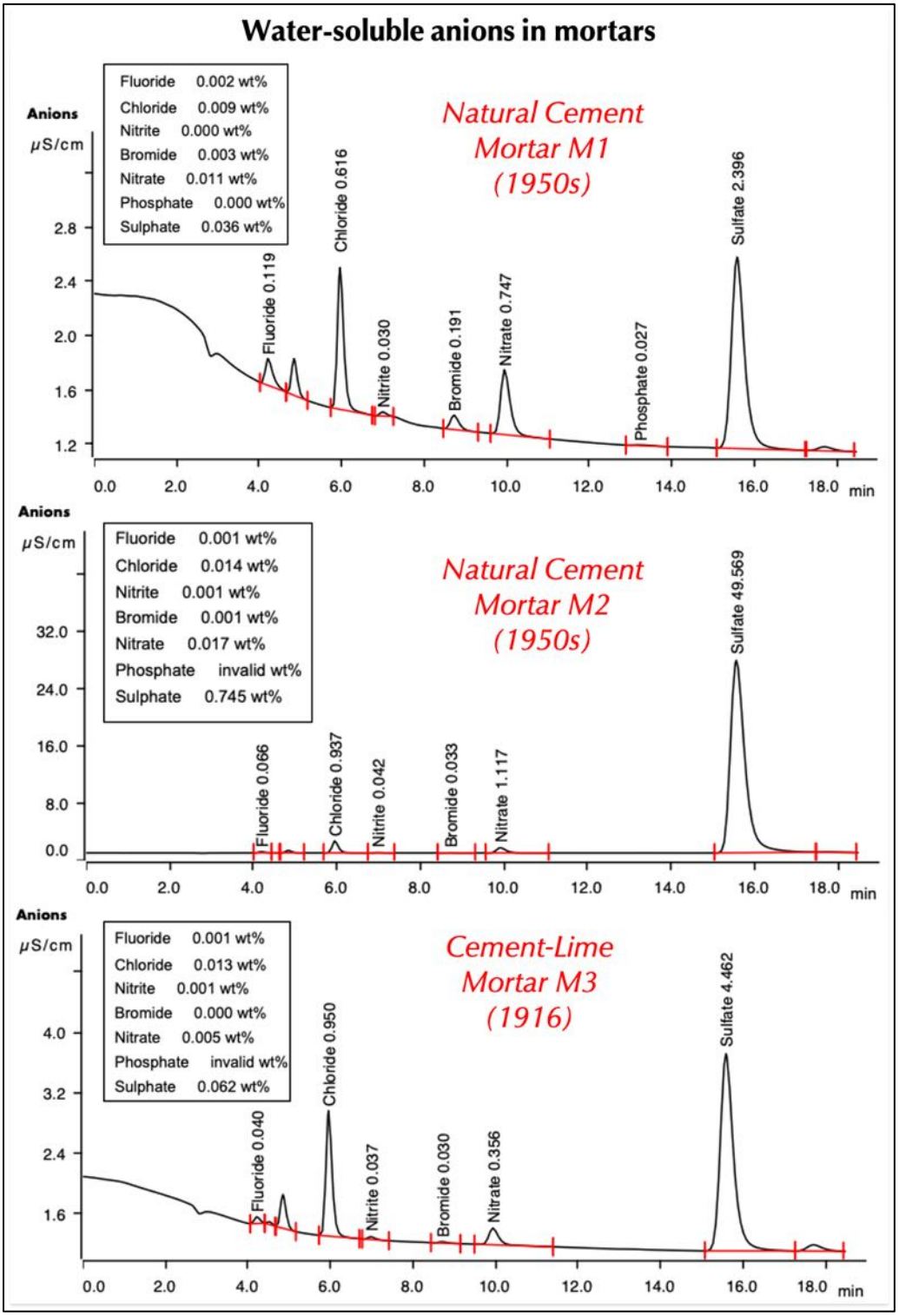

Figure 50: Ion chromatograms of water-soluble anions in mortars M1 through M3 after digesting representative portions of pulverized mortars (about a gram) in deionized water for 30 minutes at a temperature below boiling, followed by continued digestion in water at the ambient laboratory condition for 24 hours. The digested solution was filtered under vacuum through 2.5-micron followed by 0.2-micron filter papers. The final filtrates diluted to 100 ml were analyzed by ion chromatography.

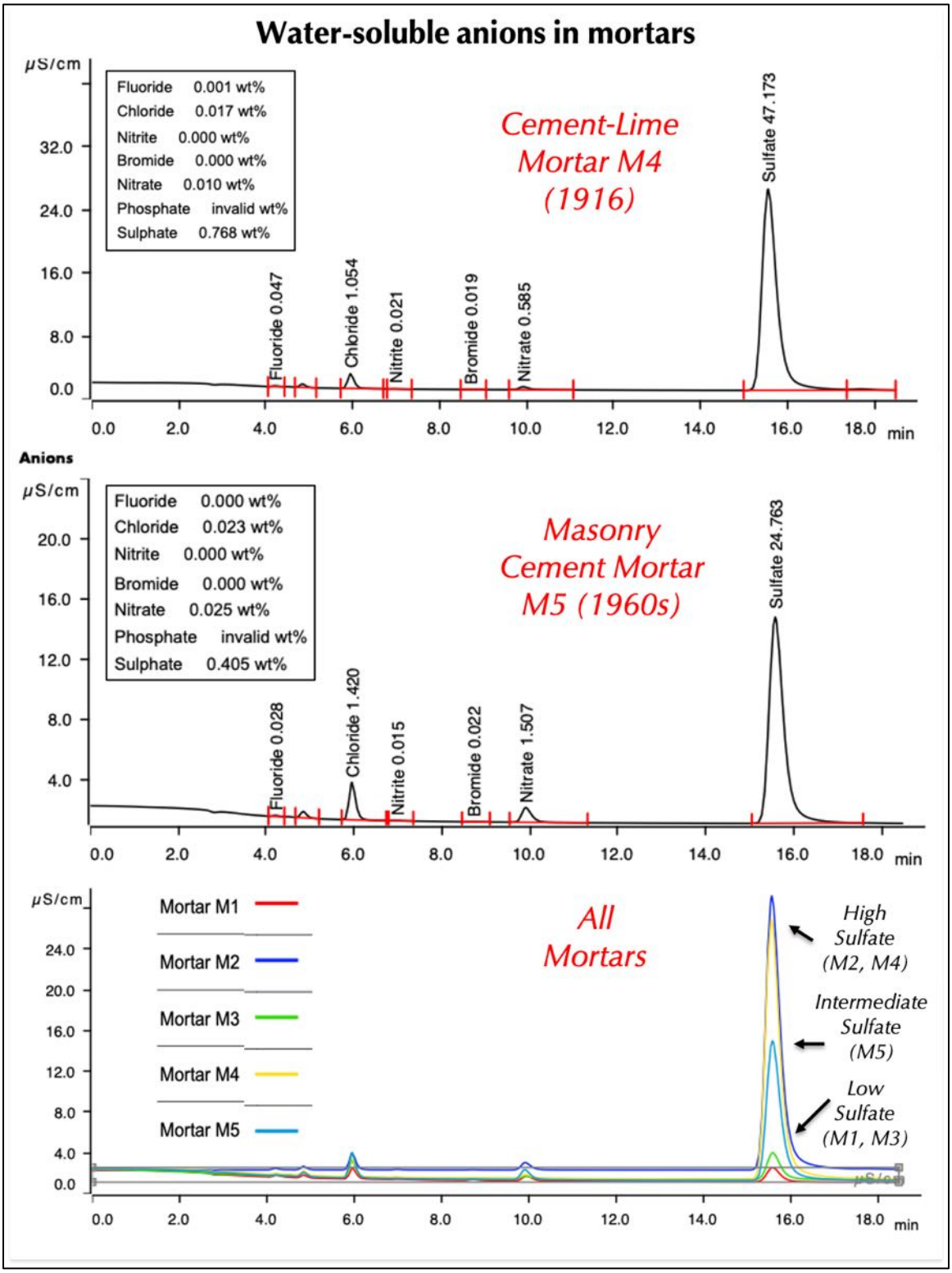

Figure 51: Ion chromatograms of water-soluble anions in mortars M4 and M5 after digesting representative portions of pulverized mortars (about a gram) in deionized water for 30 minutes at a temperature below boiling, followed by continued digestion in water at the ambient laboratory condition for 24 hours. The digested solution was filtered under vacuum through 2.5-micron followed by 0.2-micron filter papers. The final filtrates diluted to 100 ml were analyzed by ion chromatography. The bottom photo shows comparison of all five mortars to differentiate them into three groups from three different soluble sulfate contents.

Results from Chemical Analyses (Gravimetry, IC, XRF), Thermal, and XRD Studies of Masonry Mortars

Table 7 provides results obtained from chemical analyses (gravimetry), thermal analyses (TGA, DSC, DTG), X-ray diffraction, and X-ray fluorescence. Weight loss during controlled heating experiences in TGA/DSC/DTG unit of milligram levels of pulverized mortars show similarities in results as the ones obtained from losses on step-wise ignition of a gram of pulverized mortar samples in muffle furnace at 110°C, 550°C, and 950°C. Calcite content from XRD correlates with the one from TGA, quartz contents from DSC similarly show consistent results as the ones obtained from XRD after corrections for insoluble residue contents.

All these results showed the following: (i) free and combined water contents from losses up to 110-120°C are similar (0.4 to 0.5%) for all five mortars; (ii) hydrate or combined water contents from losses up to 550°C are highest in the cement-lime mortars, intermediate in natural cement mortars, and lowest in masonry cement mortar; (iii) combined/hydrate water contents of all mortars from loss on ignition from 110°C to 550°C correlates well with the losses in TGA from 200 to 600°C; (iv) carbonate contents from LOI from 550°C to 950°C as well as in TGA from 600°C to 950°C are similar in all four mortars, which showed the maximum loss in masonry cement mortar due to decomposition of calcite from abundant limestone fines and fine-grained carbonated lime, followed by cement-lime mortar and lowest in natural cement mortars; (v) quartz contents showed consistent results between DSC and XRD, latter one after correction for insoluble residue content; (vi) water-soluble chloride and sulfate contents are highest in mortars M2 (natural cement) and M4 (cement-lime), intermediate in masonry cement mortar M5, and negligible in M1 and M3.

Correlations of Results From Thermal Analyses (TGA, DSC), Gravimetry (LOI), XRD, IC, and XRF																	
Mortar Types	TGA Wt. Loss Up to 120°C	LOI from up to 110°C	TGA Wt. Loss 120°C to 200°C	TGA Wt. Loss 200°C to 600°C	LOI from 110°C to 550°C	TGA Wt. Loss > 600°C	LOI from 550°C to 950°C	Calcite Content From TGA	Calcite Content From XRD	CaO Content From XRF	LOI From XRF	Total LOI From Gravimetry	Total LOI From TGA	Sulfate Content From XRF	Water-Soluble Sulfate From IC	Quartz Content From DSC	Quartz Content From Insoluble Residue & XRD
	Free Water		Combined Water			Carbonates		Calcite		Lime	Volatiles ($H_2O + CO_2$)			Sulfate		Quartz	
Natural cement mortar, M1, 1950s	0.42	0.50	0.37	2.22	2.90	3.82	4.30	5.4	5.7	6.50	9.63	7.7	6.8	ND	0.036	45.1	65.8
Natural cement mortar, M2, 1950s	0.41	0.70	0.70	2.10	3.00	5.38	6.00	8.2	2.7	7.16	6.91	9.7	8.6	0.7450	0.745	69.5	74.2
Cement-lime mortar, M3, 1916	0.56	0.50	0.65	2.97	3.40	5.57	7.60	5.9	3.7	12.00	9.93	11.5	9.8	0.0224	0.062	44.7	46.9
Cement-lime mortar, M4, 1916	0.57	0.40	0.90	3.06	4.00	7.07	8.20	6.1	6.6	13.40	12.40	12.6	11.6	1.0400	0.768	41.2	40.6
Masonry mortar, M5, late 1960s	0.48	0.30	0.55	2.09	2.60	7.38	8.80	10.5	3.3	11.10	10.30	11.7	10.5	0.3150	0.405	60.5	57.4

Table 7: Summary of results obtained from chemical analyses (gravimetry), thermal analyses (TGA, DSC, DTG), XRD, and XRF.

Mix Proportions of Masonry Mortars from Petrographic and Chemical Data

Mortars' Compositions & Mix Proportions	Mortar M1 Natural Cement from circa 1950s	Mortar M3 Cement-Lime from circa 1916	Mortar M5 Masonry Cement circa late 1960s
Chemical Compositions			
Soluble Silica, SiO_2 (%)	1.56	2.52	2.01
Calcium Oxide, CaO (%)	6.50	12.0	11.1
Acid-Insoluble Residue (%)	82.9	70.9	72.8
Loss on Ignition: From 0°C to 110°C (Free Water) (%)	0.5	0.5	0.30
Loss on Ignition: From 110-550°C (Combined Water) (%)	2.9	3.4	2.6
Loss on Ignition: From 550-950°C (Carbonation, CO_2) (%)	4.3	7.6	8.8
Assumed Compositions & Densities			
Portland/Natural Cement Silica (SiO_2) %	20	-	21
Hydrated Lime – From CO_2, CaO, MgO, Brucite, or Soluble Silica (SiO_2) for hydraulic lime (%)	-	From CaO content, after assigning CaO for Portland Cement and assuming 63.5% CaO in Portland Cement, and converting the residual CaO to lime $Ca(OH)_2$ by multiplying the residual CaO with the factor 1.322 (mol. wt. of lime to CaO = 74.03/56 = 1.322)	
Bulk Density of Cement, (lbs./ft.^{3})	75	94 (Portland Cement)	70 (Type N), 75 (Type S), 80 (Type M)
Bulk Density of Hydrated Lime, (lbs./ft.^{3})	40	40	-
Bulk Density of Sand, (lbs./ft.^{3})	80	80	80
Calculated Volumetric Proportions			
Portland or Masonry Cement Contents (%)	Natural Cement = 100(1.56/20) = **7.8**	Portland Cement (PC) = 100(2.52/21.0) = **12.0**	Portland Cement (PC) content = 100(2.01/21.0) = **9.57** Masonry Cement (MC) = 100 – [Free water + Combined water + Sand] = 100 – (0.3+2.6+72.8) = **24.3** **PC/MC = 0.40, Type S masonry cement**
Hydrated Lime Content (%)	1.322 × [6.5 – (7.8 × 0.635)] = 2.05	1.322 × [12.0 – (12.0 × 0.635)] = 5.79	-
Sand Content (%) = Acid Insoluble Residue Content (%), For Siliceous Sand	**82.9**	**70.9**	**72.8**
Sand Content (%) = 100 – [Free Water + Combined Water + Binder], or, 100 – [Cement + Lime] For Siliceous-Calcareous Sand			
Cement Volume	7.8/75 = **0.100**	12/94 = **0.127**	24.3/75 (Type S masonry cement) = **0.324**
Hydrated Lime Volume	2.05/40 = **0.051**	5.79/40 = **0.144**	-
Sand Volume	82.9/80 = **1.036**	70.9/80 = **0.886**	72.8/80 = **0.910**
Relative Volumes of Binder Phases : Sand	Natural Cement : Lime : Sand = 0.100 : 0.051 : 1.036 = **1-part natural cement to ½ part lime to 10-part sand, (6½ times the sum of separate volumes of cement and lime)**	Portland Cement : Lime : Sand = 0.127 : 0.144 : 0.886 = **1-part Portland cement to 1-part lime to 7-part sand (3½ times the sum of separate volumes of cement and lime), similar to an ASTM C 270 Type N cement-lime mortar**	Masonry cement : Sand = 0.324: 0.910 = **1-part masonry cement to 2.8-part sand, similar to an ASTM C 270 Type S masonry cement mortar**

Table 8: Calculations of mix proportions of mortars from petrographic and chemical data.

DISCUSSIONS

Fired Clay Bricks

During firing of clay brick, a sequence of alteration occurs, which decide the properties of final brick product. The main factors concerned in manufacturing bricks are: (a) the type of raw materials, (b) fabrication method, (c) drying procedure, (d) firing temperature and (e) firing profile. These factors influence the quality of the final product. Durability and strength of bricks are often linked to their microstructure and mineralogy. In unfired clay bricks, the strength and water permeability are associated to the size and shape of the particles present and the forming process, but upon heating the nature of the mineral comprising the mass has a very significant influence because of the chemical reactions and partial fusing which occur during firing.

The porosity in brick can range from 1 to 50%, which depends on the type of clay used in manufacturing and temperature of firing. Porosity influences the compressive strength, water absorption and permeability properties of brick. During the sintering process in the brick manufacturing, initial raw materials transform into complex compounds at high temperatures. New compounds are also shaped due to chemical reactions that take place during the vitrification process, which have impacts on the steadiness of the material due to the reduction or increase in the volume of the system. Usually, porosity and water absorption of bricks show less change during firing up to 1000°C after which noticeable decrease of both occurs with increasing temperature of firing from 1000°C to 1250°C. As a result, compressive strength of bricks show a noticeable increase during firing after 1000°C.

Brick color depends on chemical composition of the raw materials (iron and calcium carbonate content) and the nature of the firing process (amount of oxygen in the kiln). For example, up to 2% iron oxide in clay fired at 900°C produces buff-colored brick in a reducing atmosphere and bright pink brick in oxidizing condition, where the same clay fired at 1100°C in oxidizing condition produces a red brick. Iron oxide (up to 7 to 10%) and manganese oxide in clay produce black brick. High lime content with iron traces in clay produces white brick, whereas low lime in clay produces gray brick. Black particles and black core in brick may result from inclusions of carbonaceous and combustible materials in clay that create reducing conditions within the brick. Within-brick color variation can come from thermal gradients developing in brick during firing. The vitrified matrix usually contain a continuous network of elongated voids.

Figure 26, and Appendix B38 to B49 show numerous optical micrographs of clay bricks from 1950s and 1916. All bricks showed: (a) tempered quartz additions as the main non-plastic component, where quartz particles are well sorted and of one population, (b) abundant elongated parallel voids creating highly porous microstructure, (c) a few dark reddish-brown grog particles of previously fired clay, and (d) the plastic component constituting aluminosilicate glass matrix from firing of clay. Overall reddish-brown color of bricks are from iron oxide component of clay and due to firing in an oxidizing condition in kiln, as opposed to the gray color tone of brick

3A and 3B which is found to be due to low carbonate content of clay and firing in a reducing condition in the kiln. Mineralogical (from XRD) and chemical (from XRF) compositions of fired clay bricks are consistent with overall amorphous fused aluminosilicate glass composition of the plastic component of bricks in which tempered quartz additives are responsible for the dominant quartz peak found in the XRD as well as contributed to the bulk silica content of bricks in XRF. Alumina, iron oxide, lime, magnesia, alkalis, titanium oxide contents are inherent from the fused clay mass whereas sulfate content may show a contribution from external salts, which is not found in any of the four bricks studied in XRF.

Bricks 3A and 3B from 1916 era are medium gray soft, highly absorptive, appeared to have very low strengths (and subsequently confirmed from 1010 psi and 790 psi strengths for 3A and 3B, respectively). These bricks are severely disintegrated and contained numerous elongated separations or lineation due to their manufacturing by hand-pressing methods. Bricks 4A and 4B from 1916s vintage are reddish-brown, relatively denser, harder, and have strengths from as low as 970 psi for disintegrated one (4A) to 3220 psi for the better one (4B) as opposed to relatively denser reddish-brown bricks from 1950s and 1960s. Bricks 1A and 1B from 1950s era are the best in appearance (no chipping), reddish-brown, and gave the highest strength of 3210 psi and 2980 psi, whereas companion Bricks 2A and 2B from 1950s are disintegrated (chipped, cracked), reddish-brown and gave strength results of 1510 psi and 1870 psi, respectively. Therefore, strength results of bricks even from the same age varied from sample-to-sample as their appearance and properties. Of all the bricks, the ones marked as 3A and 3B from 1916 are noticeably gray in color tone as opposed to reddish-brown tones of other bricks, and are the worst of all, e.g., provided the lowest strengths. Due to the overall low compressive strengths of bricks especially for the ones from 1916 era (e.g., 790 psi, 970 psi, 1010 psi strengths) replacement of those bricks with ones in conformance to the ASTM C 216 specified facing bricks are recommended.

Type of Mortar & Its Ingredients

Optical microscopy has determined: (a) the natural cement lime and siliceous sand compositions of 1950s mortars M1 and M2, (b) Portland cement, lime putty, and silcieous sand composition of 1916 mortars M3 and M4, and (c) masonry cement and siliceous sand composition of 1960s mortar M5. Original binders are determined from their characteristic mineralogies, microstructures of pastes and residual imprints of cementiitous particles left in the pastes. In the cement-lime mortar from 1916 construction, Portland cement was mixed with lime putty and silica sand. Portland cement was coarsely ground, consistent with the grinding technologies of early 20th century, henceforth left many coarse (some close to sand size) residual cement particles with dense hydration rims around many such particles. Most residual cement particles show characteristic microstructures of Portland cements in having subhedral alite or pseudomorphs of alite and skeletal interstitial dark brown ferrite phases, and, spherical belite with interstitial dark ferrite phases. In the natural cement-based mortars from 1950s construction, natural cement was mixed with lime for aided workability. Natural cement was manufactured from calcination of impure dolomitic limestones having a large range of clay and silica impurities. Due to variations in

the original compositions of impure (argillaceous) dolomitic limestone feeds, compositions of natural cements produced were diverse and so were the resultant pastes of those mortars. Finally, in the masonry cement mortar M5 from late 1960s construction, masonry cement was manufactured with a mixture of fine-grained hydrated lime, coarser grained limestone fines, and Portland cement where cement was well-hydrated leaving only pseudomorphs of alite and skeletal remains of dark interstitial ferrite phases. Silica sand was added to the lime-limestone-cement mix to prepare the proprietary brand of masonry cement.

SEM-EDS studies of pastes *per se* in all mortars showed overall enrichment of silica in siliceous sand grains and enrichment of lime in the interstitial lime-based pastes that are well-reflected in the elemental (Ca-Si-Al-Mg-etc.) maps. Additionally, paste compositions showed high magnesia due to use of dolomitic lime in natural cement or cement-lime mortars. Natural cement mortars showed highest magnesia contents in pastes, which is the characteristic feature of natural cement pastes. Alumina contents in pastes of natural cement mortars are also higher than that from cement-lime or masonry cement mortars due to contribution of alumina from natural cements. Cementation indices of pastes (paste-CI after Eckel 1922) show wide range within and between the mortars, which is not unexpected considering large compactional variations of natural cements used during 1950s era, and proprietary mix composition of masonry mortars during 1960s era, as well as variable degrees of mixing of cement and lime in the cement-lime mortar from 1916 era. A systematic trend in compositional plots of silica and lime contents of pastes against paste-CI from SEM-EDS studies of individual mortars demonstrated their respective natural cement or Portland cement and lime based compositions of original binders.

A comparison of thermograms of natural cement mortars M1 and M2 with cement-lime mortars M3 and M4 show some similarities in having: (a) endotherms from loss of free water and water from hydrate salts, following by (b) peaks from losses of structural/hydrate water around 350 to 460ºC range, followed by (c) decomposition of carbonates around 750 to 800ºC. By contrast, masonry cement mortar M5 shows (a) smallest endotherm of all mortars for loss of water from hydrate salts at 120ºC, (b) lack of any endotherm from losses of hydrate water, and (c) largest endotherm from decomposition of calcite from limestone fines and fine-grained carbonated paste at 775ºC. Loss of structural water is highest (around 3% loss in 200 to 600ºC range) in the two cement-lime mortars M3 and M4 due to higher amount of calcium silicate hydrate and calcium hydroxide components of Portland cement hydrations than the corresponding natural cement mortars M1 an M2 (which show 2.1 to 2.2% loss at 200 to 600ºC range).

FTIR studies of all four mortars showed the simple inorganic phases (e.g., quartz, calcite) that are detected in microscopy and XRD studies and lack of any polymer component in the mortars.

Ion chromatography (IC) of water-soluble salts showed detectable water-soluble chloride and sulfate contents in all mortars, which are highest in mortars M2 (natural cement) and M4 (cement-lime), intermediate in masonry cement mortar M5, and negligible in M1 and M3. Water-soluble chloride contents are 0.009%, 0.014%, 0.013%, 0.017%, and 0.023% percent by mass of mortars in samples M1 through M5, respectively. Water-soluble sulfate

contents are 0.036%, 0.745%, 0.062%, 0.768%, and 0.405% percent by mass of mortars in samples M1 through M5, respectively. Results are indicative of lack of any chloride ingress or chloride-induced distress, and, sulfate contents anticipated from contributions from binders' ingredients with no external sulfate ingress. Variations in chloride and sulfate contents as well as of other water-soluble anions are due to leaching and moisture migration through the mortars during service that have disturbed the original concentrations of these anions.

Mix Calculations

Information obtained from: (a) petrographic examinations to determine the sand compositions, binder types, as well as overall mortar types, and (b) chemical analyses of mortars to determine the soluble silica contents, water contents, and insoluble residue contents are used to calculate the volumetric proportions of mortars' ingredients. Mix calculations of mortars showed: (a) 1-part natural cement to $^{1}/_{2}$ part hydrated lime to 10-part siliceous sand mix ($6^{1}/_{2}$ times sand to sum of separate volumes of natural cement and lime) for the natural cement mortars from 1950s construction, (b) 1-part Portland cement to 1-part lime to 7-part siliceous sand ($3^{1}/_{2}$ times sand to sum of separate volumes of Portland cement and lime) for cement-lime mortar from 1916 construction, and (c) 1-part ASTM C 91 Type S masonry cement to $2^{3}/_{4}$-part siliceous sand for late 1960s masonry cement mortar.

Tuckpointing Mortars

Based on the determined natural cement-lime-siliceous sand compositions of 1950s mortars, and the determined 1-part natural cement to $^{1}/_{2}$ part hydrated lime to 10-part siliceous sand mix ($6^{1}/_{2}$ times sand to sum of separate volumes of natural cement and lime) volumetric proportions, a possible tuck-pointing mortar for both locations of 1950s mortars could be a modern-day Rosendale cement manufactured by Edison Coatings Inc., e.g., Rosendale 10C cement, or prepackaged Rosendale 10M cement-sand mix but preferably the 10C type mixed with siliceous sand used in the original mortars, where the natural cement should be in conformance to the specifications of ASTM C 10 and sand should correspond to the specification of masonry sand *a la* ASTM C 144. The final choice of binder and sand ingredients would depend on the match in appearance, compositions, and properties with the original mortars. Design and formulation of an appropriate tuck-pointing mortar should be based on trial and error on small test areas by the project engineer/architect.

Based on the determined Portland cement-lime-siliceous sand compositions of 1916 mortars, and the determined 1-part Portland cement to 1-part hydrated lime to 7-part siliceous sand mix ($3^{1}/_{2}$ times sand to sum of separate volumes of natural cement and lime) volumetric proportions, a possible tuck-pointing mortar for both locations of 1916 mortars could be 1-part Portland or blended cement (conforming ASTM C 150 or C 595, respectively) to $^{1}/_{4}$ to $1^{1}/_{2}$ part dolomitic lime (conforming ASTM C 207) to not less than $2^{1}/_{4}$ and not more than 3 times sand to the sum of the separate volumes of cement and lime by volume. The final choice of binder and sand ingredients would depend on the match in appearance, compositions, and properties with these pointing mortars, or if these mortars are to be entirely replaced then to the original mortar. The chosen mortar should bond well to the brick, as well as to the existing jointing mortars and preferably be softer than the present mortars without introducing

any undue stress from any compositional or proportional mismatch to the existing mortars or mismatch to the brick masonries.

Based on determined masonry cement and siliceous sand composition of late 1960s masonry cement mortar, and the determined 1-part masonry cement to 2 3/4-part siliceous sand volumetric proportions, a possible tuck-pointing mortar can be: (a) an ASTM C 270 Type S masonry/mortar cement and silica sand mortar (e.g., prepared by mixing 1-part ASTM C 91/C 1329 Type S or N masonry/mortar cement to 2 1/4 to 3-part ASTM C 144 masonry sand, by volume), or, (b) an air-entrained Type S cement-lime mortar (e.g., prepared by mixing 1-part ASTM C 150 Portland cement, 1/2 to 1 1/2-part ASTM C 207 Type S hydrated lime or ASTM C 1489 lime putty, and 2 1/4 to 3-part ASTM C 144 masonry sand, by volume). However, finding a match to the examined mortar may not be beneficial for overall performance of masonry if the mortar examined is inappropriate for the adjacent masonry units and intended applications. The final choice should be verified by preparing mock-up mortar batches applied over small test areas to see the match not only in the appearance and properties with the existing mortar, but also in providing overall improvement in performance and durability of the masonry wall, e.g., without incorporating any undue stresses from mismatch between the mortar and masonry units.

REFERENCES

ASTM C 10, "Standard Specification for Natural Cement," In Annual Book of ASTM Standards, Section Four Construction, Vol. 04.01 Cement; Lime; Gypsum; ASTM Committee C01 on Cement, 2017.

ASTM C 67, "Standard Test Methods for Sampling and Testing Brick and Structural Clay Tile," In Annual Book of ASTM Standards, Section Four Construction, Vol. 04.05 Chemical-Resistant Nonmetallic Materials; Vitrified Clay Pipe; Concrete Pipe; Fiber-Reinforced Cement Products; Mortars and Grouts; Masonry; Precast Concrete; ASTM Committee C15.02 on Cement, 2019.

ASTM C 91, "Standard Specification for Masonry Cement," In Annual Book of ASTM Standards, Section Four Construction, Vol. 04.01 Cement; Lime; Gypsum; ASTM Committee C01 on Cement, 2017.

ASTM C 144, "Standard Specification for Aggregate for Masonry Mortar," In Annual Book of ASTM Standards, Section Four Construction, Vol. 04.05 Chemical-Resistant Nonmetallic Materials; Vitrified Clay Pipe; Concrete Pipe; Fiber-Reinforced Cement Products; Mortars or mortars and Grouts; Masonry; Precast Concrete; ASTM Committee C12 on Mortars or mortars for Unit Masonry, 2017.

ASTM C 1324, "Standard Test Method for Examination and Analysis of Hardened Masonry Mortar," In Annual Book of ASTM Standards, Section Four Construction, Vol. 04.05 Chemical-Resistant Nonmetallic Materials; Vitrified Clay Pipe; Concrete Pipe; Fiber-Reinforced Cement Products; Mortars or mortars and Grouts; Masonry; Precast Concrete; ASTM Committee C12 on Mortars or mortars for Unit Masonry, 2017.

ASTM C 270, "Standard Specification for Mortar for Unit Masonry," In Annual Book of ASTM Standards, Section Four Construction, Vol. 04.05 Chemical-Resistant Nonmetallic Materials; Vitrified Clay Pipe; Concrete Pipe; Fiber-Reinforced Cement Products; Mortars or mortars and Grouts; Masonry; Precast Concrete; ASTM Committee C12 on Mortars or mortars and Grouts for Unit Masonry, 2017.

ASTM C 1713, "Standard Specification for Mortars or mortars for the Repair of Historic Masonry," In Annual Book of ASTM Standards, Section Four Construction, Vol. 04.05 Chemical-Resistant Nonmetallic Materials; Vitrified Clay Pipe; Concrete Pipe; Fiber-Reinforced Cement Products; Mortars or mortars and Grouts; Masonry; Precast Concrete; ASTM Committee C12 on Mortars or mortars and Grouts for Unit Masonry, 2017.

ASTM C 51, "Standard Terminology Relating to Lime and Limestone (as used by the Industry)'" In Annual Book of ASTM Standards, Section Four Construction, Vol. 04.01 Cement; Lime; Gypsum; ASTM Committee C07 on Lime, 2017.

ASTM C 856, "Standard Practice for Petrographic Examination of Hardened Concrete," In Annual Book of ASTM Standards, Section Four Construction, Vol. 04.02; ASTM Subcommittee C 9.65, 2017.

ASTM C 1723, "Standard Guide for Examination of Hardened Concrete Using Scanning Electron Microscopy," In Annual Book of ASTM Standards, Section Four Construction, Vol. 04.02; ASTM Subcommittee C 9.65, 2017.

ASTM C 1329, "Standard Specification for Mortar Cement," In Annual Book of ASTM Standards, Section Four Construction, Vol. 04.01; ASTM Subcommittee C01.11, 2016.

ASTM C 150, "Standard Specification for Portland Cement," In Annual Book of ASTM Standards, Section Four Construction, Vol. 04.01; ASTM Subcommittee C01.10, 2018.

ASTM C 1489, "Standard Specification for Lime Putty for Structural Purposes," In Annual Book of ASTM Standards, Section Four Construction, Vol. 04.01; ASTM Subcommittee C07.02, 2015.

ASTM C 207, "Standard Specification for Hydrated Lime for Masonry Purposes," In Annual Book of ASTM Standards, Section Four Construction, Vol. 04.01; ASTM Subcommittee C07.02, 2011.

ASTM C 979 "Standard Specification for Pigments for Integrally Colored Concrete,' In Annual Book of ASTM Standards, Section Four Construction, Vol. 04.01; ASTM Subcommittee C07.02, 2011.

Bartos, P. Groot, C., and Hughes, J.J. (eds.), "Historic Mortars or mortars: Characteristics and Tests", Proceedings PRO12, RILEM Publications, France, 2000.

Boynton, R., *Chemistry and Technology of Lime and Limestone, 2nd edition*, John Wiley & Sons, Inc. 1980.

Brosnan, Denis, A., Characterization of Rosendale Mortars or mortars For Fort Sumter National Monument and Degradation of Mortars or mortars by Sea Water and Frost Action, Final Report, April 19, 2012.

Callebaut, K., Elsen, J., Van Balen, K., and Viaene, W., "Nineteenth century hydraulic restoration mortars or mortars in the Saint Michael's Church (Leuven, Belgium) Natural hydraulic lime or cement?" Cement and Concrete Research, V 31, pp 397-403, 2001.

Callebaut, K., Elsen, J., Van Balen, K., and Viaene, W., Historical and scientific study of hydraulic mortars or mortars from the 19th century. In International RILEM workshop on historic mortars or mortars: Characterization and Tests; Paisley, Scotland, 12th to 14th May 1999, Edited by Barton, P., Groot, C., and Hughes, J.J., Cachan, France, RILEM Publications, 2000.

Charloa, A.E., "Mortar analysis: A comparison of European procedures." US/ICOMOS Scientific Journal: Historic Mortars or mortars & Acidic Deposition on Stone, 3 (1), pp. 2-5, 2001.

Charola, A.E., and Lazzarin, L., Deterioration of Brick Masonry Caused by Acid Rain, ACS Symposium Series, Vol. 318, pp. 250-258, 2009.

Chiari, G., Torraca, G., and Santarelli, M.L., "Recommendations for Systematic Instrumental Analysis of Ancient Mortars or mortars: The Italian Experience", *Standards for Preservation and Rehabilitation*, ASTM STP 1258, S.J. Kelley, ed., American Society for Testing and Materials, pp. 275-284, 1996.

Doebley, C.E., and Spitzer, D., "Guidelines and Standards for Testing Historic Mortars or mortars", *Standards for Preservation and Rehabilitation*, ASTM STP 1258, S.J. Kelley, ed., American Society for Testing and Materials, pp. 285-293, 1996.

Eckel, Edwin, C., *Cements, Limes, and Plasters*, John Wiley & Sons, Inc. 655pp, 1922.

Edison, M.P. (Editor), *Natural Cement*, ASTM STP 1494, American Society for Testing and Materials, 2008.

Elsen, J., "Microscopy of Historic Mortars or mortars – A Review", *Cement and Concrete Research 36*, 1416-1424, 2006.

Elsen, J., Mertens, G., and Van Balen, K., Raw materials used in ancient mortars or mortars from the Cathedral of Notre-Dame in Tournai (Belgium), Eur. J. Mineral., Vol. 23, pp. 871-882, 2011.

Elsen, J., Van Balen, K., and Mertens, G., Hydraulicity in Historic Lime Mortars or mortars: A Review, In, Valek, J, Hughes, J.J., and Groot, W.P. (Eds.), Historic Mortars or mortars Characterisation, Assessment and Repair, RILEM Book series, Volume 7, pp. 125-139, Springer, 2012.

Erlin, B., and Hime, W.G., "Evaluating Mortar Deterioration", *APT Bulletin*, Vol. 19, No. 4, pp. 8-10+54, 1987.

Goins E.S., "Standard Practice for Determining the Components of Historic Cementitious Materials," National Center for Preservation Technology and Training, Materials Research Series, NCPTT 2004.

Goins, E.S., "A standard method for the characterization of historic cementitious materials." US/ICOMOS Scientific Journal: Historic Mortars or mortars & Acidic Deposition on Stone, # (1), pp. 6-7, 2001.

Groot, C., Ashall, G., and Hughes, J., Characterization of Old Mortars or mortars with Respect to their Repair, State-of-the-art Report of RILEM Technical Committee 167-COM, 2004.

Hughes, D.C., Jaglin, D., Kozlowski, R., Mayr, N., Mucha, D., and Weber, J., "Calcination of Marls to Produce Roman Cement", pp. 84-95, In, Edison, M.P. (Editor), *Natural Cement*, ASTM STP 1494, American Society for Testing and Materials, 2007.

Hughes, J.J., Cuthbert, S., and, Bartos, P., "Alteration Textures in Historic Scottish Lime Mortars or mortars and the Implications for Practical Mortar Analysis", *Proceedings of the 7th Euroseminar on Microscopy Applied to Building Materials*, Delft, pp. 417-426, 1999.

Hughes, R.E., and Bargh, B.L., The weathering of brick: Causes, Assessment and Measurement, A Report of the Joint Agreement between the U.S. Geological Survey and the Illinois State Geological Survey, 1982.

Jana, D., "Application of Petrography In Restoration of Historic Masonry Structures", In: Hughes, J.J., Lesie, A.B. and Walsh, J.A., eds. *Proceedings of 10th Euroseminar on Microscopy Applied to Building Materials*, Paisley, 2005.

Jana, D., "Sample Preparation Techniques in Petrographic Examinations of Construction Materials: A State-of-the-art Review", *Proceedings of the 28th Conference on Cement Microscopy*, International Cement Microcopy Association, Denver, Colorado, pp. 23-70, 2006.

Jedrzejewska, H., Old mortars or mortars in Poland: a new method of investigation, Studies in Conservation 5, pp. 132-138, 1960.

Langley, W.S., Report to CRH Canada on Investigation of Failed Mortar, W.S. Langley Concrete & Materials Technology, Inc. Project No. 191271, June 2019.

Leslie, A.B., and Hughes, J.J., "Binder Microstructure in Lime Mortars or mortars: Implications for the Interpretation of Analysis Results", *Quarterly Journal of Engineering Geology & Hydrogeology*, V. 35, No. 3, pp. 257-263, 2001.

Lubell, B., van Hees, Rob. P.J., and Groot, Casper J.W.P., The role of sea salts in the occurrence of different damage mechanisms and decay on brick masonry, Construction and Building Materials, Vol. 18, pp. 119-124, 2004.

Martinet, G., Quenee, B., Proposal for a useful methodology for the study of ancient mortars or mortars, Proceedings of the International RILEM workshop "Historic Mortars or mortars: Characteristics and tests," Paisley, pp. 81-91, 2000.

Mack, Robert, and Speweik, John P., *Preservation Briefs 2*, U.S. Department of the Interior, National Park Service Cultural Resources, Heritage Preservation Services, pp. 1-16, 1998.

Middendorf, B., Baronio, G., Callebaut, K, and Hughes, J.J., "Chemical-mineralogical and physical-mechanical investigation of old mortars or mortars, Proceedings of the International RILEM workshop "Historic Mortars or mortars: Characteristics and tests," Paisley, pp. 53-61, 2000.

Middendorf, B., Hughes, J.J., Callebaut, K., Baronio, G., and Papayanni, I., Mineralogical characterization of historic mortars or mortars, In. Groot, C., et al. (eds), Characterisation of Old Mortars or mortars with Respect to their Repair, State-of-the-art Report of RILEM Technical Committee 167-COM, pp. 21-36, 2004a.

Middendorf, B., Hughes, J.J., Callebaut, K., Baronio, G., and Papayanni, I., Chemical characterization of historic mortars or mortars, In. Groot, C., et al. (eds), Characterisation of Old Mortars or mortars with Respect to their Repair, State-of-the-art Report of RILEM Technical Committee 167-COM, pp. 37-53, 2004b.

Middendorf, B., Hughes, J.J., Callebaut, K., Baronio, G., and Papayanni, I., "Investigative Methods for the Characterization of Historic Mortars or mortars – Part 1: Mineralogical Characterization," *Materials and Structures*, Vol. 38, 2005a.

Middendorf, B., Hughes, J.J., Callebaut, K., Baronio, G., and Papayanni, I., "Investigative Methods for the Characterization of Historic Mortars or mortars – Part 2: Chemical Characterization," *Materials and Structures*, Vol. 38, pp 771-780, 2005b.

Sarkar, S.L., Aimin, Xu, and Jana, Dipayan, Scanning electron microscopy and X-ray microanalysis of Concretes, pp. 231-274, In, Ramachandran, V.S. and Beaudoin, J.J. Handbook of Analytical Techniques in Concrete Science and Technology, Noyes Publications, Park Ridge, New Jersey, 2000.

Speweik, J.P., *The History of Masonry Mortar in America 1720-1995*, 2010.

Stewart, J., and Moore, J., Chemical techniques of historic mortar analysis, Proceedings of the ICCROM Symposium "Mortars or mortars, Cements, and Grouts used in the Conservation of Historic Buildings," Rome, ICCROM, Rome, pp. 297-310, 1981.

Valek, J., Hughes, J.J., and Groot, C. (eds.), *Historic Mortars or mortars: Characterization, Assessment and Repair*, Springer, RILEM Book series Vol. 7, p. 464, 2012.

Valek, J., Hughes, J.J., and Groot, C. (eds.), Historic Mortars or mortars: Characterization, Assessment and Repair, Springer, RILEM Book series Vol. 7, 2012.

Van Balen, K., Toumbakari, E.E., Blanco, M.T., Aguilera, J., Puertas, F., Sabbioni, C., Zappia, G., Riontino, C., and Gobbi, G., "Procedures for mortar type identification: A proposal." In International RILEM workshop on historic mortars or mortars: Characteristics and Tests; Paisley, Scotland, 13th to 14th May 1999, edited by Barton, P., Groot, C., and Hughes, J.J., Cachan, France: RILEM Publications, 2000.

Vyskocilova, R., W. Schwarz, D. Mucha, D. Hughes, R. Kozlowski, and J. Weber, "Hydration processes in pastes of roman and American natural cements," *ASTM STP*, vol. 4, no. 2, 2007.

Weber, J., Gadermayr, N., Kozlowski, R., Mucha, D., Hughes, D., Jaglin, D., and Schwarz, W., Microstructure and mineral composition of Roman cements produced at defined calcination conditions, Materials Characterization, Vol. 58, pp. 1217-1228, 2007.

✪ ✪ ✪ END OF TEXT ✪ ✪ ✪

APPENDIX A –
LABORATORY TESTING OF MASONRY MORTARS

Introduction[1]

Until 1970s characterization of masonry mortars were mostly based on traditional wet chemical analyses (Jedrzejewska, 1960, Stewart and Moore, 1981), where interpretation of results were often difficult if not impossible without a good knowledge of the nature of different sand and binder components in mortars. The majority of later mortar characterization proposed optical microscopy (Erlin and Hime 1987, Middendorf et al. 2000, Elsen 2006) as the first step in identification of different components of mortar based on which other analytical techniques including the wet chemistry are performed. Examples include scanning electron microscopy and X-ray microanalysis, X-ray diffraction, X-ray fluorescence, atomic absorption, thermal analysis, infrared spectroscopy, etc. (Bartos et al. 2000, Elsen 2006, Callebaut et al. 2000, Erlin and Hime 1987, Goins 2001, 2004, Groot et al. 2004, Doebley and Spitzer 1996, Chiari et al. 1996, Middendorf et al. 2000, 2004, 2005, Leslie and Hughes 2001, Martinet and Quenee 2000, Valek et al., 2012, Jana 2005, 2006). The choices of appropriate techniques depend mainly on the questions that have to be addressed, and, on the amount of material available.

Purposes of laboratory testing are: (a) to document an in place mortar by examining its sand and binder components, proportions of various ingredients, and their effects on properties and performance of the mortar, (b) evidence of any chemical or physical deterioration of the mortar from unsoundness of its ingredients to effects of potentially deleterious agents from the environment (e.g., salts), (c) records of later repointing events and their beneficial or detrimental effects on the performance of the original mortar and masonry units, and finally, (d) an assessment of an appropriate restoration mortar to ensure compatibility with the existing structure.

Currently there are two standardized procedures available that describe various laboratory techniques for analyses of masonry mortars with special emphasize to historic mortars. One is from the USA, the ASTM C 1324 "Standard Test Method for Examination and Analysis of Hardened Masonry Mortar," which includes detailed petrographic examinations, followed by chemical analyses, along with various other analytical methods to test masonry mortars as described in various literatures, e.g., XRD, thermal analysis, and infrared spectroscopy. The second one is from European studies and described in RILEM (Middendorf et al. 2004 and b, and 2005 a and b).

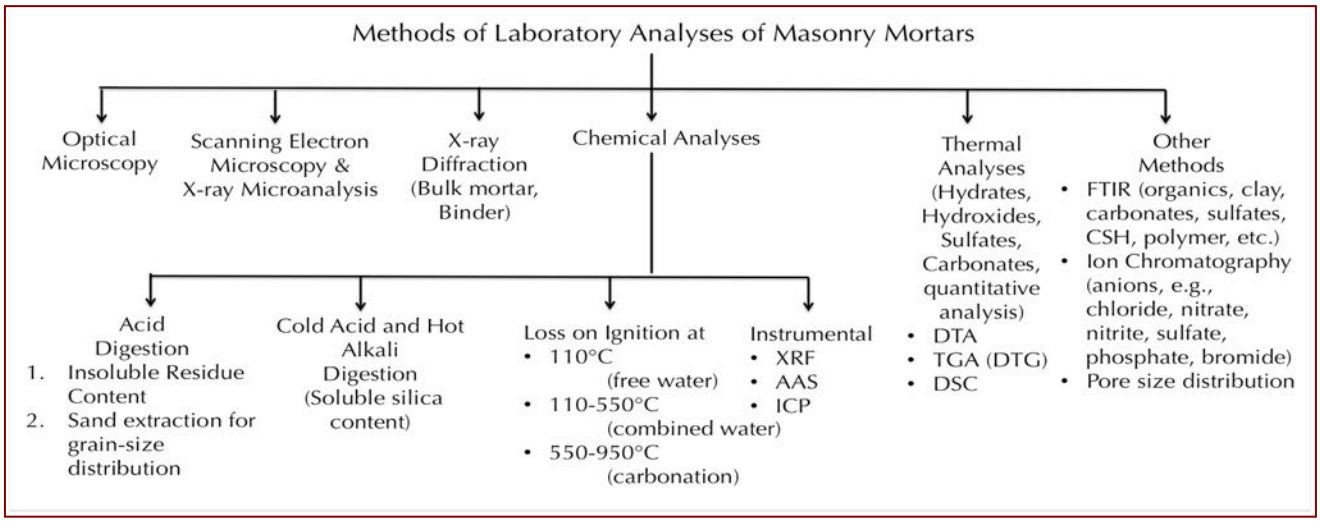

Figure A1: Various methods of laboratory analyses of masonry mortars. Optical microsocpy is the first method that provides many useful information about the mortar and its ingredeints, and dictates the subsequent methods to follow. Electron microscopy, X-ray diffraction, and various chemical analyses are commonly followed after optical microcopy to further determine the composition, microstructure, and mineralogy of sand and binder(s).

[1] For various analytical facilities for laboratory testing of mortars, please visit our website at www.cmc-concrete.com.

Sample Selection and Steps of Laboratory Analyses

Mortar samples are first photographed with a digital camera, scanned on a flatbed scanner, and examined in a low-power stereomicroscope for the preliminary examinations, e.g., to screen any unusual pieces having different appearances, e.g., representing contaminants from prior pointing episodes.

Four (4) subsets of the pieces of interest are then selected from the original amount for: (1) optical microscopy, scanning electron microscopy, and X-ray microanalysis of a representative sizable amount to cover as much of an entire 50 mm × 75 mm thin section per sample with multiple pieces as possible for chemical and mineralogical compositions, and microstructures of sand, paste, and mortar, (2) extraction of masonry sand by acid digestion for grain size distribution of sand (preferably from an un-pulverized or gently pulverized mortar), (3a) loss on ignition for water and carbonate contents, (3b) acid digestion for determination of insoluble residue content, and (3c) cold-acid then hot-alkali digestion for soluble silica content from hydraulic binders – all three after pulverizing the 3rd subset mortar to finer than 0.3 mm size and collecting aliquots of 1 gram, 1 gram, and 5 grams, respectively, and, (4) ultrafine pulverization (finer than 44-micron particle size) of 10 grams of mortar from the 4th subset for XRD, XRF, and thermal analyses. Any additional analyses, if needed, e.g., water digestion for determination of soluble salts by ion chromatography, or, infrared spectroscopy are done from the 4th subset. Organic analysis (e.g., paint or surface coating on masonry) by FTIR is done on the coating of interest from the original mortar pieces.

After preliminary visual examinations, optical microscopy is the first detailed examination that is most crucial in mortar analysis to determine the types of sand and binder used from mineralogical and textural characteristics of mortar, based on which subsequent chemical analyses are done to determine the chemical compositions of binders and proportions of sand, and binder components. Information obtained from petrographic examinations is crucial to devise the appropriate guidelines to follow for chemical methods, and to properly interpret the results of chemical analyses. For example, detection of siliceous versus calcareous versus argillaceous natures of aggregates in mortar, or the presence of any pozzolan in the binder (slag, fly ash, ceramic dusts, etc.) from petrography restricts which chemical method to follow, and how to interpret the results of such analyses, e.g., acid-insoluble residue contents. Therefore, a direct chemical analysis e.g., acid digestion of a mortar without doing a prior petrographic examination to determine the types of aggregates and binder used could lead to highly erroneous results and interpretation. Armed with petrographic and chemical data, and based on assumed compositions and bulk densities of the sand and the binder(s) similar to the ones detected from petrographic examinations volumetric proportions of sand and various binders present in the examined mortar can be calculated. The estimated mix proportions from such calculations can provide at least a rough guideline to use as a starting mix during formulation of a tuck-pointing mortar to match with the existing mortar.

Optical Microscopy for Mineralogy & Microstructure of Mortar

After preliminary non-destructive examinations, e.g., from visual examinations, photographing as-received sample with a digital camera, scanning mortar pieces on a flatbed scanner, and examining in a low-power stereomicroscope, subsequent destructive sample preparation steps are followed for examinations of detailed mineralogical and microstructural compositions of mortar sand and binders in thin sections (25 to 30 micron thickness) in (a) a higher power Stereozoom microscope from 5X to 100X, and then in a research-grade petrographic microscope from 40X to 1000X both microscopes are equipped with transmitted, reflected, polarized, and fluorescent light facilities, as well as photo-micrographic capabilities with advanced high-resolution microscope cameras.

The main purposes of optical microscopy of masonry mortar are characterization of: (a) aggregates, e.g., type(s), chemical and mineralogical compositions, nominal maximum size, shape, angularity, grain-size distribution, soundness, alkali-aggregate reactivity, etc. (b) paste, e.g., compositions and microstructures to diagnose various type(s) of binder(s) used, (c) air, e.g., presence or absence of air entrainment, air content, etc., (d) alterations, e.g., lime leaching, carbonation, staining, etc. due to interactions with the environmental agents during service, and effects of such alterations on properties and performance of mortar; and (e) deteriorations, e.g., chemical and/or physical deteriorations during service, cracking from various mechanisms, salt attacks, possible reasons for the lack of bond if reported from the masonry unit, etc.

Four essential steps followed during optical microscopy are: (1) visual examination of as-received, fresh fractured, and sectioned surfaces of mortar in a stereo-microscope, (2) preparation of a large-area (50 × 75 mm) thin section of homogeneous thickness (25-30 micron), (3) observation of thin section in a transmitted-light stereo-zoom microscope from 5X to 100X preferably with polarized-light facilities to observe large-scale distribution of sand and mortar microstructure, and finally (4) observation of thin section in a petrographic microscope from 40X to 600X equipped with transmitted and reflected polarized and fluorescent-light facilities for examinations of sand and binder compositions and microstructures.

For thin section preparation, representative fragments are oven-dried at 40°C to a constant mass and placed in a flexible (e.g., molded silicone) sample holder, then encapsulated with a colored dye (e.g., blue dye commonly used in sedimentary petrography, or, fluorescent dye, Elsen 2006) mixed low-viscosity epoxy resin under vacuum to impregnate the capillary pore spaces of mortar, improve the overall integrity of sample during sectioning by the cured epoxy, highlight porous areas of mortar, alterations, cracks, voids, reaction products, etc. The epoxy-encapsulated cured solid block of sample is then de-molded and processed through a series of coarse to fine grinding on metal and resin-bonded diamond grinding discs with water or a lubricant, eventually a perfectly flat clean ground surface is glued to a large-area (50 × 75 mm) glass slide. Careful precision sectioning and precision grinding of the sample is then done in a thin-sectioning machine (e.g., Buehler, Logitech, Ingram-Wards, Microtrim, Struers) till the thickness is down to 50-60 micron. Final thinning down to 25-30 micron thickness is done on a glass plate with fine (5-15 micron) alumina abrasive. Thin section is eventually polished with various fine (1 micron to 0.25 micron size) diamond abrasives on polishing wheels for examinations in a petrographic microscope, and eventually in SEM-EDS. Sample preparation steps are described in detail in Jana (2006).

Steps followed during light optical microscopical examinations of a mortar sample include:

a. Visual examinations of mortar fragments, as received, to select fragments for detailed optical microscopy; initial digital and flatbed scanner photography of mortar as received;
b. Low-power stereomicroscopic examinations of saw-cut and freshly fractured sections of mortar for evaluation of variations in color, grain-size and appearances of sand, and the nature of the mortar paste;
c. Examinations of oil immersion mounts for special features and materials from mortar in a petrographic microscope;
d. Examinations of colored (blue or fluorescent) dye-mixed epoxy-impregnated polished thin sections of mortar fragments in a transmitted-light Stereozoom microscope for determination of size, shape, angularity, and distribution of sand, as well as abundance and distribution of void and pore spaces that are highlighted by the colored dye-mixed epoxy;
e. Image analyses of photomicrographs of mortar thin sections for estimations of pores, voids, intergranular open spaces, and shrinkage microcracks by using Image J or other image analysis software where multiple photomicrographs are collected in plane polarized light mode by using a high-resolution Stereozoom microscope equipped with transmitted and polarizing light facilities and stitched to get a representative coverage;
f. Examinations of colored (blue or fluorescent) dye-mixed epoxy-impregnated polished thin sections of mortar fragments in a petrographic microscope for detailed compositional, mineralogical, textural, and microstructural analyses of aggregates and binders in mortars, along with diagnoses of evidence of any deleterious processes and alterations (e.g., lime leaching, precipitation of secondary deposits and alteration products, salts);
g. Examinations of polished thin or solid section in reflected-light (epi-illumination) mode of petrographic microscope after etching the surface with acid to identify various non-hydrated hydraulic phases (e.g., C_2S, C_3S, C_3A, etc. Middendorf et al., 2005);
h. Examinations of any physical or chemical deterioration of mortar or signs of improper construction practices from microstructural evidences;
i. Stereo-microscopical examinations of size, shape, and color variations of sand extracted after hydrochloric acid digestion; and finally,
j. Selection of areas of interest to be examined by scanning electron microscopy.

CMC has a large assortment of optical microscopes from early 20th century to many latest advanced Nikon, Olympus, Leitz, Zeiss stereozoom and petrographic microscopes and several petrographic sample preparation and photomicrography facilities that can be found in our website at www.cmc-concrete.com.

Figure A2: Top - Optical microscopy laboratory in CMC which houses a variety of optical microscopes including low-power stereomicroscopes, high-power transmitted, reflected, fluorescent, and polarized-light stereozoom microscope, metallurgical microscopes, petrographic microscopes with reflected, transmitted, fluorescent, and polarized light facilities, fluorescent microscopes, inverted microscopes, comparison microscopes, etc. Mortar examinations are done on stereomicroscopes, fluorescent light microscopes, and petrographic microscopes. Bottom – Thin sectioning equipment from Buehler and Microtec that prepare 25 to 30 micron thick thin-sections impregnated in clear, blue, or fluorescent dye-mixed epoxy for observations in petrographic and stereozoom microscopes (left), Nikon Eclipse E600 POL petrographic microscope (2nd from left), Nikon SMZ-10A stereomicroscope (3rd from left) and Olympus SZX-12 transmitted-light stereozoom microscope (rightmost) all having photomicrographic capabilities with advanced high-resolution microscope cameras (e.g., Jenoptik Progres Gryphax, Luminera Infinity series) for documenting compositional and microstructural features from optical microscopical examinations of masonry mortar.

Scanning Electron Microscopy & X-Ray Microanalyses for Mineralogy, Microstructure, and Microchemical Compositions of Mortar

Figure A3: CamScan Series 2 scanning electron microscope in CMC that is attached to a backscatter detector, a secondary electron detector and an energy-dispersive X-ray detector.

Methods followed in scanning electron microscopy and energy-dispersive X-ray fluorescence spectroscopy (SEM-EDS) include: (a) secondary electron imaging (SEI) to determine the surface texture, microstructure and morphology of the examined surface, (b) backscatter electron (BSE) imaging to determine compositions of various phases from various shades of darkness/grayness from average atomic numbers of phases from the darkest pore spaces to brightest iron minerals (via minerals e.g., thaumasite, periclase, ettringite, quartz, dolomite, monosulfate, gypsum, calcite, C-S-H, aluminate, calcium hydroxide, belite, alite, free lime, and ferrite having progressively increasing average atomic numbers and brightness in BSE image), (c) X-ray elemental mapping (dot mapping) of an area of interest to differentiate various phases, (d) point-mode or area (raster)-mode analysis of specific area/phase of interest on a polished thin or solid section, and (e) average compositional analysis of a specific phase or an area on a polished thin or solid section or small subset of a sample.

The main purposes of SEM-EDS analyses of mortar are to: (a) observe the morphology and microstructure of various phases of sand and binder, (b) characterize the typical fine-grained microstructure of hydrated hydraulic components that are too fine to be examined by optical microscopy and not well crystallize to be detected by XRD; (c) determine the major element oxide compositions, and compositional variations of paste, and from that determine the type of binder used, especially to differentiate non-hydraulic calcitic and dolomitic lime mortars from hydraulic lime varieties, natural cements, pozzolans, slag cements, Portland cements, etc. all from their characteristic differences in compositions and hydraulicities (e.g., cementation index of Eckel 1922); (d) determine composition of residual hydraulic phases to assess the raw feed and calcination processes used in binder manufacturing; (e) assess hydration, carbonation, and alteration products of binders, (f) investigate effects of various environmental alterations of paste and its role on properties and performance of mortar, (g) detect salts and other potentially deleterious constituents, (h) detect pigments and fillers, (i) examine compositional variations

across multiple coats of binder installed, etc.; and eventually (i) complement and confirm the results of optical microscopy.

Due to characteristic difference in compositions of pastes made using various binders, e.g., non-hydraulic lime (CaO dominants over all other oxides), variably hydraulic lime (CaO with variable SiO_2 contents depending on hydraulicity), dolomitic lime (high CaO and MgO), natural cement (CaO, SiO_2, Al_2O_3, and MgO contents are high, high MgO and FeO contents are characteristic), and Portland cement (CaO and SiO_2 contents are higher than all other oxides), SEM-EDS analysis of paste is a powerful method for detection of the original binder components in the mortar. Effects of chemical alterations and various chemical deteriorations of a mortar (e.g., lime leaching, secondary calcite precipitates, gypsum deposits, etc.) can also be detected effectively by SEM-EDS.

SEM-EDS analysis is done in a CamScan Series 2 scanning electron microscope (Figure A3) equipped with a high-resolution column 40Å tungsten, 40 kV electron optics zoom condenser 75° focusing lens operating at 20 kV, equipped with a variable geometry secondary electron detector, backscatter electron detector, EDS detector for observations of microstructures at high-resolution, compositional analysis, and quantitative determinations of major element oxides from various areas of interest, respectively. Revolution 4Pi software is used for digital storage of secondary election and backscatter electron images, elemental mapping, and analysis along a line, a point, or an area of interest.

Portion(s) of interest on the polished 50 mm × 75 mm size thin section used for optical microscopy are subsequently coated with a thin conductive carbon or gold-palladium film and placed on a custom-made aluminum sample holder to fit inside the large multiported chamber of CamScan SEM equipped with the eucentric 50 × 100 mm motorized stage. Procedures for SEM examinations are described in ASTM C 1723. Sarkar et al. (2000) described various applications of SEM-EDS in concrete and other construction materials.

Acid Digestion for Siliceous Sand Content and Size Distribution of Sand

Acid digestion is perhaps the most commonly used test of masonry mortar, which is done to: (a) extract sand from mortar by dissolving the binder fractions so that grain-size distribution of sand can be done by sieve analysis, and (b) assess sand content in the mortar. Sand content after acid digestion is determined both from: (a) 1.00 gram of pulverized mortar (finer than 0.3 mm size) digested in 50-ml dilute (1+3) HCl (heated rapidly but below boiling), and, (b) from digesting a representative bulk mortar *per se* (for harder mortars perhaps with light pulverization) in multiple fresh batches of (1+3) HCl at ambient temperature. The former usually gives better result due to small amount, pulverization to easily remove the binder fraction for digestion, and use of rapidly heated acid, whereas latter method requires multiple episodes of digestion in fresh acid and is time-consuming. Acid digestion is also done as the first step to determine soluble silica content in a mortar as described below, which is contributed from the hydraulic components in binder.

All these goals of acid digestion depend on the assumptions that: (i) sand is siliceous in composition and does not contain any acid-soluble constituents (e.g., carbonates), and, (ii) binder entirely dissolves in acid and does not contain any acid-insoluble constituents (gypsum, clay, etc.). Applicability of acid digestion to assess these tasks should therefore be first verified by optical microscopy to confirm the siliceous nature of sand without any appreciable acid-soluble constituents, and calcareous nature of binder, and none without any appreciable argillaceous (clay) constituents.

For grain-size distribution of sand (for mortar found from optical microscopy to contain siliceous sand), a few representative fragments of (preferably not pulverized or lightly pulverized in a porcelain mortar and pestle for harder mortars to break down to smaller size fraction without crushing the sand to retain the original sand size) are selected for digestion in multiple fresh batches of (1+3) dilute hydrochloric acid to dissolve away all binder fractions and extract, wash, and oven-dry the acid-insoluble component of aggregate. Usually multiple episodes of acid digestion in fresh batches of acid and filtration of residues are needed to entirely remove the binder fractions without losing the finer fractions of sand. Sand particles thus extracted are washed, oven-dried, and sieved in an automatic mini sieve shaker (e.g., from Gilson) through various U.S. Sieves from No. 4 (4.75 mm) through 8 (2.36 mm), 16 (1.18 mm), 30 (0.6 mm), 50 (0.3 mm), 100 (0.15 mm), and 200 (0.075 mm) for determination of the size, shape, angularity, and color of sands retained on various sieves. Grain-size distribution

of sand is then compared with ASTM C 144 specifications for masonry sand. Photomicrographs of sand retained on each sieve are then taken with a stereomicroscope to record the sand color. For low amount of mortar, or, for mortar having calcareous sand, image analysis (e.g., ImageJ) on stitched photomicrographs of thin sections taken from multiple areas can be done to determine the sand-size distribution (Elsen et al. 2011).

Cold-Acid & Hot-Alkali Digestion for Soluble Silica Content

Digestion of a pulverized sample of mortar in a cold acid followed by further digestion of residue in a hot alkali hydroxide solution are done to determine the soluble silica content contributed from the hydraulic component of binder, where cold acid digestion usually dissolves most of the binder without affecting the sand, followed by hot alkali hydroxide digestion to dissolve remaining soluble silica from calcium silicate hydrate component of paste or in mortars containing hydraulic binders. The soluble silica content corresponds to the silica mostly contributed from the hydraulic binder components (and a minor amount from any soluble silica component in the aggregates).

For determination of soluble silica content (modified from ASTM C 1324), 5.00 grams of pulverized mortar (finer than 0.3 mm size, without excessive fines) is first digested in 100-mL cold (at 3 to 5°C) HCl and filtered through two 2.5-micron filter papers (filtrate#1). The residue with filter papers is then digested again in hot (below boiling) 75-ml NaOH, and filtered through two 2.5-micron filter papers (filtrate# 2). The two filtrates from acid and alkali digestions are then combined, re-filtered twice with 2.5-micron and then through 0.45-micron filter paper to remove any suspended silica fines, brought to 250 mL volume with distilled water, and then used for soluble silica determination by an analytical method, such as atomic absorption spectroscopy (AAS), inductive coupled plasma optical emission spectroscopy (ICP-OES), or X-ray fluorescence spectroscopy (XRF). Multiple steps of filtrations from 2.5-micron to submicron (0.2-micron pore size) filter papers are necessary to remove any suspended silica that can skew the result. Instrument to be used for such determination must be calibrated with several silica standards in matrices similar to the one used in mortar analysis. CMC uses an XRF unit that is calibrated with filtrates from a series of laboratory-prepared standards of Portland cement and silica sand mortars (moist cured at *w/c* of 0.50 for at least 30 days) having various proportions of cements (SiO_2 contents of standards ranging from 1 to 10%) for determining SiO_2 Kα X-ray intensities from known stoichiometric silica (cement) contents of standards (using exact 5.00 grams as samples) prepared by the same procedure of cold HCl-digestion/filtration/hot NaOH-digestion/2nd filtration/combination of two filtrates/re-filtration steps followed for mortars. Hydraulic binder content is then calculated as: [(soluble SiO_2, weight percent in sample as calculated above) divided by assumed soluble SiO_2 content in binder] ×100, where assumed SiO_2 contents of binders varies, e.g., 21% in Portland cement, 20% in natural cement, 27% in slag cement, 7 to 10% in hydraulic lime, etc., or, more preferably, from the average paste-SiO_2 content determined from SEM-EDS for binder content.

Losses on Ignition for Free & Combined Water Contents, and, Carbonate Content

Losses in weight of a mortar on step-wise heating from ambient to 110°C, 550°C, and 950°C temperatures liberate free water from capillary pore spaces by 110°C, combined water from dehydroxylation of various hydrous phases (calcium silicate hydrate, calcium hydroxide, etc.) by 550°C, and liberation of carbon dioxide from decomposition of carbonated paste and carbonate minerals by 950°C. Such losses in weight are measured by following the procedures of ASTM C 1324 by heating 1.00 gram of pulverized mortar (finer than 0.3 mm) in an alumina crucible in a muffle furnace in a controlled step-wise heating at a heating rate of 10ºC/min. Mortars having hydraulic binders and hydration products of such provide measurable combined water contents after calcination to 550°C whereas those having high calcareous components (high-calcium lime, mortar having calcareous sand) produce high weight loss during ignition to 950°C. Usually, a good correlation is found between weight losses at 550°C from dehydration of combined water and soluble silica contents contributed from hydraulic binders amongst series of mortars containing variable amounts of hydraulic phases.

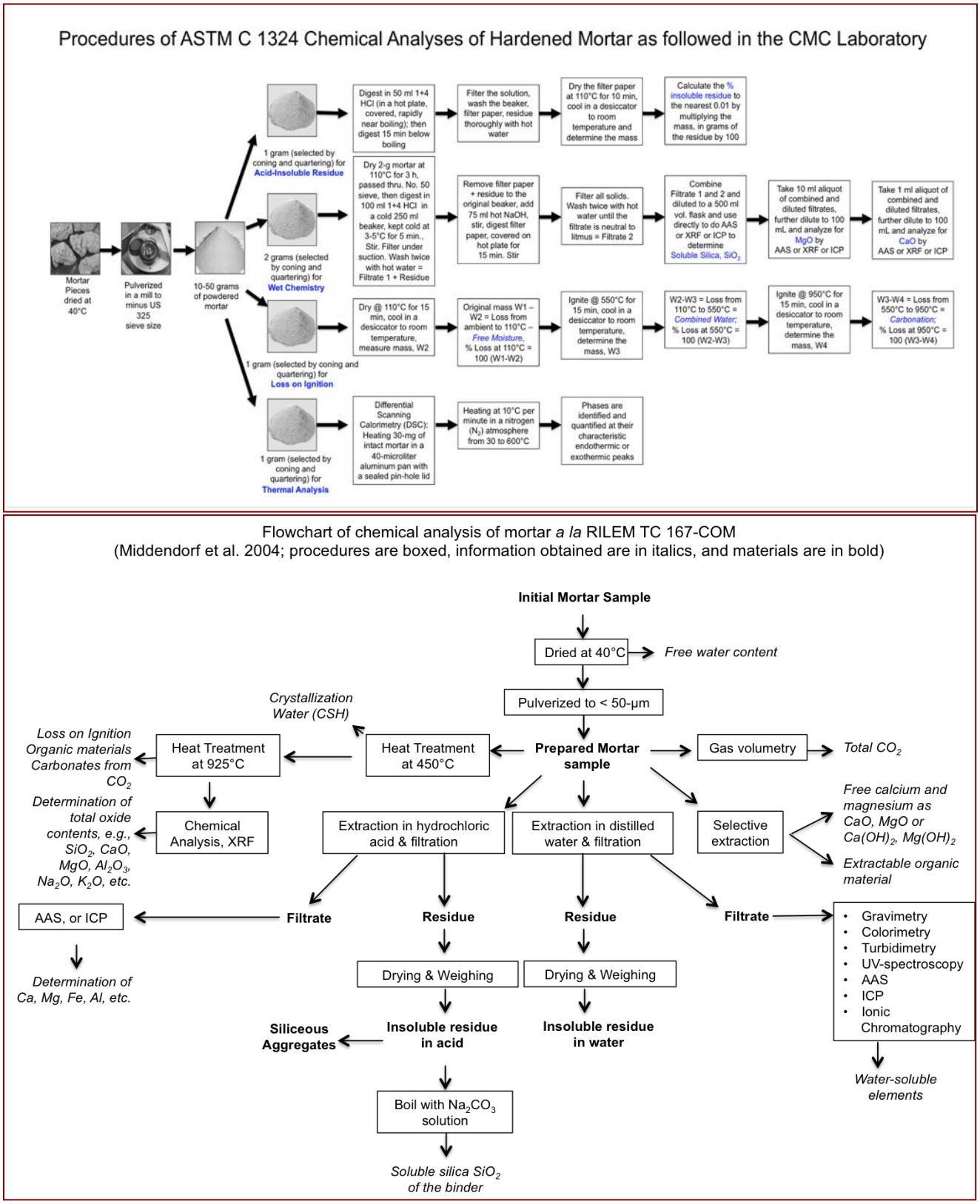

Figure A4: Flow charts for various chemical analyses of masonry mortar according to the US (top, ASTM C 1324) and European (bottom, RILEM) standards.

X-Ray Diffraction for Mineralogy of Mortar

X-ray diffraction (XRD) is a powerful method for: (a) determination of bulk mineralogical composition of mortar, including its aggregate and binder mineralogies (e.g., quartz in sand from major diffraction peaks at 26.65º, 20.85º, 50.14º 2θ, or calcite in sand or carbonated lime binder from major peaks at 29.41º, 39.40º, 43.15º 2θ, or Portlandite in binder from major peaks at 34.09º, 18.09º, 47.12º 2θ); (b) individual primary mineralogy and alteration products of aggregate at various size fractions, and binder phases; (c) detection of dolomitic lime binder from brucite in the mortar from major peaks at 38.02º, 18.59º, 50.86º 2θ; (d) detection of use of lime (portlandite), gypsum (11.59º, 20.72º, 29.11º 2θ), or cement binders from their characteristic mineralogies; (e) detection of any potentially deleterious constituents, e.g., deleterious salts, or efflorescence deposits; (f) detection of a mineral oxide-based pigmenting component in the mortar; and (g) detection of components that are difficult to detect by microscopical methods.

X-ray diffraction can be done on: (i) pulverized (to finer than 45 micron) portion of bulk mortar, or (ii) on the sand extracted from the mortar by acid digestion, if sand has a complex mineralogy, or also (iii) on the binder-fraction by separating the sand from the binder from a carefully ground mortar (in a mortar and pestle) and passing the ground mass through US 200 sieve (75 micron) to collect the fraction rich in binder. Since sands used in mortars are commonly siliceous, XRD pattern of bulk mortar shows quartz as the dominant mineral that surpasses peaks for all other phases (e.g., calcite, dolomite, clay, secondary deposits); hence binder separation is sometimes useful to detect minor minerals of interest (e.g., salts or pigments). For binder mineralogy, mortar is first dried at 40°C to a constant mass, then carefully crushed without pulverizing the sand, and sieved through a 75-micron opening screen to retain sand-rich fraction on the sieve and obtain the passed binder-rich fraction for further pulverization down to finer than 45 micron. Salts and other soft components can also be analyzed from binder fraction. Efflorescence salts on masonry walls are also analyzed routinely in XRD.

For sample preparation, a Rocklab (Sepor Mini-Thor Ring) pulverizer is used to grind mortar sample down to finer than 100 microns. Usually, a few drops of anhydrous alcohol are added to reduce decomposition of hydrous phases from the heat generated from grinding. Approximately 10 grams of sample is ground first in the pulverizer, from which about 8.0 grams of sample is selected, mixed with an appropriate binder (e.g., three Herzog grinding aid pellets from Oxford Instruments having a total binder weight of 0.6 gram for 8 grams of sample for a fixed binder proportion of 7.5 percent); the mixture is then further ground in Rocklab pulverizer and in a McCrone micronizing mill with anhydrous alcohol down to finer than 45-micron size. Approximately 7.0 grams of binder-mixed pulverized sample thus prepared is weighed into an aluminum sample cup and inserted in a stainless steel die press to prepare the sample pellet. A 25-ton Spex X-press is used to prepare 32 mm diameter pellet from the pulverized sample (see Figure A5 for sample preparation). The pressed pellet is then placed in a custom-made circular sample holder for XRD and excited with the copper radiation of 1.54 angstroms. Sample holders made with quartz or silicon are best for working with very small quantities of sample because these holders create no diffraction peaks between 2° and 90° 2θ (Middendorf et al. 2005).

XRD is carried out in a Siemens D5000 Powder diffractometer (θ-2θ goniometer) employing a long line focus Cu X-ray tube, divergent and anti-scatter slits fixed at 1 mm, a receiving slit (0.6 mm), diffracted and incident beam Soller slits (0.04 rad), a curved graphite diffracted beam monochromator, and a sealed proportional counter. Siemens D5000 is equipped with (a) a horizontal stage (fixed), (b) an X-ray generator with CuKα, fine focus sealed tube source, (c) large diameter goniometer (600 mm), low divergence collimator, and Soller slits, (d) fixed detector slits 0.05, 0.2, 0.6, 1.0, 2.0, and 6.0, and (e) Scintillation detector. Generator settings used are 40 kV and 30 mA. Tests are usually run at 2θ from 4° to 64° with a step scan of 0.02° and a dwell time of one second.

The resulting diffraction patterns are collected by DataScan 4 software of Materials Data, Inc. (MDI), analyzed by Jade software of MDI with ICDD PDF-4 (Minerals 2019) diffraction data. Phase identification, and quantitative analyses were carried out with MDI's Search/Match, Easy Quant, and Rietveld modules, respectively.

Figure A5: Siemens D5000 X-ray diffractometer in CMC that is connected to PC through MDI Datascan to collect diffraction data. XRD results are analyzed with MDI Jade software with search-match, easy quant, and Rietveld modules. The bottom row shows sample preparation for XRD where a Sepor Ring pulverizer (2nd from left) followed by McCrone micronizing mill (leftmost one) pulverized the sample to finer than 45-micron size. The pulverized sample is mixed with an appropriate binder and pressed in a 25-ton Spex press to form a 32-mm diameter pellet. Small amount of sample (i.e. not enough to prepare a pellet) is pulverized and spread over a quartz plate coated with a thin film of Vaseline.

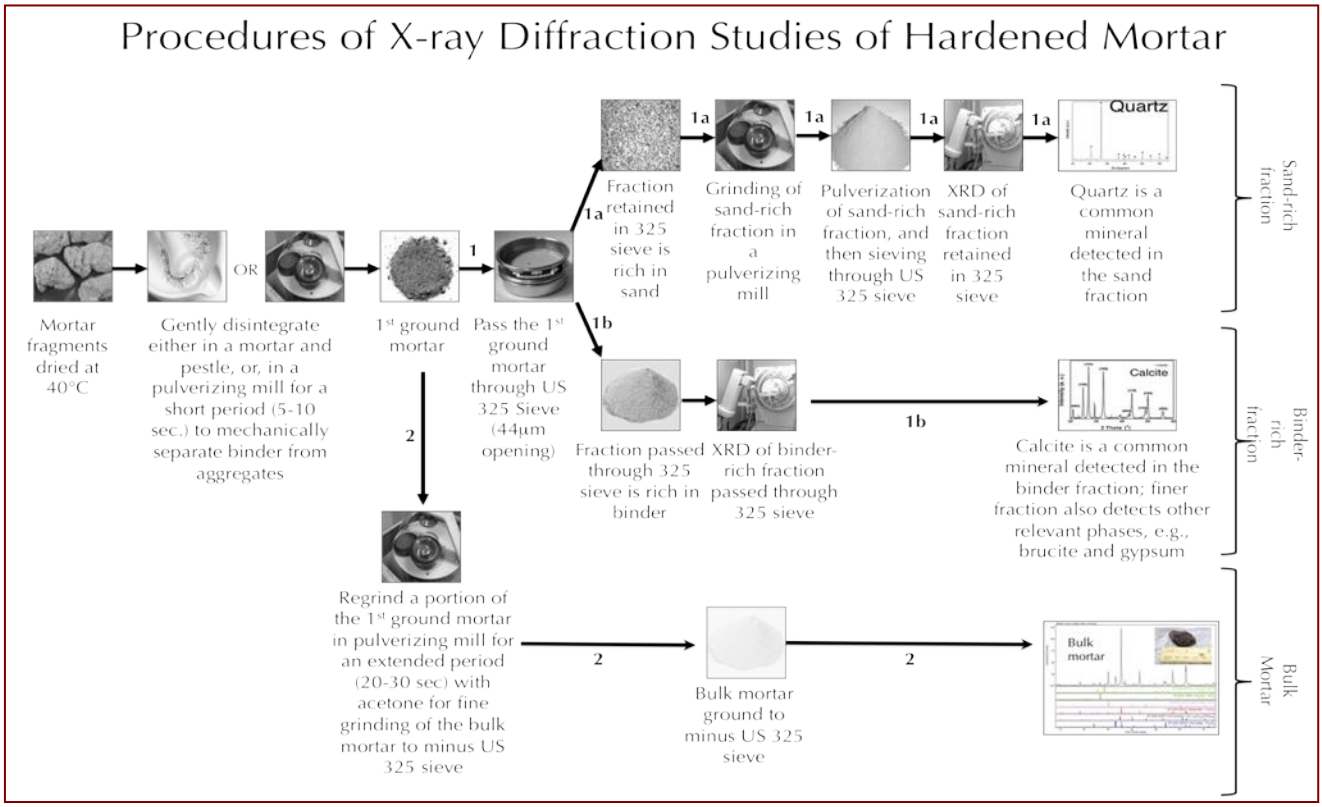

Figure A6: Various procedures for X-ray diffraction analysis of bulk mortar, and sand and/or binder fraction extracted from mortar.

X-Ray Fluorescence Spectroscopy for Chemical Composition of Mortar

X-ray fluorescence (XRF) is used for determining: (a) major element oxide composition of mortar, and (b) soluble silica content of filtrate after digestion of mortar in cold-HCl and hot-NaOH. Major element oxide compositions provide clues about the siliceous sand content of mortar from silica content, type of binder used (e.g., a dolomitic lime or natural cement based binder gives a characteristically higher magnesia than a calcitic lime or Portland cement based binder), calculation of lime content in a cement-lime mortar from bulk CaO content from XRF, effect of alterations and deteriorations (e.g., salt ingress in a mortar from marine environment can be diagnosed from excessive sodium, sulfate, etc.), etc. A series of standards from Portland cements, lime, gypsum, to various rocks, and masonry mortars of certified compositions (e.g., from USGS, GSA, NIST, CCRL, Brammer, or measured by ICP) are used to calibrate the instrument for various oxides and empirical calculations are done from such calibrations to determine oxide compositions of mortars. For mortars with highly unusual compositions (e.g. severely salt-contaminated mortar) a standardless FP calculation is done to determine the best possible composition.

An energy-dispersive bench-top X-ray fluorescence unit from Rigaku Americas Corporation (NEX-CG) is used (Figure A7). Rigaku NEX CG delivers rapid qualitative and quantitative determination of major and minor atomic elements in a wide variety of sample types with minimal standards. Unlike conventional EDXRF analyzers, the NEX CG was engineered with a unique close-coupled Cartesian Geometry (CG) optical kernel that dramatically increases signal-to-noise. By using monochromatic secondary target excitation, instead of conventional direct excitation, sensitivity is further improved. The resulting dramatic reduction in background noise, and simultaneous increase in element peaks, result in a spectrometer capable of routine trace element analysis even in difficult sample types. The instrument is calibrated by using various certified (CCRL, NIST, GSA, and Brammer) reference standards of cements and rocks. The same pellet used for XRD for mineralogical compositions is used for XRF to determine the chemical composition.

Figure A7: Rigaku NEX-CG in CMC, which can perform analyses of 9 pressed pellet or fused bead of mortar. Samples are prepared either as pressed pellet (usually the one already prepared for XRD) or can also accommodate fused bead with proper calibrate of standard beads.

Thermal Analyses for Determination of Hydrous, Carbonate, and Sulfate Phases in Mortar

Thermal analyses encompass: (1) thermogravimetric analysis (TGA), which measures the weight loss in a mortar as it is heated, where weight loss can be related to specific physical decomposition of a phase of interest at a specific temperature that is characteristic of the phase from which both the phase composition and the abundance can be determined; (2) differential thermal analysis (DTA, or first derivative of TGA i.e. DTG) measuring temperature difference between the sample and an inert standard (Al_2O_3) both are heated at the same rate and time where endothermic peaks are recorded when the standard continues to increase in temperature during heating but the sample does not due to decompositions (e.g., dehydration of hydrous or decarbonation of carbonate phases); the endothermic or exothermic transitions are characteristic of particular phase, which can be identified and quantified using DTA (or DTG); and (3) differential scanning calorimetry (DSC), which follows the same basic principle as DTA, whereas temperature differences are measured in DTA, during heating using DSC energy is added to maintain the same and the reference material (Al_2O_3) at the same temperature; this energy use is recorded and used as a measure of the calorific value of the thermal transitions that the sample experiences; this is particularly useful for detection of quartz that undergoes polymorphic (α to β form) transitions and no weight loss.

Thermal analyses are done to determine the presence and quantitative amounts of: (a) hydrates (e.g., combined water liberated from paste dehydration during decomposition of calcium-silicate-hydrate component in paste at 180-190ºC); (b) sulfates (gypsum from decompositions at 125ºC, and 185-200ºC, ettringite at 120-130ºC, thaumasite at 150ºC); (c) brucite from its dehydroxylation at 300-400ºC to confirm the presence of dolomitic lime;

(d) hydrate water from decomposition of Portlandite component of paste at 400-600ºC; (e) quartz from polymorphic transformation (α to β form) at 573ºC; (f) cryptocrystalline calcite in the carbonated lime matrix from decomposition at 620-690ºC, or magnesite at 450-520ºC, or (g) coarsely crystalline calcite e.g., in limestone by decomposition at 680-800ºC or (h) dolomite at 740-800ºC and 925ºC, and (i) phase transition of belite (C_2S) at 693ºC, etc. Phases are determined from their characteristic decomposition temperatures occurring mostly as endothermic peaks or polymorphic transition temperatures as for quartz.

Figure A8: Mettler-Toledo simultaneous TGA/DSC1 unit in CMC that can accommodate 32 samples. The top left photo shows the TGA/DSC1 unit with sample robot for automation as well as the sample holder for pressing aluminum sample holders. Sample is pulverized in a ring pulverizer shown in the bottom left, then a small amount (usually 30-70 mg) is weighed in a precision balance (shown 2nd from left in bottom row) and taken in an alumina sample holder (without lid). For DSC measurements up to 600°C, sometimes sample is taken in an aluminum holder and pressed in sample press (3rd from left in bottom row) and pierced with a needle for release of volatiles from decomposition. A PolyScience chiller (rightmost one in the bottom row) is used to cool the furnace. An ultrapure nitrogen gas is purged through the system during analyses.

Simultaneous TGA and DSC analyses are done in a Mettler Toledo TGA/DSC 1 unit (Figure A8) on 30-70 mg of finely ground (<0.6 mm) mortar in alumina crucible (70 µl, no lid) from 30°C to 1000°C at a heating rate of 10°C/min with high purity nitrogen as purge gas at a flow rate of 75.0 ml/min. By using one of the three removable sensor types the TGA/DSC 1 simultaneously measures heat flow in addition to weight change. The instrument offers high resolution (ultra-microgram resolution over the whole measurement range), efficient automation (with a reliable sample robot for high sample throughput), wide measurement range (measure small and large sample masses and volumes) broad temperature scale (analyze samples from ambient to 1100°C), superior ultra-micro balance, simultaneous DSC heat flow measurement (for simultaneous detection of thermal

events, e.g., polymorphic alpha-to-beta transition of quartz and quartz content), and a gastight cell (ensures a properly defined measurement environment).

Infrared Spectroscopy for Determination of Organic Components in Mortar

Fourier-transform infrared spectroscopy (FT-IR) measures interaction between applied infrared radiation and the molecules in the compounds of interest (Middendorf et al. 2005). Bonds between atoms have distinctive geometrics and natural states of rotation and vibration. Incident infrared radiation will excite these vibrations and rotations when a critical wavelength is reached that can impart energy to the bond. At this point the atomic bond that is being excited will absorb that wavelength of infrared radiation. If the sample is placed between the source of radiation and a detector these times of absorption of infrared radiation can be recorded as reduced intensity and can be related to specific types of atomic bonds characteristic of particular functional groups in compounds (e.g., CO^{3-}group in carbonates). FT-IR is particularly useful for detection of admixture, additives, and polymer resins. FT-IR is used mainly to identify various organic components (functional groups) in mortar (e.g., methyl CH_3, organic acids CO-OH, carbonates CO_3) from their characteristic spectral fingerprints in FT-IR spectrum. FT-IR can also be used for detection of main mineral phases in a hydraulic binder, CSH, carbonates, gypsum, and clays (Middendorf et al. 2005). Organic compounds such as synthetic (e.g., acrylics, polyesters) and natural resins, carbohydrates, colorants, oils and fats, proteins, waxes as well as inorganic compounds, e.g., corrosion products, minerals, pigments, paints, fillers, stone, glass, and ceramics can be detected by this technique.

FT-IR measurements are done in a Perkin Elmer Spectrum 100 FT-IR spectrophotometer (Figure A9) running with Spectrum 10 software. Samples were measured using attenuated total reflection (ATR) on a single bounce diamond/ZnSe ATR crystal. Sample was measured between a frequency range of 4000 to 650 cm^{-1}. Each run was collected at 4 cm^{-1} resolution with Strong Beer-Norton apodization. Data were collected with a temperature-stabilized deuterated triglycine sulfate (DTGS) detector by placing the sample in contact with the ATR crystal and by applying force from the pressure applicator supplied with the ATR accessory. The application of pressure enabled the sample to be in intimate contact with the ATR crystal, ensuring a high-quality spectrum was achieved. Additionally, more conventional KBr pellet is also used for samples on as-needed basis.

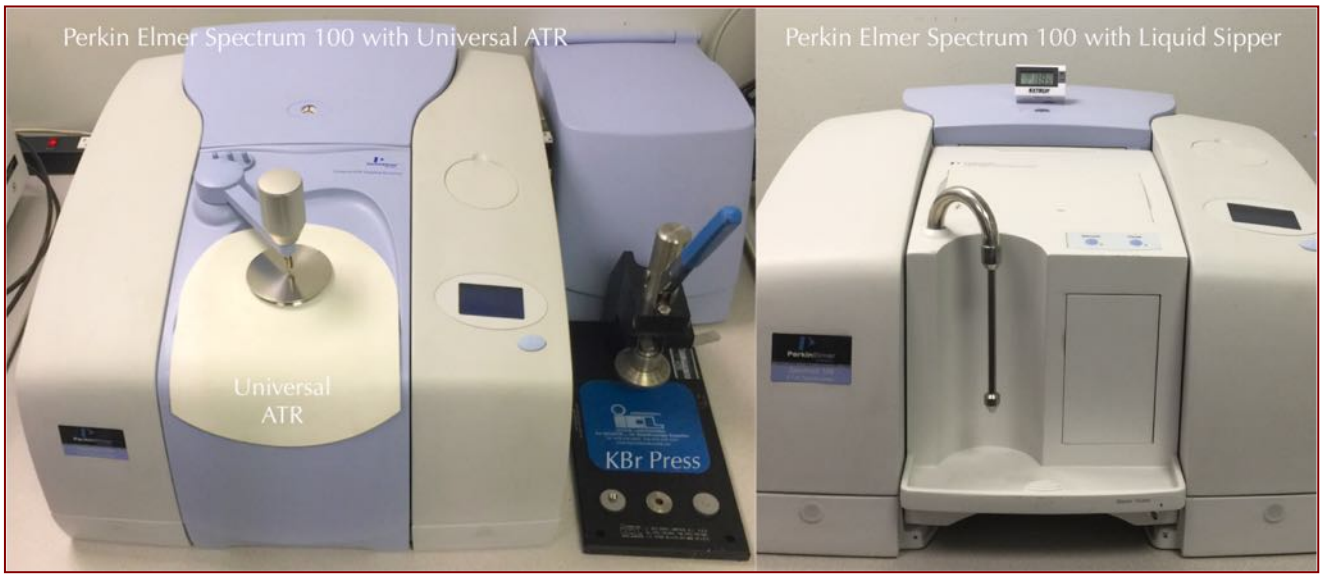

Figure A9: Perkin Elmer Spectrum 100 FT-IR unit in CMC with Universal ATR and Liquid Sipper attachments. The FT-IR unit can analyze a sample as-received in the Universal ATR (left), or as a pressed pellet after mixing with KBr powder in a KBr press (middle), or as a liquid either directly in Universal ATR or in Liquid Sipper unit (right).

Ion Chromatography for Determination of Water-Soluble Cations and Anions in Mortar

Salts can cause various deteriorations in masonry from: (a) mere aesthetic issues of surface efflorescence by precipitation from evaporation of leachates on the masonry wall surfaces followed by atmospheric carbonation of the precipitates where salts deposit as individual crystals or as crust to (b) more serious internal distress in mortar and masonry units from crystallization inside the pores (sub-fluorescence or crypto-fluorescence) from expansive forces associated with crystallization of salt from supersaturated solutions. Some common salts in masonry are calcium carbonates (e.g., calcite, vaterite), magnesium carbonate (magnesite), sodium carbonate hydrate and bicarbonate (thermonatrite, trona, nahcolite), sulphates (gypsum, thenardite, epsomite, melanterite, mirabilite, glauberite, or ettringite and thaumasite from oxidation of sulfides or cement hydrates), and chlorides (halite, sylvite, calcium oxychloride from deicing salts, salt-bearing aggregates, ground water). X-ray diffraction and SEM-EDS can determine many of these salts as long as they are present in detectable amounts.

Ion chromatography is an established technique for analyses of various water-soluble anions and cations in salts (e.g., chloride, sulfate, and nitrate anions, and magnesium, calcium, alkali, ammonium cations) to assess magnitude of environmental impacts on masonry units and mortars, and subsequent effects of such salt ingress. Masonry samples are pulverized, digested in ultrapure deionized water to dissolve all water-soluble salts, then solid residues are filtered out, and finally water-digested filtrates are analyzed by an ion chromatograph.

Procedures followed in Ion chromatography are described in ASTM D 4327 "Standard Test Method for Anions in Water by Chemically Suppressed Ion Chromatography." Briefly, an aliquot of 1 gram of pulverized sample (passing No. 50 sieve) is digested in 50 ml distilled water for 6 to 8 hours on a magnetic stirrer at a temperature below boiling point of water; then the digested sample is filtered through two 2.5-micron filter papers using vacuum, followed by a second filtration through micro-filter (0.2 micron) paper, then the filtrate is either used directly or diluted to 100 to 250 ml with distilled water depending on the concentration of ions, and used for analysis to get ppm-level cations (calcium, magnesium, sodium, potassium, lithium, ammonium), and anions (fluoride, chloride, nitrite, bromide, nitrate, phosphate, and sulfate) in the water-digested sample in Metrohm IC units (Figure A10). The instruments are calibrated against multiple custom-made Metrohm standard solutions having all the ions of interest from 0.1-ppm to 100-ppm levels. To check the accuracy of the instrument, a 50-ppm standard solution was run first prior to the analysis of samples.

Figure A10: Various ion chromatography units used in CMC for determination of water-soluble ions after digestion of pulverized masonry mortar in deionized water to determine various anions (sulfate, chloride, nitrate, nitrite, phosphate, bromide) extracted from mortar.

Information Obtained from Various Laboratory Methods

Information	Optical Microscopy	SEM-EDS	XRD	XRF	Chemical (Gravimetry)	Chemical (Titration & IC)	Sieve Analyses of Sand	Thermal	FTIR
Mortar Sand Type	X	X	X	X					
Sand Composition	X	X	X	X					
Sand Mineralogy	X	X	X						
Sand Soundness	X	X							
Sand Fineness	X						X		
Sand Grading & Color	X						X		
Mortar Binder Type(s)	X	X	X					X	
Binder Composition	X	X	X					X	
Binder Microstructure	X	X							
Portland Cement	X	X	X	X				X	
Hydrated Calcitic Lime	X	X						X	
Dolomitic Lime	X	X	X					X	
Hydraulic Lime	X	X						X	X
Masonry Cement	X	X							
Natural Cement	X	X							
Carbonation	X	X	X					X	X
Carbonated Paste vs. Carbonate Sand	X							X	
Fillers	X	X						X	
Organic Components		X						X	X
Surface Treatments	X	X				X			X
Clay Contaminants	X		X					X	X
Mortar Type	X	X			X				
Masonry Discoloration	X	X	X	X		X		X	
Masonry Cracking	X	X	X						
Mortar Softening	X	X			X				
Mortar Crumbling	X	X	X		X				
Mortar Cracking	X	X	X	X			X	X	
Mortar Discoloration	X	X	X	X		X			
Mortar Shrinkage, Stiffening	X	X							
Bond to Masonry	X	X							
Masonry Efflorescence	X	X	X	X					

Information	Optical Microscopy	SEM-EDS	XRD	XRF	Chemical (Gravimetry)	Chemical (Titration & IC)	Sieve Analyses of Sand	Thermal	FTIR
Salt Attack	X	X	X			X		X	
Lime Leaching	X	X				X			
Polymer		X						X	X
Mix Proportion	X	X	X	X	X				
Tuckpointing Mortar Suggestions	X	X	X	X	X		X	X	X
Miscellaneous Failure Analysis	X	X	X	X	X			X	X

Table 9: Information obtained from various laboratory methods.

Steps Followed in Laboratory Analyses

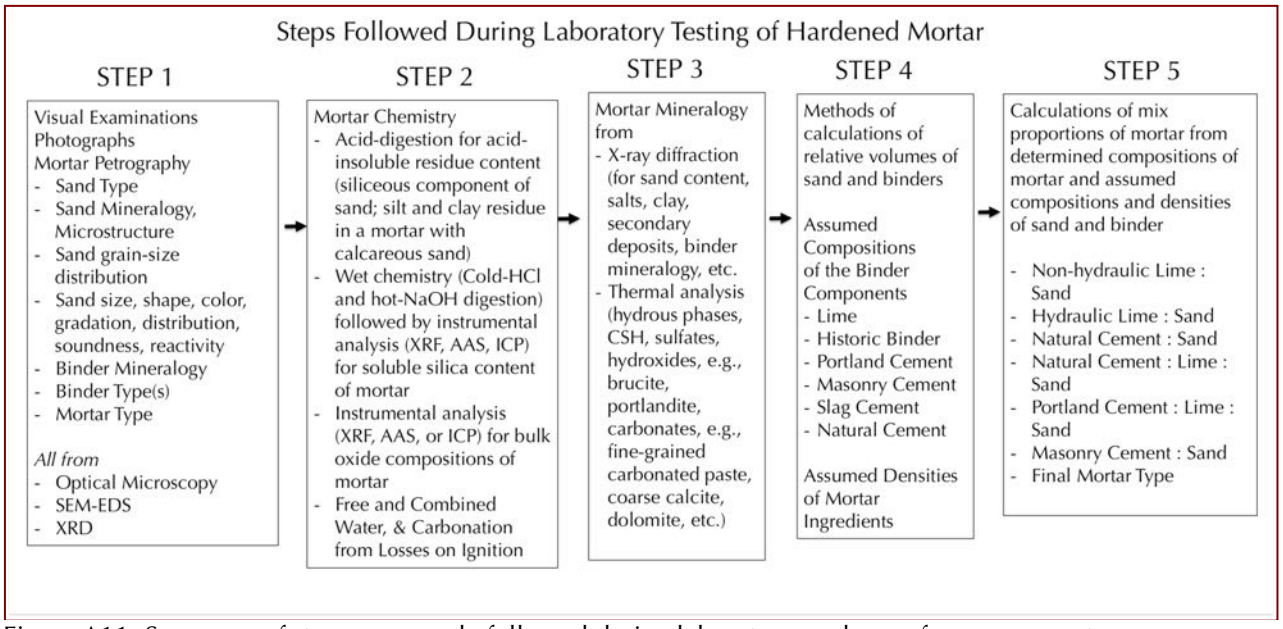

Figure A11: Sequence of steps commonly followed during laboratory analyses of masonry mortars.

Mix Calculations from Petrography & Chemical Analyses of Mortar

ASTM C 1324 provides procedures of calculations of volumetric proportions of Portland cement, lime, and sand in a modern cement-lime mortar containing siliceous or calcareous sand, and proportion of Portland cement in a masonry cement and masonry cement to sand proportion in a masonry cement mortar. Such approaches can be extended for other mortars having other binder types from non-hydraulic lime, to hydraulic lime, to natural cement, slag cement etc. These approaches, however, are based on many underlying assumptions that are important to know and verify against the results of laboratory tests to validate for a particular mortar, especially of historic nature. For example, for mix calculations in a common modern-day Portland cement-lime-silica sand mortar, such approach assumes fixed composition of cement (21% silica and 63.5% lime), fixed composition of magnesian or dolomitic lime (brucite), negligible effect of pozzolanic and other cementitious materials, negligible soluble silica or lime contribution from sand, etc. The following Figure provides examples of various approaches of mix calculations for mortars containing a wide range of sand and binder.

Binders and Sand	Assumed Compositions and Methods of Calculation	Assumed Bulk Density (lbs./ft^3)
High-Calcium Non-hydraulic Lime	[CO_2 data from loss on ignition at 950°C divided by 0.594], where 0.594 is ratio of molecular weights of CO_2 to $Ca(OH)_2$ i.e. 44/74.09	40
Magnesian Non-hydraulic Lime	[100 times (brucite content in mortar from TGA/DSC/5.8)], assuming magnesian lime has 71% CaO and 4% MgO, or 5.8% brucite, since ratio of molecular weights of brucite to MgO (58.32 / 40.32) is 1.447	40
Dolomitic Non-hydraulic Lime	[100 times (brucite content in mortar from TGA or DSC divided by 42)], assuming dolomitic lime has 41% CaO and 29% MgO, or 42% brucite, since ratio of molecular weights of brucite to MgO (58.32 / 40.32) is 1.447	40
Calcitic or Magnesian Hydraulic Lime	[100 times (soluble silica in mortar/0.07] assuming hydraulic lime has 7% SiO_2, or average SiO_2 content calculated from SEM-EDS data of paste	40
Dolomitic Hydraulic Lime	[100 times (soluble silica in mortar/0.07] assuming hydraulic lime has 7% SiO_2, or average SiO_2 content calculated from SEM-EDS data of paste Or [100 times (brucite content in mortar from TGA/DSC/38)], assuming lime has 38% CaO and 26% MgO, or 38% brucite, since ratio of molecular weights of brucite to MgO (58.32 / 40.32) is 1.447	40
Portland Cement in Cement-Lime Mortar	100 × [Soluble silica in mortar / 21.0], assuming 21% silica in Portland cement	94
Calcitic Lime in Portland Cement-Lime Mortar	Lime content = 1.322 × CaO assignable to Lime, which is [CaO content of Mortar – (CaO assignable to portland cement, which is portland cement content × 0.635, assuming 63.5% CaO in portland cement)], where the factor 1.322 comes from ratio of molecular weights of $Ca(OH)_2$ to CaO i.e. 74.09/56.03	40
Dolomitic Lime in Portland Cement-Lime Mortar	100 times (brucite content in mortar from TGA/DSC/42)], assuming dolomitic lime has 41% CaO and 29% MgO, or 42% brucite, since ratio of molecular weights of brucite to MgO (58.32 / 40.32) is 1.447	40
Slag Cement	100 × [Soluble silica in mortar / 27.0], assuming 27% silica in slag cement, or average SiO_2 content determined from SEM-EDS data	90
Natural Cement	100 × [Soluble silica in mortar / 20.0], assuming 20% silica in natural cement, or average SiO_2 content determined from SEM-EDS data	75
Masonry Cement	(i) 100 – [Sand + Total Water], if sand is all siliceous and hence sand content is obtained directly from the acid-insoluble residue content; (ii) PC content (from the soluble silica data) divided by factor 0.50, 0.66, or 0.75 with an assumed masonry cement type of N, S, or M, respectively. MC Type (M, S, N) is determined from PC/MC = 0.75 (for M), 0.66 (for S), or 0.50(for N) – if sand has calcareous component	70 (Type N) 75 (Type S) 80 (Type M)
Gypsum Plaster	Gypsum content from XRD or thermal analysis times 0.843 (ratio of molecular weight of plaster to gypsum)	70
Sand	If sand contains acid-soluble component (carbonates), Sand content = 100 – [Total Binder + Total Water from LOI to 550°C i.e. free plus hydrated water]; If sand has no acid-soluble component (i.e. all siliceous sand) Sand content is directly obtained from the acid-insoluble residue content	80

Figure A12: Various procedures followed for calculations of binder-to-sand volumetric proportions from (a) the determined sand and binder, (b) calculated contents of ingredients, and (c) assumed bulk densities of sand and binders.

Flow Chart of Procedures Followed in Laboratory Analyses of Masonry Mortars

Finally, Figure A13 provides step-by-step procedures followed during laboratory analyses of masonry mortars.

Laboratory Analyses of Masonry Mortars

Initial Mortar (50 to 100 grams) [Photographed with digital camera & flat-bed scanner, As-received condition, total weight, and dimensions of largest piece are documented]

Intact Pieces (20+ g)

1. *Optical Microscopy*

I. Perform visual examination of mortar as received, then saw-cut and fractured surfaces and with a low-power stereomicroscope,
II. Take digital and flat bed scanner photos of intact piece(s),
III. Encapsulate the piece for thin section microscopy in a flexible mold with a low-viscosity colored or fluorescent dye-mixed epoxy to highlight voids, pores, cracks, etc.,
IV. Prepare thin section (< 30 micron thickness) and polish the thin section for optical and SEM-EDS analyses,
V. Scan the thin section on a flat-bed scanner with the thin section residue,
VI. Take transmitted light high-power stereo-zoom photomicrographs of thin sections from different areas to be stitched to determine volumes and size distributions of pore spaces and sand grains by Image J,
VII. Take plane and crossed polarized-light photomicrographs of sand and binder fractions in thin section from a petrographic microscope and determine areas for further studies by SEM-EDS,
VIII. Do detailed petrographic examinations to determine the sand and binder compositions, sand mineralogy and texture, binder phases, residual binders, alterations, and products of any deleterious reactions, immersion mounts of specific areas of interest, etc.

2. *SEM-EDS*

I. Put conductive coating only on the portion of polished thin section intended for SEM-EDS studies from optical microscopy,
II. Take backscatter and/or secondary electron images, and if needed X-ray elemental maps,
III. Select multiple areas on paste to determine oxide compositions and Eckel's cementation indices,
IV. Tabulate the paste composition variations across the backscatter/secondary electron image.
V. Determine chemical compositions of resides left from the original components of the binders, as well as the hydration and carbonation and other alteration products

Lightly hand-ground in a Mortar & Pestle (30+ g)

3. *Acid Digestion - Sand Color & Sand Size Distribution* (10 g)

I. Take 10 g. of mortar lightly ground in mortar & pestle and digest in HCl (1+3) in a 250 ml beaker on a magnetic stirrer until all sand separates and settles at the bottom of beaker,
II. Filter all through two 2.5 micron filter paper, wash the beaker, filter paper, and all sand residue with dist. water,
III. Dry the residue at 110°C in an oven for 10 min., gently brush out from the filter paper and collect, then sieve the entire sand residue through No. 4 through 200 sieves in a mini sieve shaker (e.g., from Gilson),
IV. Determine the mass retained on each sieve, and on the pan (finer than No. 200 sieve),
V. Take photomicrographs of sand particles retained on each sieve for sand color variations in a stereomicroscope.

4. *Acid & Alkali Digestion – Soluble Silica for Hydraulic Binder* (5 g)

I. Grind 10 g of lightly ground fraction from mortar & pestle in a WC pulverizer for 30 sec.
II. Sieve thru. No. 50 sieve, collect the fraction passing the sieve,
III. Re-grind the residue retained on sieve for 15 sec. and mix thoroughly with the previous fraction;
IV. Use 5.00 g of thus prepared powder (passing No. 50 sieve) for digestion in 100 ml cold (3-5°C/38-41°F) HCl (1+4) in a 250 ml beaker for 15 min. on a magnetic stirrer,
V. Filter thru. two 2.5 micron filter paper and keep the filtrate# 1,
VI. Digest the residue with filter paper in 75 ml hot NaOH (below boiling) on hot plate for 15 min. on magnetic stirrer,
VII. Cool down to room temp. and filter thru. two 2.5 micron filter paper and collect filtrate# 2,
VIII. Combine these two filtrates, filter the combined filtrates thru. two 2.5 micron filter paper to remove any suspended silica (especially for sand-rich mortars, or if mortar is grounded too long); then dilute to 250 ml in a volumetric flask with dist. water, an aliquot (about 10 ml) is then used for XRF for soluble silica determination against the calibrations with standard PC mortars of known soluble silica contents prepared in the same way.

5. *Acid Digestion – Acid-Insoluble Residue Content for Siliceous Sand Content* (2 g)

I. Take 1-2 g of prepared mortar powder from Step 4 iii (passing No. 50 sieve) and digest in 50 ml HCl (1+3) in a 250 ml beaker (covered) on a hot pate rapidly near boiling, then 15 min. at a temp. below boiling, then cool down to room temperatures,
II. Filter thru. two pre-weighed 2.5 micron filter papers, washing the beaker, paper, and residue thoroughly with hot water,
III. Dry the filter paper at 110C for 10 min, cool in a desiccator to room temp. and measure the weight.
IV. Subtract from mass of dry filter paper to determine acid-insoluble residue content.

6. *Chemical Analysis – Loss On Ignition for Free and Combined Water Content, and Carbonate plus Carbonation* (2 g)

I. Take 1-2 g (W_1) of prepared mortar powder from Step 3 iii (passing No. 50 sieve) in a tarred porcelain crucible (keep a record of mass of the empty crucible),
II. Dry at 110°C for 15 min in a muffle furnace pre-set to 110°C, cool in a desiccator to room temp. and measure the mass (W_2) by subtracting the empty crucible mass from the total mass,
III. Ignite at 550°C for 15 min. in the muffle furnace pre-set to 550°C, cool in a desiccator to room temp. and measure the mass (W_3) by subtracting the empty crucible mass from the total mass,
IV. Ignite at 950°C for 15 min. in the muffle furnace pre-set to 950°C, cool in a desiccator to room temp. and measure the mass (W_4) by subtracting the empty crucible mass from the total mass,
V. Calculate the losses on ignition at 110°C, 550°C, and 950°C for free water, combined water, and carbonate plus degree of carbonation, respectively.

7. *Mineralogy of Bulk Mortar, Extracted Sand, Extracted Binder, or Salt from XRD* (at least 8 g)

I. Weigh 8.00 g of mortar (or extracted sand or binder as needed) lightly ground in a mortar & pestle, add three grinding/pelletizing aid tablets (e.g., from Oxford Instruments) and pulverize in a suitable mill to minimize contamination (e.g., Rocklab pulverizer with WC bowl or McCrone Micronizing Mill with agate) for 3 min. with anhydrous alcohol to get <45 micron size particles passing U.S. No. 325 sieve,
II. Take 6.8 to 7.0 g. of ground <45 micron prepared mass in an aluminum sample holder inside a stainless steel die to prepare a 32 mm pellet with 25 ton pressure for 1 min,
III. Use the prepared pellet for XRD and then use the same pellet for XRF.
IV. Do XRD on the binder-rich fraction, or salt either on a shallow-depth sample holder or preferably on a zero background quartz plate for small volume of sample.

8. *Bulk Mortar's Composition from X-Ray Fluorescence (XRF)* (same pellet used in XRD)

I. Use the same pellet prepared for XRD in the XRF, or, use a fused bead if sample volume is low to prepare a pellet. In either method, have calibrations of measured oxides with adequate standard.
II. XRF can also be used with proper calibrations for soluble silica determination on the filtrates after acid and alkali digestions, as described in Section 3.

9. *Thermal Analyses* (0.1 g), TGA, DTG, DSC, DTA, for quantitative analysis of various hydrous, sulfate, and carbonate phases in mortar, content of dolomitic lime added from the brucite content in mortar as determined from TGA or DSC, etc.

I. Simultaneous TGA and DSC analyses can be done on 30-70 mg of finely ground (<0.6 mm) mortar in alumina crucible (70 µl, no lid) from 30°C to 1000°C at a heating rate of 10°C/min with high purity nitrogen as purge gas at a flow rate of 75.0 ml/min .

10. *Infrared Spectroscopy,* for determination of various organic additives, and clays in mortar

I. Take an aliquot of powder prepared for thermal analysis and use that in Universal ATR of FTIR.
II. Alternately, digest a pulverized mortar in acetone to extract the organic additive and analyze the liquid in FTIR for characteristic functional groups.

11. *Ion Chromatography of Water-Soluble Salts* (1 g)

I. Take an aliquot of 1 gram powder prepared for chemical analysis (i.e. passing U.S. No. 50 sieve), digest in distilled or deionized water for at least 24 hours in a beaker on a magnetic stirrer, filter the solid residues out to collect the filtrate and analyze the filtrate for soluble salts (chloride, sulfate, nitrate, nitrite, phosphate, etc.) by ion chromatography.

Figure A13: Step-by-step procedures followed for various laboratory analyses of masonry mortars.

APPENDIX B -
OPTICAL MICROGRAPHS OF THIN SECTIONS OF BRICKS AND MORTARS

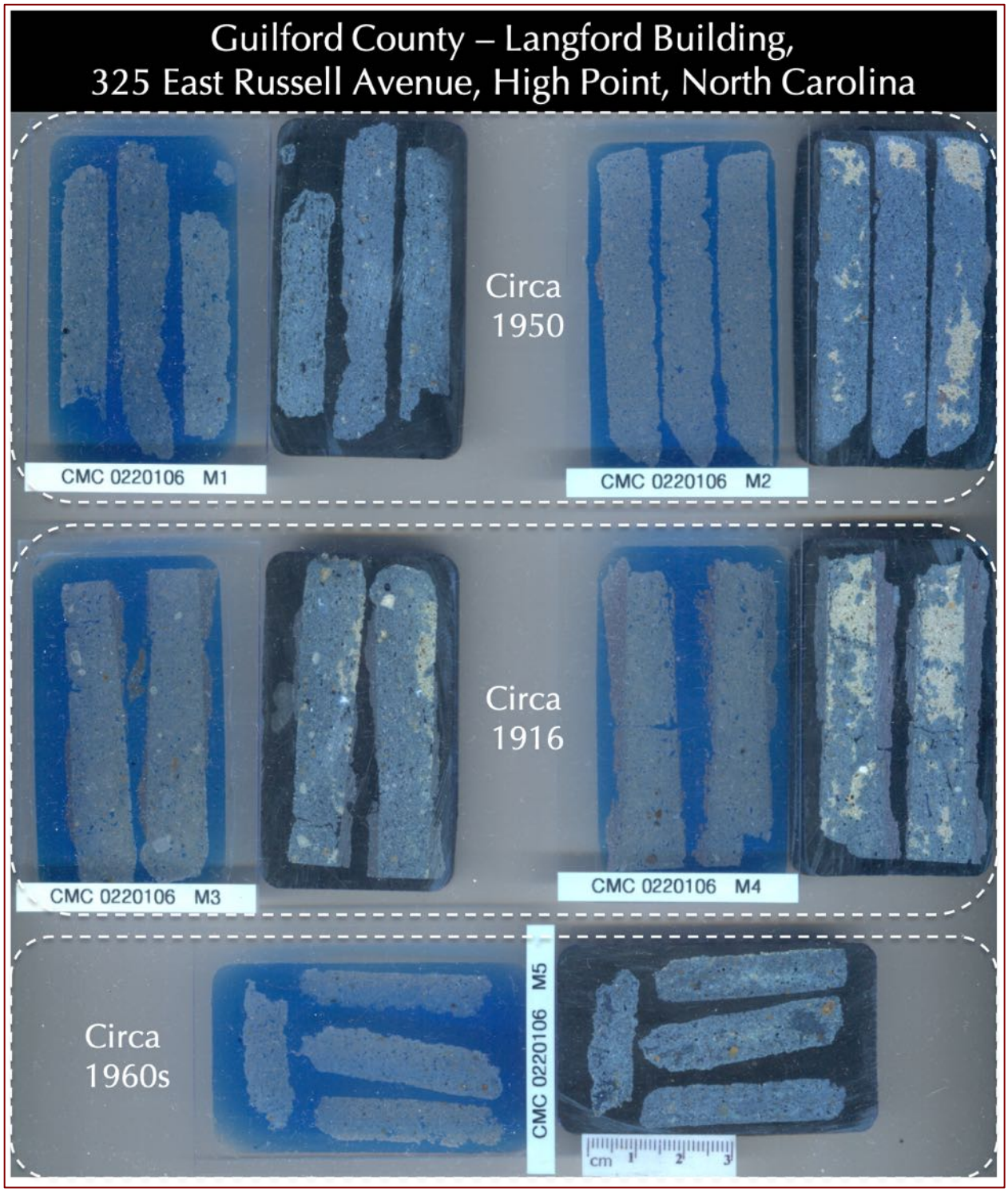

Figure B1: Blue dye-mixed epoxy-impregnated thin sections and residues left after preparation of thin sections of representative pieces of masonry mortars. Thin sections were polished and examined in: (a) high-power stereo-zoom microscope in transmitted, reflected, and polarized light modes, (b) in a petrographic microscope in plane and cross polarized light modes, and, eventually, after selecting areas of interest from opitcal microsopy, thin sections were coated with thin film of conductive gold film and examined in (c) a scanning electron microscope with attached secondary electron detector, backscatter electron detector, and energy-dispersive X-ray fluorescent detector.

Micrographs of Thin Section of Natural Cement Mortar M1 from 1950s

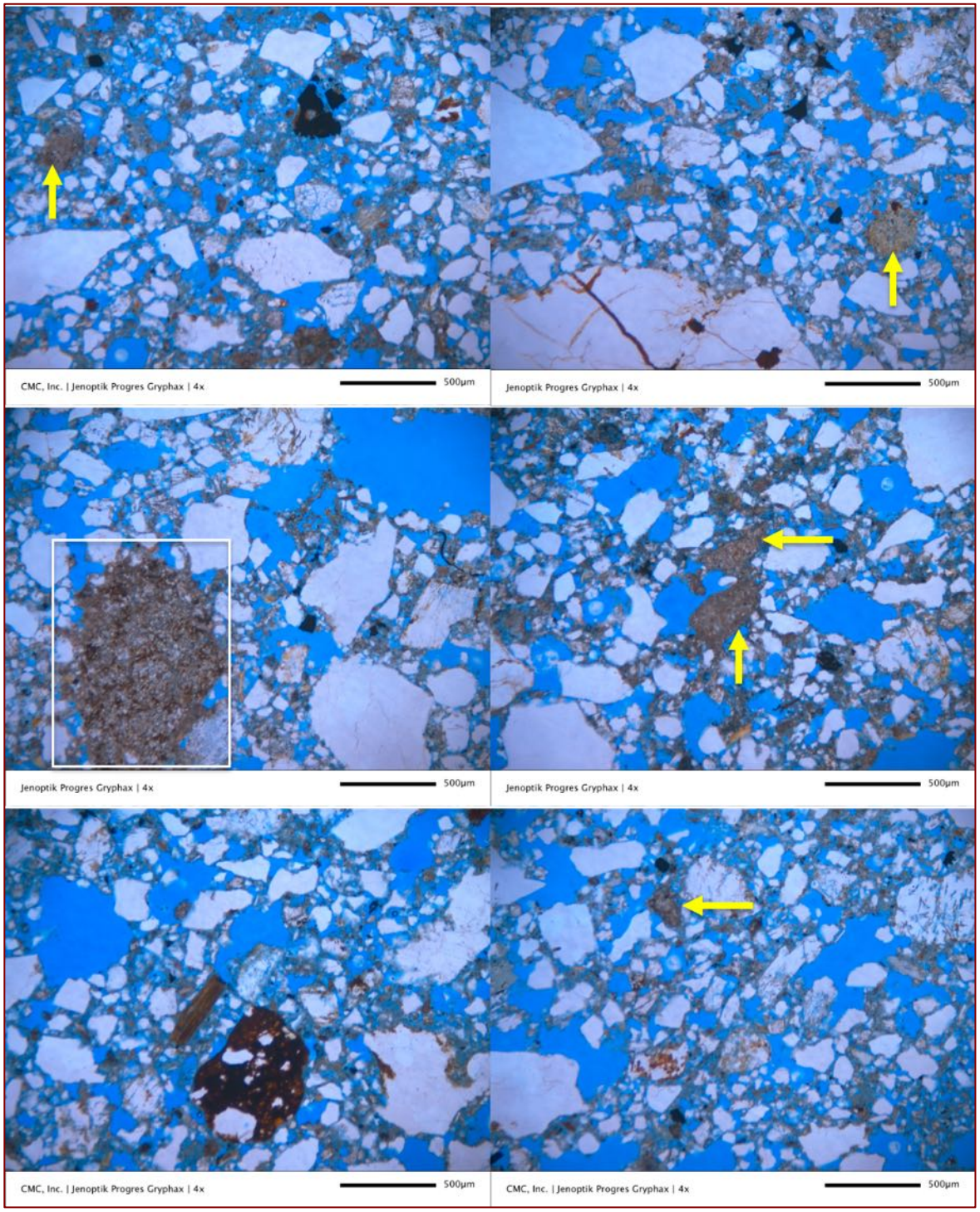

Figure B2: Mortar M1 (1950s) Natural cement mortar - Micrographs of thin section of 1950s natural cement mortar viewed in plane polarized light mode in a petrographic microscope showing: (a) crushed siliceous natural sand aggregate particles that are well-graded, well-distributed, and have been sound during their service, (b) interstitial paste that is highly porous and contains many hydrated and residual phases of the original binder components, and (d) many brown colored variably calcined residual impure dolomitic limestone raw feeds (some are marked in arrows and boxed) that are indicative of use of natural cement binder in the mortar. Notice many impure dolomitic limestone particles left from calcination process are sand-sized.

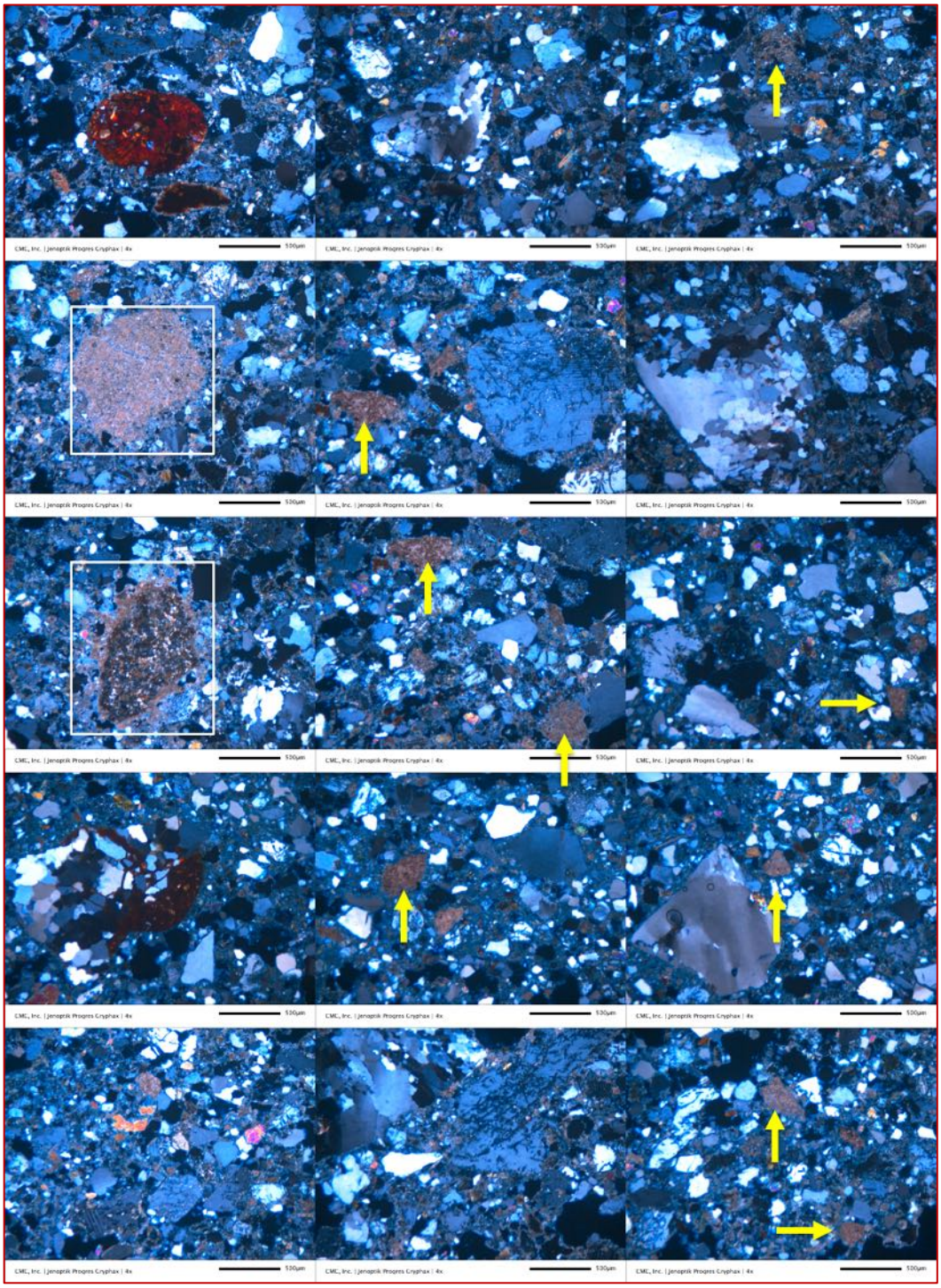

Figure B3: Mortar M1 (1950s) Natural cement mortar - Micrographs of thin section of 1950s natural cement mortar viewed in cross polarized light mode in a petrographic microscope showing: (a) crushed siliceous natural sand aggregate particles that contain major amounts of strained and unstrained quartz and quartzite, subordinate amount of feldspar, and trace amounts of colored mica and mafic minerals; sand particles are well-graded, well-distributed, and have been sound during their service, (b) interstitial paste that is highly porous and contains many hydrated and residual phases of the original binder components, and (d) many brown colored variably calcined residual impure dolomitic limestone raw feeds (some are marked in arrows and boxed) that are indicative of use of natural cement binder in the mortar. Notice many impure dolomitic limestone particles left from calcination process are sand-sized.

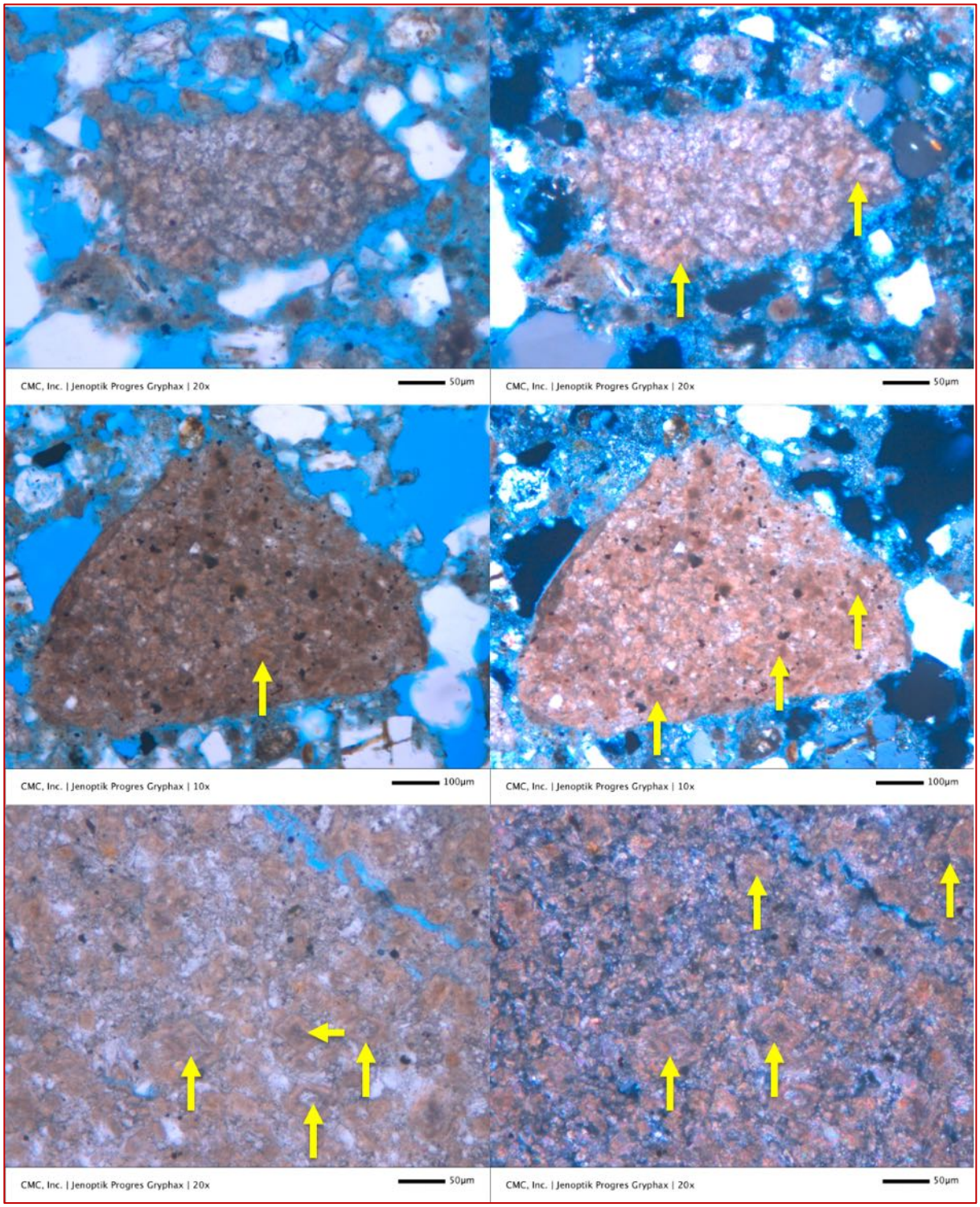

Figure B4: Mortar M1 (1950s) Natural cement mortar - Micrographs of thin section of 1950s natural cement mortar viewed in plane polarized light mode in a petrographic microscope (except the bottom right photo that was taken in crossed polarized mode of the correspinding photo at bottom left) showing: (a) internal mineralogy and texture of impure dolomitic limestone particles that were used as raw feed in the kiln for production of natural cement, (b) many rhombic-shaped dolomite crystals in the dolomitic limestone particles, many of which are marked with arrows, and (c) interstitial calcite and siliceous component from silica and clay minerals in the matrix of limestone (especially seen in the bottom row photos) that upon calcination and reaction with calcined calcite and dolomite have provided the necessary hydraulicity of natural cement.

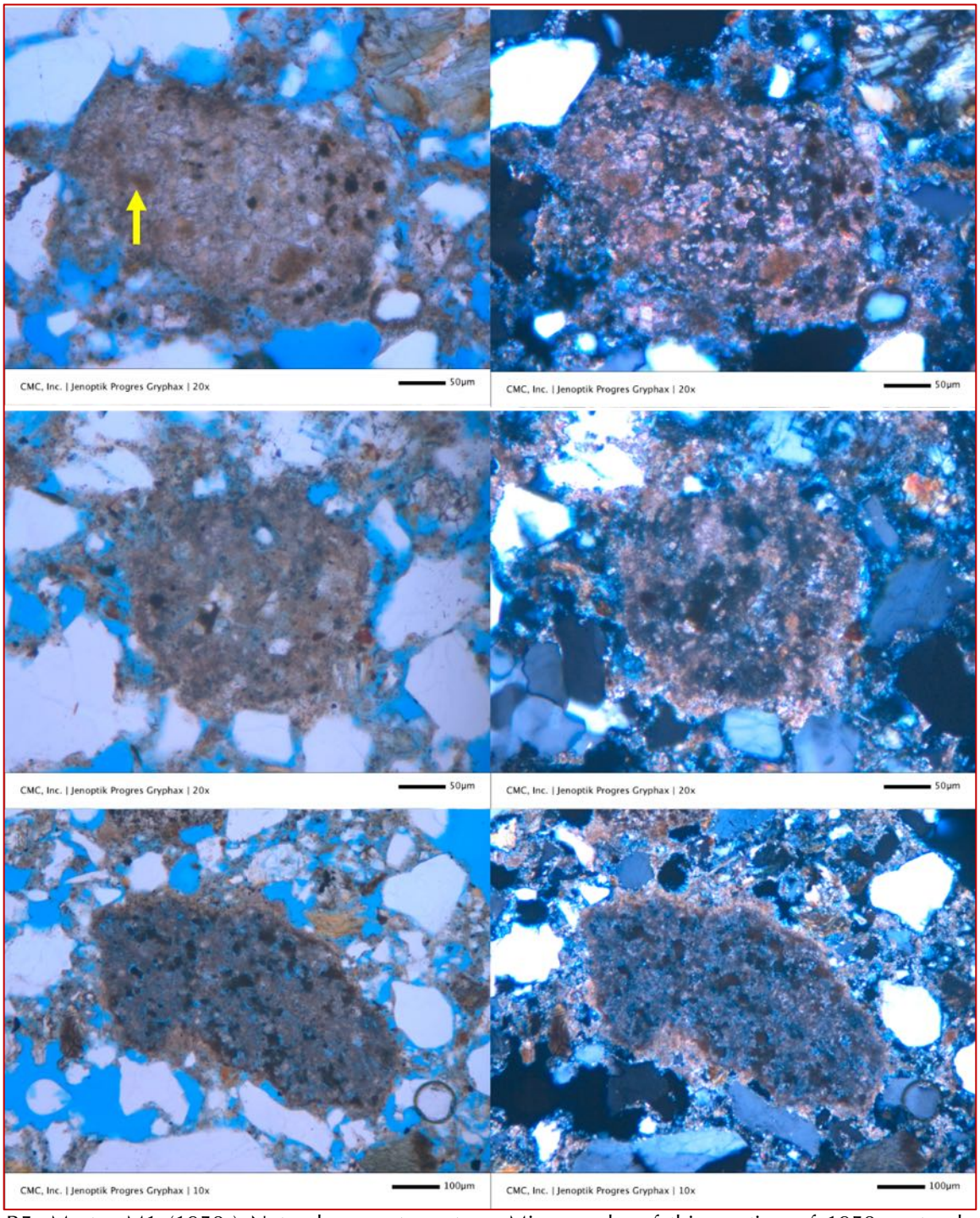

Figure B5: Mortar M1 (1950s) Natural cement mortar - Micrographs of thin section of 1950s natural cement mortar viewed in plane (left column) and corresponding crossed (right column) polarized light mode in a petrographic microscope showing: (a) internal mineralogy and texture of impure dolomitic limestone particles that were used as raw feed in the kiln for production of natural cement, (b) a few rhombic-shaped dolomite crystals in the dolomitic limestone particles, one of which is marked with an arrow in the top left photo, and (c) interstitial calcite and siliceous component from silica and clay minerals in the matrix of limestone (especially seen in the bottom row photos) that upon calination and reaction with calcined calcite and dolomite have provided the necessary hydraulicity of natural cement. Particles in the middle and bottom row show advanced stages of calcination and subsequent hydration where most of the matrix contains amorphous phase, appears near-isotropic in crossed polarized light mode, which is the main phase responsible for hydraulicity of natural cement.

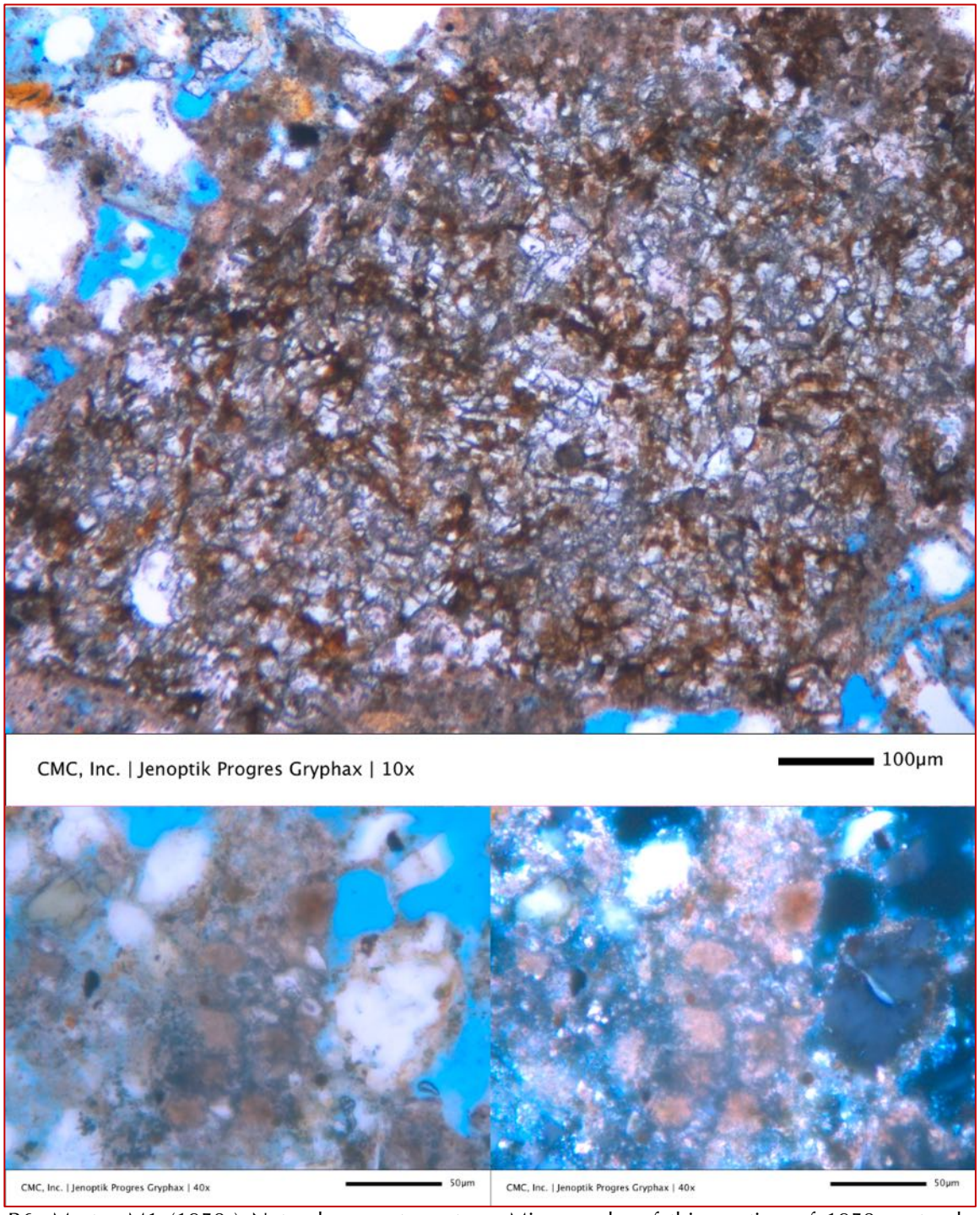

Figure B6: Mortar M1 (1950s) Natural cement mortar - Micrographs of thin section of 1950s natural cement mortar viewed in plane polarized light mode in a petrographic microscope in the top, and in plane and corresponding crossed polarized mode (bottom) showing: (a) internal mineralogy and texture of calcined impure dolomitic limestone particles that were used as raw feed in the kiln for production of natural cement, (b) many calcium-magnesium-alumina-silicate phases in the top photo formed from calination of dolomitic limestone, and (c) interstitial calcite and siliceous component from silica and clay minerals in the matrix of limestone (especially seen in the bottom row photos) that upon calination and reaction with calcined calcite and dolomite have provided the necessary hydraulicity of natural cement. The particle in the bottom row shows near-isotropic nature of the matrix in the crossed polar mode due to calcination and subsequent hydration of the interstitial amorphous phase.

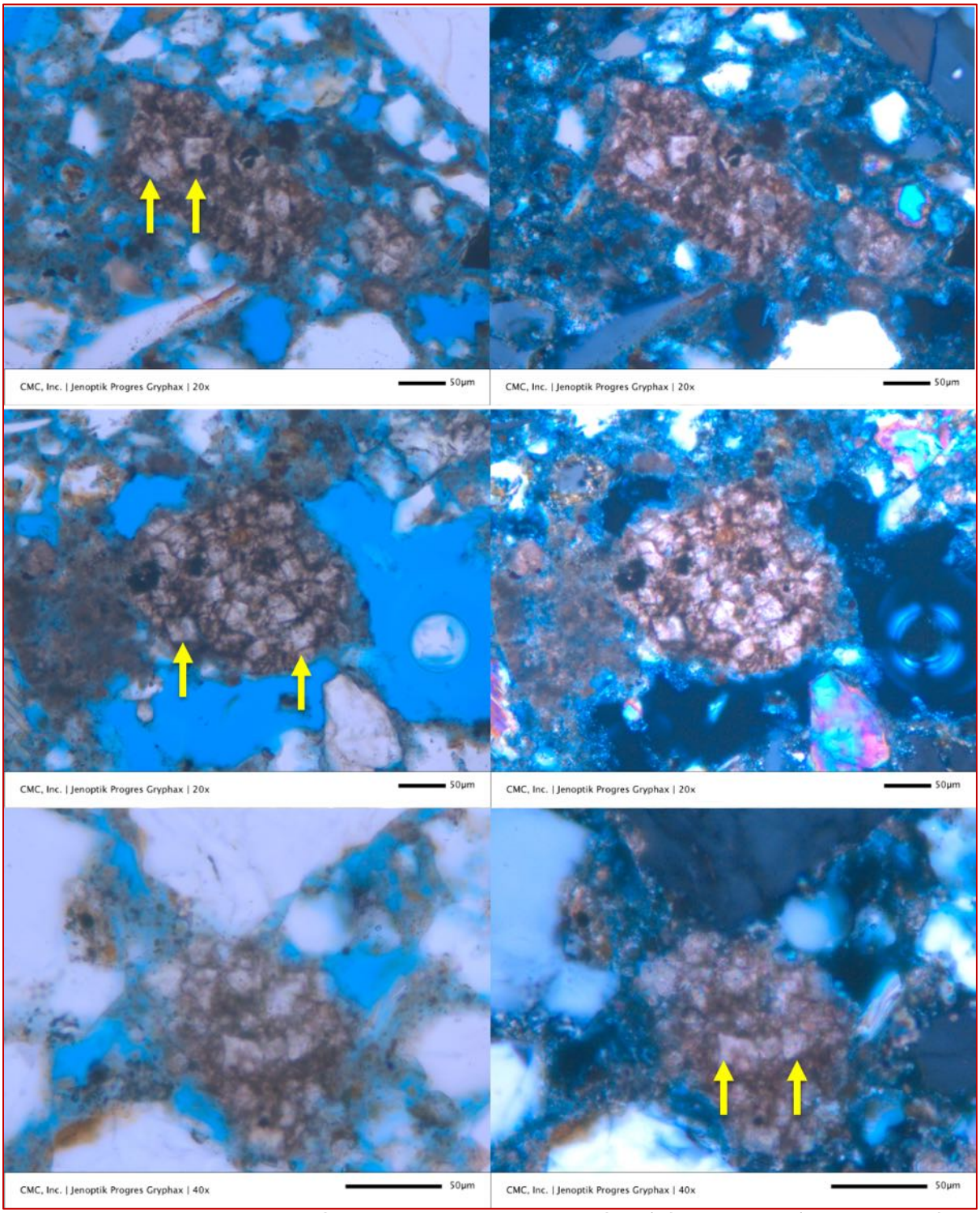

Figure B7: Mortar M1 (1950s) Natural cement mortar – Micrographs of thin section of 1950s natural cement mortar viewed in plane (left column) and corresponding cross (right column) polarized light mode in a petrographic microscope showing: (a) internal mineralogy and texture of impure dolomitic limestone particles that were used as raw feed in the kiln for production of natural cement, (b) many rhombic-shaped dolomite crystals in the dolomitic limestone particles, many of which are marked with arrows, many show dark brown rims around the rhombs due to migration of iron phases in the dolomite during calcination process, and (c) interstitial calcite and siliceous component from silica and clay minerals in the matrix of impure limestone that upon calcination and reaction with calcined calcite and dolomite have provided the necessary hydraulicity of natural cement.

Micrographs of Thin Section of Natural Cement Mortar M2 from 1950s

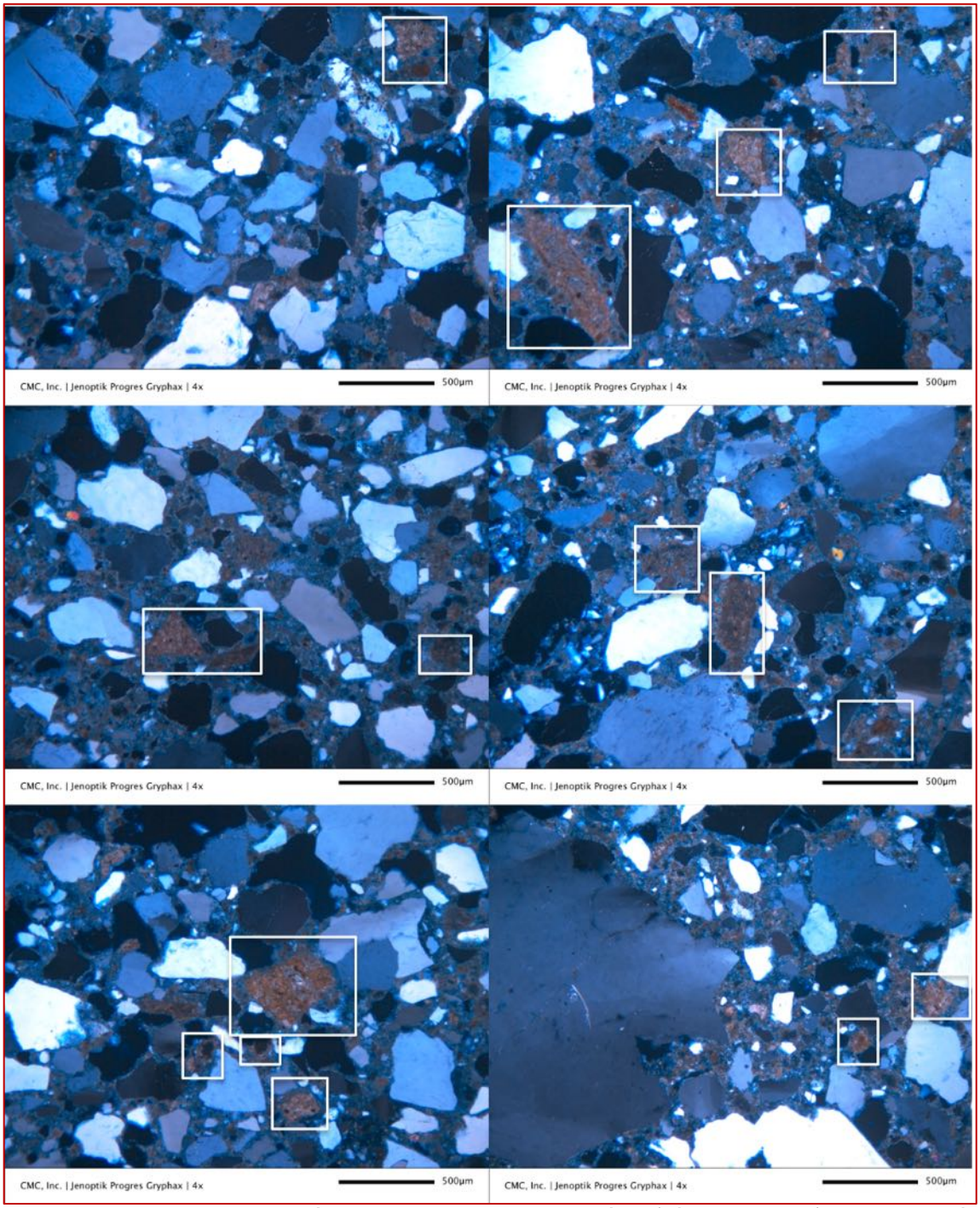

Figure B8: Mortar M2 (1950s) Natural cement mortar - Micrographs of thin section of 1950s natural cement mortar viewed in cross polarized light mode in a petrographic microscope showing: (a) crushed siliceous natural sand aggregate particles that contain major amounts of strained and unstrained quartz and quartzite, and subordinate amount of feldspar; sand particles are well-graded, well-distributed, and have been sound during their service, (b) interstitial paste that is porous and contains many hydrated and residual phases of the original binder components, and (d) many brown colorer variably calcined residual impure dolomitic limestone raw feeds (some are marked in arrows and boxed) that are indicative of use of natural cement binder in the mortars. Notice many impure dolomitic limestone particles left from calcination process are sand-sized.

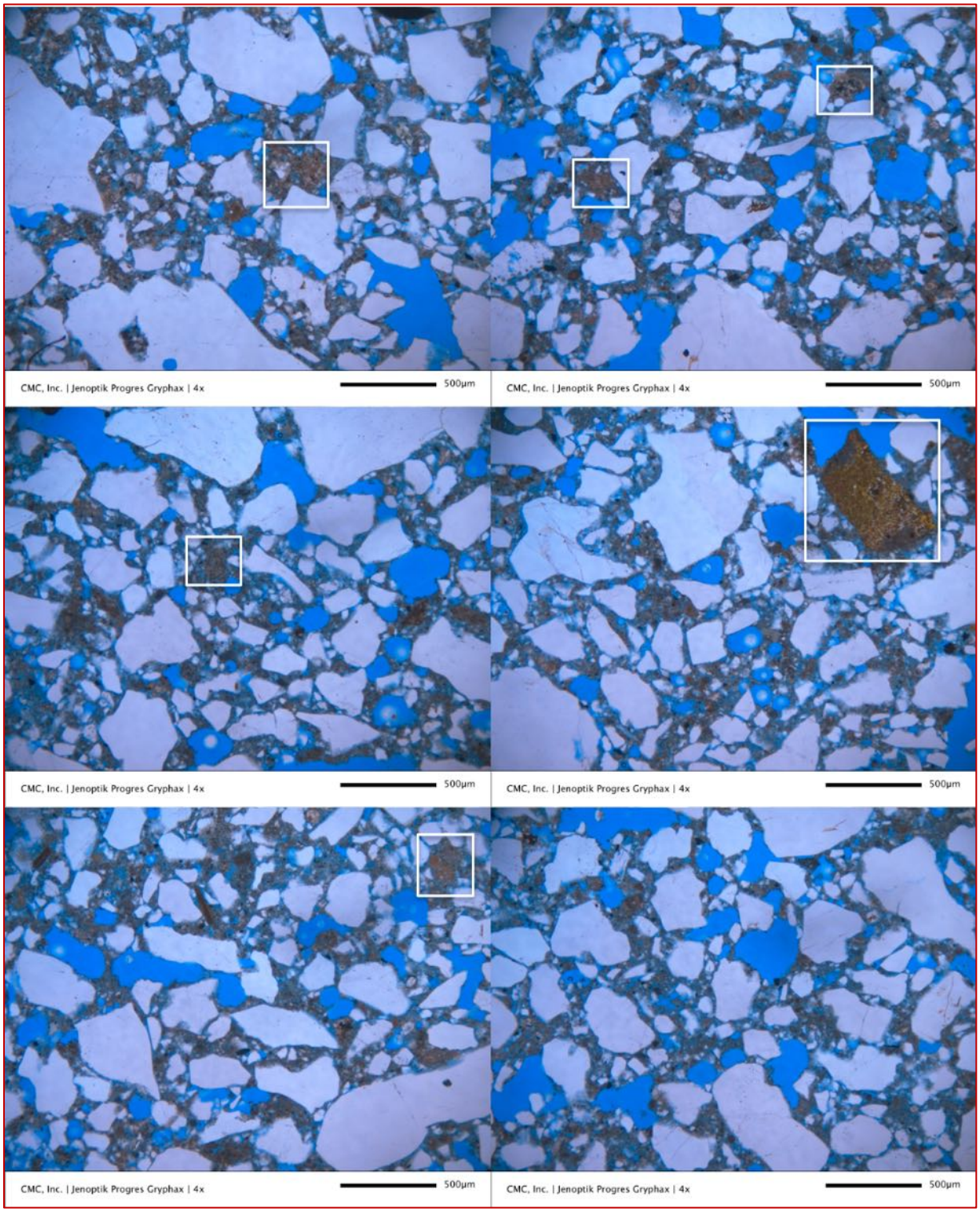

Figure B9: Mortar M2 (1950s) Natural cement mortar - Micrographs of thin section of 1950s natural cement mortar viewed in plane polarized light mode in a petrographic microscope showing: (a) crushed siliceous natural sand aggregate particles that are well-graded, well-distributed, and have been sound during their service, (b) interstitial paste that is highly porous and contains many hydrated and residual phases of the original binder components, and (d) many brown colored variably calcined residual impure dolomitic limestone raw feeds (some are marked in arrows and boxed) that are indicative of use of natural cement binder in the mortar. Notice many impure dolomitic limestone particles left from calcination process are sand-sized.

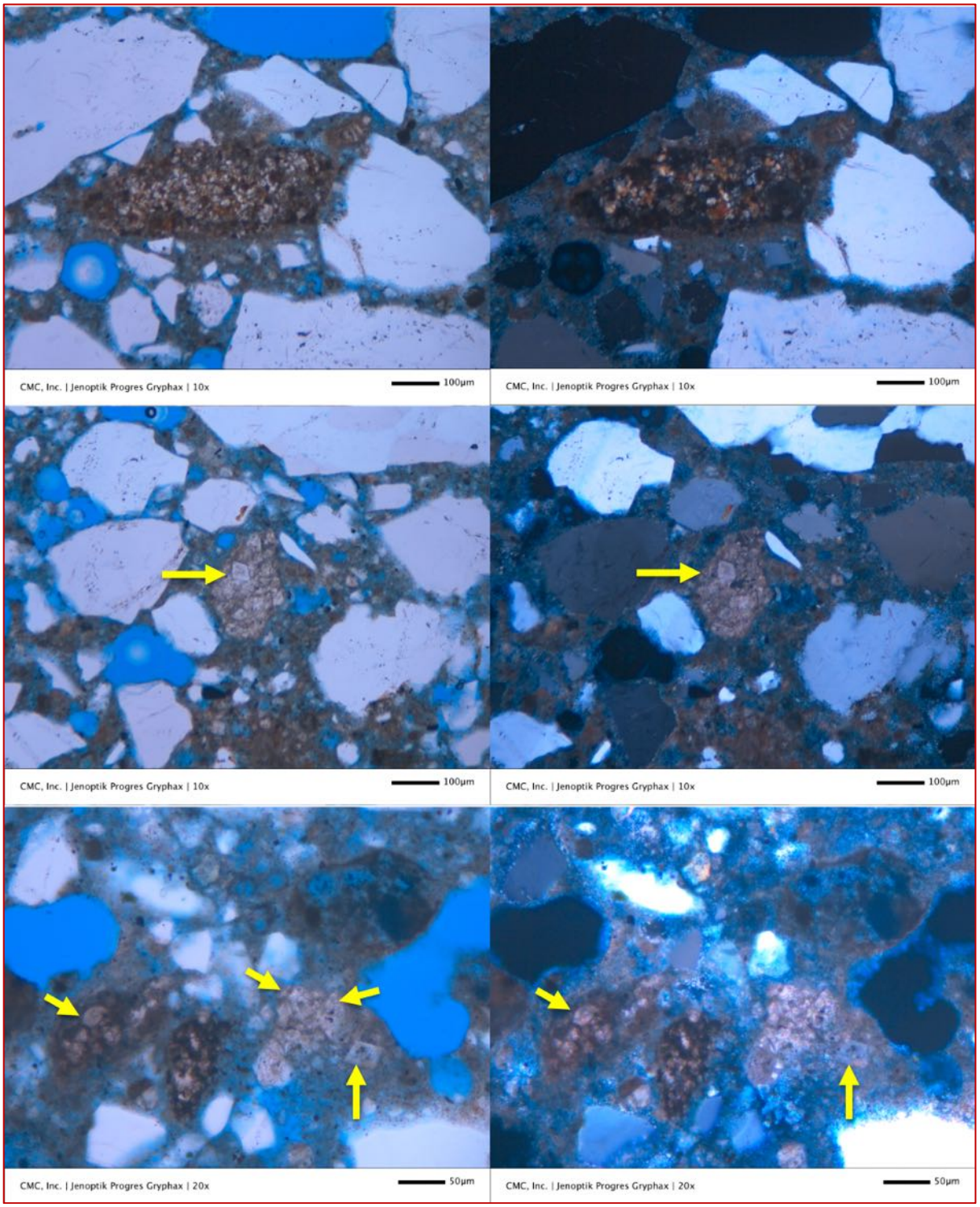

Figure B10: Mortar M2 (1950s) Natural cement mortar - Micrographs of thin section of 1950s natural cement mortar viewed in plane (left column) and corresponding cross (right column) polarized light mode in a petrographic microscope showing: (a) internal mineralogy and texture of impure dolomitic limestone particles that were used as raw feed in the kiln for production of natural cement, (b) many rhombic-shaped dolomite crystals in the dolomitic limestone particles, many of which are marked with arrows, many show dark brown rims around the rhombs due to migration of iron phases in the dolomite during calcination process, and (c) interstitial calcite and siliceous component from silica and clay minerals in the matrix of impure limestone that upon calcination and reaction with calcined calcite and dolomite have provided the necessary hydraulicity of natural cements.

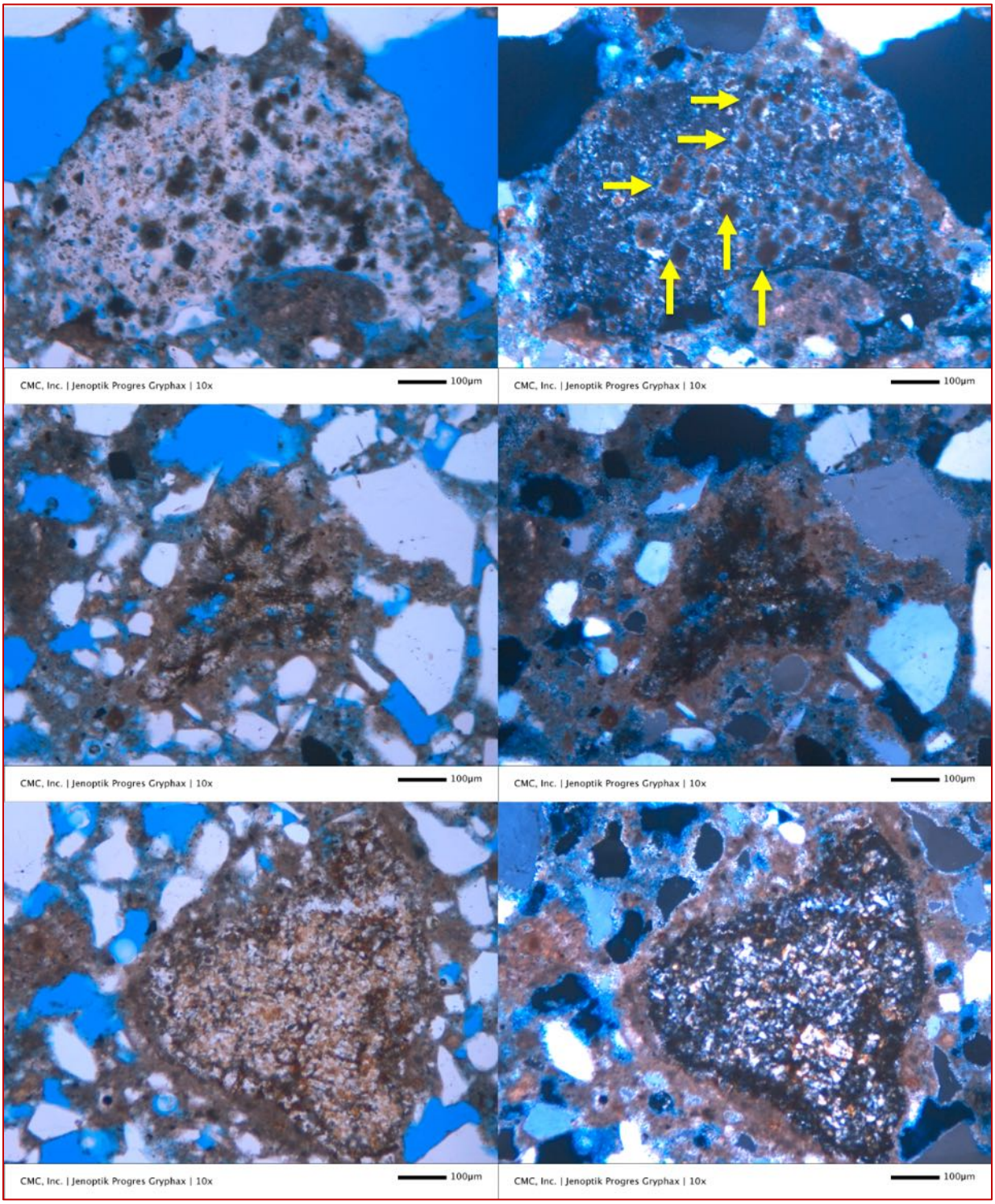

Figure B11: Mortar M2 (1950s) Natural cement mortar - Micrographs of thin section of 1950s natural cement mortar viewed in plane (left column) and corresponding crossed (right column) polarized light mode in a petrographic microscope showing: (a) internal mineralogy and texture of impure dolomitic limestone particles that were used as raw feed in the kiln for production of natural cement, (b) a few rhombic-shaped dolomite crystals in the dolomitic limestone particles, and (c) advanced stages of calcination and subsequent hydration where most of the matrix contains amorphous phase, appearing near-isotropic in crossed polarized light mode, which is the main phase responsible for hydraulicity of natural cement. Bottom row shows many calcium-aluminate-silicate minerals in a residual cement formed from calcination process.

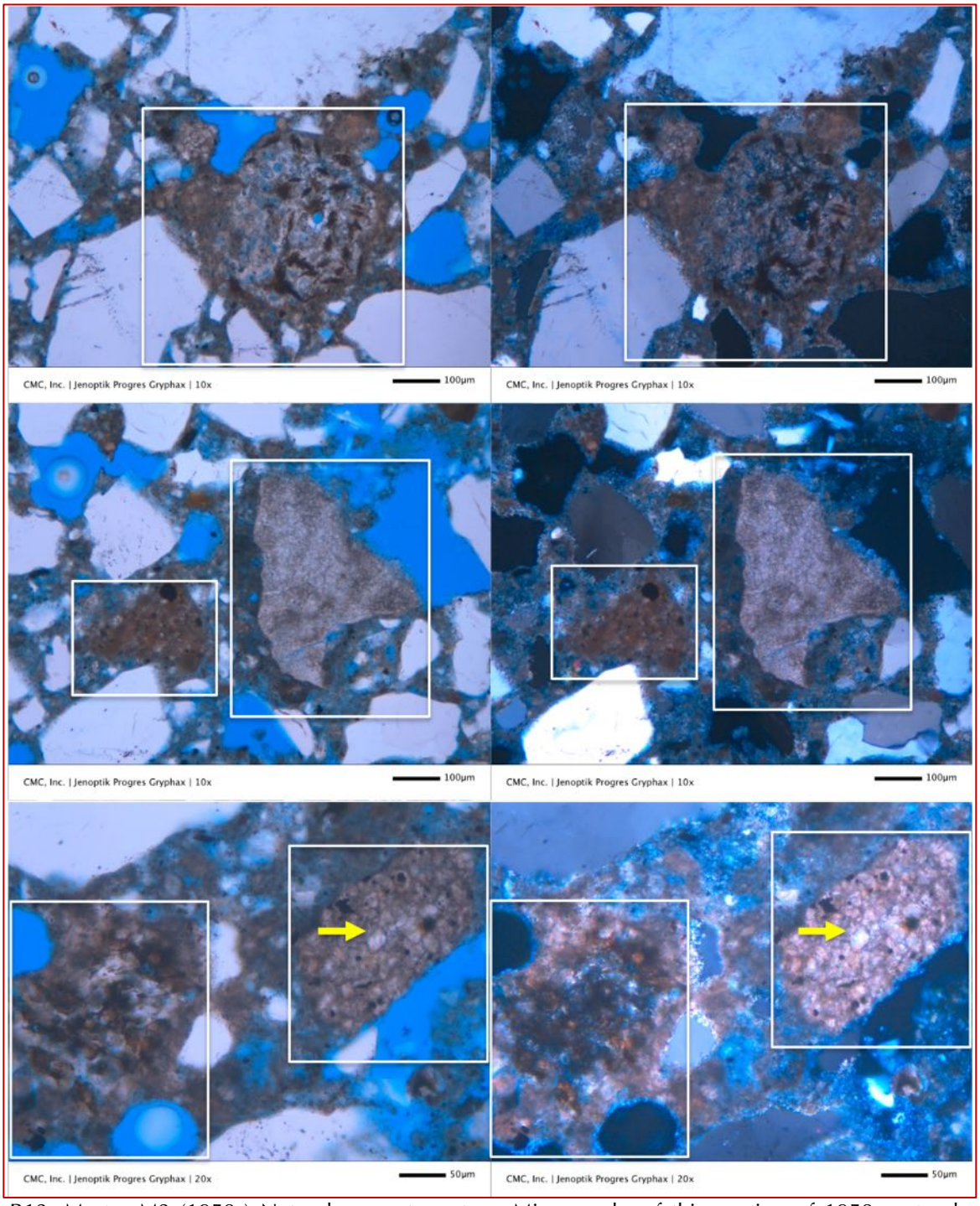

Figure B12: Mortar M2 (1950s) Natural cement mortar - Micrographs of thin section of 1950s natural cement mortar viewed in plane (left column) and corresponding crossed (right column) polarized light mode in a petrographic microscope showing: (a) internal mineralogy and texture of impure dolomitic limestone particles that were used as raw feed in the kiln for production of natural cement, (b) a few rhombic-shaped dolomite crystals in the dolomitic limestone particles, one of which is marked with an arrow in the bottom row, and (c) interstitial calcite and siliceous component from silica and clay minerals in the matrix of limestone (esepcially seen in the bottom row photos) that upon calination and reaction with calcined calcite and dolomite have provided the necessary hydraulicity of natural cement. Particles in the top row show advanced stages of calcination and subsequent hydration where most of the matrix contains amorphous phase, appearing near-isotropic in crossed polarized light mode, which is the main phase responsible for hydraulicity of natural cement.

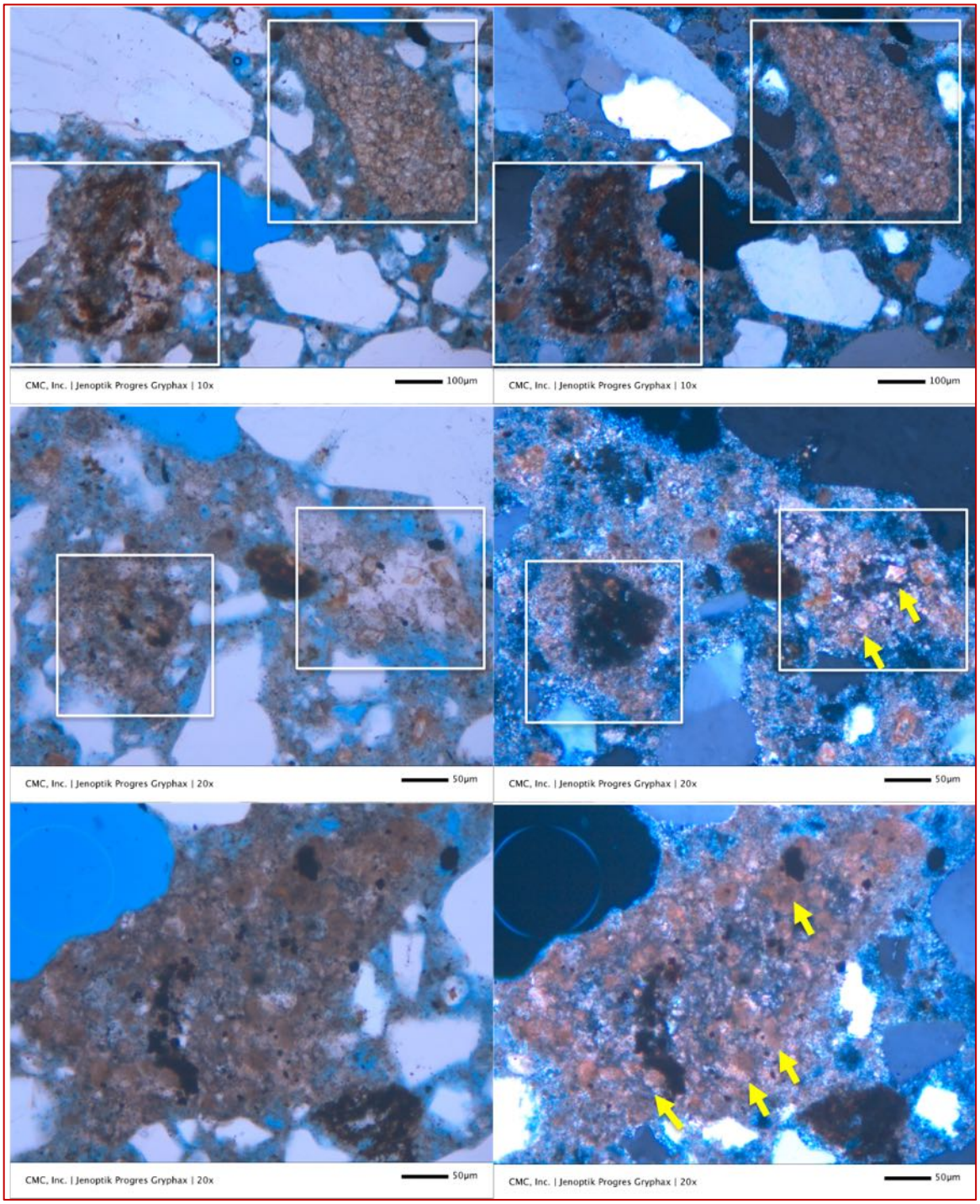

Figure B13: Mortar M2 (1950s) Natural cement mortar – Micrographs of thin section of 1950s natural cement mortar viewed in plane (left column) and corresponding crossed (right column) polarized light mode in a petrographic microscope showing: (a) internal mineralogy and texture of impure dolomitic limestone particles that were used as raw feed in the kiln for production of natural cement, (b) a few rhombic-shaped dolomite crystals in the dolomitic limestone particles, some are marked with arrows in the bottom right photo, and (c) interstitial calcite and siliceous component from silica and clay minerals in the matrix of limestone that upon calcination and reaction with calcined calcite and dolomite have provided the necessary hydraulicity of natural cement. Particles in all three rows show advanced stages of calcination and subsequent hydration where most of the matrix contains amorphous phase appearing near-isotropic in crossed polarized light mode, which is the main phase responsible for hydraulicity of natural cement.

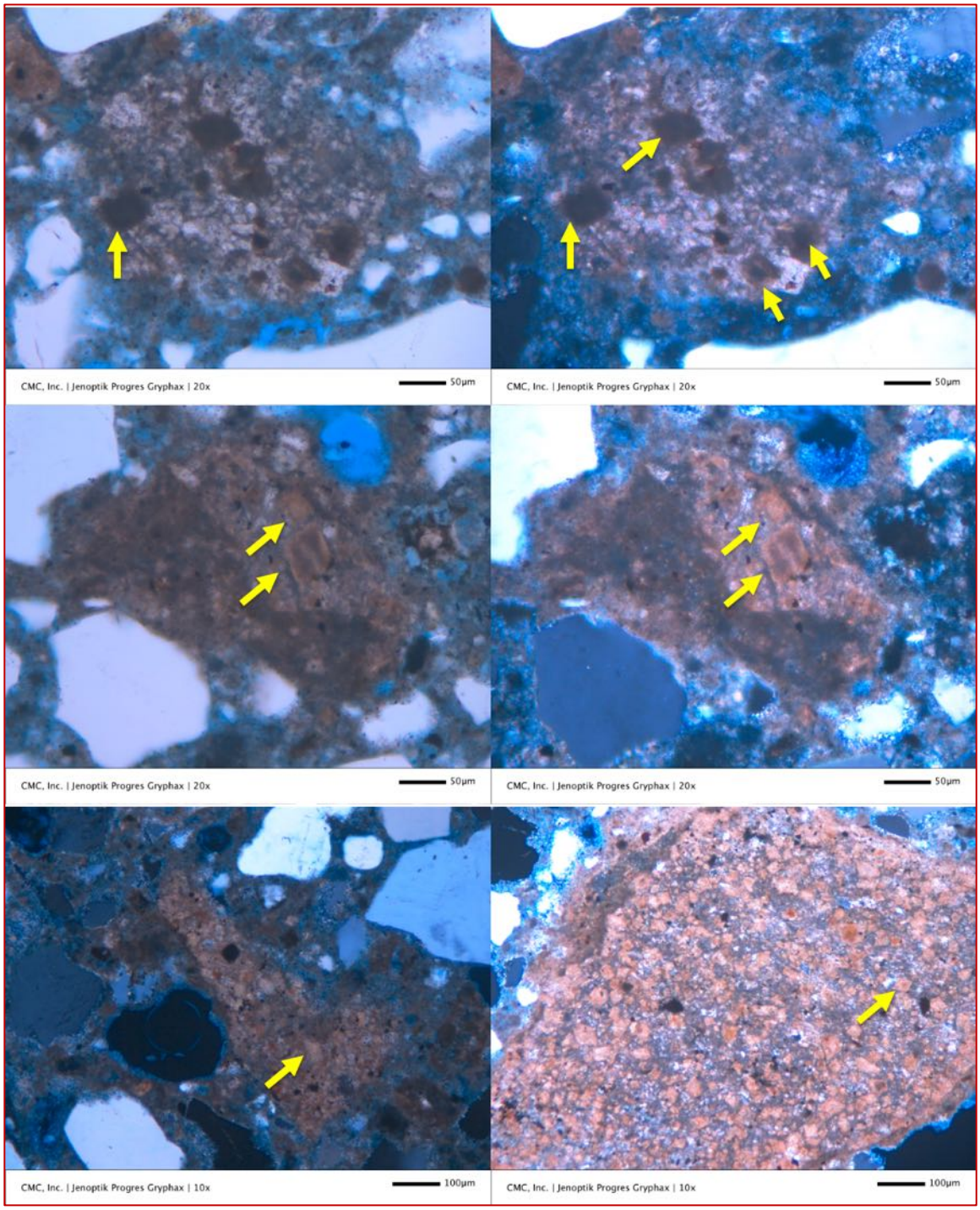

Figure B14: Mortar M2 (1950s) Natural cement mortar - Micrographs of thin section of 1950s natural cement mortar viewed in plane (left column) and corresponding crossed (right column) polarized light mode in a petrographic microscope showing: (a) internal mineralogy and texture of impure dolomitic limestone particles that were used as raw feed in the kiln for production of natural cement, (b) a few rhombic-shaped dolomite crystals in the dolomitic limestone particles marked with arrows, and (c) interstitial calcite and siliceous component from silica and clay minerals in the matrix of limestone that upon calcination and reaction with calcined calcite and dolomite have provided the necessary hydraulicity of natural cement. Particles in the top and middle rows show advanced stages of calcination and subsequent hydration where most of the matrix contains amorphous phase appearing near-isotropic in crossed polarized light mode, which is the main phase responsible for hydraulicity of natural cement.

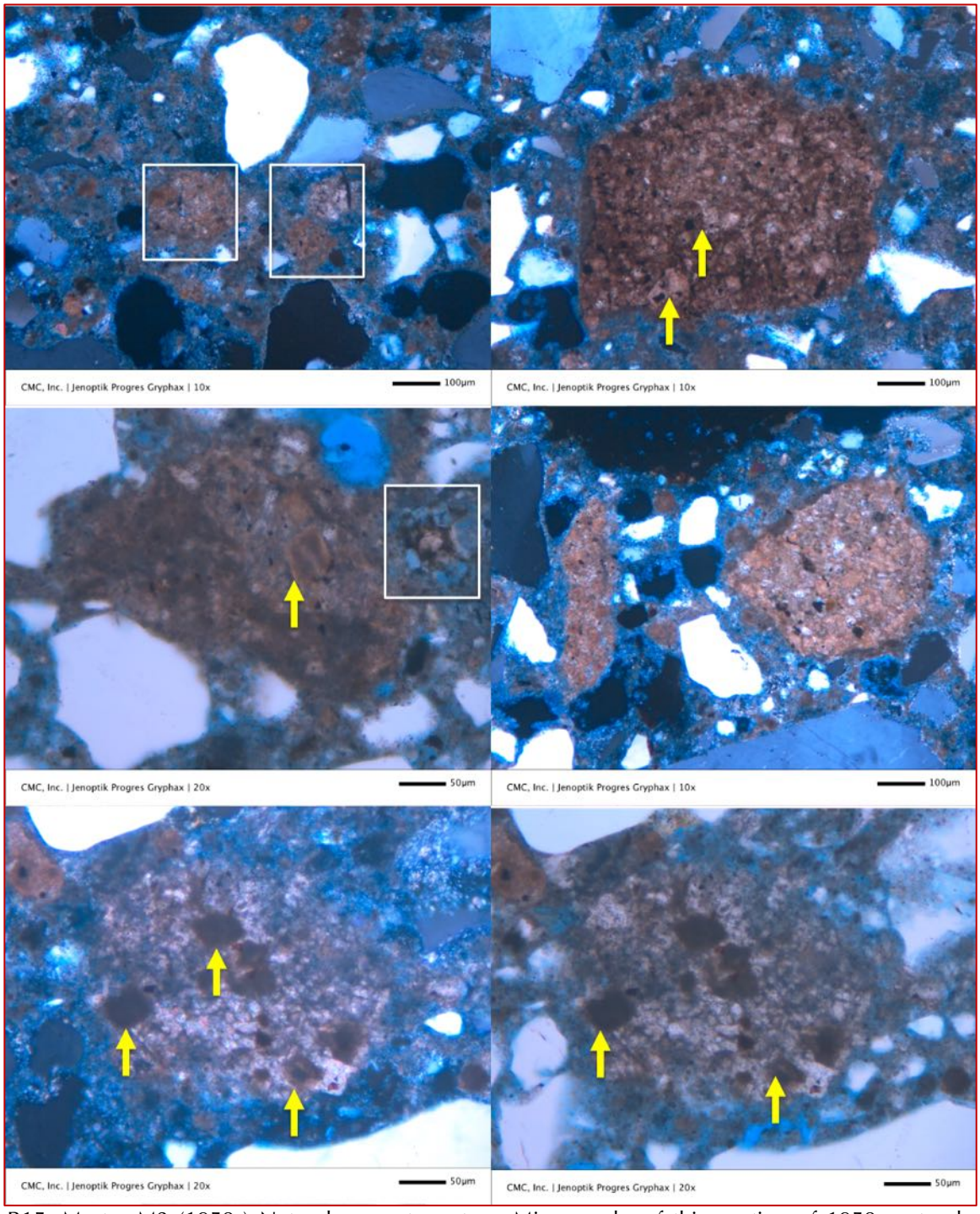

Figure B15: Mortar M2 (1950s) Natural cement mortar - Micrographs of thin section of 1950s natural cement mortar viewed in plane (left column) and corresponding crossed (right column) polarized light mode in a petrographic microscope showing: (a) internal mineralogy and texture of impure dolomitic limestone particles that were used as raw feed in the kiln for production of natural cement, (b) a few rhombic-shaped dolomite crystals in the dolomitic limestone particles marked with arrows, and (c) interstitial calcite and siliceous component from silica and clay minerals in the matrix of limestone that upon calcination and reaction with calcined calcite and dolomite have provided the necessary hydraulicity of natural cement. Particles in the bottom row show advanced stages of calcination and subsequent hydration where most of the matrix contains amorphous phase appearing near-isotropic in crossed polarized light mode, which is the main phase responsible for hydraulicity of natural cement.

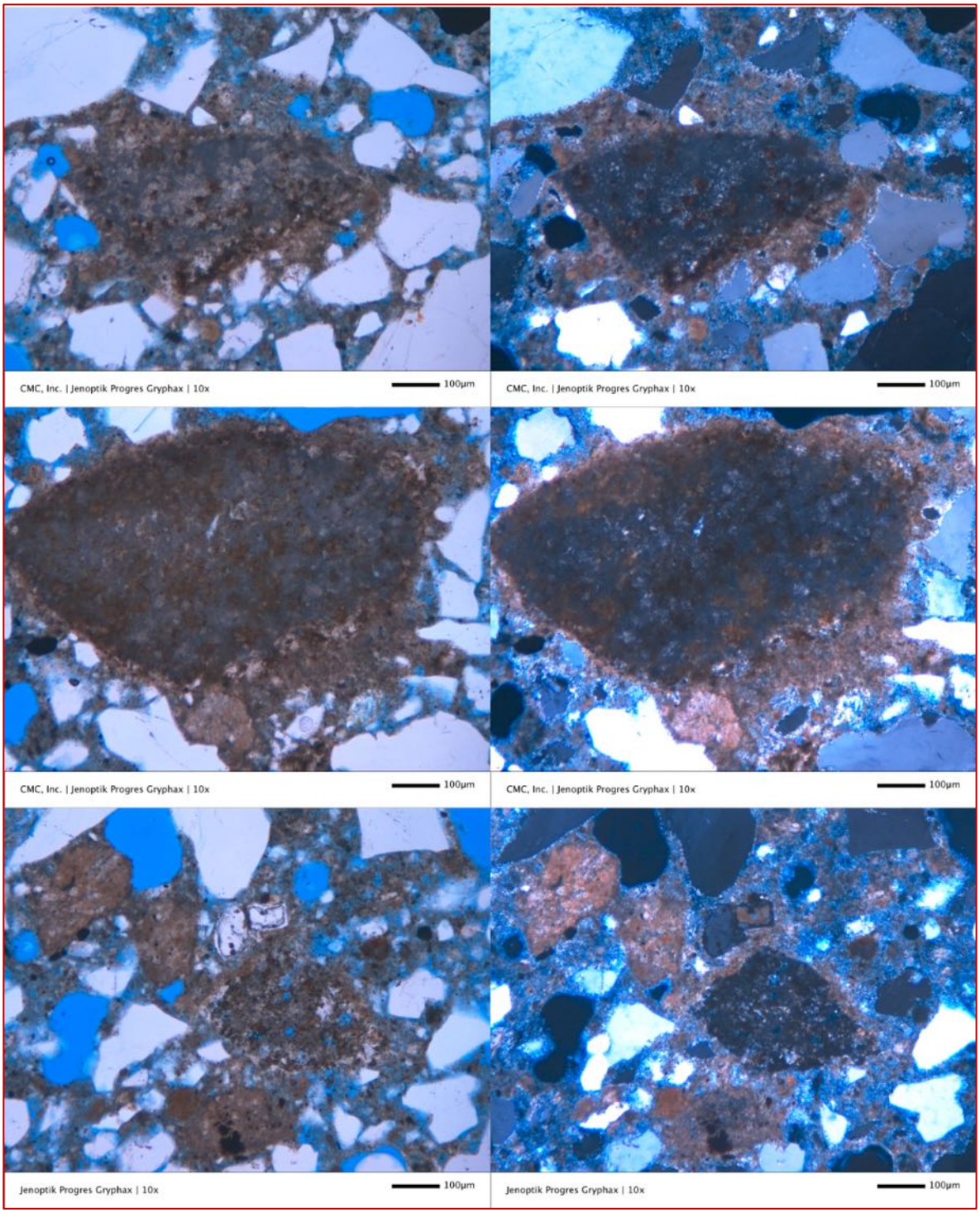

Figure B16: Mortar M2 (1950s) Natural cement mortar - Micrographs of thin section of 1950s natural cement mortar viewed in plane (left column) and corresponding crossed (right column) polarized light mode in a petrographic microscope showing: (a) internal mineralogy and texture of impure dolomitic limestone particles that were used as raw feed in the kiln for production of natural cement, (b) a few rhombic-shaped dolomite crystals in the dolomitic limestone particles, and (c) interstitial calcite and siliceous component from silica and clay minerals in the matrix of limestone that upon calcination and reaction with calcined calcite and dolomite have provided the necessary hydraulicity of natural cement. Particles in all three rows show advanced stages of calcination and subsequent hydration where most of the matrix contains amorphous phase appearing near-isotropic in crossed polarized light mode, which is the main phase responsible for hydraulicity of natural cement.

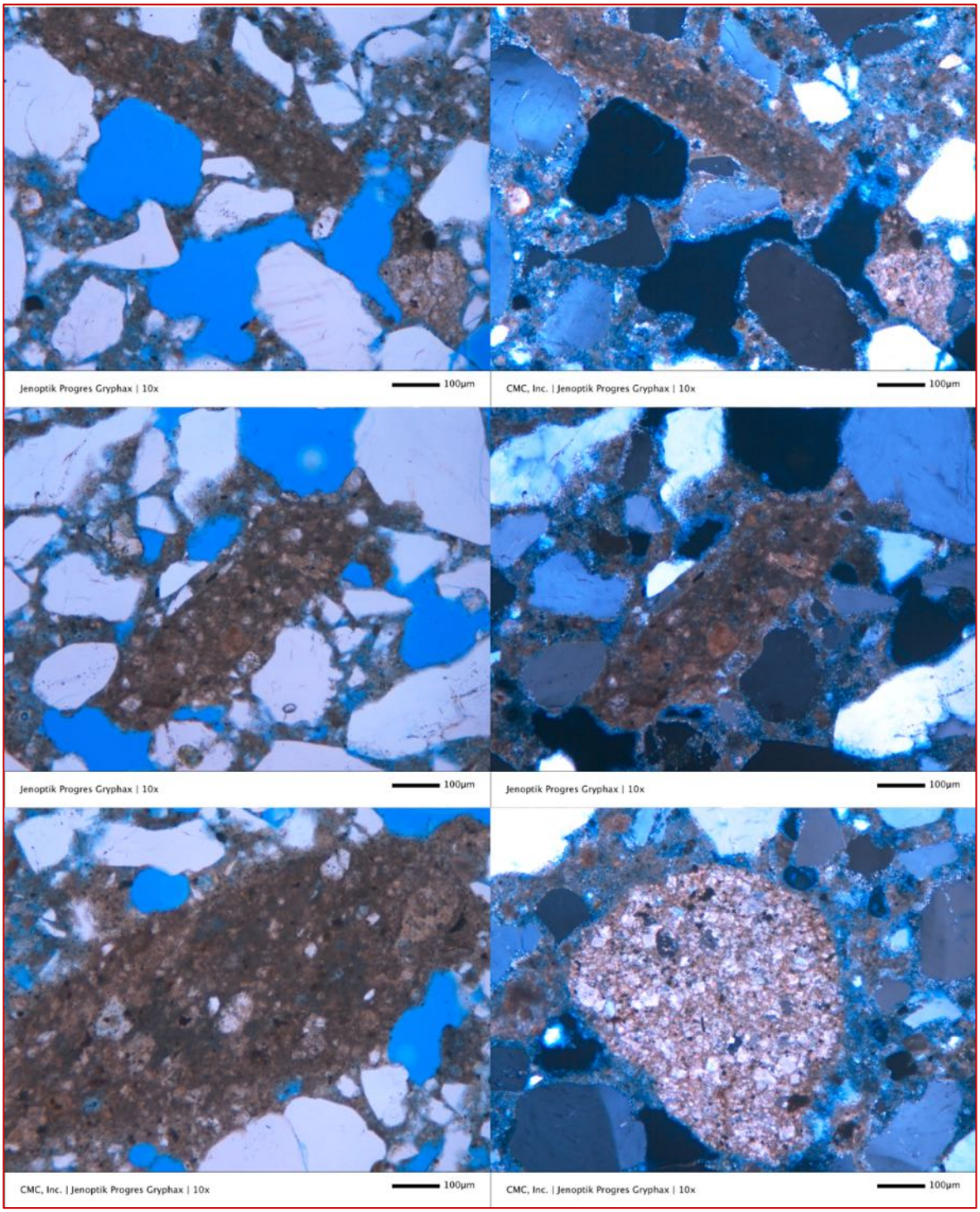

Figure B17: Mortar M2 (1950s) Natural cement mortar - Micrographs of thin section of 1950s natural cement mortar viewed in plane (left column) and corresponding crossed (right column) polarized light mode in a petrographic microscope showing: (a) internal mineralogy and texture of impure dolomitic limestone particles that were used as raw feed in the kiln for production of natural cement, (b) a few rhombic-shaped dolomite crystals in the dolomitic limestone particles, and (c) interstitial calcite and siliceous component from silica and clay minerals in the matrix of limestone that upon calcination and reaction with calcined calcite and dolomite have provided the necessary hydraulicity of natural cement. Particles in top and middle rows show advanced stages of calcination and subsequent hydration where most of the matrix contains amorphous phase appearing near-isotropic in crossed polarized light mode, which is the main phase responsible for hydraulicity of natural cement.

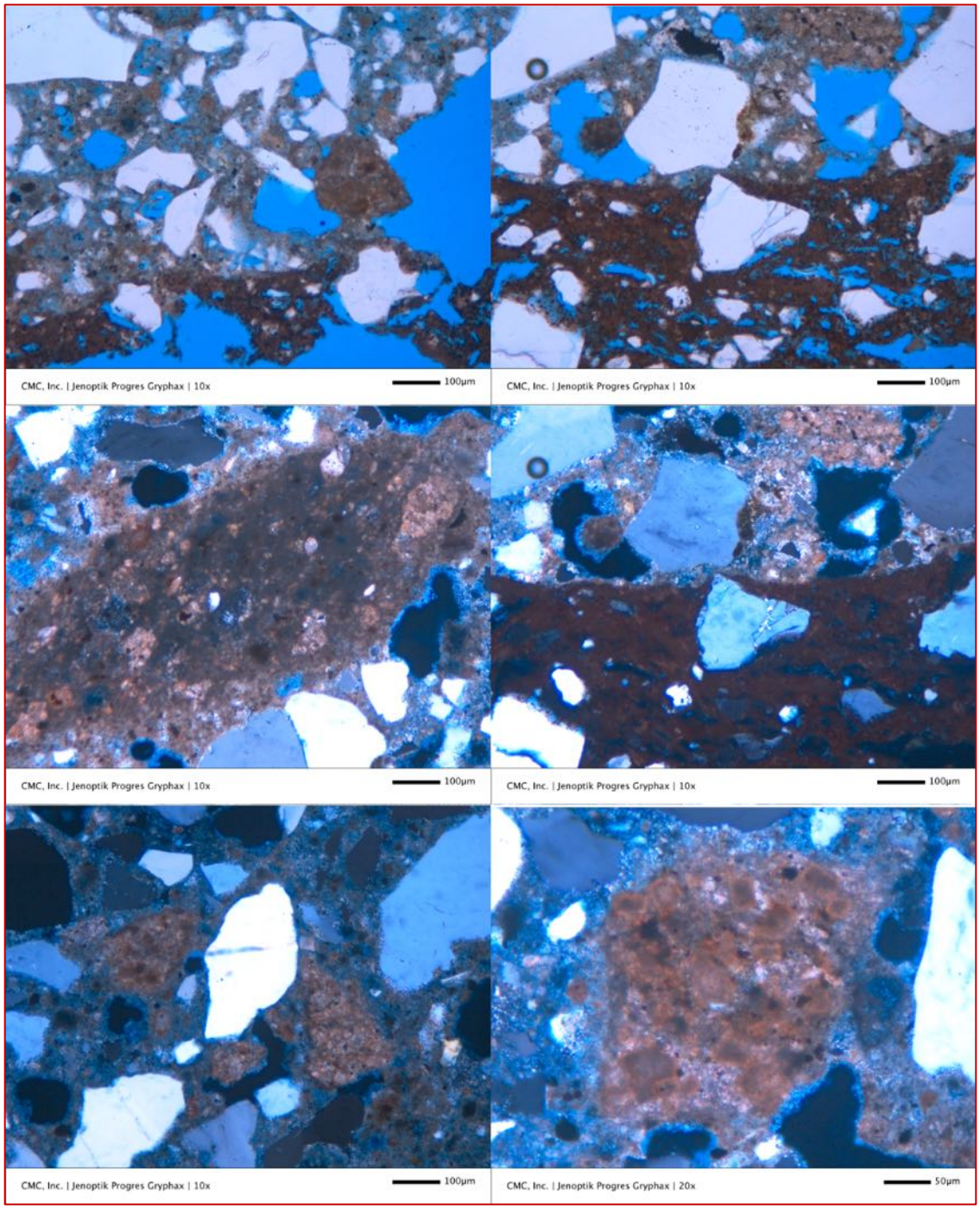

Figure B18: Mortar M2 (1950s) Natural cement mortar - Micrographs of thin section of 1950s natural cement mortar viewed in plane (left column) and corresponding crossed (right column) polarized light mode in a petrographic microscope showing: (a) internal mineralogy and texture of impure dolomitic limestone particles that were used as raw feed in the kiln for production of natural cement, (b) a few rhombic-shaped dolomite crystals in the dolomitic limestone particles, and (c) interstitial calcite and siliceous component from silica and clay minerals in the matrix of limestone that upon calination and reaction with calcined calcite and dolomite have provided the necessary hydraulicity of natural cement. Particle in all middle left photo shows advanced stages of calcination and subsequent hydration where most of the matrix contains amorphous phase appearing near-isotropic in crossed polarized light mode, which is the main phase responsible for hydraulicity of natural cement. Top row shows portion of clay brick adhered to the mortar where brick contains characteristic elongated voids, tempered quartz and reddish-brown aluminosilicate glass matrix.

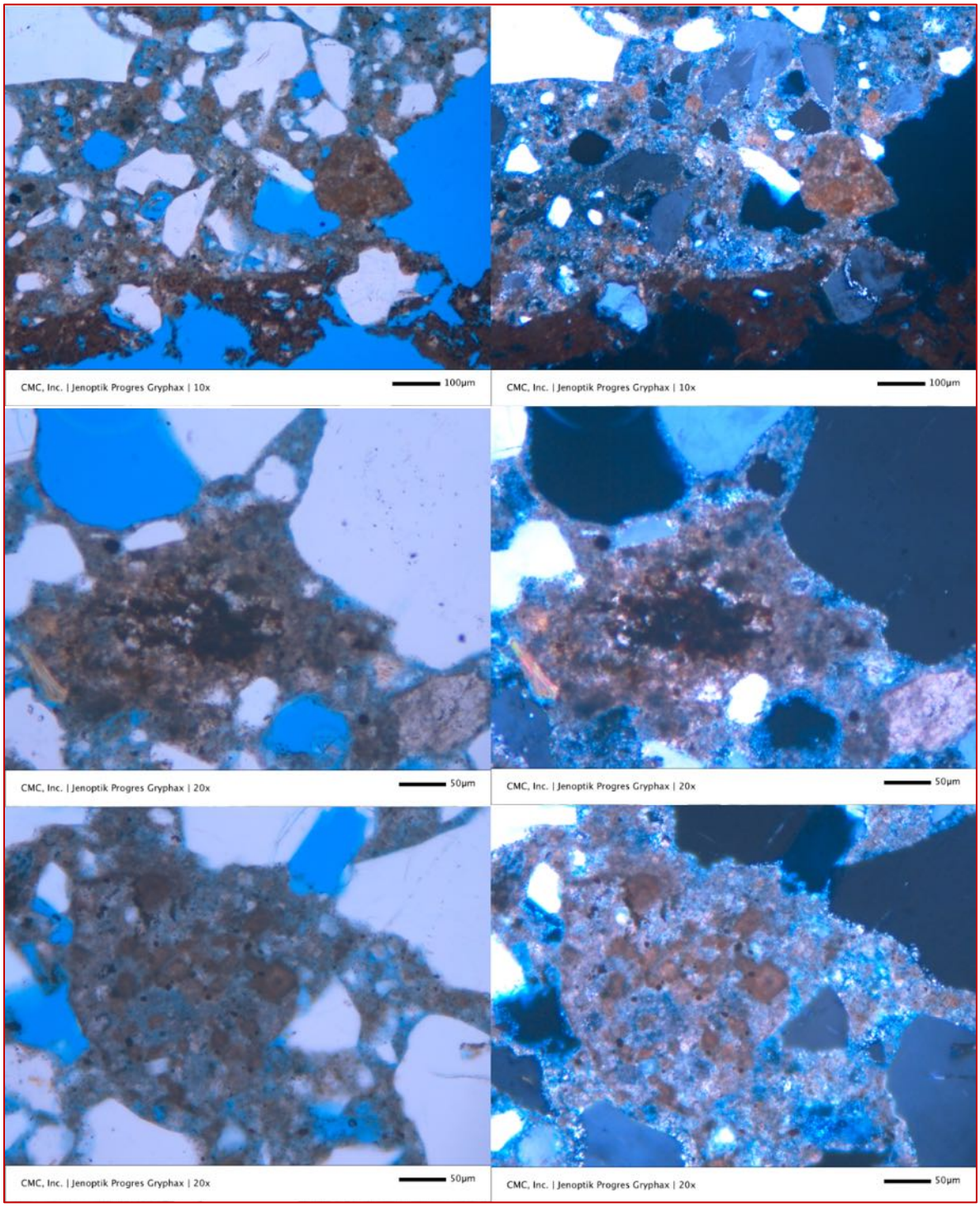

Figure B19: Mortar M2 (1950s) Natural cement mortar - Micrographs of thin section of 1950s natural cement mortar viewed in plane (left column) and corresponding crossed (right column) polarized light mode in a petrographic microscope showing: (a) internal mineralogy and texture of impure dolomitic limestone particles that were used as raw feed in the kiln for production of natural cement, (b) a few rhombic-shaped dolomite crystals in the dolomitic limestone particles (especially seen in the bottom row), and (c) interstitial calcite and siliceous component from silica and clay minerals in the matrix of limestone that upon calcination and reaction with calcined calcite and dolomite have provided the necessary hydraulicity of natural cement. Top row shows portion of clay brick adhered to the mortar where brick contains characteristic elongated voids, tempered quartz and reddish-brown aluminosilicate glass matrix.

Micrographs of Thin Section of Cement-Lime Mortar M3 from 1916

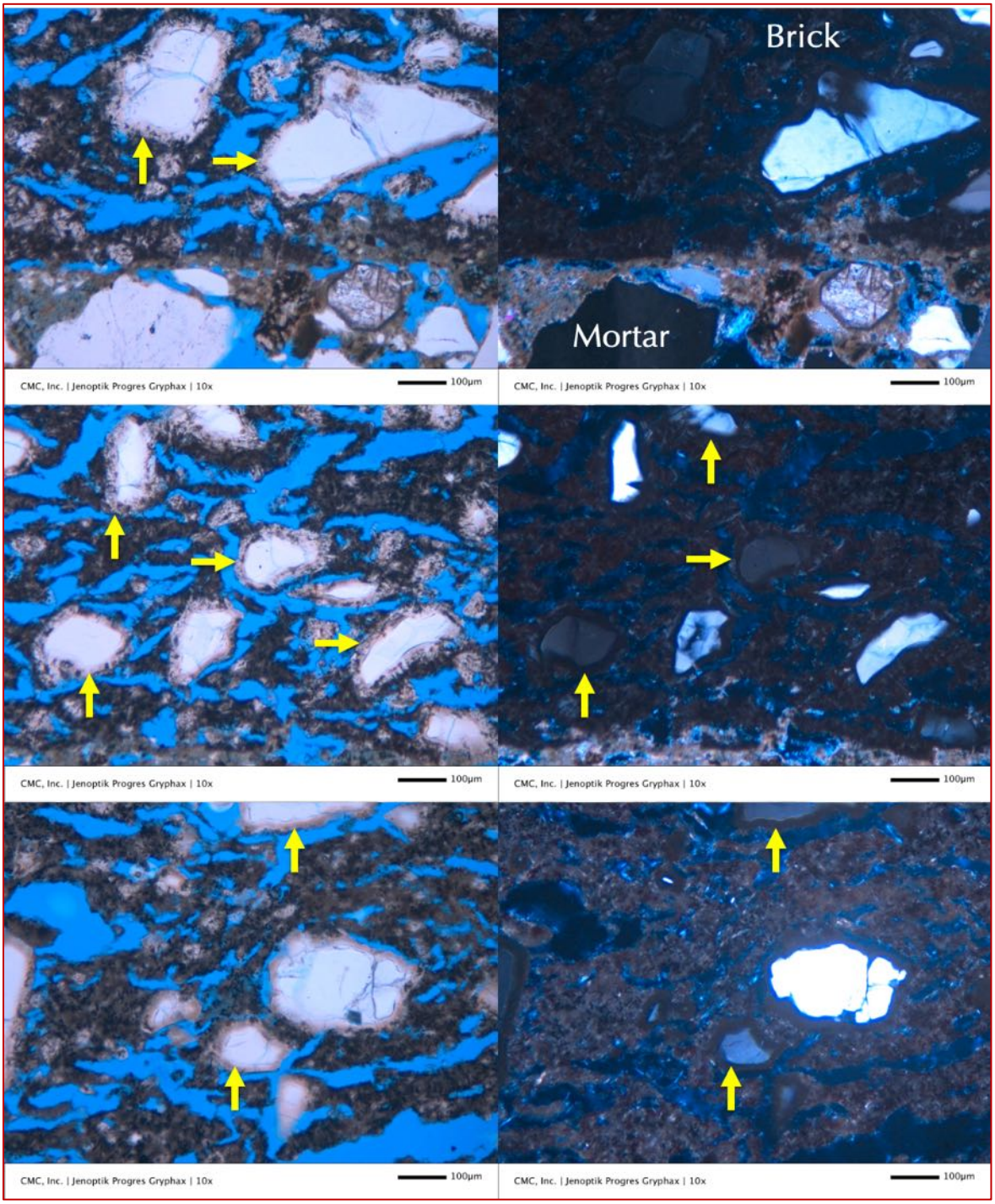

Figure B20: Mortar M3 (1916) Cement-lime mortar – Micrographs (left in PPL and right in corresponding XPL mode) of clay brick adhered to 1916 cement-lime mortar where brick shows characteristic: (a) elongated parallel voids from loss of water during drying after molding and subsequent baking; (b) tempered quartz additive in brick where quartz grains are angular, well-graded, show glassy reacted rims around particles from reactions with glassy matrix during baking (some are shown with arrows); and (c) dark gray aluminosilicate glass matrix of brick, which is not reddish-brown as in the other bricks due to low carbonate content of clay and reducing condition of kiln. The top row shows adhered cement-lime mortar where mortar contains silica sand and carbonated paste. Notice the highly porous nature of brick from abundance of elongated parallel voids.

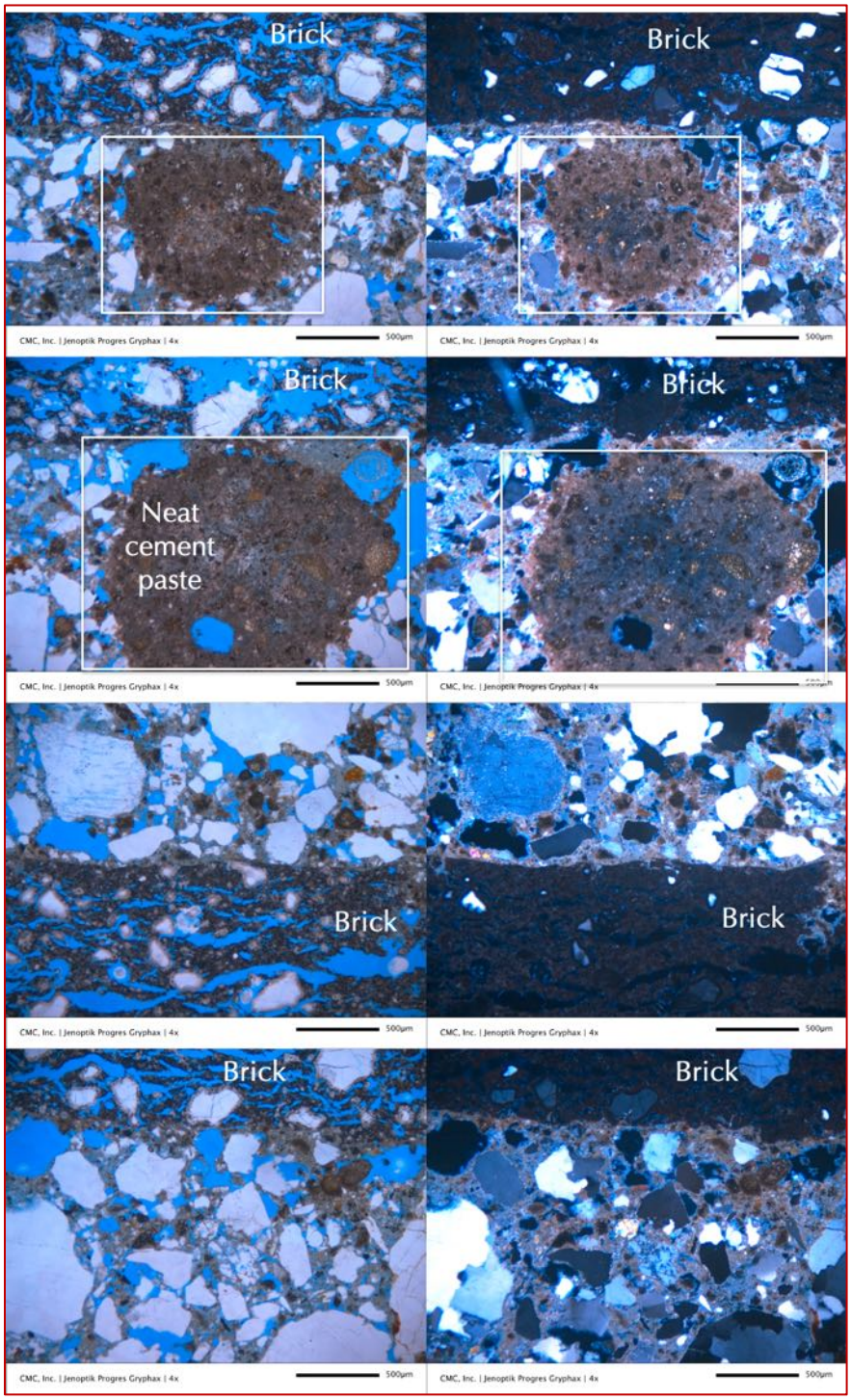

Figure B21: Mortar M3 (1916) Cement-lime mortar – Micrographs (left in PPL and right in corresponding XPL mode) of 1916 cement-lime mortar showing: (a) clumps of neat Portland cement paste that are boxed in 1st and 2nd rows; (b) clay bricks with characteristic elongated voids, tempered quartz additive and glassy matrix in brick, adhered to cement-lime mortar in the 1st, 3rd, and 4th rows; (c) natural silica sand particles in the mortar and tempered quartz in clay bricks (all photos) where sand particles in mortar as well as in brick are well-graded, well-distributed, and sound. Notice the highly porous nature of brick from abundance of elongated parallel voids. The cement-lime mortar is also porous and non-air-entrained.

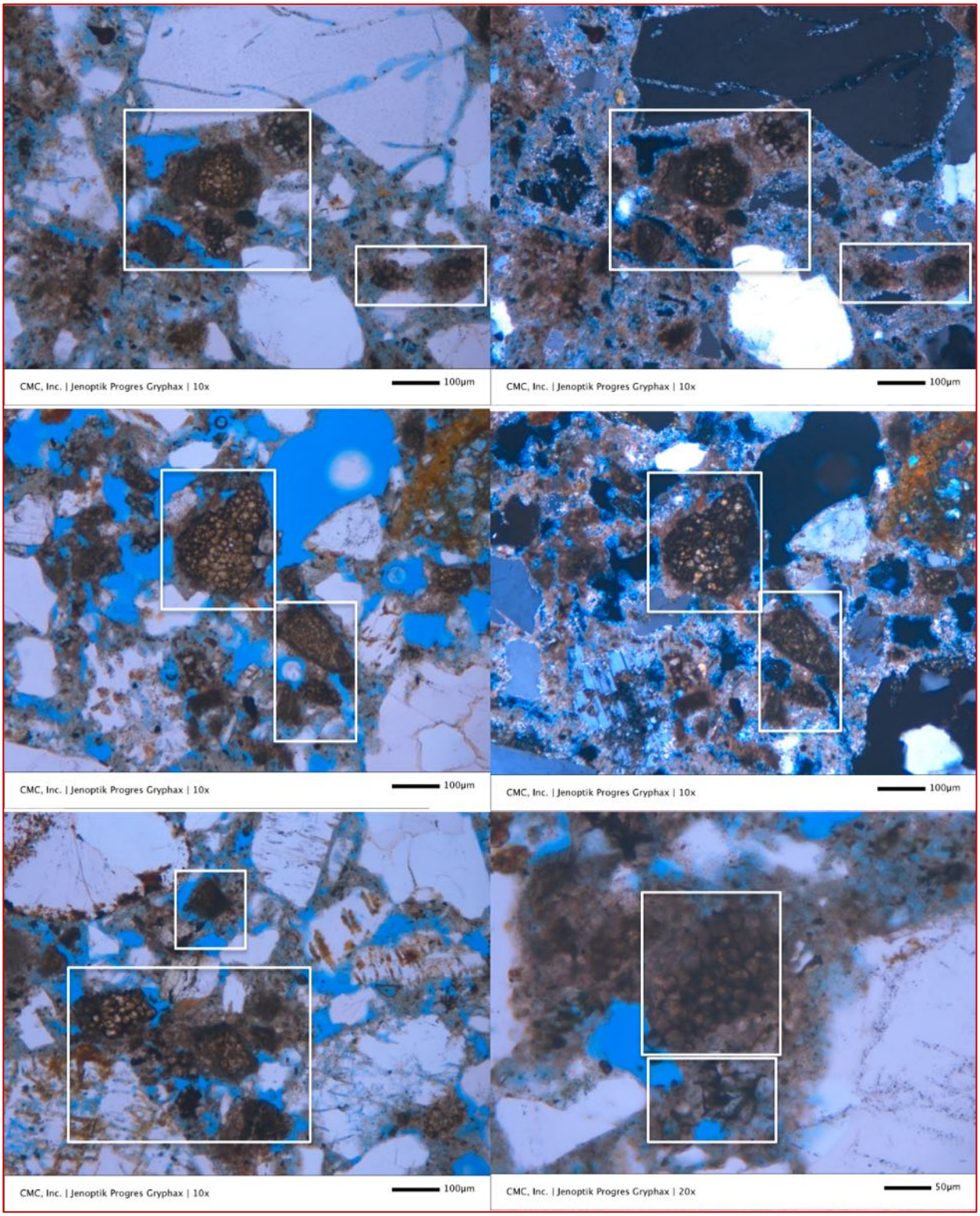

Figure B22: Mortar M3 (1916) Cement-lime mortar – Micrographs (left in PPL and right in corresponding XPL mode) of cement-lime mortar showing many residual Portland cement particles and associated dense paste of hydration products of cement (many are boxed) where residual cement particles show characteristic mineralogies (subhedral alite, anhedral belite clusters, and interstitial dark brown ferrite) and textures of Portland cement. Grain sizes of residual cement particles indicate use of coarsely ground Portland cement consistent with its reported age of early 20th century.

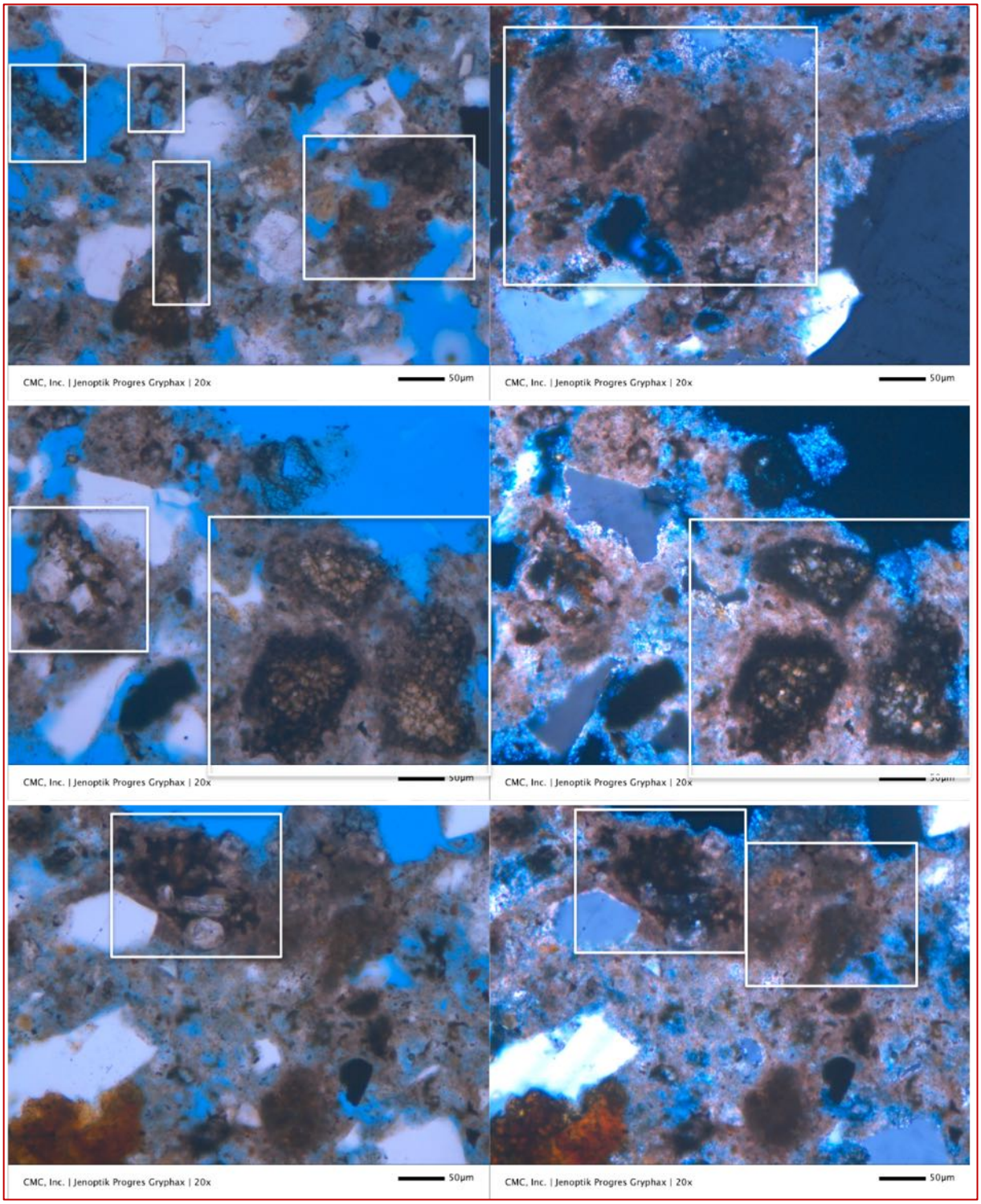

Figure B23: Mortar M3 (1916) Cement-lime mortar - Micrographs of cement-lime mortar showing many residual Portland cement particles and associated dense paste of hydration products of cement (many are boxed) where residual cement particles show characteristic mineralogies (subhedral alite, anhedral belite clusters, and interstitial dark brown ferrite) and textures of Portland cement. Grain sizes of residual cement particles indicate use of coarsely ground Portland cement consistent with its reported age of early 20th century. Paste shows variable porosities from porous paste to denser pastes, latter preferentially around residual cement particles. Paste is highly carbonated as evidenced by characteristic golden yellow birefringence in crossed polarized light photos in the right column.

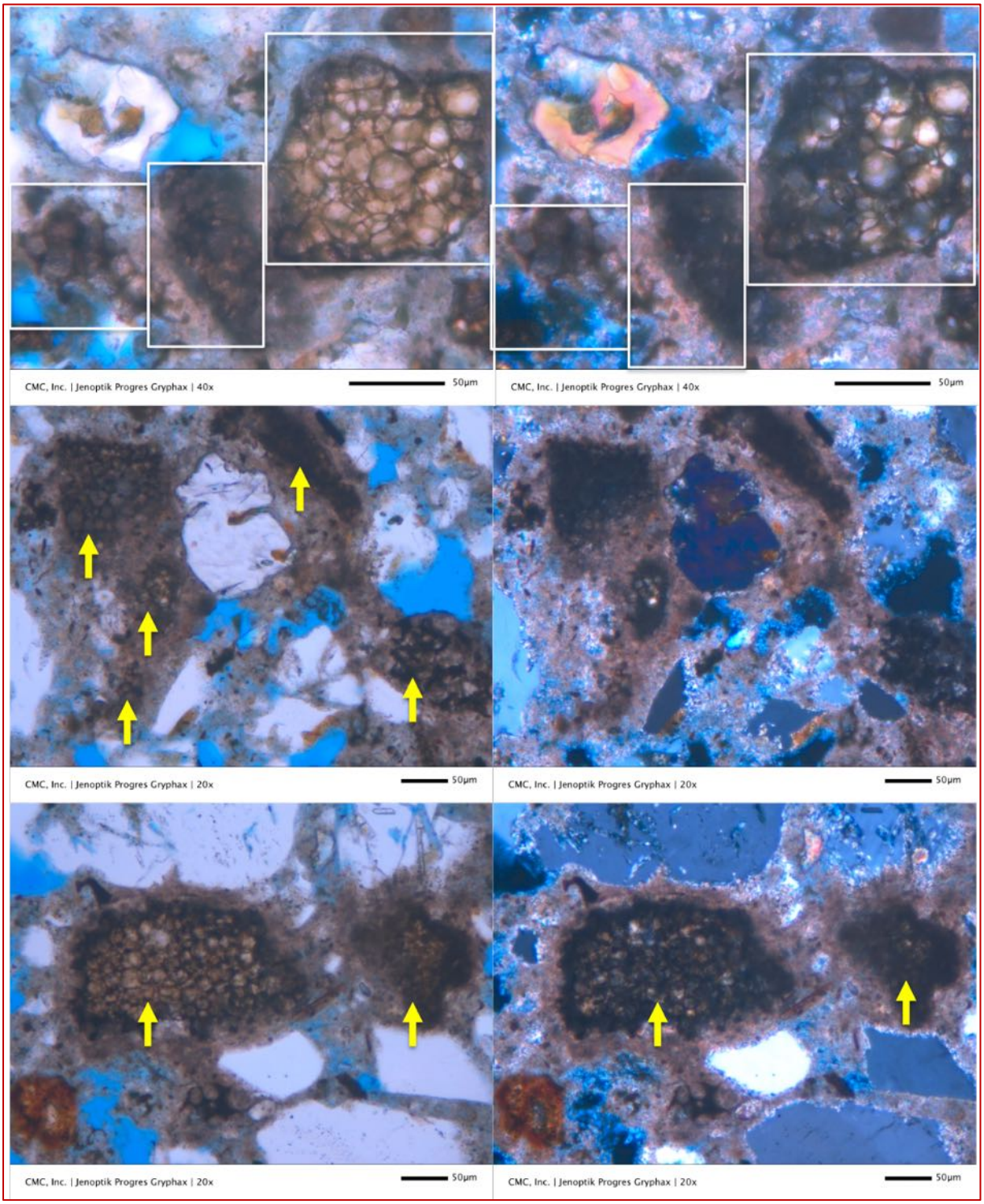

Figure B24: Mortar M3 (1916) Cement-lime mortar - Micrographs (left in PPL and right in corresponding XPL mode) of cement-lime mortar showing many residual Portland cement particles and associated dense paste of hydration products of cement (many are boxed and shown by arrows) where residual cement particles show characteristic mineralogies (subhedral alite, anhedral belite clusters, and interstitial dark brown ferrite) and textures of Portland cement. Grain sizes of residual cement particles indicate use of coarsely ground Portland cement consistent with its reported age of early 20th century. Paste shows variable porosities from porous paste to denser pastes, latter preferentially around residual cement particles. Paste is highly carbonated as evidenced by characteristic golden yellow birefringence in crossed polarized light photos in the right column.

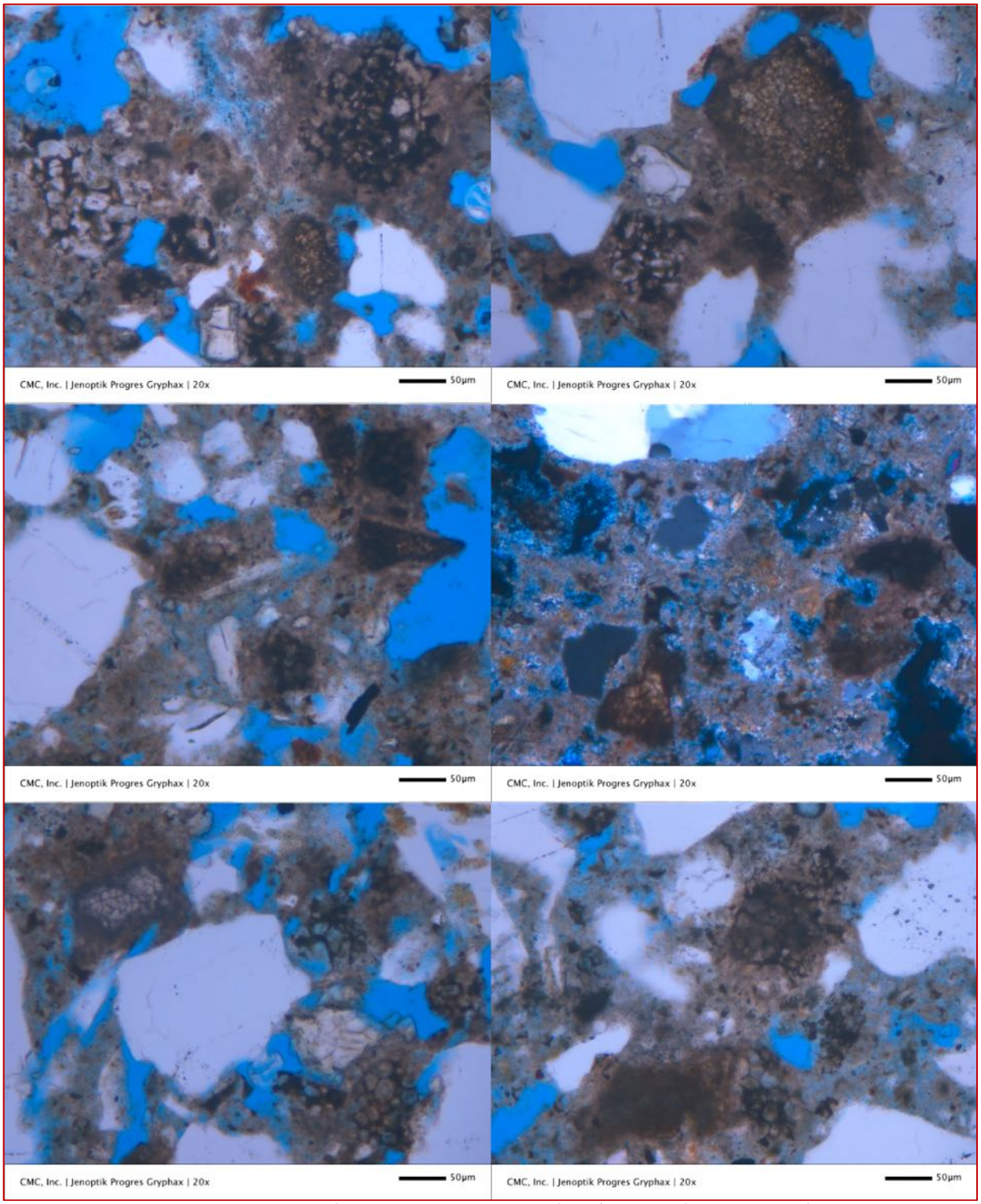

Figure B25: Mortar M3 (1916) Cement-lime mortar - Micrographs of cement-lime mortar showing many residual Portland cement particles and associated dense paste of hydration products of cement where residual cement particles show characteristic mineralogies (subhedral alite, anhedral belite clusters, and interstitial dark brown ferrite) and textures of Portland cement. Grain sizes of residual cement particles indicate use of coarsely ground Portland cement consistent with its reported age of early 20th century. Paste shows variable porosities from porous paste to denser pastes, latter preferentially around residual cement particles. Paste is highly carbonated as evidenced by characteristic golden yellow birefringence in crossed polarized light in the middle right photo.

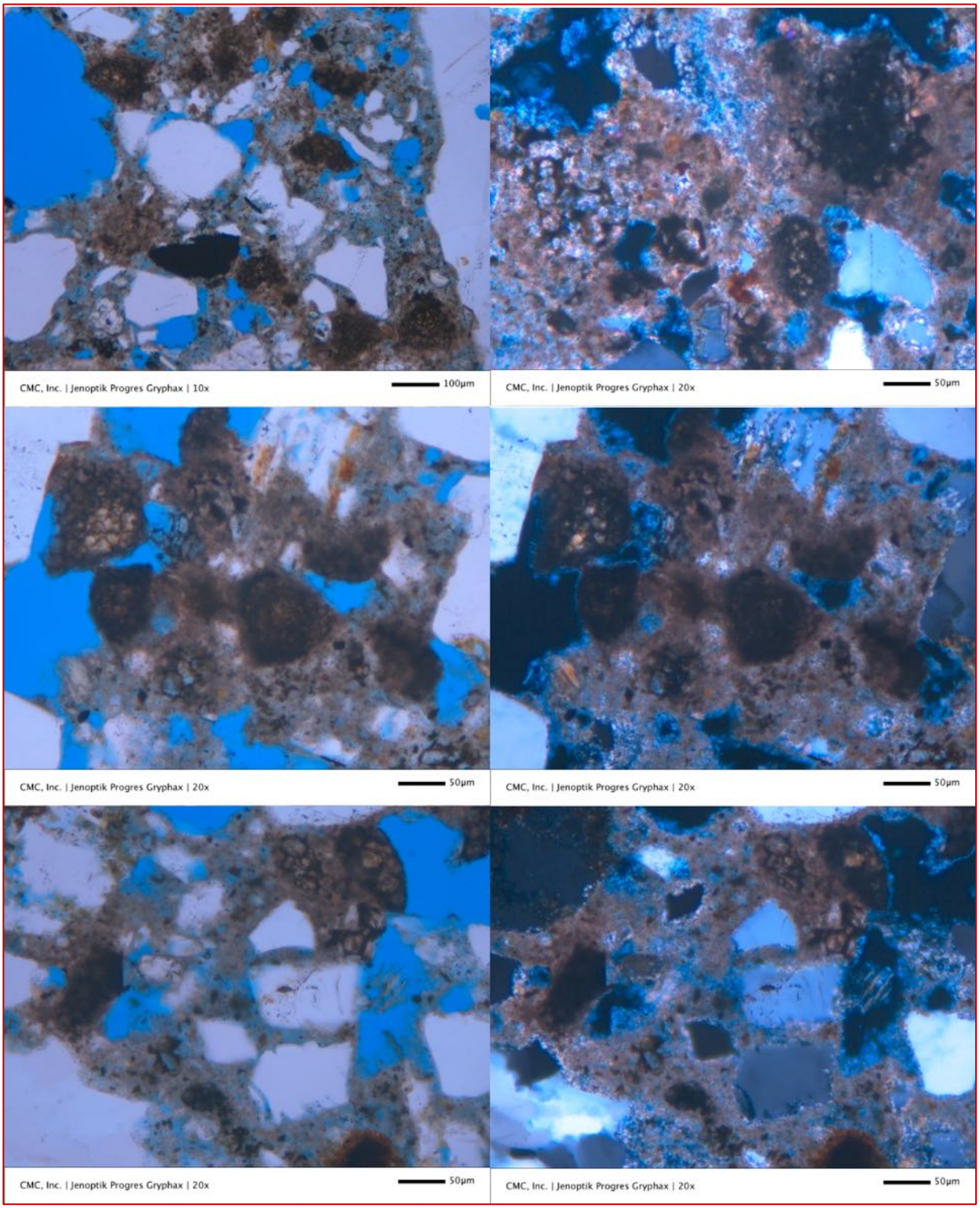

Figure B26: Mortar M3 (1916) Cement-lime mortar - Micrographs of cement-lime mortar showing many residual Portland cement particles and associated dense paste of hydration products of cement where residual cement particles show characteristic mineralogies (subhedral alite, anhedral belite clusters, and interstitial dark brown ferrite) and textures of Portland cement. Grain sizes of residual cement particles indicate use of coarsely ground Portland cement consistent with its reported age of early 20th century. Paste shows variable porosities from porous paste to denser paste, latter preferentially around residual cement particles. Paste is highly carbonated as evidenced by characteristic golden yellow birefringence in crossed polarized light photos in the right column.

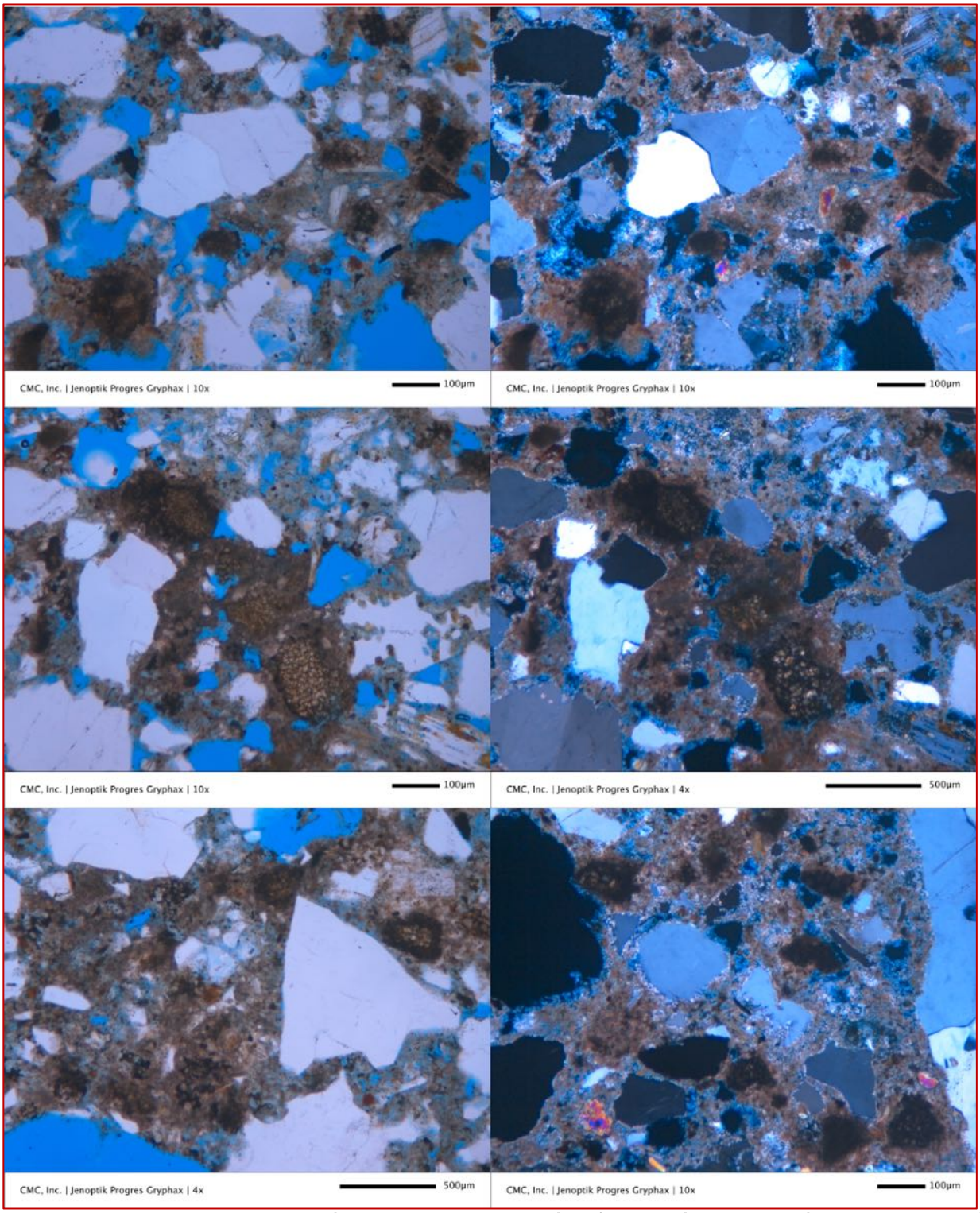

Figure B27: Mortar M3 (1916) Cement-lime mortar - Micrographs of cement-lime mortar showing many residual Portland cement particles and associated dense paste of hydration products of cement where residual cement particles show characteristic mineralogies (subhedral alite, anhedral belite clusters, and interstitial dark brown ferrite) and textures of Portland cement. Grain sizes of residual cement particles indicate use of coarsely ground Portland cement consistent with its reported age of early 20th century. Paste shows variable porosities from porous paste to denser pastes, latter preferentially around residual cement particles. Paste is highly carbonated as evidenced by characteristic golden yellow birefringence in crossed polarized light photos in the right column.

Micrographs of Thin Section of Cement-Lime Mortar M4 from 1916

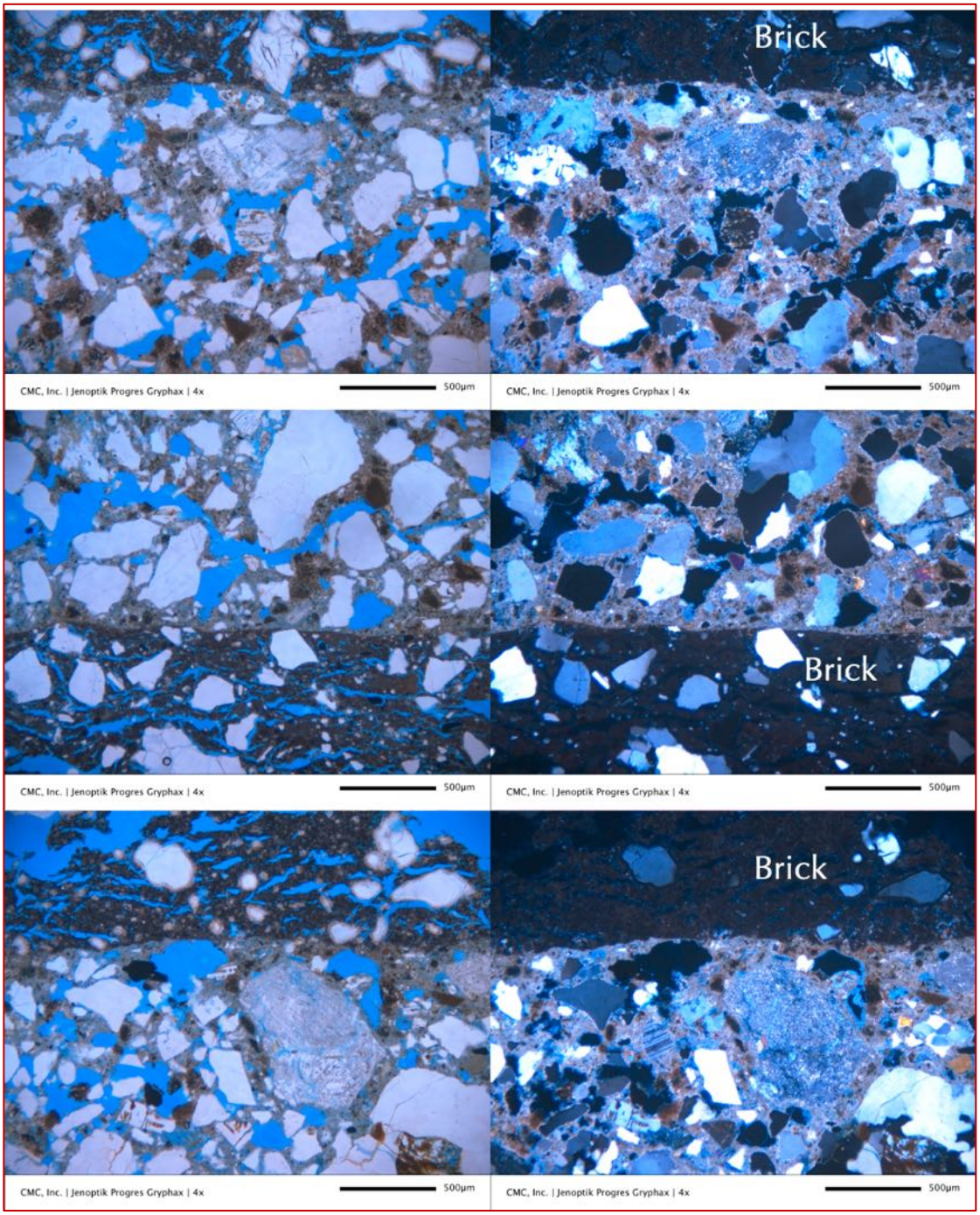

Figure B28: Mortar M4 (1916) Cement-lime mortar - Micrographs (left in PPL and right in corresponding XPL mode) of clay brick adhered to 1916 cement-lime mortar where brick shows characteristic: (a) elongated parallel voids from loss of water during drying after molding and subsequent baking; (b) tempered quartz additive in brick where quartz grains are angular, well-graded (without any glassy reaction rims around tempered quartz as seen in the brick adhered to M3 mortar); and (c) dark gray aluminosilicate glass matrix of brick, which is reddish-brown as opposed to gray in the brick adhered to M3 mortar. The adhered cement-lime mortar shows silica sand and carbonated paste. Notice the highly porous nature of brick from abundance of elongated parallel voids. Mortar is carbonated, non-air-entrained and porous where entrapped voids in mortar are highlighted by blue epoxy in plane polarized light photos in the left column.

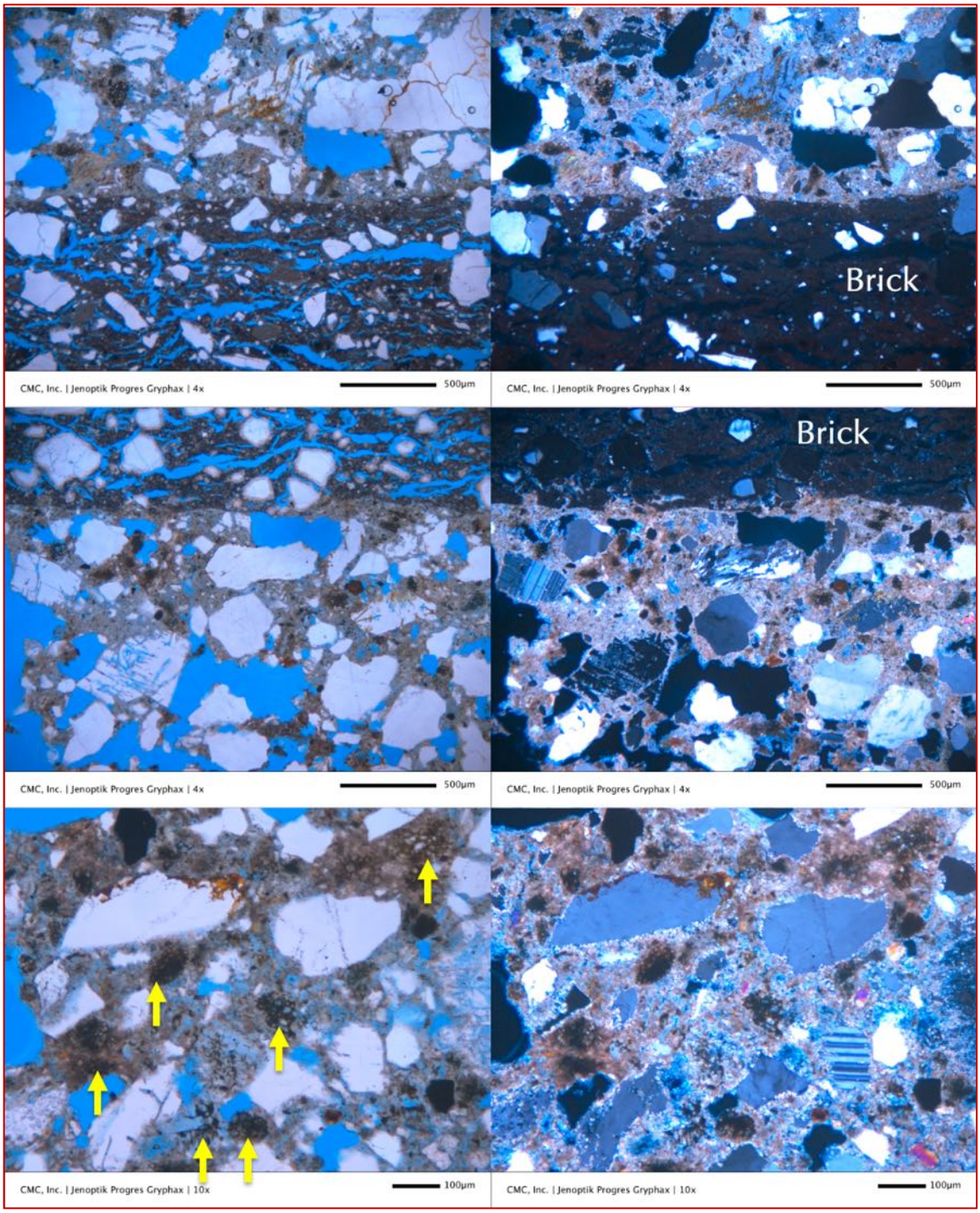

Figure B29: Mortar M4 (1916) Cement-lime mortar - Micrographs (left in PPL and right in corresponding XPL mode) of clay brick adhered to 1916 cement-lime mortar where brick shows characteristic: (a) elongated parallel voids from loss of water during drying after molding and subsequent baking; (b) tempered quartz additive in brick where quartz grains are angular, well-graded (without any glassy reaction rims around tempered quartz as seen in the brick adhered to M3 mortar); and (c) dark gray aluminosilicate glass matrix of brick, which is reddish-brown as opposed to gray in the brick adhered to M3 mortar. The adhered cement-lime mortar shows silica sand and carbonated paste. Notice the highly porous nature of brick from abundance of elongated parallel voids. Mortar is carbonated, non-air-entrained and porous where entrapped voids in mortar are highlighted by blue epoxy in plane polarized light photos in the left column. Paste contains many residual Portland cement particles that are not as coarse as in M3 mortar (some are marked with arrows in bottom left photo).

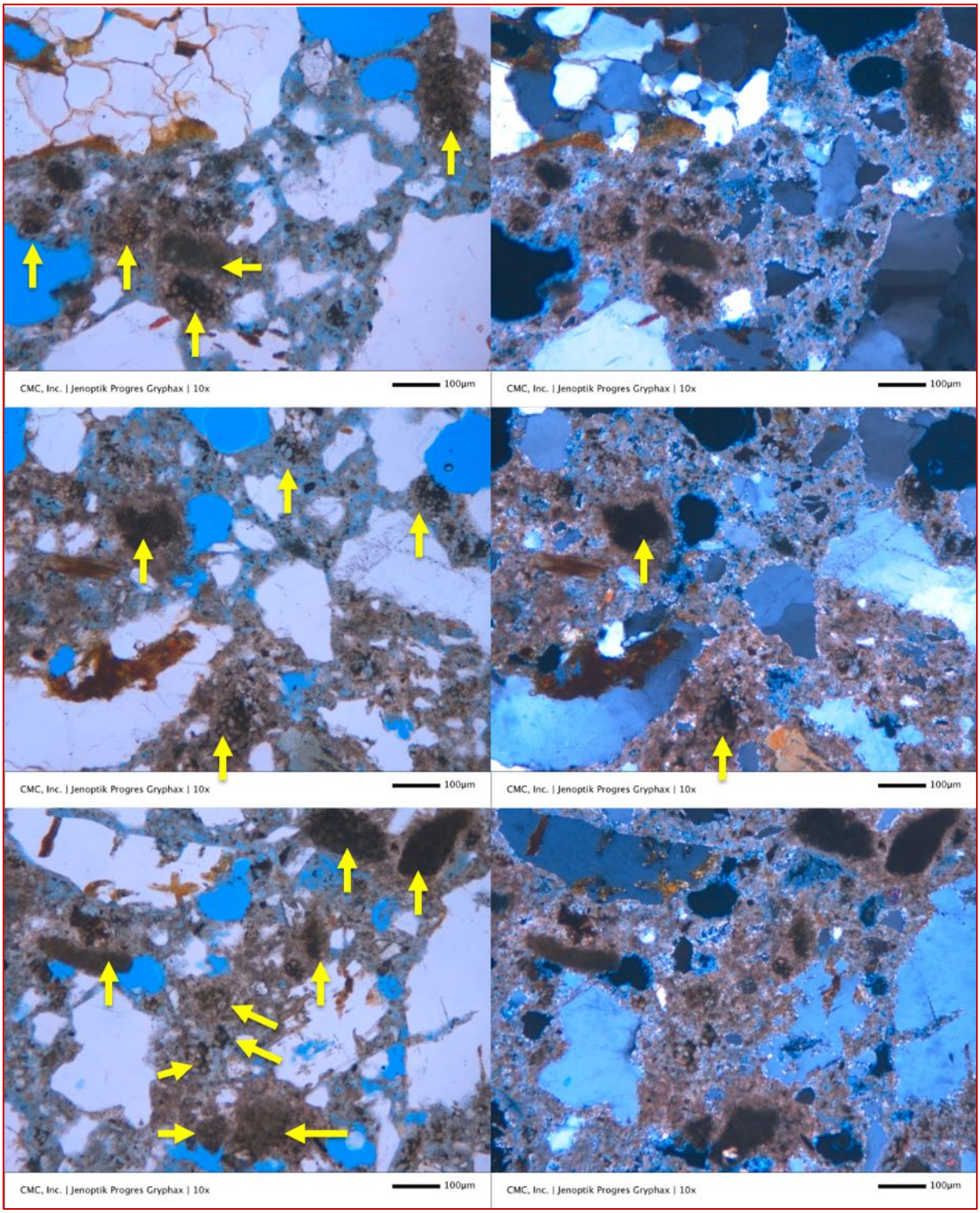

Figure B30: Mortar M4 (1916) Cement-lime mortar - Micrographs of cement-lime mortar showing many residual Portland cement particles and associated dense paste of hydration products of cement where residual cement particles show characteristic mineralogies (subhedral alite, anhedral belite clusters, and interstitial dark brown ferrite) and textures of Portland cement (many are marked with arrows). Grain sizes of residual cement particles are not as coarse as seen in the M3 mortar indicating finer grain size of cement used in M4 mortar than the one used in M3 mortar. Paste shows variable porosities from porous paste to denser pastes, latter preferentially around residual cement particles. Paste is highly carbonated as evidenced by characteristic golden yellow birefringence in crossed polarized light photos in the right column.

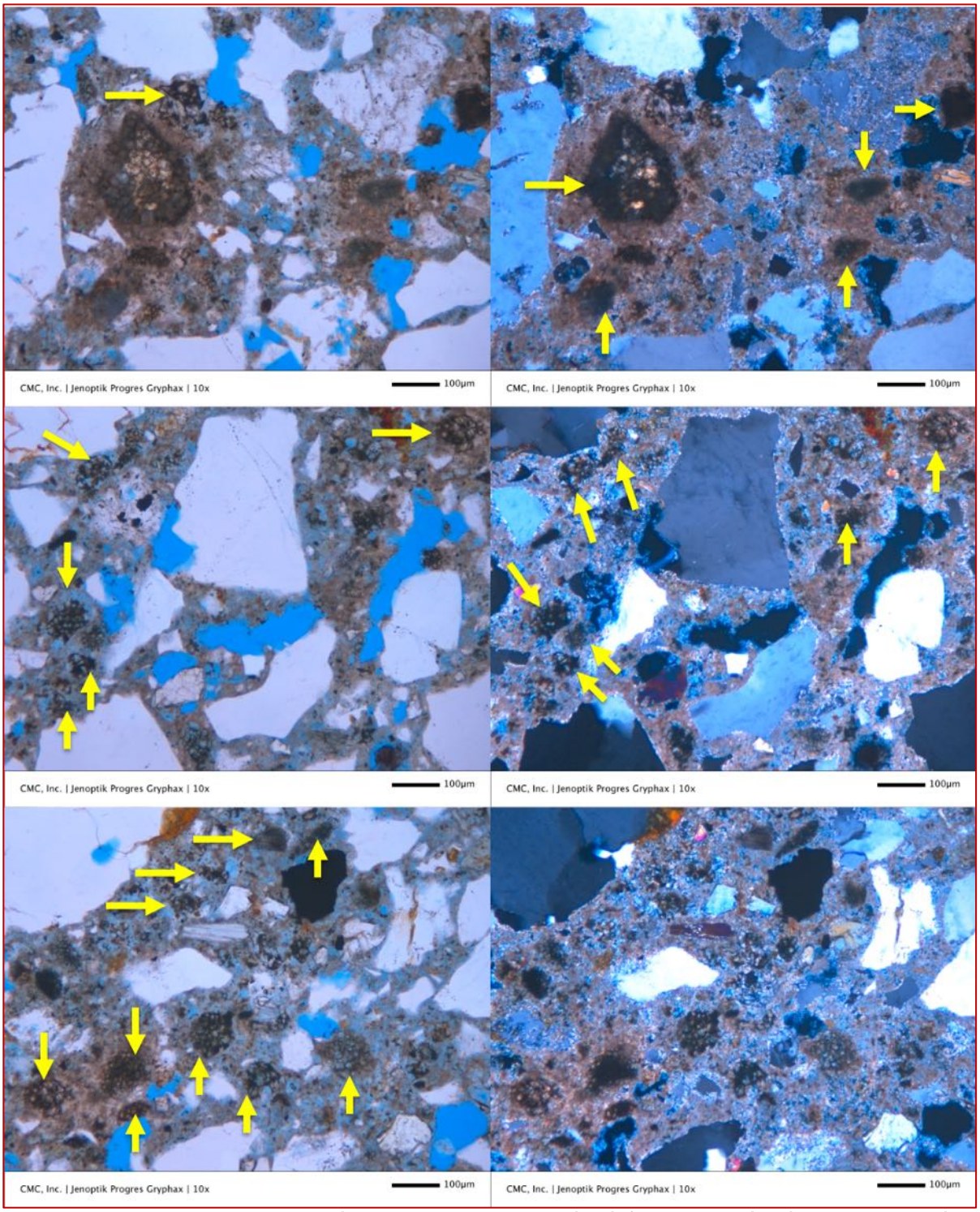

Figure B31: Mortar M4 (1916) Cement-lime mortar - Micrographs (left in PPL and right in corresponding XPL mode) of cement-lime mortar showing many residual Portland cement particles and associated dense paste of hydration products of cement where residual cement particles show characteristic mineralogies (subhedral alite, anhedral belite clusters, and interstitial dark brown ferrite) and textures of Portland cement (many are marked with arrows). Grain sizes of residual cement particles are not as coarse as seen in the M3 mortar indicating finer grain size of cement used in M4 mortar than the one used in M3 mortar. Paste shows variable porosities from porous paste to denser pastes, latter preferentially around residual cement particles. Paste is highly carbonated as evidenced by characteristic golden yellow birefringence in crossed polarized light photos in the right column.

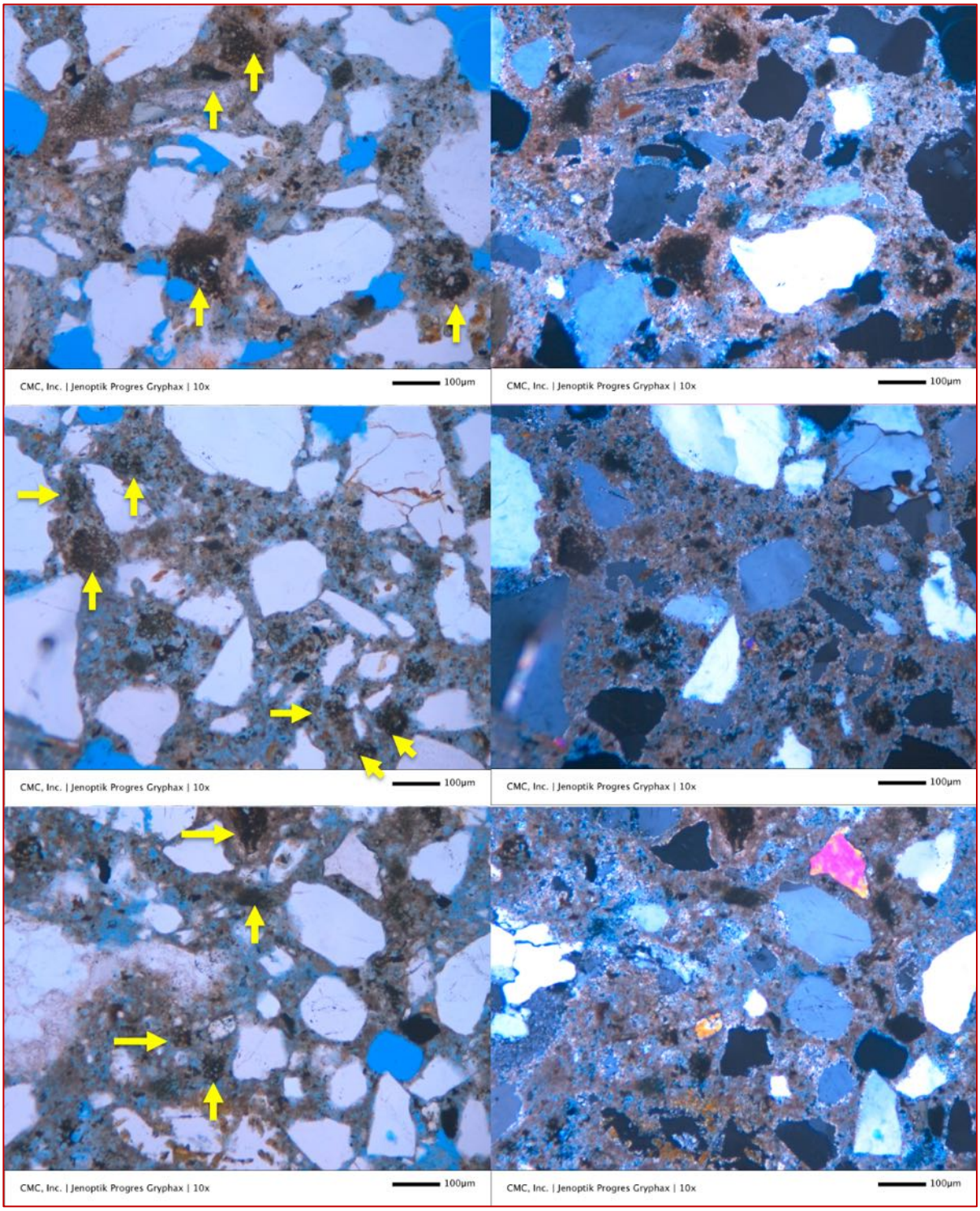

Figure B32: Mortar M4 (1916) Cement-lime mortar - Micrographs (left in PPL and right in corresponding XPL mode) of cement-lime mortar showing many residual Portland cement particles and associated dense paste of hydration products of cement where residual cement particles show characteristic mineralogies (subhedral alite, anhedral belite clusters and interstitial dark brown ferrite) and textures of Portland cement (many are marked with arrows). Grain sizes of residual cement particles are not as coarse as seen in the M3 mortar indicating finer grain size of cement used in M4 mortar than the one used in M3 mortar. Paste shows variable porosities from porous paste to denser paste, latter preferentially around residual cement particles. Paste is highly carbonated as evidenced by characteristic golden yellow birefringence in crossed polarized light photos in the right column.

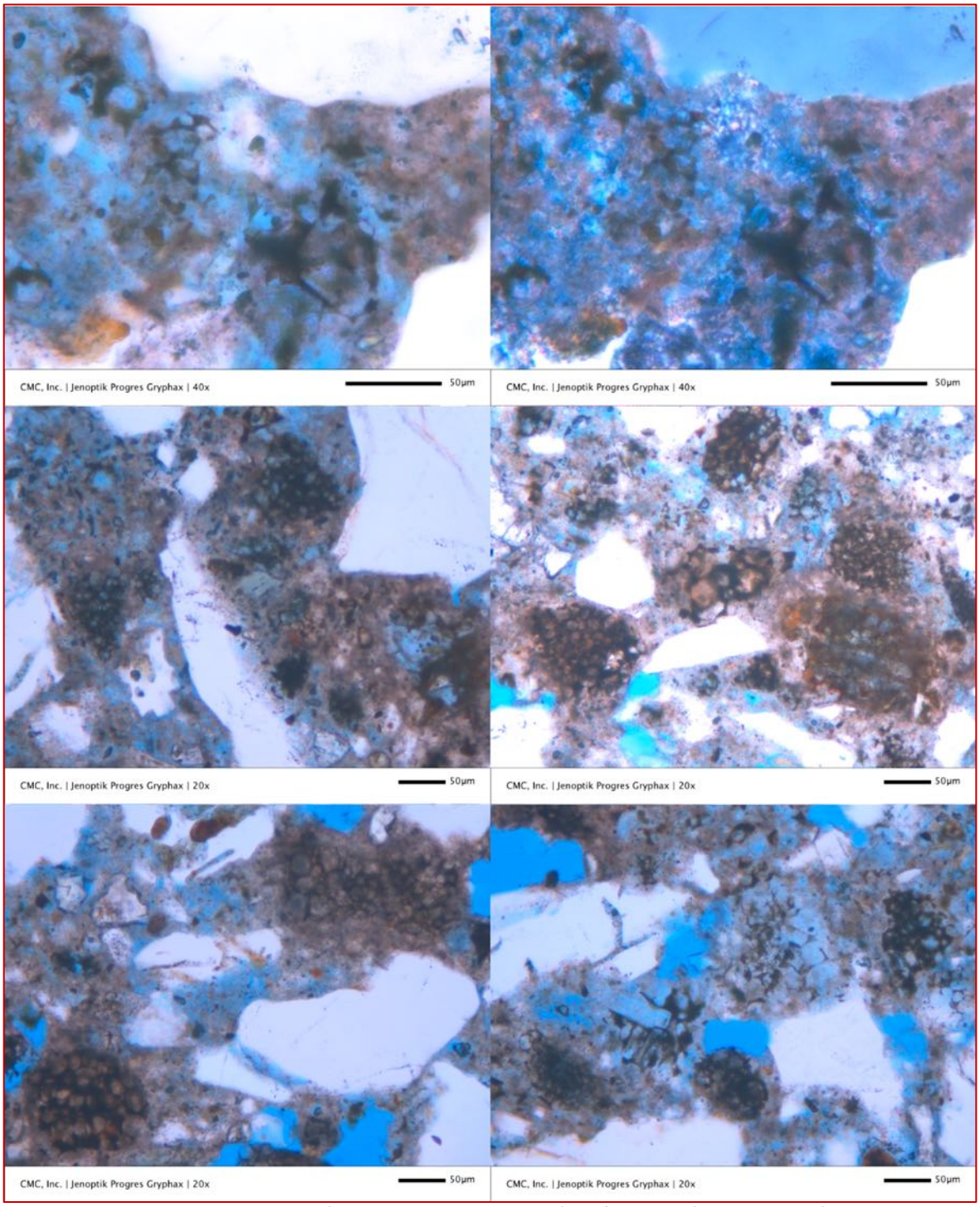

Figure B33: Mortar M4 (1916) Cement-lime mortar - Micrographs of cement-lime mortar showing many residual Portland cement particles and associated dense paste of hydration products of cement where residual cement particles show characteristic mineralogies (subhedral alite, anhedral belite clusters, and interstitial dark brown ferrite) and textures of Portland cement (many are marked with arrows). Grain sizes of residual cement particles are not as coarse as seen in the M3 mortar indicating finer grain size of cement used in M4 mortar than the one used in M3 mortar. Paste shows variable porosities from porous paste to denser paste, latter preferentially around residual cement particles. These photos were taken at higher magnification than the previous one to show textures of residual cement particles where calcium-silicate phases are mostly hydrated leaving pseudomorphs of alite and belite with interstitial dark ferrite phases (prominent in the top row).

Micrographs of Thin Section of Masonry Cement Mortar M5 from Late 1960s

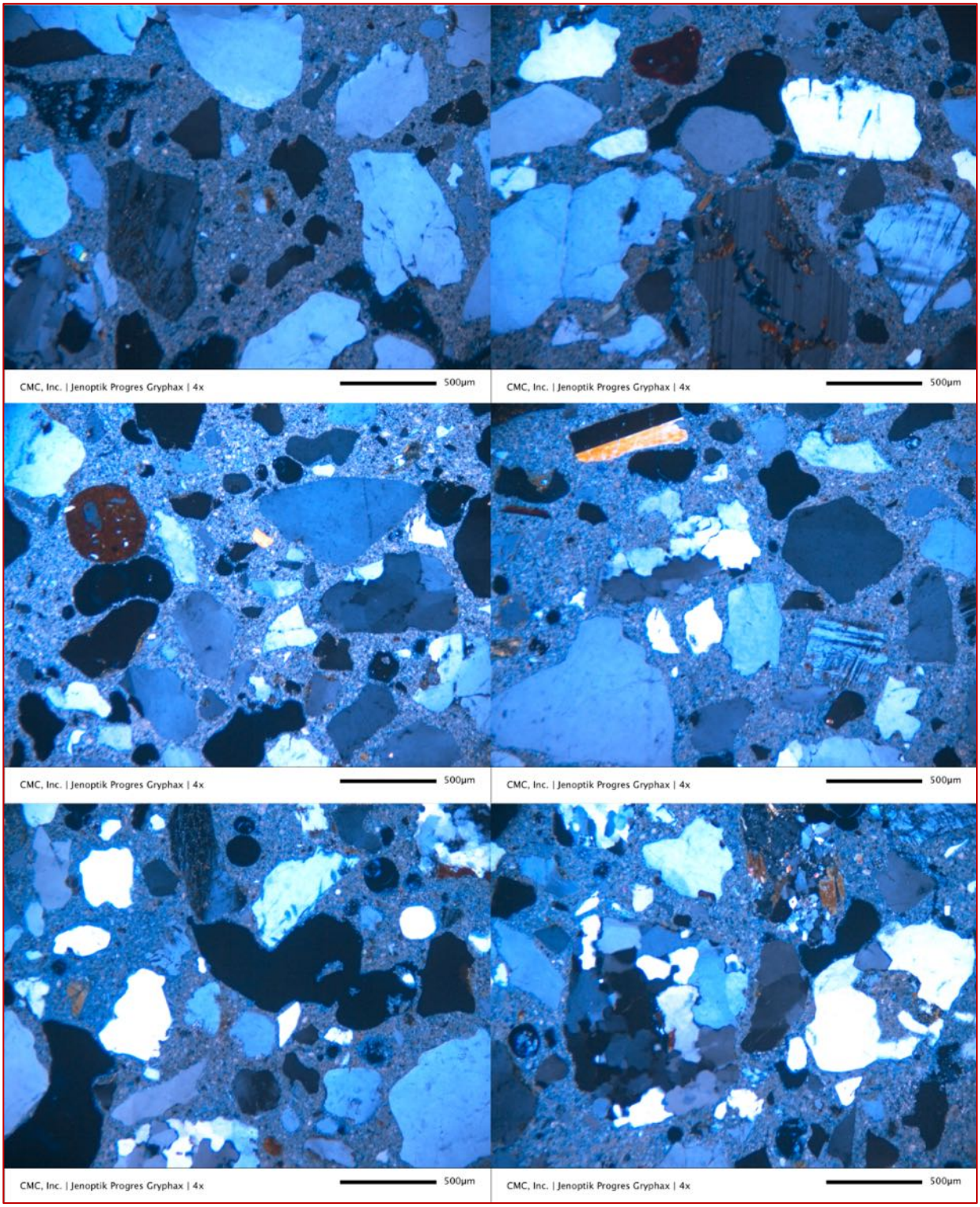

Figure B34: Mortar M5 (Late 1960s) Masonry cement mortar – Micrographs of masonry cement mortar from late 1960s showing: (a) natural siliceous sand aggregate consisting of major amount of quartz, and subordinate amounts of feldspar and quartzite particles, and (b) carbonated paste which is characteristic of many modern-day masonry cement mortars. Unlike modern-day masonry cements which are characteristically air-entrained, however, the present mortar is non-air-entrained.

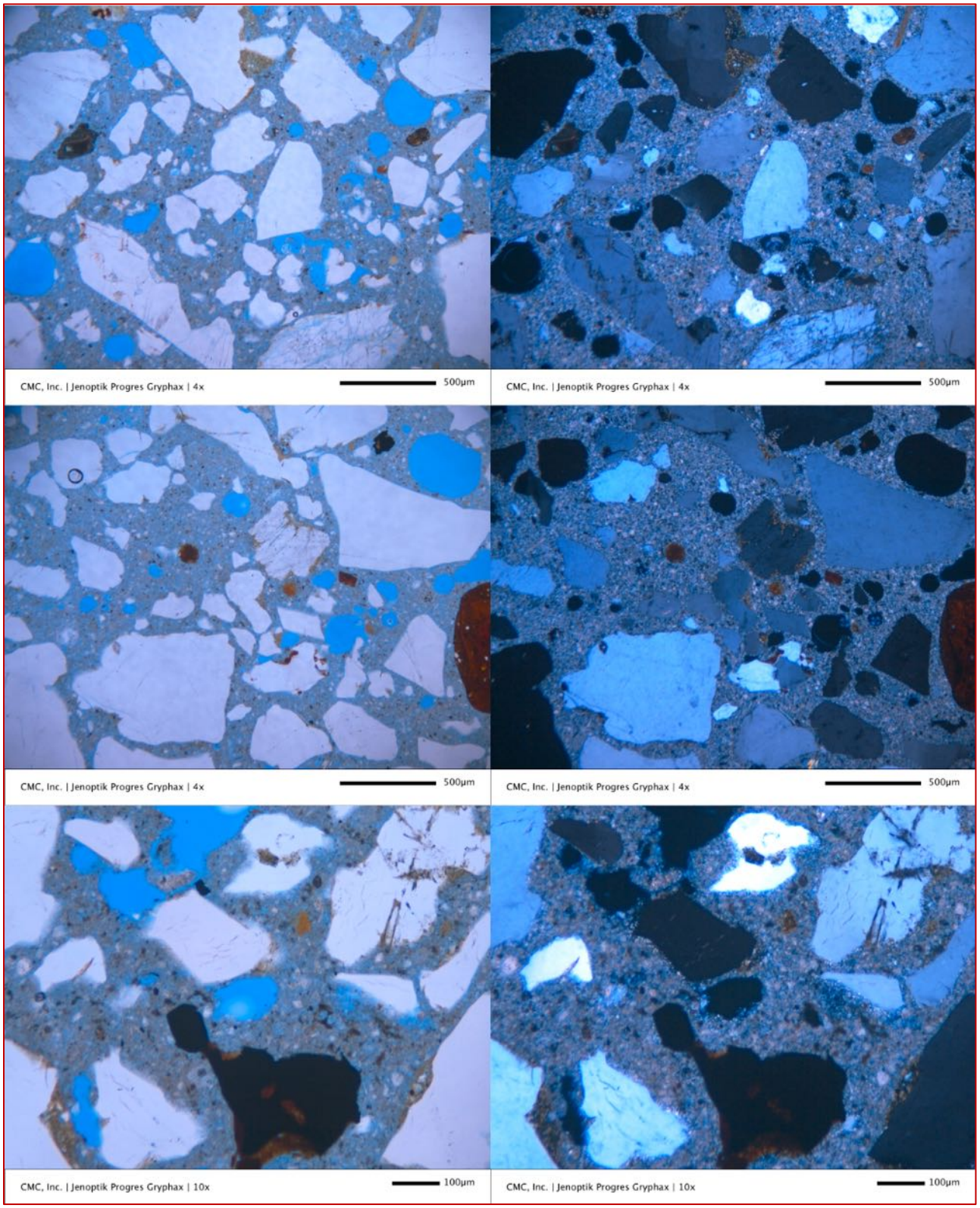

Figure B35: Mortar M5 (Late 1960s) Masonry cement mortar - Micrographs (left in PPL and right in corresponding XPL mode) of masonry cement mortar from late 1960s showing: (a) natural siliceous sand aggregate consisting of major amount of quartz, and subordinate amounts of feldspar and quartzite particles, and (b) carbonated paste which is characteristic of many modern-day masonry cement mortars. Unlike modern-day masonry cements which are characteristically air-entrained, however, the present mortar is non-air-entrained.

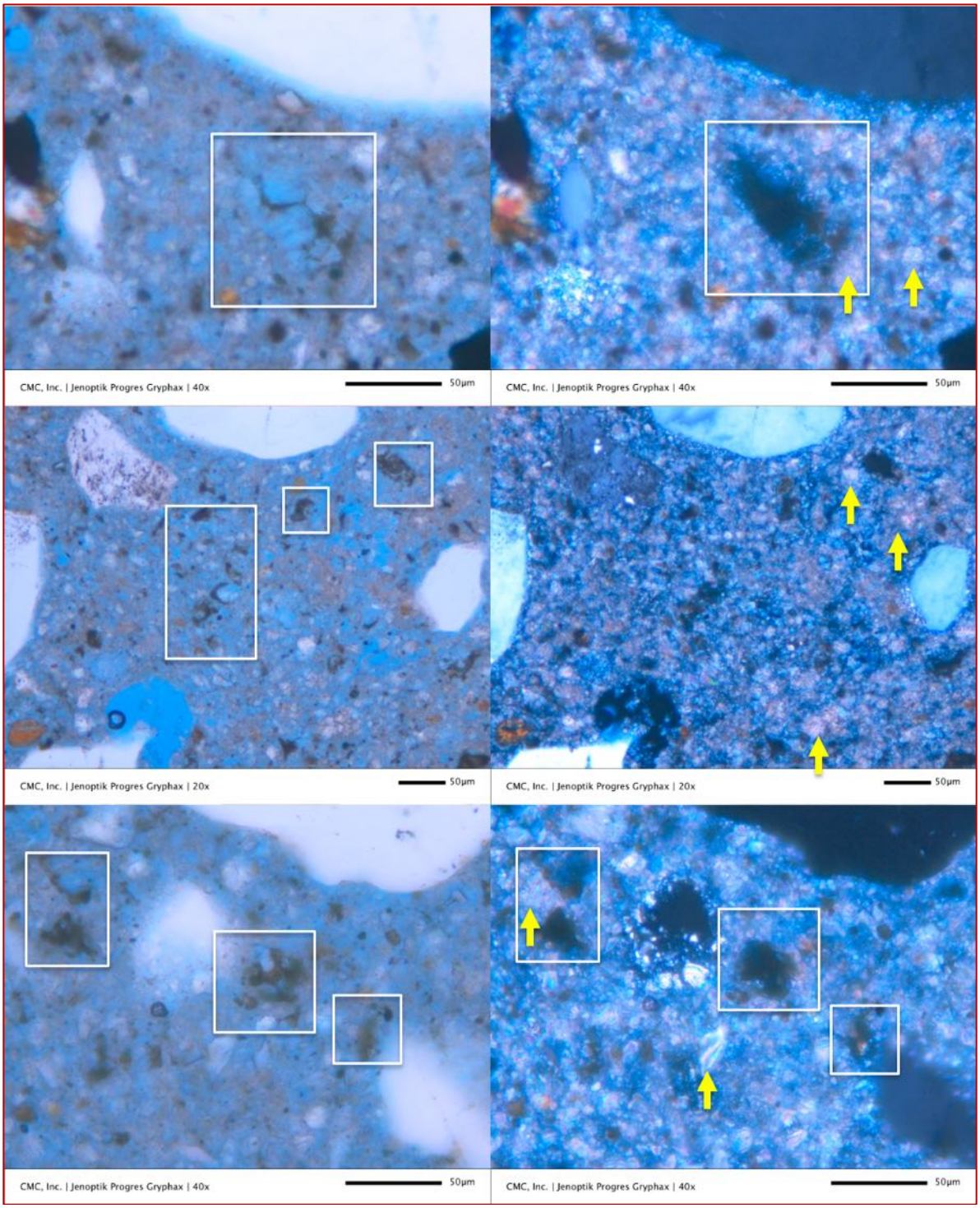

Figure B36: Mortar M5 (Late 1960s) Masonry cement mortar - Micrographs (left in PPL and right in corresponding XPL mode) of masonry cement mortar from late 1960s showing carbonated paste, which is characteristic of many modern-day masonry cement mortars. Unlike modern-day masonry cements which are characteristically air-entrained, however, the present mortar is non-air-entrained. Within the carbonated paste are: (a) relics of well-hydrated and carbonated Portland cement particles some of which are boxed, carbonated hydrated lime, and limestone fine particles having the fineness of Portland cement. Masonry cement used had a higher lime content and lower Portland cement content, e.g., similar to or probably of higher lime than many modern-day Type N masonry cement mortars.

Micrographs of Thin Section of Bricks

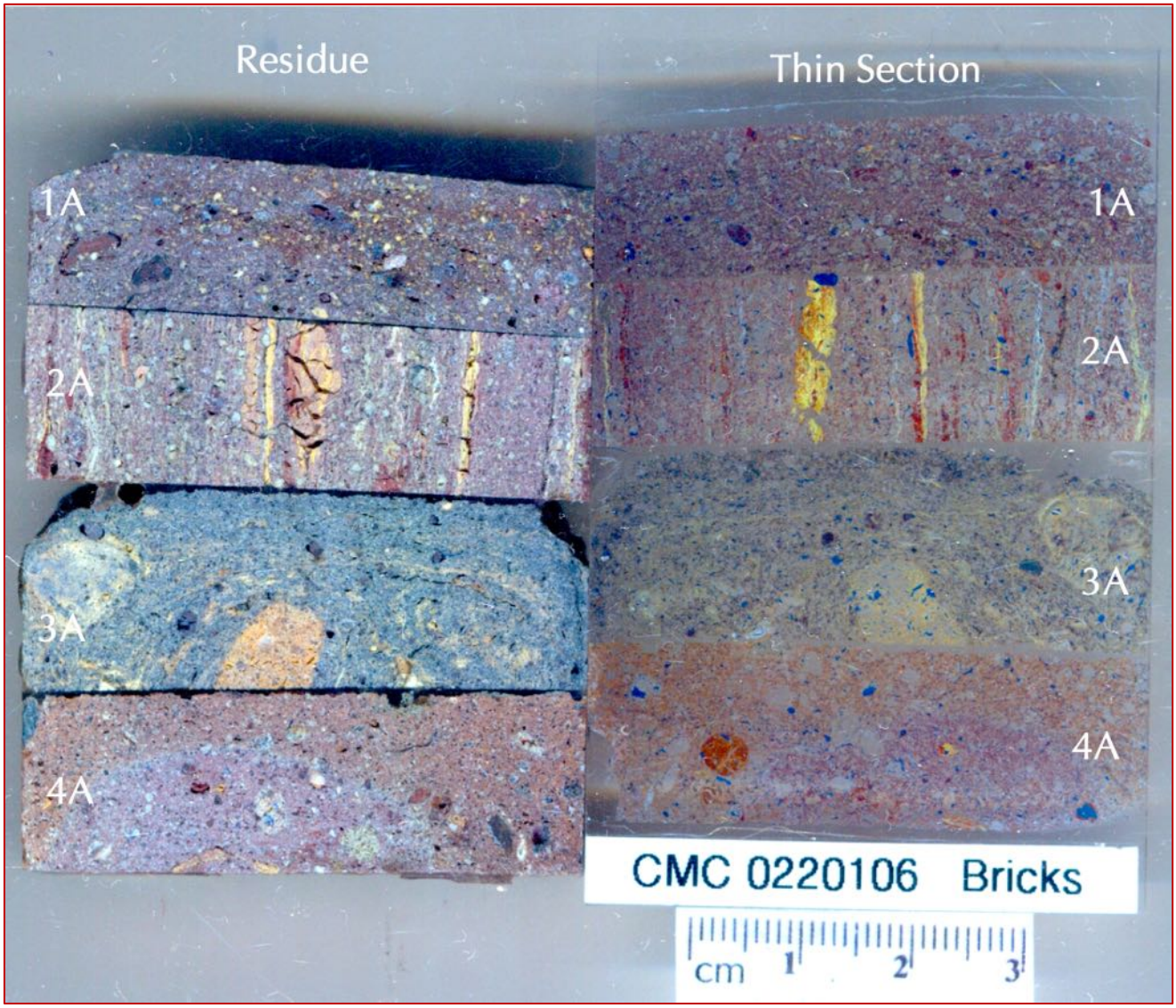

Figure B37: Blue dye-mixed epoxy-impregnated thin section and residue left after preparation of thin section of clay bricks from samples 1A and 2A of 1950s vintage, and 3A and 4A of 1916 vintage. Blue epoxy has highlighted pore spaces and voids in the bricks, thus revealed highly porous natures of all four bricks.

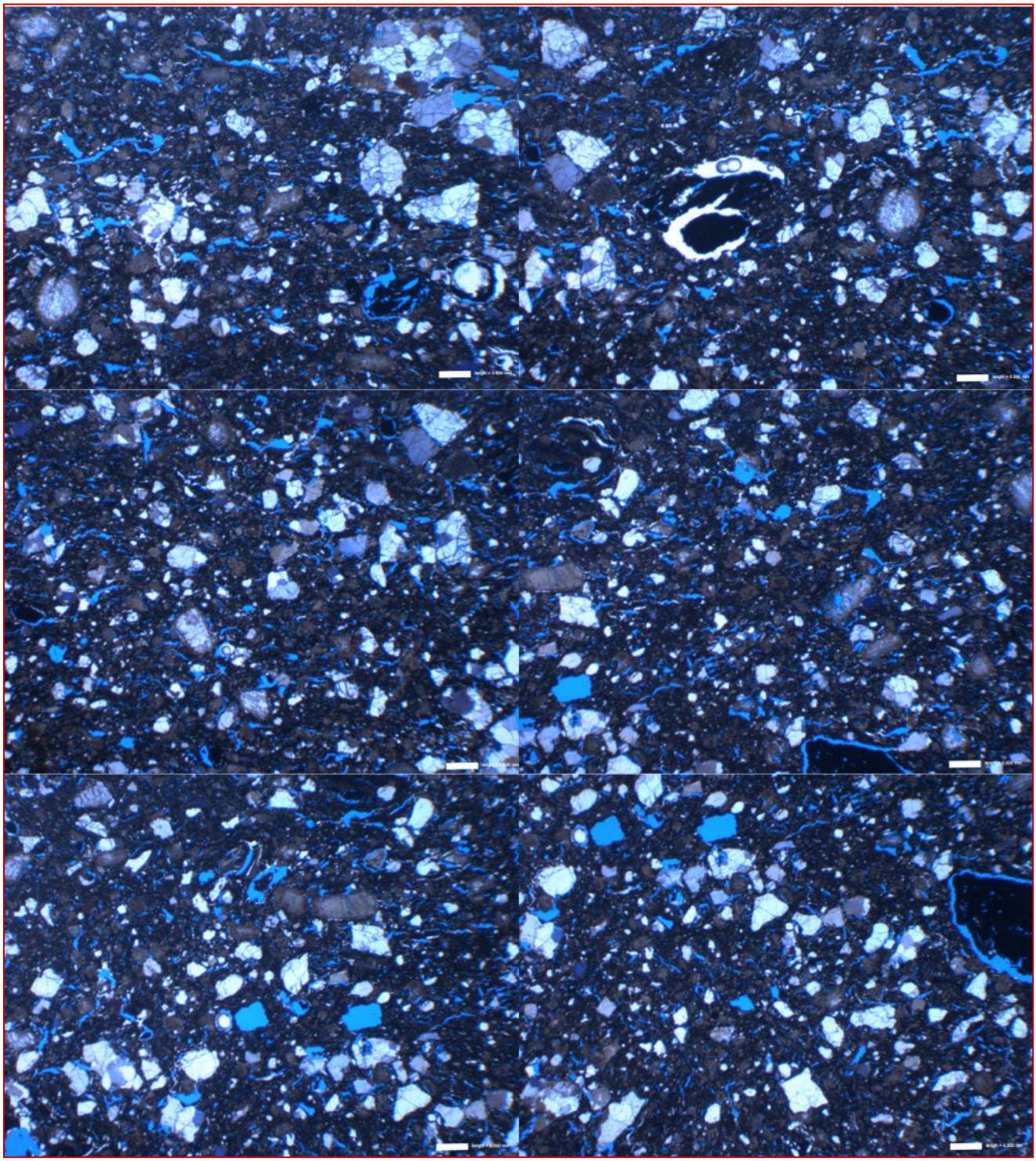

Figure B38: Micrographs of thin section of Brick 1A from 1950s vintage (taken using a transmitted-light stereo-zoom microscope) showing: (a) tempered quartz additive where quartz grains are crushed, well-graded, well-distributed, and representative of one population, (b) a few grog particles of previously fired bricks having rims of separations from surrounding aluminosilicate matrix of host brick, (c) reddish-brown aluminosilicate glassy matrix of fired clay, and (d) abundant elongated voids of separation from shrinkage during drying after molding followed by subsequent baking. Notice the porous nature of the brick from abundance of void spaces highlighted by blue epoxy. White scale bar in the bottom right corner in each photo is 0.5 mm in length.

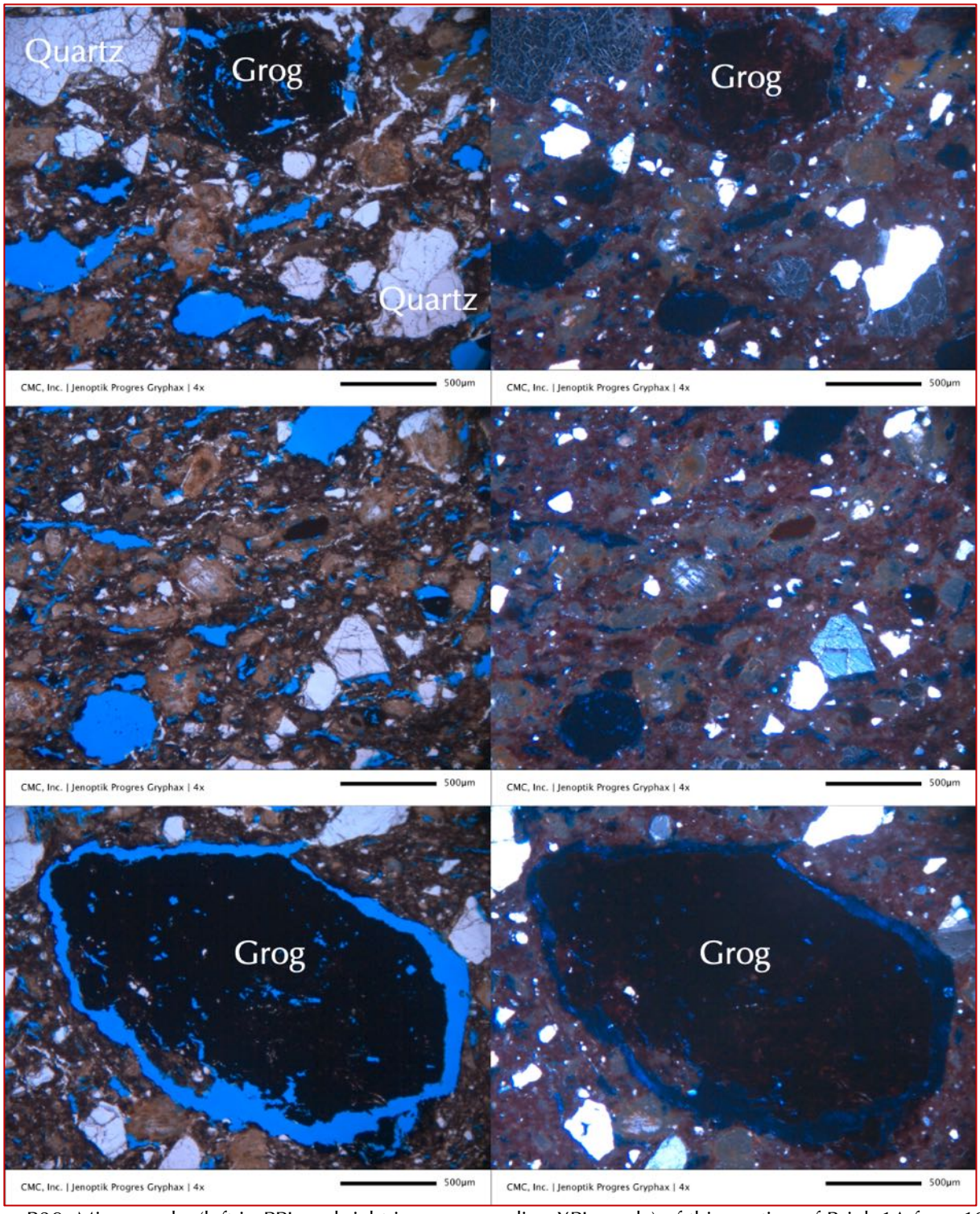

Figure B39: Micrographs (left in PPL and right in corresponding XPL mode) of thin section of Brick 1A from 1950s vintage (taken using a petrographic microscope) showing: (a) tempered quartz additive where quartz grains are crushed, well-graded, well-distributed, and representative of one population, (b) a few grog particles of previously fired bricks having rims of separations from surrounding aluminosilicate matrix of host brick, (c) reddish-brown aluminosilicate glass matrix of fired clay, and (d) abundant elongated voids of separation from shrinkage during drying after molding followed by subsequent baking. Notice the porous nature of the brick from abundance of void spaces highlighted by blue epoxy.

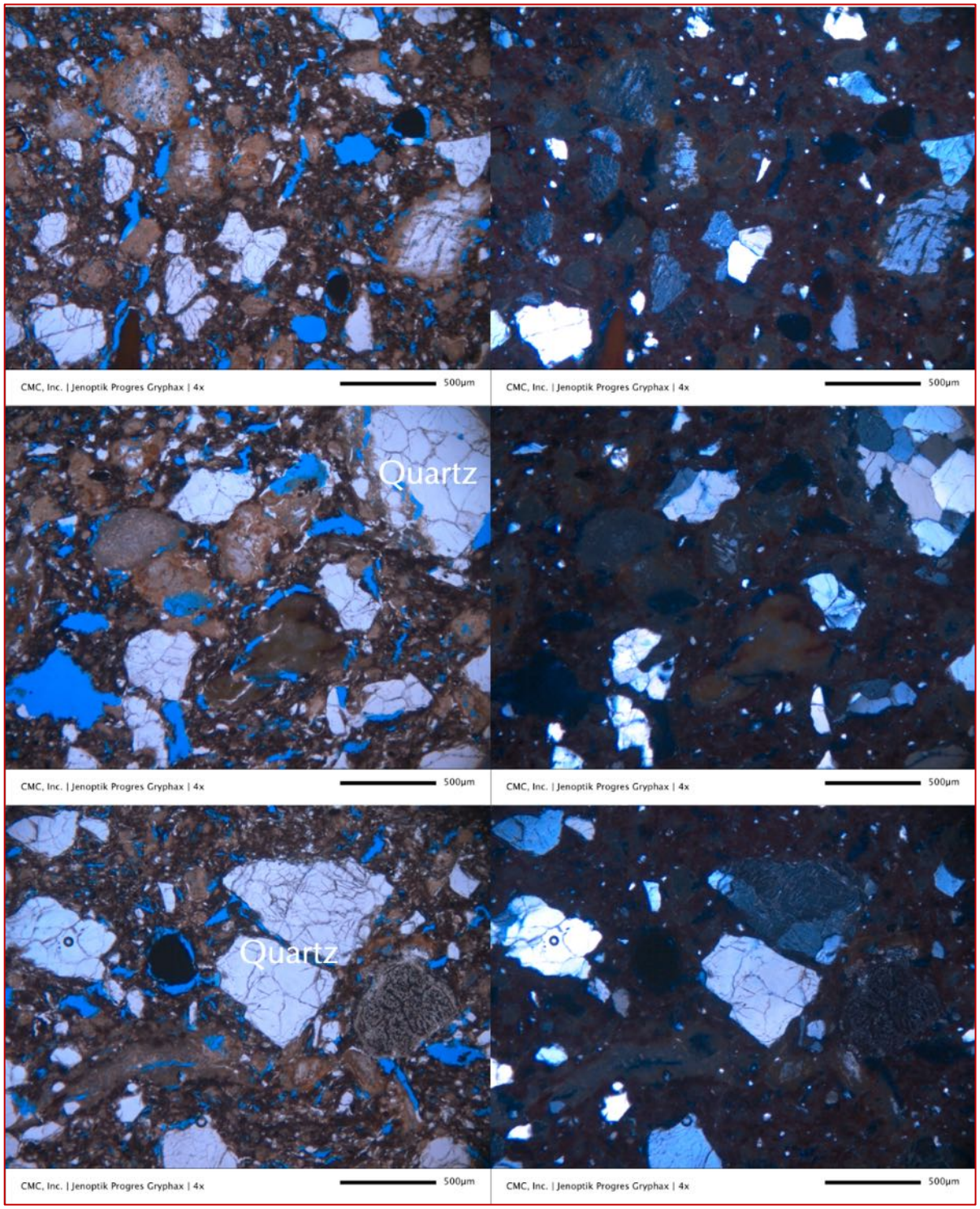

Figure B40: Micrographs (left in PPL and right in corresponding XPL mode) of thin section of Brick 1A from 1950s vintage (taken using a petrographic microscope) showing: (a) tempered quartz additive where quartz grains are crushed, well-graded, well-distributed, and representative of one population, (b) a few grog particles of previously fired bricks having rims of separations from surrounding aluminosilicate matrix of host brick, (c) reddish-brown aluminosilicate glass matrix of fired clay, and (d) abundant elongated voids of separation from shrinkage during drying after molding followed by subsequent baking. Notice the porous nature of the brick from abundance of void spaces highlighted by blue epoxy.

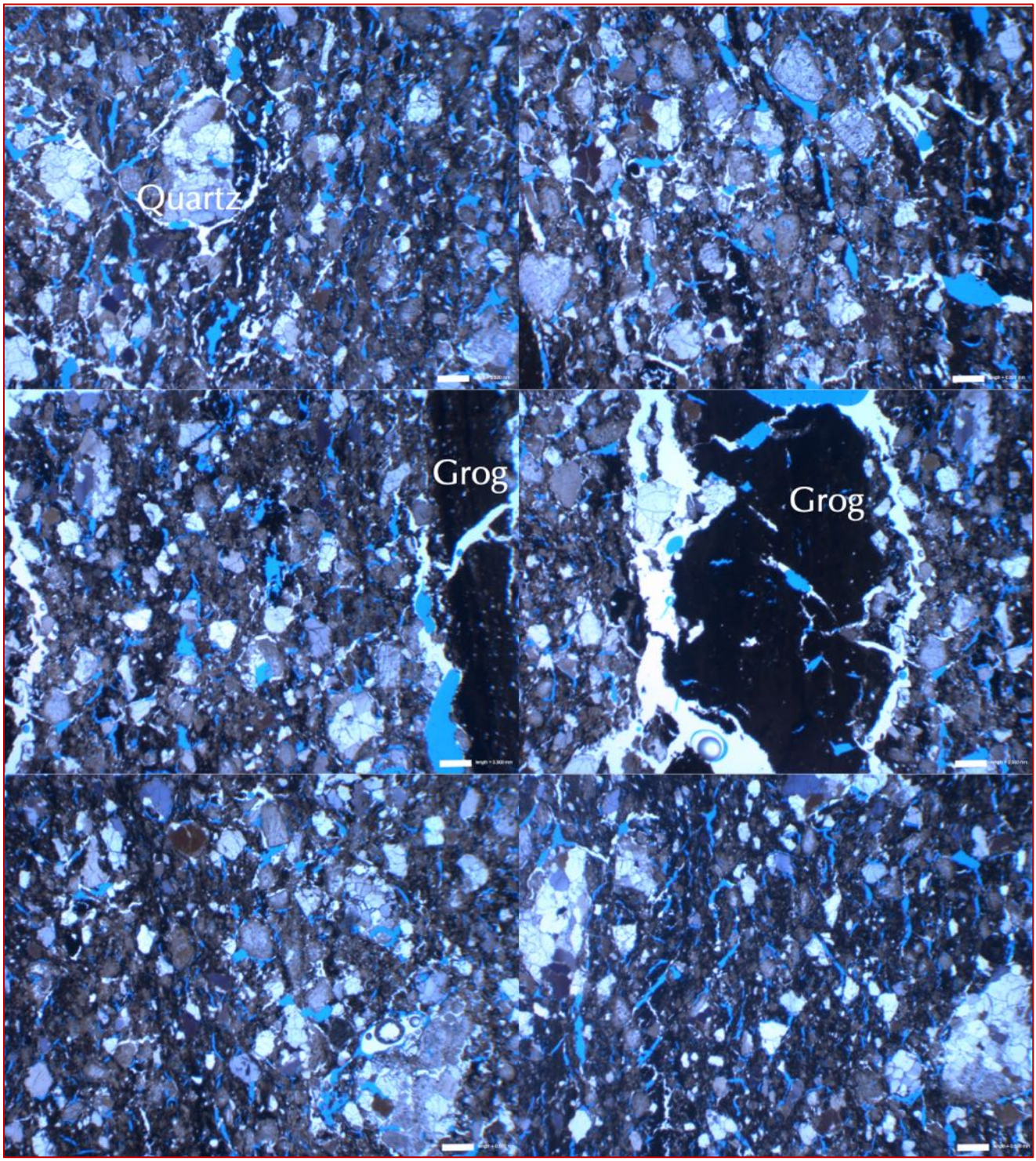

Figure B41: Micrographs of thin section of Brick 2A from 1950s vintage (taken using a transmitted-light stereo-zoom microscope) showing: (a) tempered quartz additive where quartz grains are crushed, well-graded, well-distributed, and representative of one population, (b) a few grog particles of previously fired bricks having rims of separations from surrounding aluminosilicate matrix of host brick, (c) reddish-brown aluminosilicate glass matrix of fired clay, and (d) abundant elongated voids of separation from shrinkage during drying after molding followed by subsequent baking. Notice the porous nature of the brick from abundance of void spaces highlighted by blue epoxy. White scale bar in the bottom right corner in each photo is 0.5 mm in length.

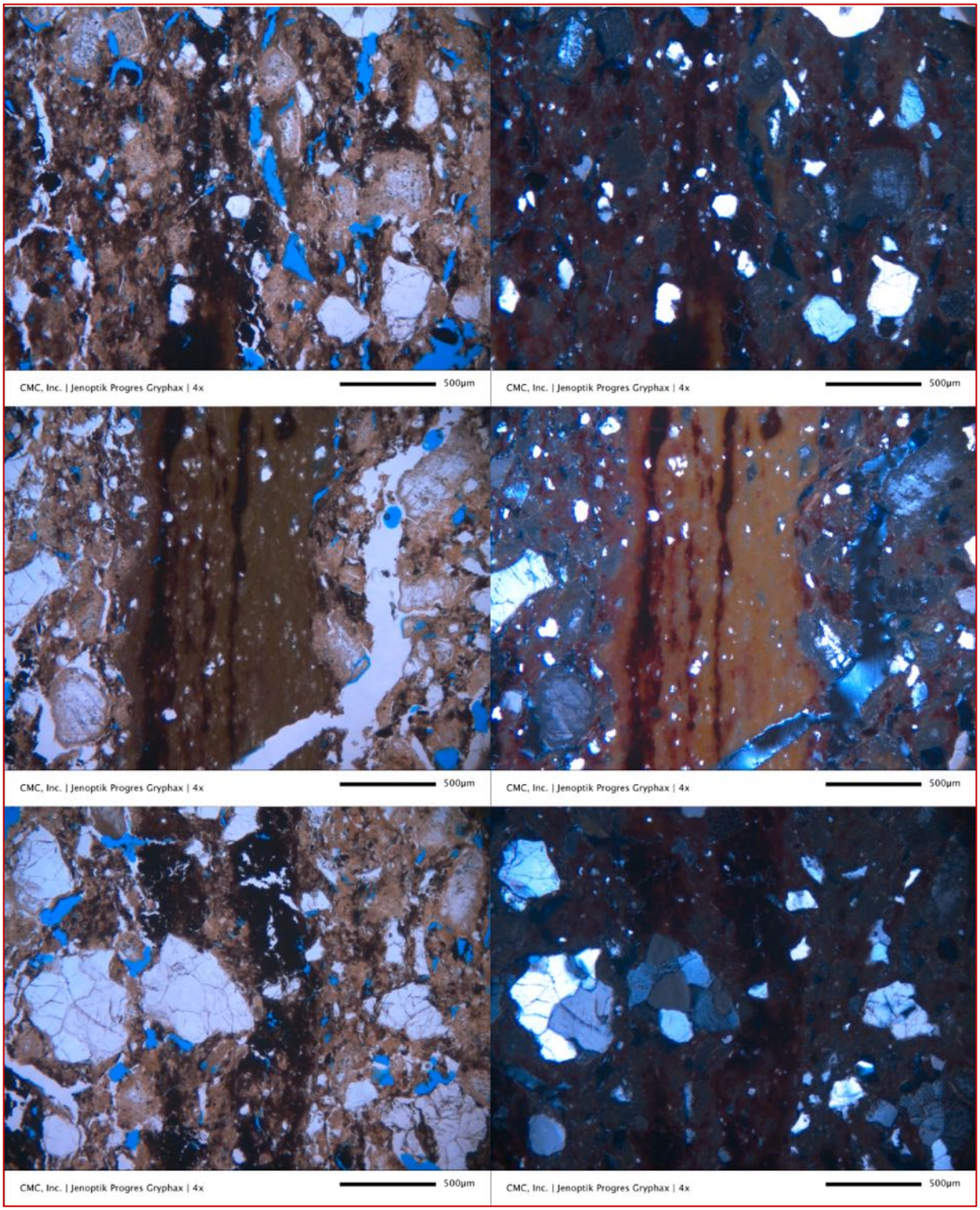

Figure B42: Micrographs (left in PPL and right in corresponding XPL mode) of thin section of Brick 2A from 1950s vintage (taken using a petrographic microscope) showing: (a) tempered quartz additive where quartz grains are crushed, well-graded, well-distributed, and representative of one population, (b) a few grog particles of previously fired bricks having rims of separations from surrounding aluminosilicate matrix of host brick, (c) reddish brown aluminosilicate glass matrix of fired clay, and (d) abundant elongated voids of separation from shrinkage during drying after molding followed by subsequent baking. Notice the porous nature of the brick from abundance of void spaces highlighted by blue epoxy.

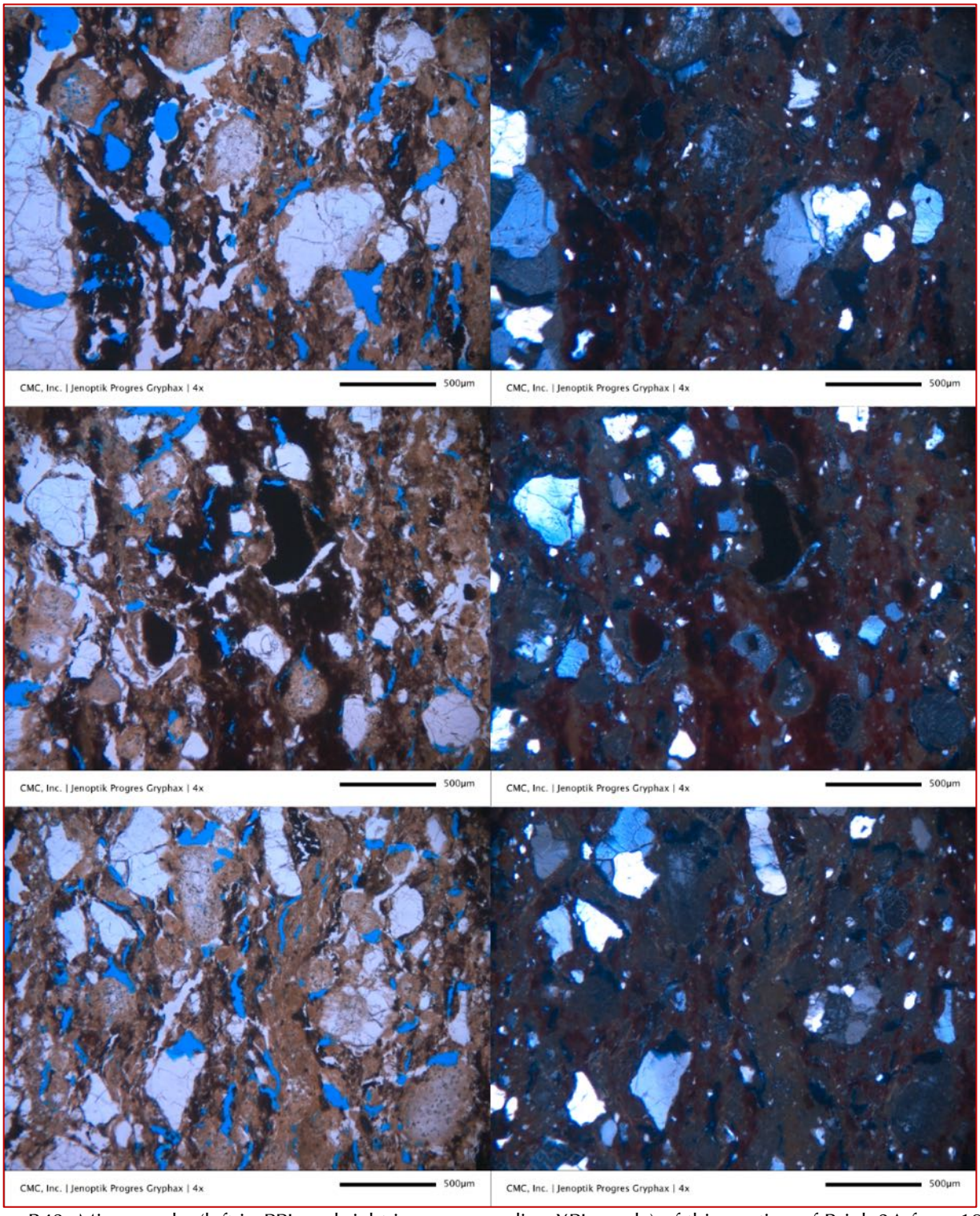

Figure B43: Micrographs (left in PPL and right in corresponding XPL mode) of thin section of Brick 2A from 1950s vintage (taken using a petrographic microscope) showing: (a) tempered quartz additive where quartz grains are crushed, well-graded, well-distributed, and representative of one population, (b) a few grog particles of previously fired bricks having rims of separations from surrounding aluminosilicate matrix of host brick, (c) reddish-brown aluminosilicate glassy matrix of fired clay, and (d) abundant elongated voids of separation from shrinkage during drying after molding followed by subsequent baking. Notice the porous nature of the brick from abundance of void spaces highlighted by blue epoxy.

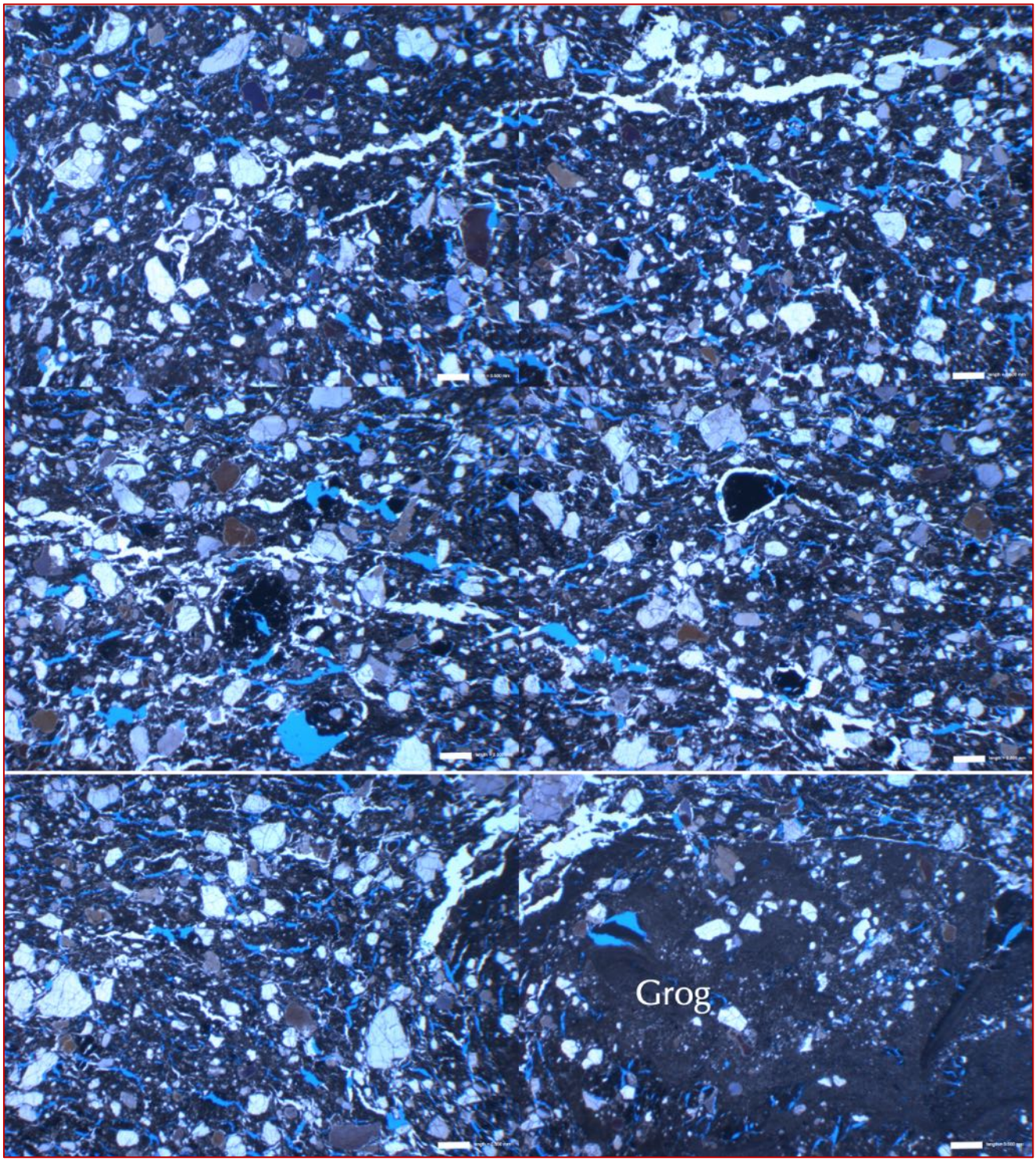

Figure B44: Micrographs of thin section of Brick 3A from 1916 vintage (taken using a transmitted-light stereo-zoom microscope) showing: (a) tempered quartz additive where quartz grains are crushed, well-graded, well-distributed, and representative of one population, (b) a few grog particles of previously fired bricks having rims of separations from surrounding aluminosilicate matrix of host brick, (c) lack of reddish-brown aluminosilicate glassy matrix of fired clay that is found in other bricks, and (d) abundant elongated voids of separation from shrinkage during drying after molding followed by subsequent baking. Notice the porous nature of the brick from abundance of void spaces highlighted by blue epoxy. White scale bar in the bottom right corner in each photo is 0.5 mm in length.

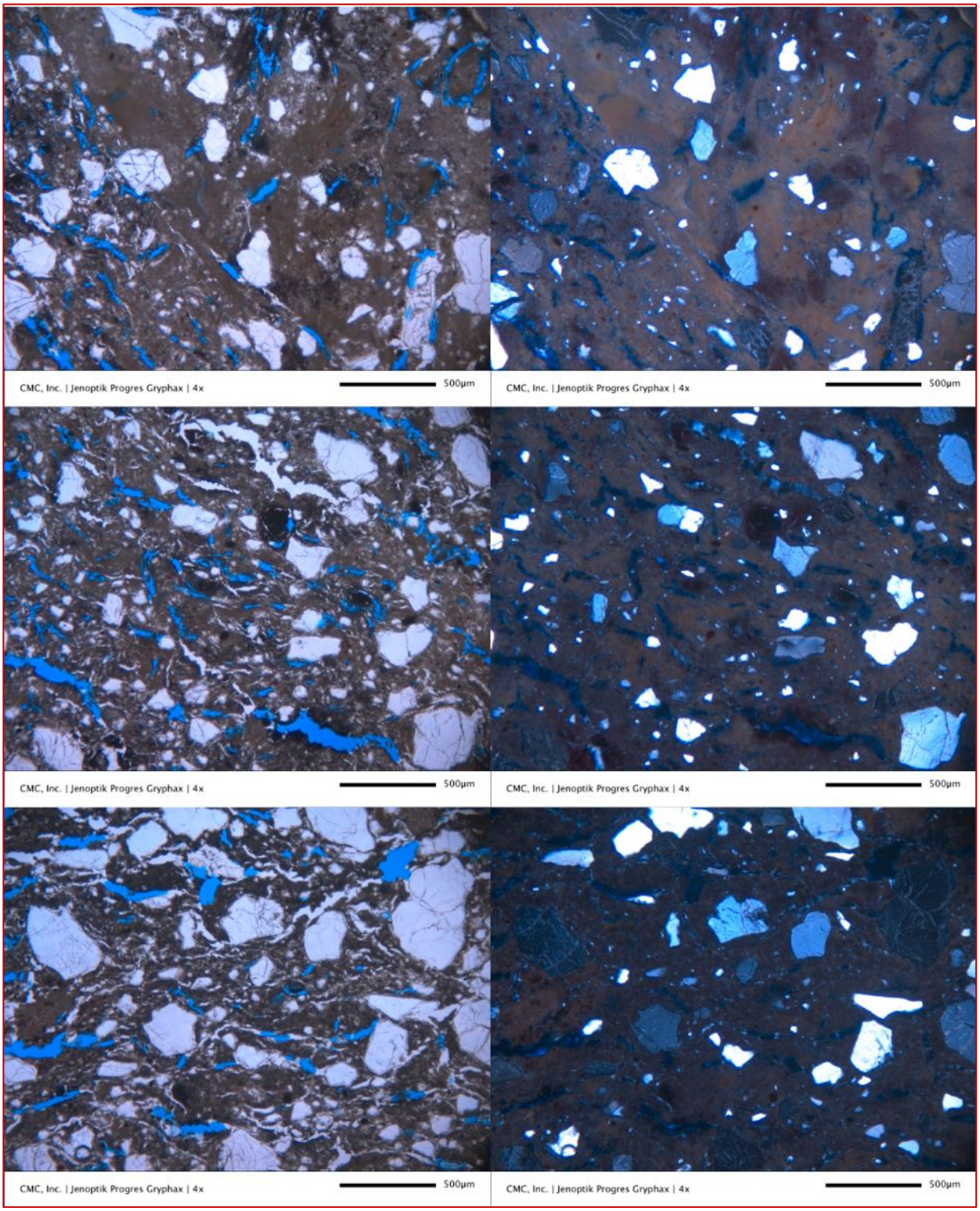

Figure B45: Micrographs (left in PPL and right in corresponding XPL mode) of thin section of Brick 3A from 1916 vintage (taken using a petrographic microscope) showing: (a) tempered quartz additive where quartz grains are crushed, well-graded, well-distributed, and representative of one population, (b) a few grog particles of previously fired bricks having rims of separations from surrounding aluminosilicate matrix of host brick, (c) lack of reddish-brown aluminosilicate glass matrix of fired clay found in other bricks, and (d) abundant elongated voids of separation from shrinkage during drying after molding followed by subsequent baking. Notice the porous nature of the brick from abundance of void spaces highlighted by blue epoxy.

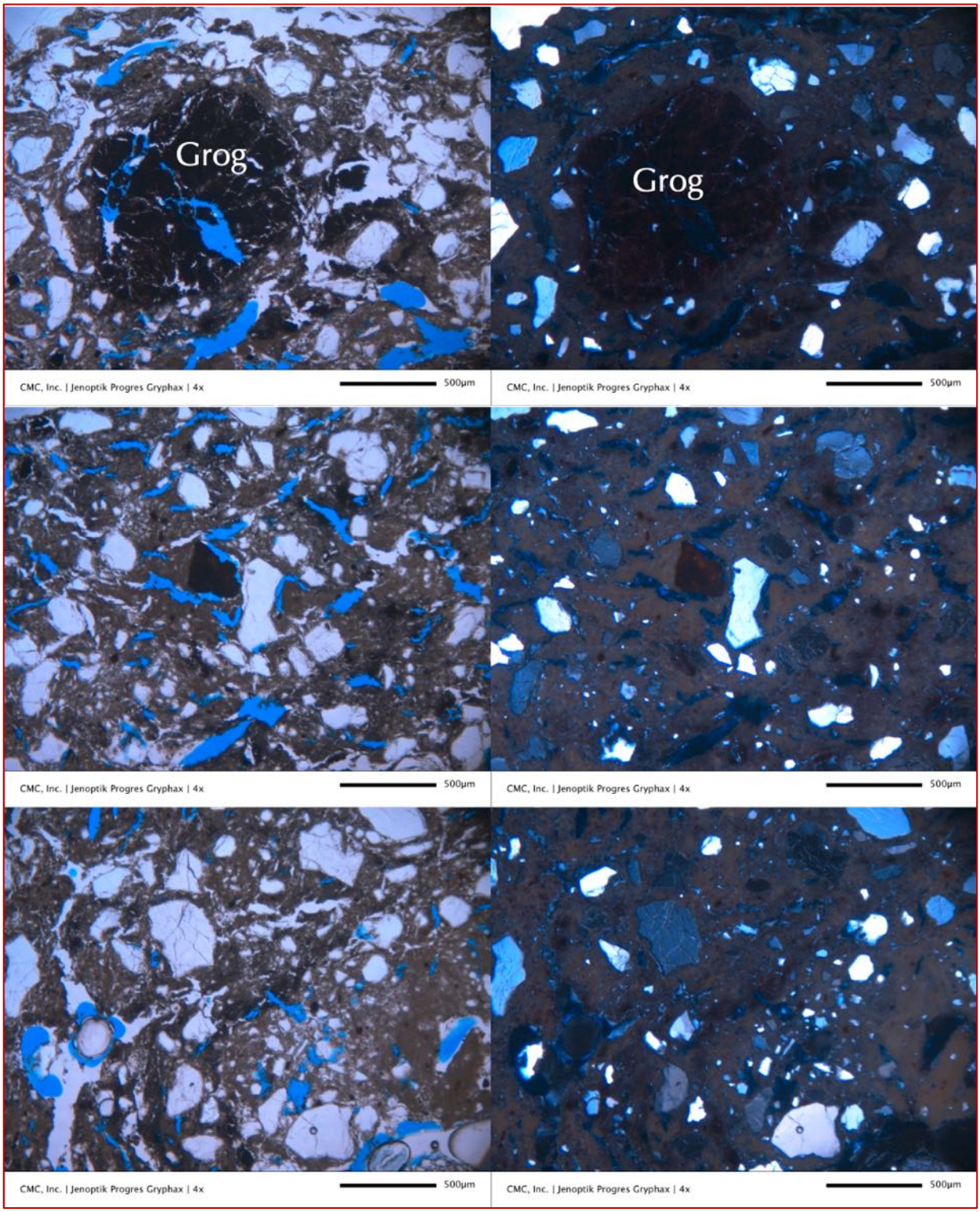

Figure B46: Micrographs (left in PPL and right in corresponding XPL mode) of thin section of Brick 3A from 1916 vintage (taken using a petrographic microscope) showing: (a) tempered quartz additive where quartz grains are crushed, well-graded, well-distributed, and representative of one population, (b) a few spherical grog particles of previously fired bricks having rims of separations from surrounding aluminosilicate matrix of host brick, (c) lack of reddish-brown aluminosilicate glass matrix of fired clay found in other bricks, and (d) abundant elongated voids of separation from shrinkage during drying after molding followed by subsequent baking. Notice the porous nature of the brick from abundance of void spaces highlighted by blue epoxy.

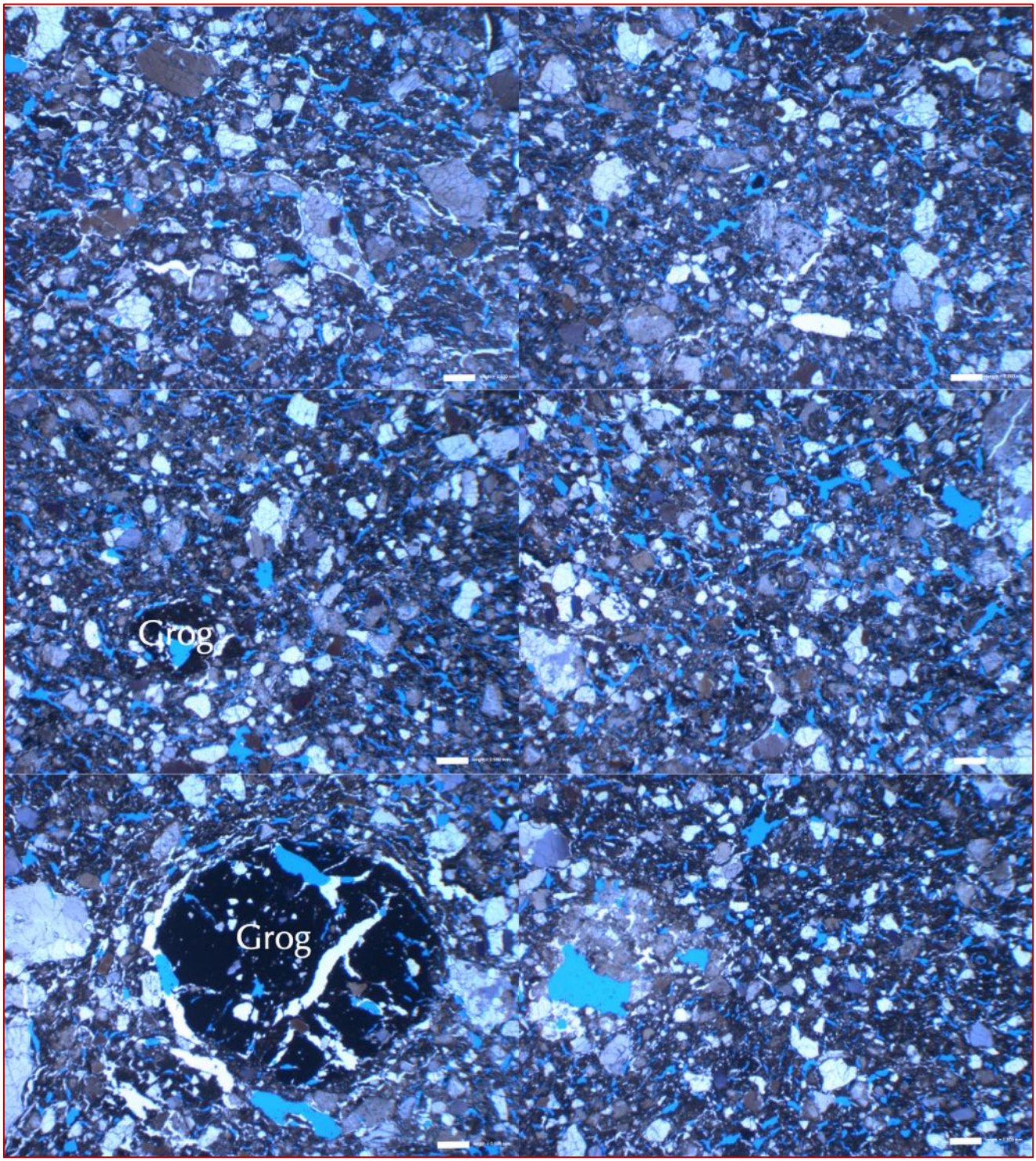

Figure B47: Micrographs of thin section of Brick 4A from 1916 vintage (taken using a transmitted-light stereo-zoom microscope) showing: (a) tempered quartz additive where quartz grains are crushed, well-graded, well-distributed, and representative of one population, (b) a few spherical grog particles of previously fired bricks having rims of separations from surrounding aluminosilicate matrix of host brick, (c) reddish-brown aluminosilicate glass matrix of fired clay, and (d) abundant elongated voids of separation from shrinkage during drying after molding followed by subsequent baking. Notice the porous nature of the brick from abundance of void spaces highlighted by blue epoxy.

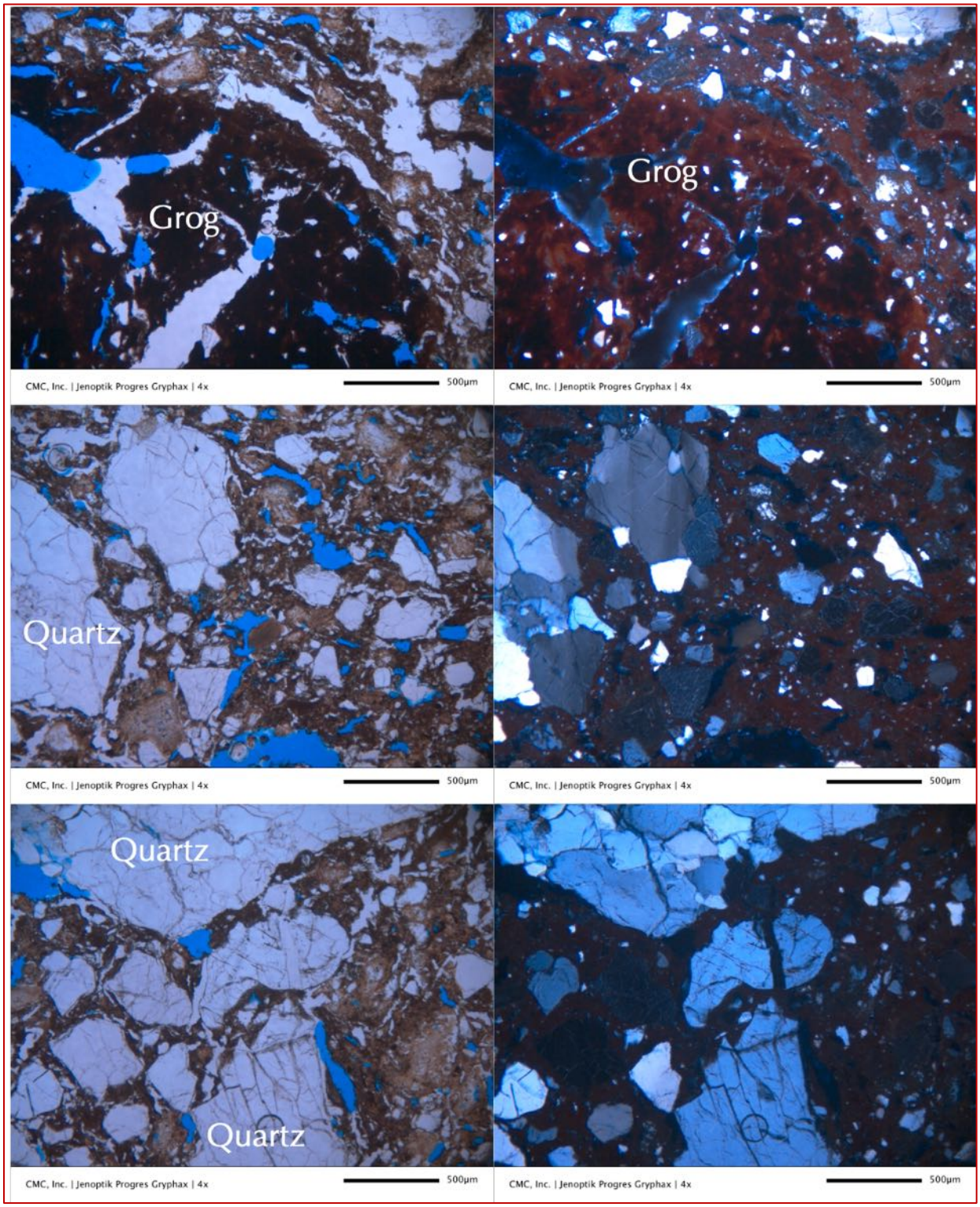

Figure B48: Micrographs (left in PPL and right in corresponding XPL mode) of thin section of Brick 4A from 1916 vintage (taken using a petrographic microscope) showing: (a) tempered quartz additive where quartz grains are crushed, well-graded, well-distributed, and representative of one population, (b) a few grog particles of previously fired bricks having rims of separations from surrounding aluminosilicate matrix of host brick, (c) reddish-brown aluminosilicate glass matrix of fired clay, and (d) abundant elongated voids of separation from shrinkage during drying after molding followed by subsequent baking. Notice the porous nature of the brick from abundance of void spaces highlighted by blue epoxy.

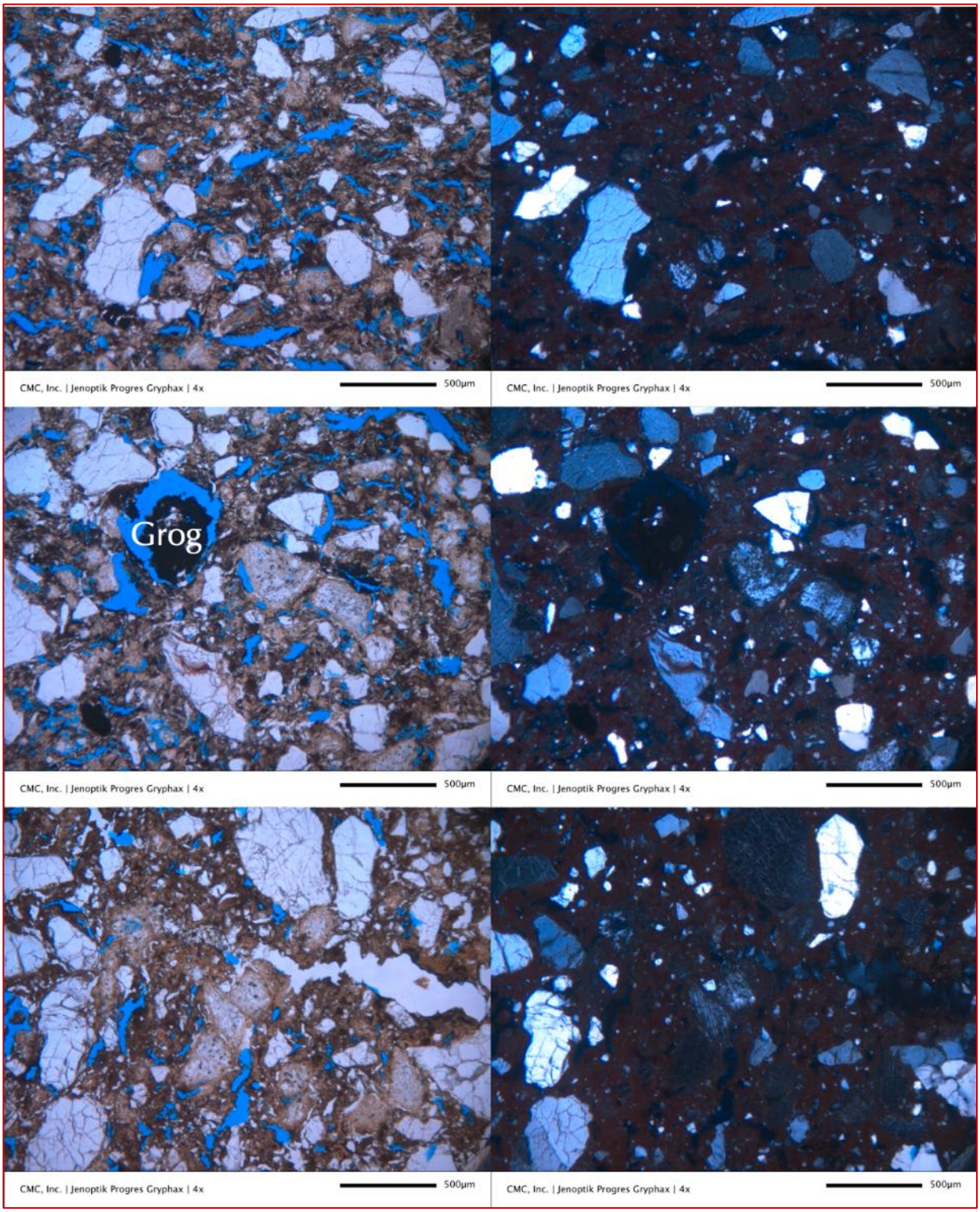

Figure B49: Micrographs (left in PPL and right in corresponding XPL mode) of thin section of Brick 4A from 1916 vintage (taken using a petrographic microscope) showing: (a) tempered quartz additive where quartz grains are crushed, well-graded, well-distributed, and representative of one population, (b) a few grog particles of previously fired bricks having rims of separations from surrounding aluminosilicate matrix of host brick, (c) reddish-brown aluminosilicate glass matrix of fired clay, and (d) abundant elongated voids of separation from shrinkage during drying after molding followed by subsequent baking. Notice the porous nature of the brick from abundance of void spaces highlighted by blue epoxy.

APPENDIX C

SEM-EDS STUDIES OF BRICKS AND MORTARS

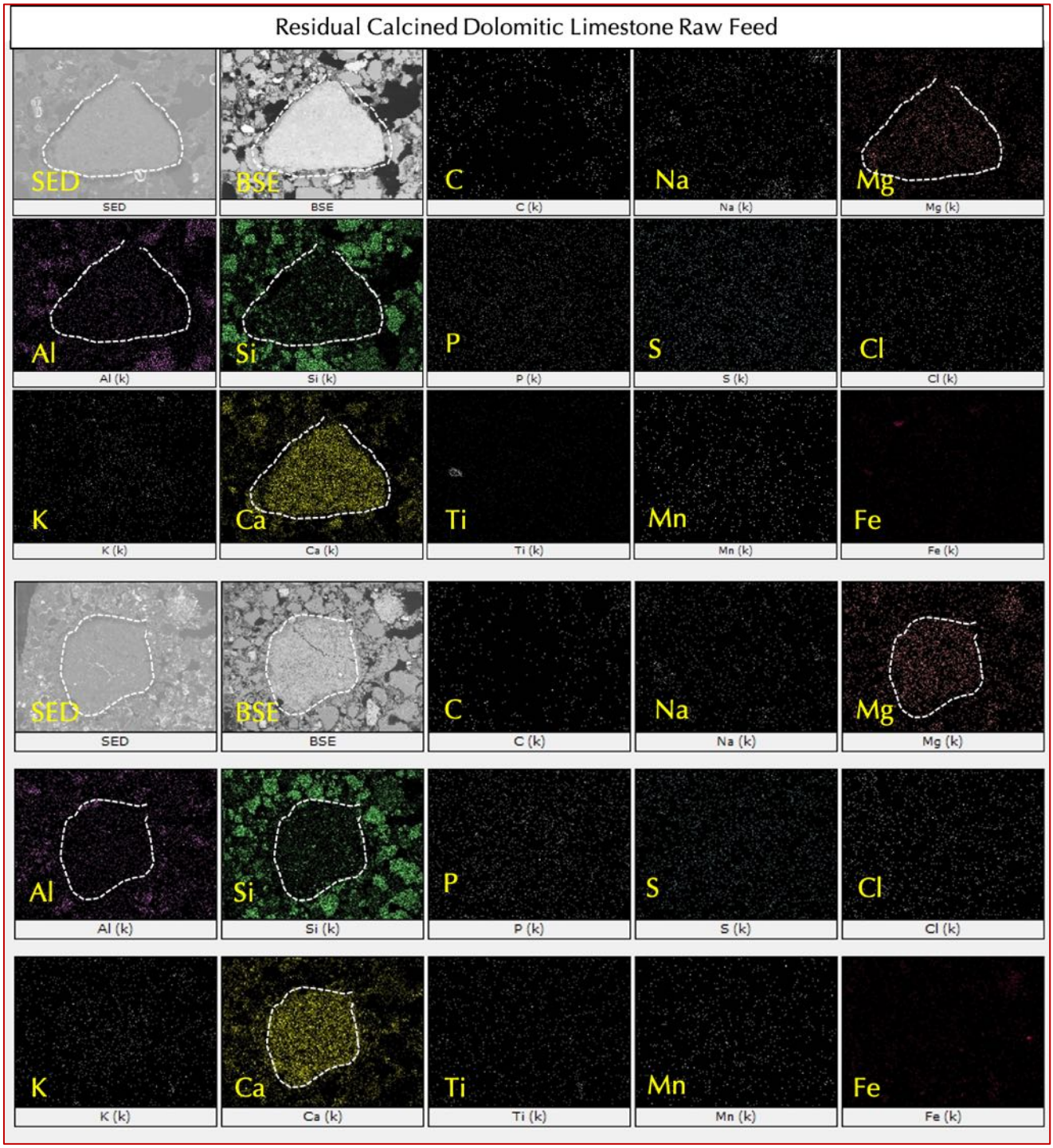

Figure C1: X-ray elemental maps of carbon (C), sodium (Na), aluminum (Al), silicon (Si), phosphorus (P), sulfur (S), chlorine (Cl), potassium (K), calcium (Ca), titanium (Ti), manganese (Mn), and iron (Fe) taken from an energy-dispersive X-ray fluorescence spectrometer attached to a scanning electron microscope showing: (a) characteristic enrichment of Ca and to a lesser extent Mg and Si of residual calcined impure dolomitic limestone feed of natural cement in natural cement mortar in M1 shown in two sets, at the top and bottom, where the residual natural cement particle of interest is marked with dashed lines; and (b) enrichment in Al and Si but depletion of Ca in the paste fraction of mortar around the residual cement particle. Secondary electron image (SED) and corresponding backscatter electron image (BSE) of each set of elemental maps is also shown.

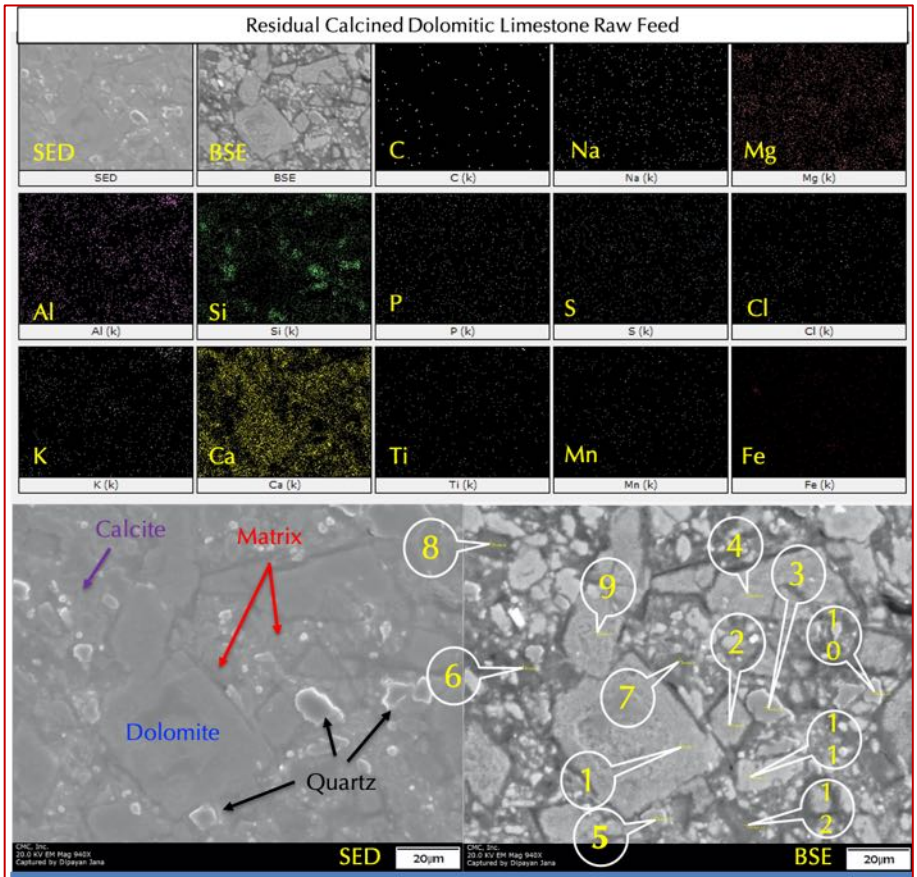

Probe	CaO	SiO2	Al2O3	Na2O	MgO	SO3	K2O	TiO2	FeO	P2O5	CO2	Total	Phase	Paste Cl
1	**76.22**	**6.95**	0.04	0.00	**9.76**	0.12	0.07	0.07	0.12	0.18	6.47	100.00	Dolomite	-
2	**74.27**	**6.82**	0.82	0.00	**10.13**	0.32	0.00	0.09	0.83	0.15	6.56	99.99	Dolomite	-
3	0.11	**93.42**	0.15	0.00	0.00	0.51	0.12	0.00	0.35	0.00	5.33	99.99	Quartz	-
4	**57.90**	9.01	0.67	0.04	**11.76**	0.78	0.02	0.00	0.74	0.79	18.29	100.00	Dolomite	-
5	0.53	**92.26**	0.72	0.00	0.00	0.06	0.18	0.00	0.00	0.93	5.32	100.00	Quartz	-
6	**8.94**	**39.43**	**11.39**	0.10	**22.19**	2.25	0.04	0.01	1.49	0.35	13.82	100.01	Matrix	-
7	**12.98**	**43.38**	**10.76**	0.16	**18.71**	1.40	1.11	0.00	1.46	0.26	9.78	100.00	Matrix	-
8	**7.25**	**40.63**	**11.48**	0.19	**25.66**	2.24	0.14	0.00	0.67	0.27	11.46	99.99	Matrix	-
9	**76.53**	**3.47**	0.27	0.00	**10.83**	0.50	0.02	0.00	0.22	0.28	7.89	100.01	Dolomite	-
10	0.44	**91.59**	0.51	0.00	0.00	0.04	0.29	0.00	0.05	0.35	6.73	100.00	Quartz	-
11	**95.72**	0.10	0.00	0.00	0.00	0.01	0.00	0.00	0.10	0.15	3.91	99.99	Calcite	-
12	**23.46**	**30.56**	7.67	0.18	**16.80**	1.90	0.80	0.16	1.70	0.66	16.11	100.00	Matrix	-

Subhedral to Euhedral Dolomite Rhombs, Anhedral Calcite and Quartz, Interstitial Matrix (Mg-Si-Al)

Figure C2: X-ray elemental maps (top), secondary electron image (SED, middle left), backscatter electron image (BSE, middle right), and X-ray elemental compositions at the tips of callouts shown in the backscatter electron image of interior of a residual calcined impure dolomitic limestone particle in the 1950s natural cement mortar M1 showing (i) euhedral dolomite rhombs, (ii) interstitial anhedral calcite grains, and (iii) interstitial calcined clay-silica matrix in the residual natural cement of calcium raw feed. Each phase is color-coded in the Table of compositions with characteristic components shown in bold.

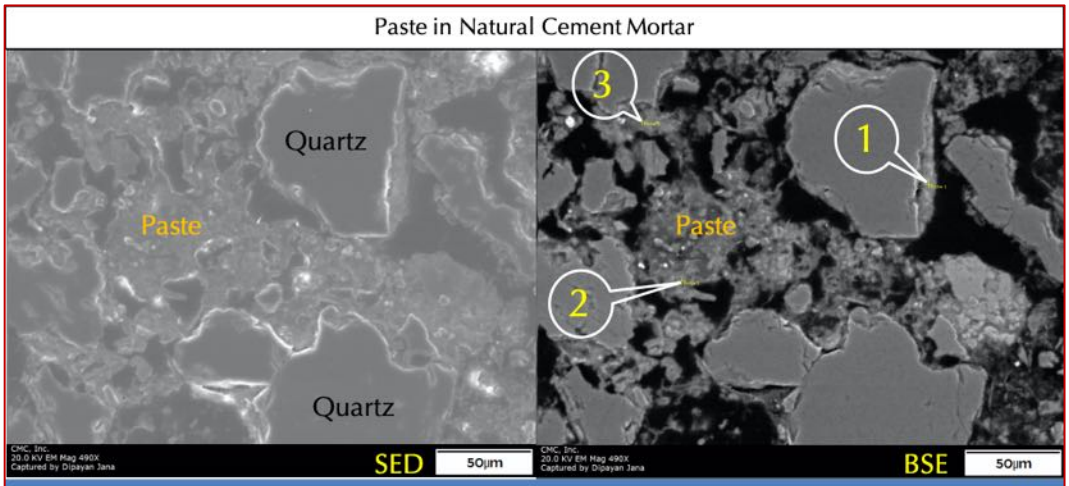

Probe	CaO	SiO2	Al2O3	Na2O	MgO	SO3	K2O	TiO2	FeO	P2O5	CO2	Total	Phase	Paste Cl
1	1.02	31.21	21.37	0.22	4.28	0.36	1.36	0.27	18.79	1.47	19.64	99.99	Paste ?	-
2	20.46	35.02	10.55	0.48	13.85	2.71	0.05	0.03	2.18	1.13	13.55	100.0	Paste	2.79
3	26.71	31.51	9.16	0.27	12.12	2.16	0.03	0.04	2.42	0.83	14.75	100.0	Paste	2.29

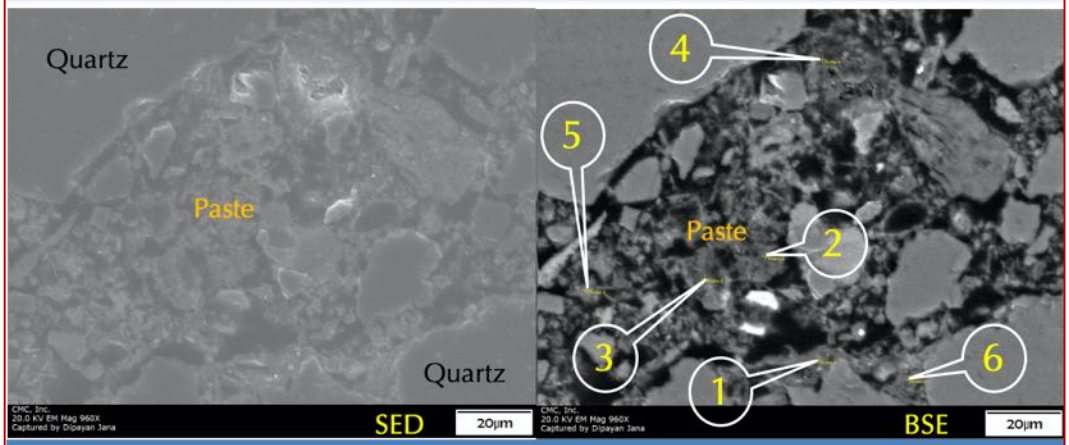

Probe	CaO	SiO2	Al2O3	Na2O	MgO	SO3	K2O	TiO2	FeO	P2O5	CO2	Total	Phase	Paste Cl
1	4.54	41.47	20.83	0.10	3.00	1.06	0.23	0.21	6.19	1.13	21.27	100.0	Paste ?	-
2	19.19	33.77	6.97	0.00	5.68	1.81	0.15	0.18	1.88	0.95	29.42	100.0	Paste	3.81
3	20.47	29.70	7.43	0.03	6.23	1.40	0.37	0.15	2.22	1.11	30.88	100.0	Paste	3.18
4	12.56	18.14	20.85	0.00	1.13	1.28	0.03	0.75	1.68	1.08	42.49	100.0	Paste	5.30
5	33.60	14.36	7.59	0.08	3.89	2.61	0.13	0.17	4.13	1.09	32.35	100.0	Paste	1.32
6	0.48	48.58	30.38	0.00	1.02	0.29	0.27	0.02	2.03	0.00	16.93	100.0	Paste ?	-

Figure C3: Secondary electron image (SED), backscatter electron image (BSE), and X-ray elemental compositions at the tips of callouts shown in the BSE images of paste in the 1950s natural cement mortar M1 showing (i) characteristic enrichment of magnesia in the paste compared to a Portland cement paste, (ii) variable calcium and silica contents of paste depending on degree of hydration of original natural cement, subsequent leaching during service, and lime content along with natural cement, and (iii) variable and higher carbon content in the paste due to variable and higher porosities of paste, respectively.

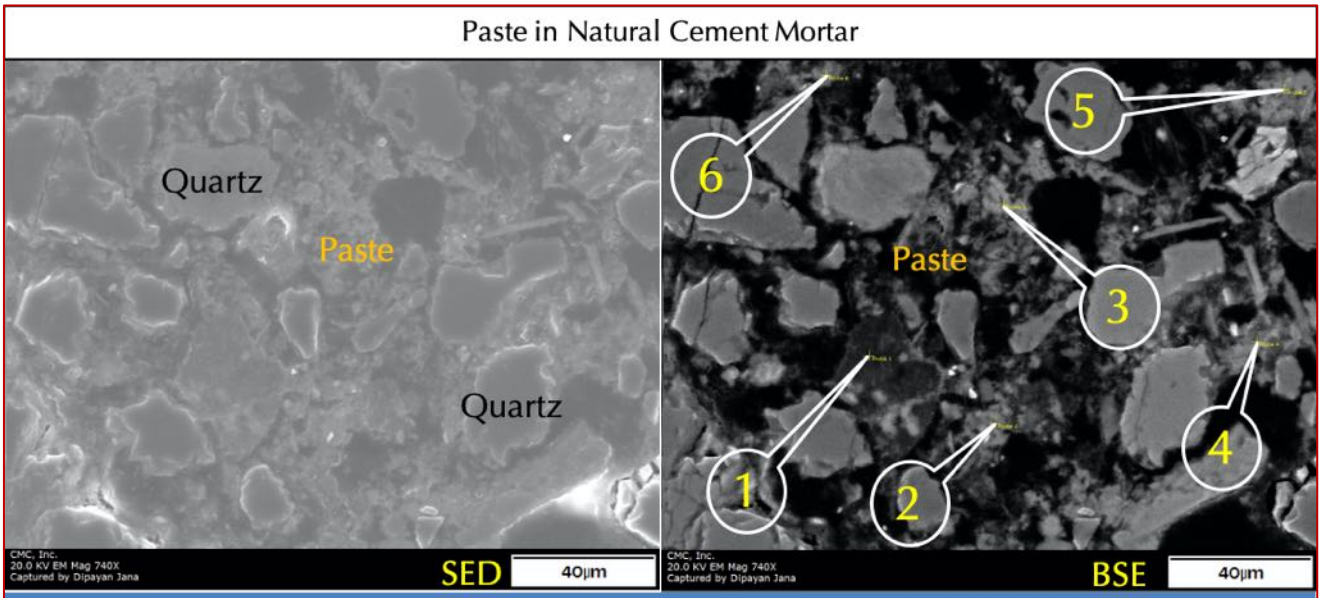

Probe	CaO	SiO2	Al2O3	Na2O	MgO	SO3	K2O	TiO2	FeO	P2O5	CO2	Total	Phase	Paste Cl
1	4.51	29.21	11.93	0.00	11.78	3.90	0.15	0.32	1.58	2.46	34.15	100.0	Paste ?	4.57
2	**42.15**	**14.74**	**5.61**	0.37	**3.87**	**2.91**	0.06	0.06	1.31	0.95	27.97	100.0	Paste	1.02
3	**45.75**	**21.23**	**7.12**	0.53	**2.99**	**2.80**	0.09	0.01	2.70	1.13	15.65	100.0	Paste	1.39
4	**65.52**	**10.33**	**4.24**	0.59	**3.49**	**2.86**	0.09	0.37	1.48	0.97	10.06	100.0	Paste	0.49
5	**31.43**	**27.77**	**10.95**	0.09	**6.32**	**0.93**	0.81	0.73	6.89	1.45	12.62	100.0	Paste	2.35
6	**45.17**	**17.40**	**7.09**	0.24	**4.30**	**2.41**	0.01	0.05	1.25	0.91	21.15	100.0	Paste ?	1.12

Figure C4: Secondary electron image (SED), backscatter electron image (BSE), and X-ray elemental compositions at the tips of callouts shown in the BSE images of paste in the 1950s natural cement mortar M1 showing (i) characteristic enrichment of magnesia in the paste compared to a Portland cement paste, (ii) variable calcium and silica contents of paste depending on degree of hydration of original natural cement, subsequent leaching during service, and lime content along with natural cement, and (iii) variable and higher carbon content in the paste due to variable and higher porosities of paste, respectively.

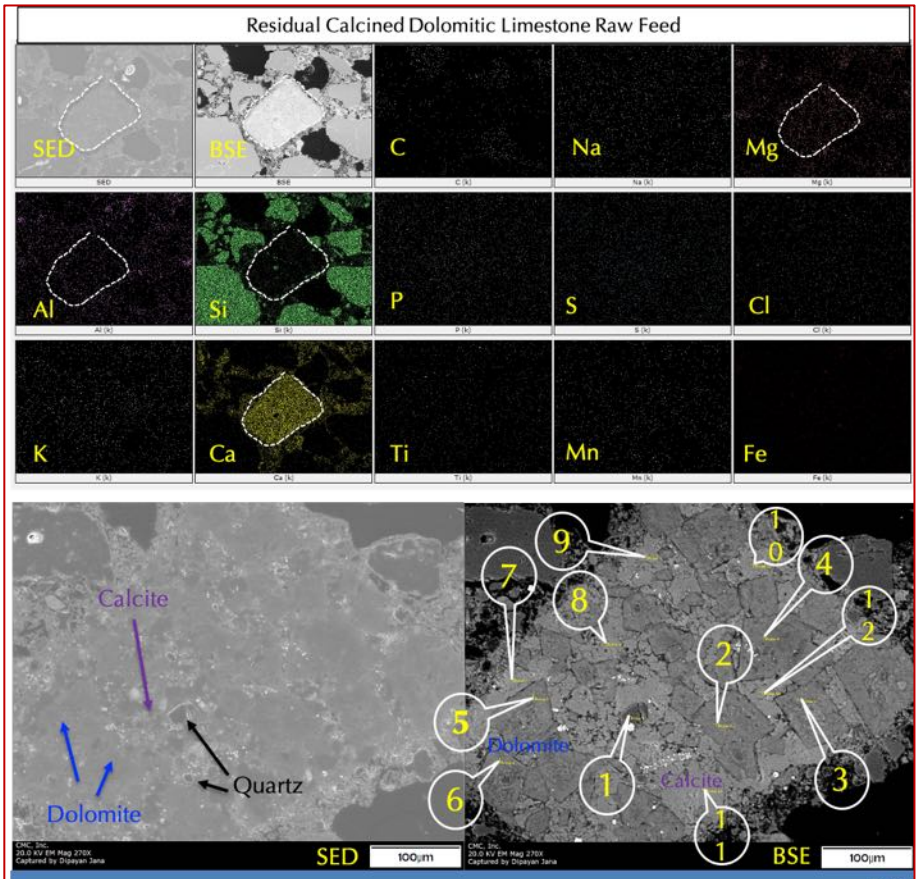

Probe	CaO	SiO2	Al2O3	Na2O	MgO	SO3	K2O	TiO2	FeO	P2O5	CO2	Total	Phase	Paste Cl
1	0.43	**96.91**	0.02	0.00	0.00	0.08	0.00	0.00	0.07	0.18	2.31	100.0	Quartz	-
2	**80.17**	2.67	0.00	0.00	**6.00**	0.23	0.00	0.00	2.79	0.66	7.47	100.0	Dolomite	-
3	**81.85**	2.31	0.05	0.00	**5.96**	0.75	0.00	0.09	0.92	0.56	7.51	100.0	Dolomite	-
4	**81.41**	0.61	0.00	0.02	**6.25**	0.32	0.00	0.09	3.23	0.81	7.25	100.0	Dolomite	-
5	**79.57**	3.68	0.17	0.09	**6.57**	0.46	0.02	0.00	1.80	0.76	6.87	100.0	Dolomite	-
6	**82.16**	3.34	0.33	0.08	**5.54**	0.56	0.13	0.00	0.02	0.98	6.85	100.0	Dolomite	-
7	**95.15**	0.43	0.00	0.00	0.00	0.06	0.05	0.00	0.33	0.34	3.64	100.0	Calcite	-
8	**93.15**	0.70	1.80	0.00	0.00	0.09	0.02	0.01	0.05	0.64	3.52	100.0	Calcite	-
9	**94.47**	0.53	0.00	0.00	0.02	0.17	0.03	0.00	0.31	0.24	4.24	100.0	Calcite	-
10	**96.34**	0.01	0.00	0.00	0.00	0.03	0.00	0.00	0.00	0.28	3.33	100.0	Calcite	-
11	**95.34**	0.35	0.00	0.00	0.00	0.11	0.00	0.09	0.05	0.30	3.75	100.0	Calcite	-
12	**95.46**	0.33	0.00	0.00	0.00	0.01	0.04	0.00	0.32	0.34	3.50	100.0	Calcite	-

Subhedral to Euhedral Dolomite Rhombs, Anhedral Calcite and Quartz, Interstitial Matrix (Mg-Si-Al)

Figure C5: X-ray elemental maps (top), secondary electron image (SED, middle left), backscatter electron image (BSE, middle right), and X-ray elemental compositions at the tips of callouts shown in the backscatter electron image of interior of a residual calcined impure dolomitic limestone particle in the 1950s natural cement mortar M2 showing (i) euhedral dolomite rhombs, (ii) interstitial anhedral calcite grains, and (iii) interstitial calcined clay-silica matrix in the residual natural cement of calcium raw feed. Each phase is color-coded in the Table of compositions with characteristic components shown in bold.

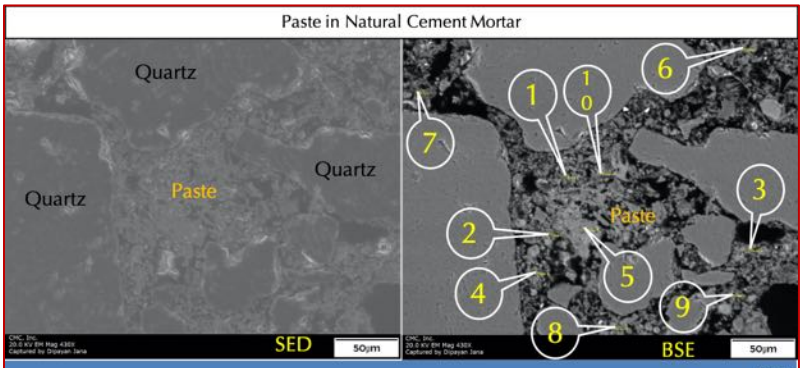

Probe	CaO	SiO2	Al2O3	Na2O	MgO	SO3	K2O	TiO2	FeO	P2O5	CO2	Total	Phase	Paste Cl
1	19.84	44.02	3.35	0.00	1.75	1.75	0.20	0.09	0.76	0.33	27.91	100.0	Paste ?	5.72
2	38.25	17.62	4.00	0.09	4.94	2.23	0.26	0.00	1.44	0.82	30.35	100.0	Paste	1.21
3	35.54	21.86	10.70	0.01	7.69	3.01	0.41	0.33	2.40	0.32	17.74	100.0	Paste	1.61
4	37.69	22.31	4.19	0.16	9.32	2.63	0.26	0.53	0.57	0.24	22.10	100.0	Paste	1.33
5	45.98	19.25	5.87	0.19	8.22	2.96	0.55	0.03	1.49	0.81	14.65	100.0	Paste	1.07
6	24.34	15.11	4.49	0.00	5.70	1.93	0.34	0.02	1.04	0.45	46.57	99.99	Paste ?	1.48
7	4.53	19.30	4.94	0.17	1.95	0.22	0.00	0.52	0.93	0.29	67.16	100.0	Paste ?	8.28
8	38.21	18.59	4.35	0.08	8.53	2.58	0.53	0.00	1.44	0.34	25.35	100.0	Paste	1.15
9	17.22	23.15	5.42	0.15	2.59	1.63	0.99	8.81	1.81	0.33	37.89	99.99	Paste	3.46
10	50.88	17.15	5.92	0.02	5.59	3.66	0.56	0.10	1.28	0.08	14.76	100.0	Paste	0.94

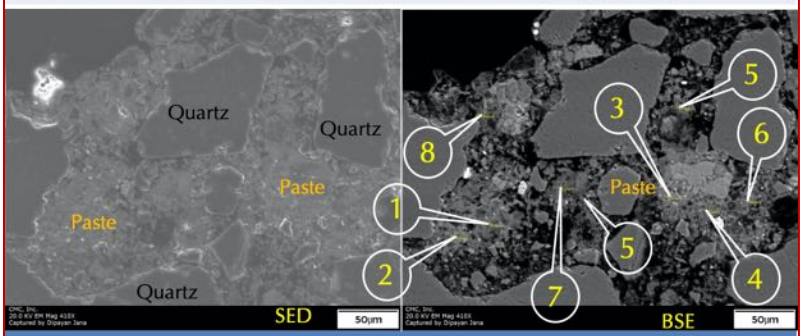

Probe	CaO	SiO2	Al2O3	Na2O	MgO	SO3	K2O	TiO2	FeO	P2O5	CO2	Total	Phase	Paste Cl
1	37.26	26.20	6.70	0.00	15.58	2.08	0.02	0.04	1.43	0.81	9.88	100.0	Paste	1.38
2	43.77	21.99	4.79	0.13	5.27	1.65	0.29	0.93	1.47	0.27	19.44	100.0	Paste	1.33
3	58.61	19.40	4.41	0.01	6.24	1.21	0.23	0.16	2.48	0.21	7.04	100.0	Paste	0.90
4	40.92	14.97	3.35	0.05	5.09	2.48	0.16	0.12	1.37	0.56	30.92	100.0	Paste	0.97
5	38.45	16.74	5.13	0.34	4.91	1.53	0.09	4.85	1.73	0.87	25.36	100.0	Paste	1.19
6	34.90	30.22	5.55	0.02	8.38	2.48	0.54	0.16	1.72	0.79	15.25	100.0	Paste	1.97
7	33.49	18.31	2.75	0.13	3.34	1.86	0.27	0.04	0.39	0.45	38.98	100.0	Paste	1.43
8	37.71	18.82	3.98	0.00	5.17	2.40	0.52	0.04	1.41	0.87	29.08	100.0	Paste	1.29

Figure C6: Secondary electron image (SED), backscatter electron image (BSE), and X-ray elemental compositions at the tips of callouts shown in the BSE images of paste in the 1950s natural cement mortar M2 showing (i) characteristic enrichment of magnesia in the paste compared to a Portland cement paste, (ii) variable calcium and silica contents of paste depending on degree of hydration of original natural cement, subsequent leaching during service, and lime content along with natural cement, and (iii) variable and higher carbon content in the paste due to variable and higher porosities of paste, respectively.

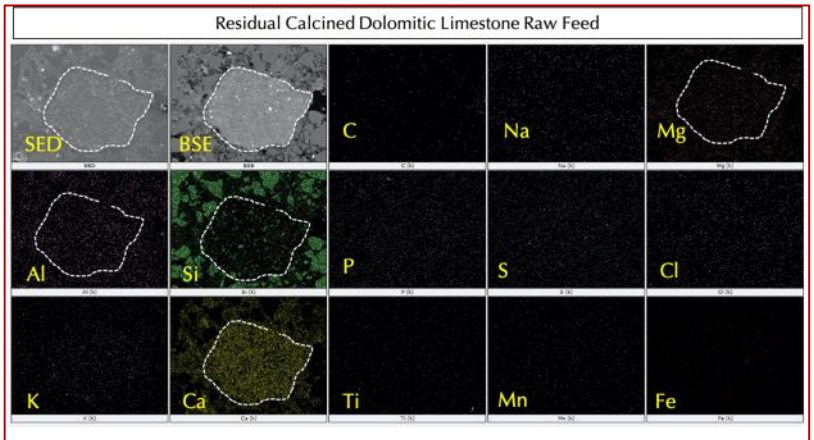

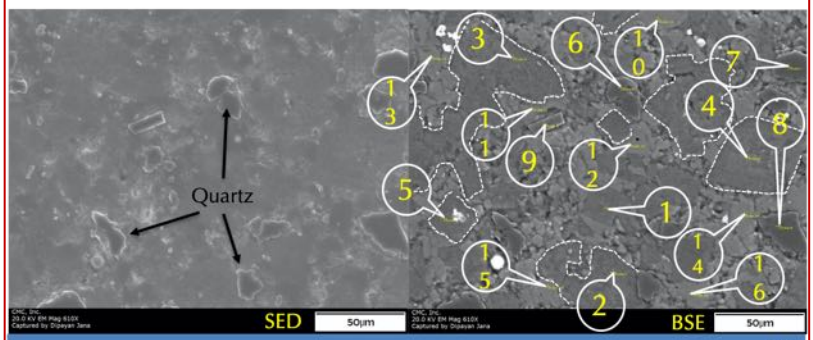

Probe	CaO	SiO2	Al2O3	Na2O	MgO	SO3	K2O	TiO2	FeO	P2O5	CO2	Total	Phase	Paste Cl
1	88.43	2.19	0.15	0.11	1.02	0.27	0.13	0.10	0.00	0.55	7.05	100.0	Quartz	-
2	**78.93**	3.01	0.31	0.00	**7.02**	0.21	0.02	0.00	1.18	0.43	8.88	100.0	Dolomite	-
3	**76.97**	3.14	0.41	0.00	**8.47**	0.10	0.09	0.00	1.82	0.86	8.13	100.0	Dolomite	-
4	**75.87**	3.49	0.69	0.06	**7.19**	0.26	0.00	0.33	0.45	0.74	10.92	100.0	Dolomite	-
5	**81.59**	1.96	0.29	0.04	**5.84**	0.30	0.00	0.07	1.73	0.31	7.86	100.0	Dolomite	-
6	0.47	**95.54**	0.02	0.00	0.00	0.09	0.01	0.00	0.05	0.81	3.00	100.0	Quartz	-
7	0.18	**94.99**	0.02	0.00	0.00	0.32	0.00	0.03	0.31	0.90	3.25	100.0	Quartz	-
8	0.36	**94.57**	0.16	0.06	0.00	0.29	0.02	0.00	0.08	0.95	3.49	100.0	Quartz	-
9	0.61	**43.66**	**31.99**	1.42	**5.66**	0.46	0.04	0.00	**9.15**	0.66	6.36	100.0	Mineral	-
10	**92.09**	2.23	0.01	0.00	0.65	0.10	0.10	0.24	0.00	0.10	4.47	100.0	Calcite	-
11	**87.40**	3.60	0.04	0.00	1.34	0.29	0.33	0.00	0.35	1.01	5.66	100.0	Calcite	-
12	**95.48**	0.00	0.00	0.00	0.00	0.15	0.21	0.14	0.14	0.57	3.31	100.0	Calcite	-
13	**93.59**	1.48	0.09	0.02	0.03	0.05	0.01	0.04	0.04	0.09	4.57	100.0	Calcite	-
14	**94.96**	0.21	0.00	0.03	0.22	0.14	0.05	0.03	0.00	0.35	4.02	100.0	Calcite	-
15	**93.15**	0.73	0.00	0.00	0.63	0.05	0.00	0.00	0.18	0.32	4.94	100.0	Calcite	-
16	**94.56**	0.62	0.00	0.00	0.07	0.07	0.00	0.00	0.00	0.73	3.95	100.0	Calcite	-

Subhedral to Euhedral Dolomite Rhombs, Anhedral Calcite and Quartz, Interstitial Matrix (Mg-Si-Al)

Figure C7: X-ray elemental maps (top), secondary electron image (SED, middle left), backscatter electron image (BSE, middle right), and X-ray elemental compositions at the tips of callouts shown in the backscatter electron image of interior of a residual calcined impure dolomitic limestone particle in the 1950s natural cement mortar M2 showing (i) euhedral dolomite rhombs, (ii) interstitial anhedral calcite grains, and (iii) interstitial calcined clay-silica matrix in the residual natural cement of calcium raw feed. Each phase is color-coded in the Table of compositions with characteristic components shown in bold.

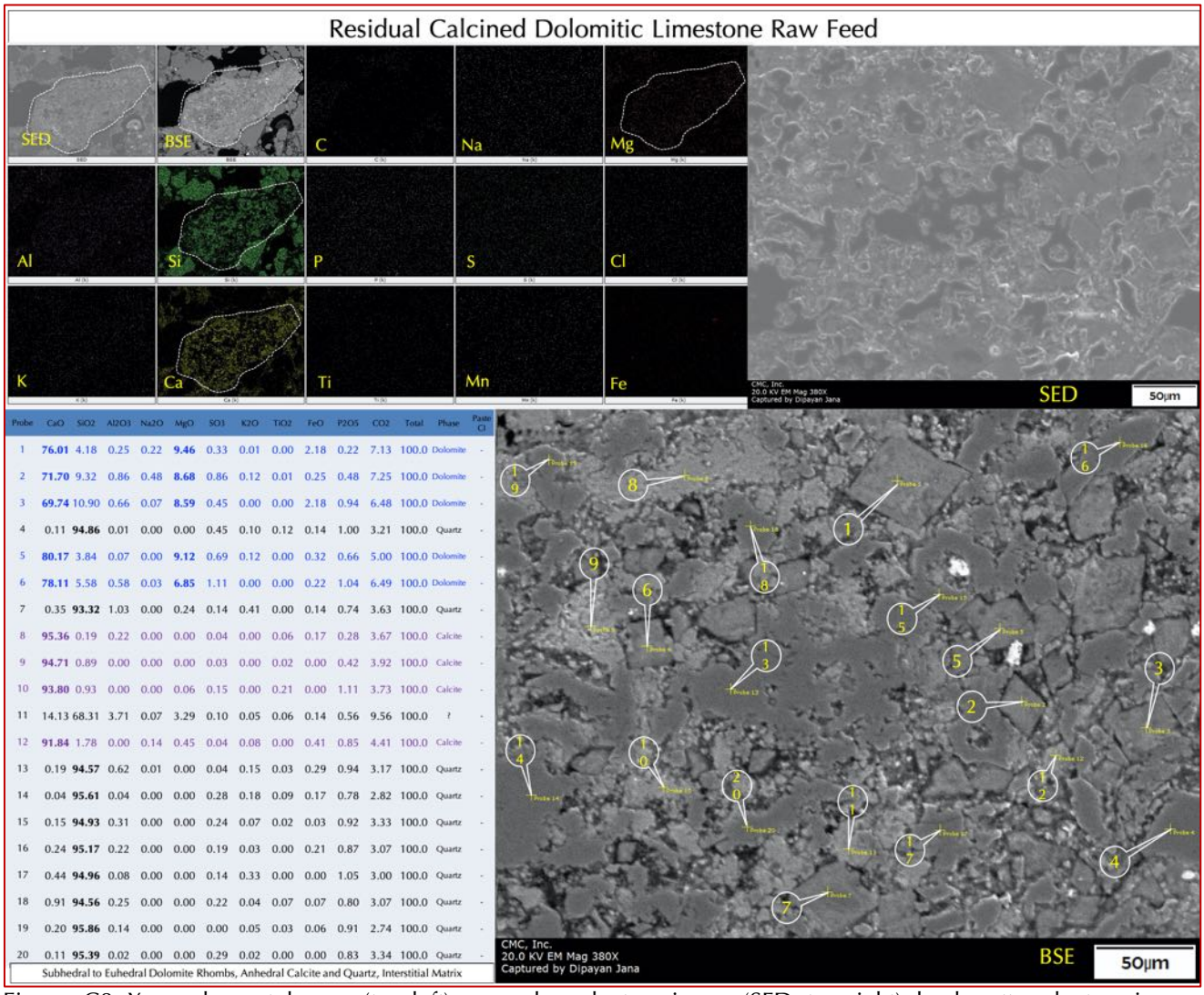

Probe	CaO	SiO2	Al2O3	Na2O	MgO	SO3	K2O	TiO2	FeO	P2O5	CO2	Total	Phase	Paste Cl
1	**76.01**	4.18	0.25	0.22	**9.46**	0.33	0.01	0.00	2.18	0.22	7.13	100.0	Dolomite	-
2	**71.70**	9.32	0.86	0.48	**8.68**	0.86	0.12	0.01	0.25	0.48	7.25	100.0	Dolomite	-
3	**69.74**	10.90	0.66	0.07	**8.59**	0.45	0.00	0.00	2.18	0.94	6.48	100.0	Dolomite	-
4	0.11	**94.86**	0.01	0.00	0.00	0.45	0.10	0.12	0.14	1.00	3.21	100.0	Quartz	-
5	**80.17**	3.84	0.07	0.00	**9.12**	0.69	0.12	0.00	0.32	0.66	5.00	100.0	Dolomite	-
6	**78.11**	5.58	0.58	0.03	**6.85**	1.11	0.00	0.00	0.22	1.04	6.49	100.0	Dolomite	-
7	0.35	**93.32**	1.03	0.00	0.24	0.14	0.41	0.00	0.14	0.74	3.63	100.0	Quartz	-
8	**95.36**	0.19	0.22	0.00	0.00	0.04	0.00	0.06	0.17	0.28	3.67	100.0	Calcite	-
9	**94.71**	0.89	0.00	0.00	0.00	0.03	0.00	0.02	0.00	0.42	3.92	100.0	Calcite	-
10	**93.80**	0.93	0.00	0.00	0.06	0.15	0.00	0.21	0.00	1.11	3.73	100.0	Calcite	-
11	14.13	68.31	3.71	0.07	3.29	0.10	0.05	0.06	0.14	0.56	9.56	100.0	?	-
12	**91.84**	1.78	0.00	0.14	0.45	0.04	0.08	0.00	0.41	0.85	4.41	100.0	Calcite	-
13	0.19	**94.57**	0.62	0.01	0.00	0.04	0.15	0.03	0.29	0.94	3.17	100.0	Quartz	-
14	0.04	**95.61**	0.04	0.00	0.00	0.28	0.18	0.09	0.17	0.78	2.82	100.0	Quartz	-
15	0.15	**94.93**	0.31	0.00	0.00	0.24	0.07	0.02	0.03	0.92	3.33	100.0	Quartz	-
16	0.24	**95.17**	0.22	0.00	0.00	0.19	0.03	0.00	0.21	0.87	3.07	100.0	Quartz	-
17	0.44	**94.96**	0.08	0.00	0.00	0.14	0.33	0.00	0.00	1.05	3.00	100.0	Quartz	-
18	0.91	**94.56**	0.25	0.00	0.00	0.22	0.04	0.07	0.07	0.80	3.07	100.0	Quartz	-
19	0.20	**95.86**	0.14	0.00	0.00	0.00	0.05	0.03	0.06	0.91	2.74	100.0	Quartz	-
20	0.11	**95.39**	0.02	0.00	0.00	0.29	0.02	0.00	0.00	0.83	3.34	100.0	Quartz	-

Subhedral to Euhedral Dolomite Rhombs, Anhedral Calcite and Quartz, Interstitial Matrix

Figure C8: X-ray elemental maps (top left), secondary electron image (SED, top right), backscatter electron image (BSE, bottom right), and X-ray elemental compositions at the tips of callouts shown in the backscatter electron image of interior of a residual calcined impure dolomitic limestone particle in the 1950s natural cement mortar M2 showing (i) euhedral dolomite rhombs, (ii) interstitial anhedral calcite grains, and (iii) interstitial calcined clay-silica matrix in the residual natural cement of calcium raw feed. Each phase is color-coded in the Table of compositions with characteristic components shown in bold.

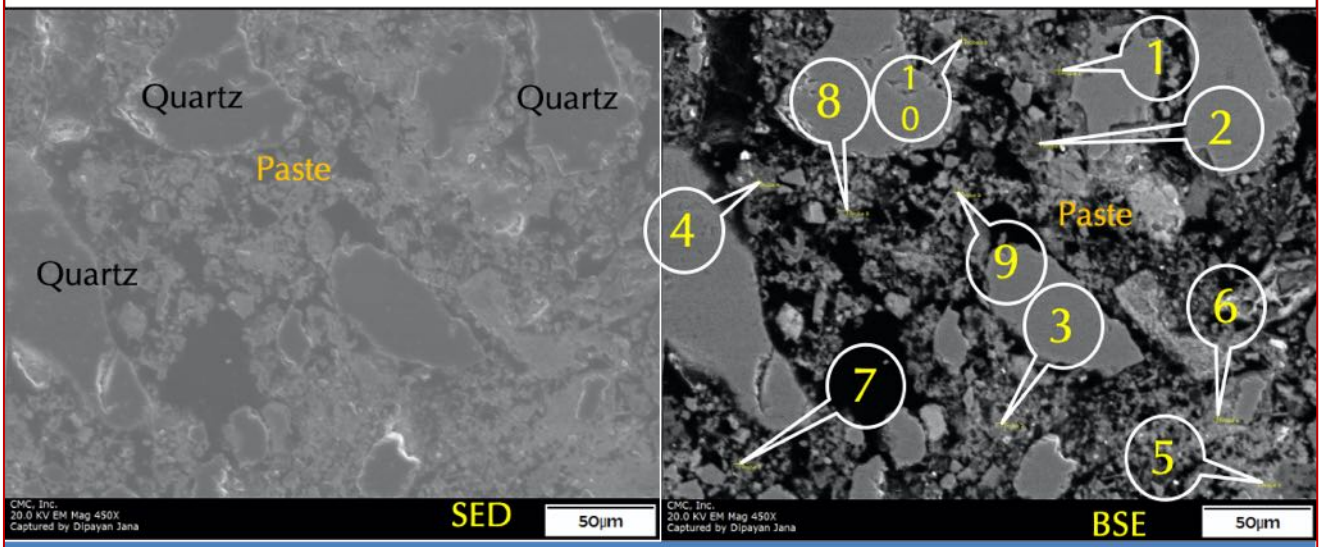

Probe	CaO	SiO2	Al2O3	Na2O	MgO	SO3	K2O	TiO2	FeO	P2O5	CO2	Total	Phase	Paste Cl
1	24.39	26.65	10.14	0.02	5.92	2.65	1.00	0.00	1.32	1.29	26.63	100.0	Leached Paste	2.65
2	7.78	38.53	10.20	0.45	9.90	2.08	1.11	0.53	3.51	1.46	24.46	100.0	Leached Paste	5.62
3	57.55	11.19	5.62	0.09	9.79	1.80	0.90	0.34	3.17	1.04	8.51	100.0	Paste	0.56
4	20.62	29.98	6.39	0.08	9.84	2.57	0.37	0.18	1.62	0.97	27.39	100.0	Leached Paste	2.68
5	6.84	19.60	5.34	0.21	3.42	1.54	0.23	0.27	1.51	0.61	60.43	100.0	Leached Paste	5.32
6	62.67	13.71	3.24	0.16	5.52	2.18	1.18	0.18	0.34	1.08	9.73	100.0	Paste	0.60
7	39.50	16.09	5.79	0.01	3.58	2.68	0.68	0.11	1.53	0.65	29.38	100.0	Paste	1.18
8	56.16	12.96	3.63	0.60	3.65	2.02	0.54	0.08	1.63	0.90	17.84	100.0	Paste	0.68
9	38.55	19.46	8.58	0.00	6.82	3.33	1.06	0.45	1.71	1.51	18.51	100.0	Paste	1.35
10	23.24	23.37	8.37	0.00	4.66	2.09	0.63	0.15	4.90	1.47	31.12	100.0	Leached Paste	2.62

Figure C9: Secondary electron image (SED), backscatter electron image (BSE), and X-ray elemental compositions at the tips of callouts shown in the BSE images of paste in the 1950s natural cement mortar M2 showing (i) characteristic enrichment of magnesia in the paste compared to a Portland cement paste, (ii) variable calcium and silica contents of paste depending on degree of hydration of original natural cement, subsequent leaching during service, and lime content along with natural cement, and (iii) variable and higher carbon content in the paste due to variable and higher porosities of paste, respectively.

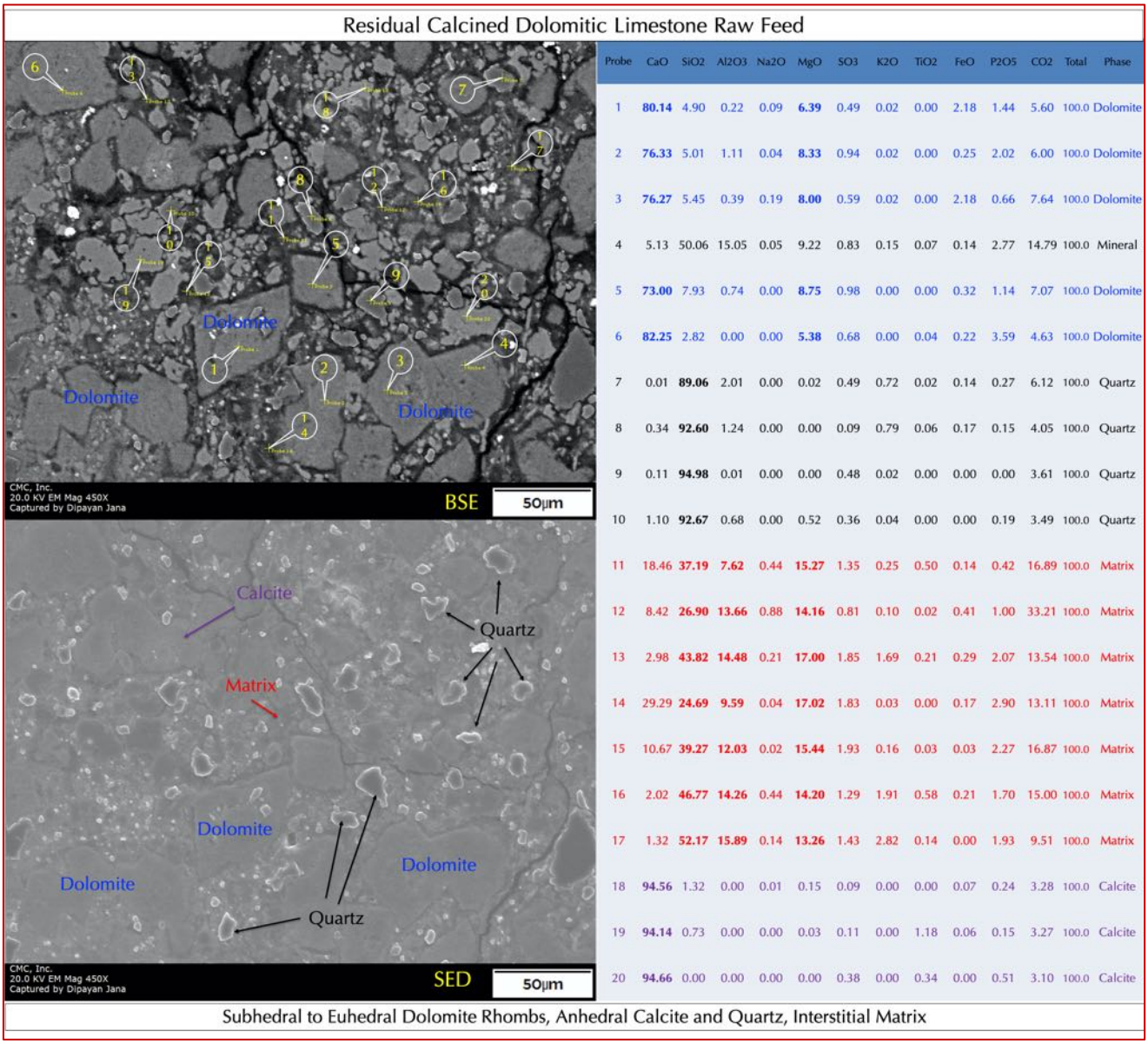

Probe	CaO	SiO2	Al2O3	Na2O	MgO	SO3	K2O	TiO2	FeO	P2O5	CO2	Total	Phase
1	**80.14**	4.90	0.22	0.09	**6.39**	0.49	0.02	0.00	2.18	1.44	5.60	100.0	Dolomite
2	**76.33**	5.01	1.11	0.04	**8.33**	0.94	0.02	0.00	0.25	2.02	6.00	100.0	Dolomite
3	**76.27**	5.45	0.39	0.19	**8.00**	0.59	0.02	0.00	2.18	0.66	7.64	100.0	Dolomite
4	5.13	50.06	15.05	0.05	9.22	0.83	0.15	0.07	0.14	2.77	14.79	100.0	Mineral
5	**73.00**	7.93	0.74	0.00	**8.75**	0.98	0.00	0.00	0.32	1.14	7.07	100.0	Dolomite
6	**82.25**	2.82	0.00	0.00	**5.38**	0.68	0.00	0.04	0.22	3.59	4.63	100.0	Dolomite
7	0.01	**89.06**	2.01	0.00	0.02	0.49	0.72	0.02	0.14	0.27	6.12	100.0	Quartz
8	0.34	**92.60**	1.24	0.00	0.00	0.09	0.79	0.06	0.17	0.15	4.05	100.0	Quartz
9	0.11	**94.98**	0.01	0.00	0.00	0.48	0.02	0.00	0.00	0.00	3.61	100.0	Quartz
10	1.10	**92.67**	0.68	0.00	0.52	0.36	0.04	0.00	0.00	0.19	3.49	100.0	Quartz
11	18.46	**37.19**	**7.62**	0.44	**15.27**	1.35	0.25	0.50	0.14	0.42	16.89	100.0	Matrix
12	8.42	**26.90**	**13.66**	0.88	**14.16**	0.81	0.10	0.02	0.41	1.00	33.21	100.0	Matrix
13	2.98	**43.82**	**14.48**	0.21	**17.00**	1.85	1.69	0.21	0.29	2.07	13.54	100.0	Matrix
14	29.29	**24.69**	**9.59**	0.04	**17.02**	1.83	0.03	0.00	0.17	2.90	13.11	100.0	Matrix
15	10.67	**39.27**	**12.03**	0.02	**15.44**	1.93	0.16	0.03	0.03	2.27	16.87	100.0	Matrix
16	2.02	**46.77**	**14.26**	0.44	**14.20**	1.29	1.91	0.58	0.21	1.70	15.00	100.0	Matrix
17	1.32	**52.17**	**15.89**	0.14	**13.26**	1.43	2.82	0.14	0.00	1.93	9.51	100.0	Matrix
18	**94.56**	1.32	0.00	0.01	0.15	0.09	0.00	0.00	0.07	0.24	3.28	100.0	Calcite
19	**94.14**	0.73	0.00	0.00	0.03	0.11	0.00	1.18	0.06	0.15	3.27	100.0	Calcite
20	**94.66**	0.00	0.00	0.00	0.00	0.38	0.00	0.34	0.00	0.51	3.10	100.0	Calcite

Figure C10: Secondary electron image (SED), backscatter electron image (BSE), and X-ray elemental compositions at the tips of callouts shown in the backscatter electron image of interior of a residual calcined impure dolomitic limestone particle in the 1950s natural cement mortar M2 showing (i) euhedral dolomite rhombs, (ii) interstitial anhedral calcite grains, and (iii) interstitial calcined clay-silica matrix in the residual natural cement of calcium raw feed. Each phase is color-coded in the Table of compositions with characteristic components shown in bold.

Paste in Natural Cement Mortar

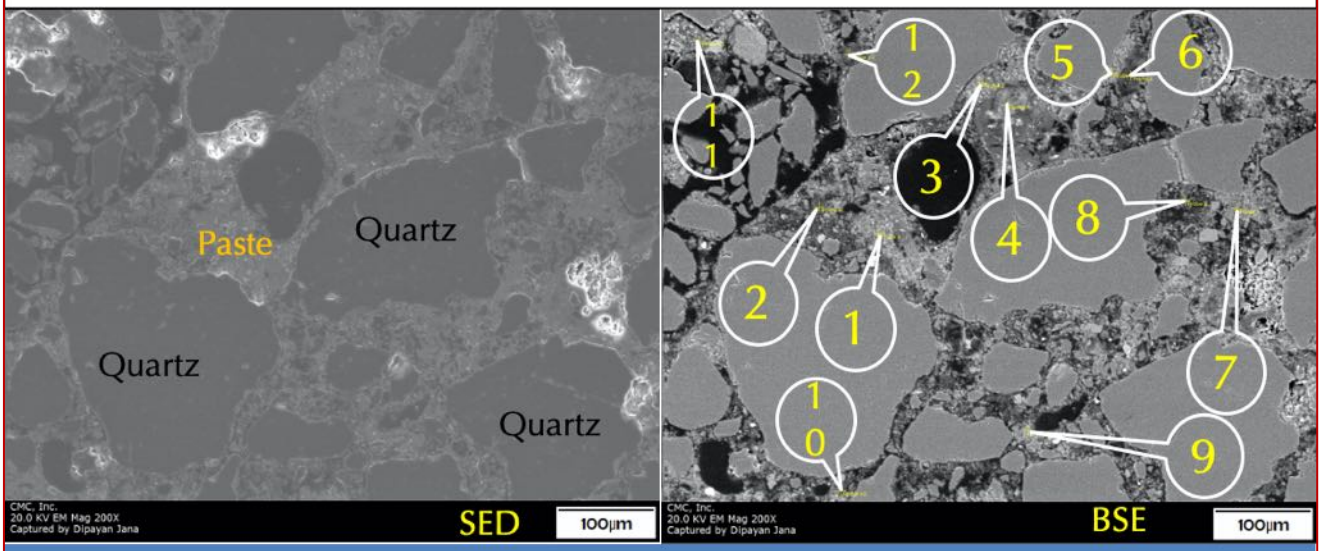

Probe	CaO	SiO2	Al2O3	Na2O	MgO	SO3	K2O	TiO2	FeO	P2O5	CO2	Total	Phase	Paste Cl
1	**49.75**	**32.34**	4.33	0.00	4.67	1.07	1.28	0.48	1.62	0.72	3.73	100.0	Paste	1.71
2	14.76	**49.83**	3.21	0.06	3.83	0.41	0.08	0.11	1.87	0.59	**25.25**	100.0	Leached Paste	-
3	8.44	**74.03**	1.62	0.00	0.56	0.64	0.11	0.10	0.26	1.61	**12.62**	100.0	Leached Paste	-
4	**43.20**	**14.09**	11.86	0.00	3.31	2.87	0.90	0.38	3.22	1.24	18.94	100.0	Paste	1.14
5	**40.75**	**26.69**	5.95	0.16	5.56	2.74	0.42	0.29	1.38	1.24	14.81	100.0	Paste	1.69
6	8.22	**35.85**	2.45	0.03	6.17	1.34	0.71	0.09	0.62	1.26	**43.25**	100.0	Leached Paste	-
7	28.41	**32.49**	3.39	0.05	3.63	1.67	0.75	0.01	0.69	1.07	**27.85**	100.0	Leached Paste	-
8	**26.78**	**17.94**	6.55	0.00	5.90	2.30	0.86	0.33	2.07	1.44	35.83	100.0	Paste	1.68
9	**40.36**	**24.28**	6.63	0.05	6.18	3.26	0.75	0.19	1.91	1.02	15.39	100.0	Paste	1.56
10	0.00	**95.41**	0.04	0.00	0.00	0.04	0.00	0.00	0.00	1.16	3.34	100.0	Quartz	-
11	21.58	**25.66**	17.51	0.07	3.34	1.86	0.41	0.05	1.64	1.64	**26.24**	100.0	Leached Paste	-
12	8.25	**43.46**	3.66	0.26	11.64	1.90	0.32	0.00	0.21	1.06	**29.25**	100.0	Leached Paste	-

Figure C11: Secondary electron image (SED), backscatter electron image (BSE), and X-ray elemental compositions at the tips of callouts shown in the BSE images of paste in the 1950s natural cement mortar M2 showing (i) characteristic enrichment of magnesia in the paste compared to a Portland cement paste, (ii) variable calcium and silica contents of paste depending on degree of hydration of original natural cement, subsequent leaching during service, and lime content along with natural cement, and (iii) variable and higher carbon content in the paste due to variable and higher porosities of paste, respectively.

Residual Calcined Dolomitic Limestone Raw Feed

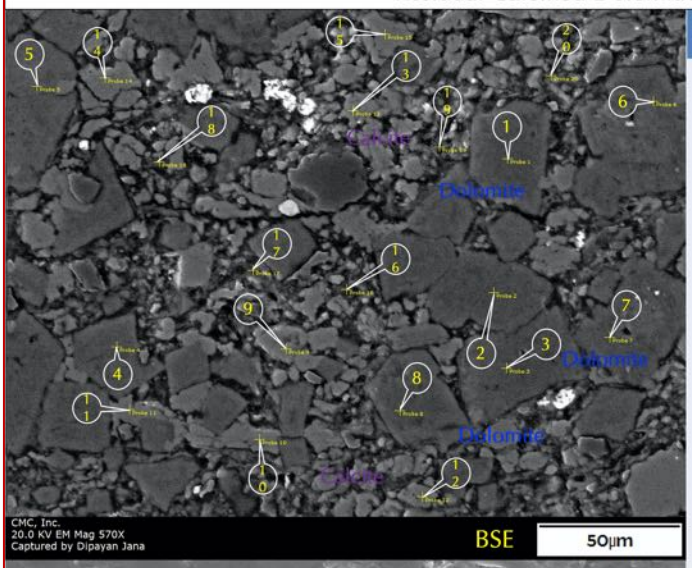

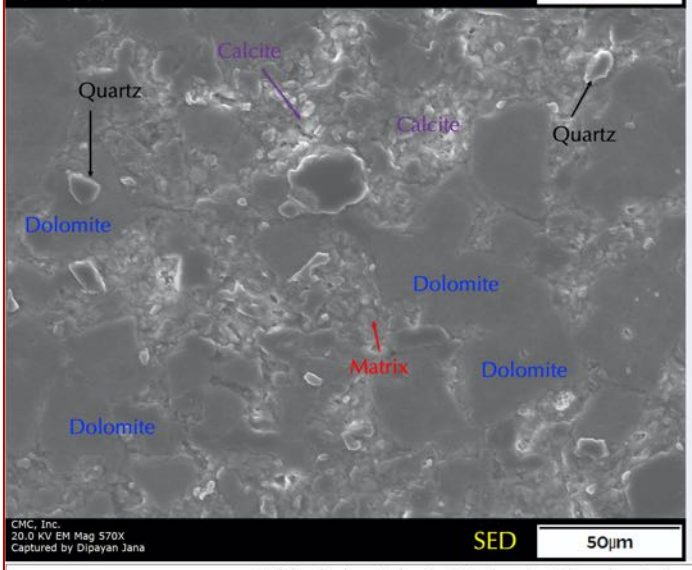

Probe	CaO	SiO2	Al2O3	Na2O	MgO	SO3	K2O	TiO2	FeO	P2O5	CO2	Total	Phase
1	**55.03**	2.40	0.29	0.00	**25.48**	1.18	0.00	0.03	0.00	0.19	**15.40**	100	Dolomite
2	**71.87**	2.21	0.13	0.00	**17.46**	0.47	0.00	0.00	0.00	0.11	**7.75**	100	Dolomite
3	**57.00**	2.22	0.75	0.00	**25.52**	0.66	0.00	0.02	0.03	0.46	**13.34**	100	Dolomite
4	**59.94**	9.54	1.89	0.00	**11.86**	0.81	0.00	0.00	0.60	0.23	**15.12**	100	Dolomite
5	**81.12**	3.37	0.32	0.00	**5.75**	0.64	0.00	0.00	0.34	0.24	**8.22**	100	Dolomite
6	**50.80**	4.70	1.54	0.13	**21.20**	1.60	0.00	0.00	4.09	0.54	**15.39**	100	Dolomite
7	**58.32**	6.11	1.67	0.07	**13.66**	1.08	0.11	0.01	0.64	0.65	**17.68**	100	Dolomite
8	**53.10**	3.23	0.27	0.00	**25.08**	0.68	0.00	0.00	0.31	0.22	**17.10**	100	Dolomite
9	**93.42**	0.34	0.00	0.00	0.09	0.03	0.00	0.00	0.07	0.06	**5.98**	100	Calcite
10	**89.54**	1.75	0.23	0.32	0.70	0.63	0.07	0.14	0.04	0.79	**5.78**	100	Calcite
11	**94.20**	0.58	0.00	0.00	0.05	0.08	0.00	0.00	0.03	0.48	**4.58**	100	Calcite
12	**91.44**	1.89	0.06	0.00	0.53	0.11	0.15	0.02	0.26	0.04	**5.50**	100	Calcite
13	**87.69**	2.68	0.35	0.00	1.53	0.13	0.13	0.03	0.40	0.78	**6.29**	100	Calcite
14	**83.99**	4.07	0.71	0.07	0.83	0.13	0.14	0.10	0.14	0.66	**9.16**	100	Calcite
15	**93.81**	1.19	0.00	0.00	0.03	0.07	0.00	0.00	0.13	0.16	**4.60**	100	Calcite
16	13.36	**43.65**	**14.78**	0.03	8.23	0.21	**4.92**	0.64	1.63	1.05	**11.49**	100	Matrix
17	17.71	**35.89**	**18.02**	0.32	9.82	0.14	**3.89**	0.36	1.72	0.83	**11.30**	100	Matrix
18	42.30	**25.19**	**8.38**	0.04	6.51	0.26	**1.64**	0.00	0.62	1.14	**13.92**	100	Matrix
19	6.47	**48.29**	**18.60**	0.52	8.45	0.23	**3.93**	0.30	1.07	1.04	**11.11**	100	Matrix
20	31.21	**29.68**	**12.15**	0.27	6.78	0.67	**2.68**	0.85	1.27	0.24	**14.20**	100	Matrix

Subhedral to Euhedral Dolomite Rhombs, Anhedral Calcite and Quartz, Interstitial Matrix

Figure C12: Secondary electron image (SED), backscatter electron image (BSE), and X-ray elemental compositions at the tips of callouts shown in the backscatter electron image of interior of a residual calcined impure dolomitic limestone particle in the 1950s natural cement mortar M2 showing (i) euhedral dolomite rhombs, (ii) interstitial anhedral calcite grains, and (iii) interstitial calcined clay-silica matrix in the residual natural cement of calcium raw feed. Each phase is color-coded in the Table of compositions with characteristic components shown in bold.

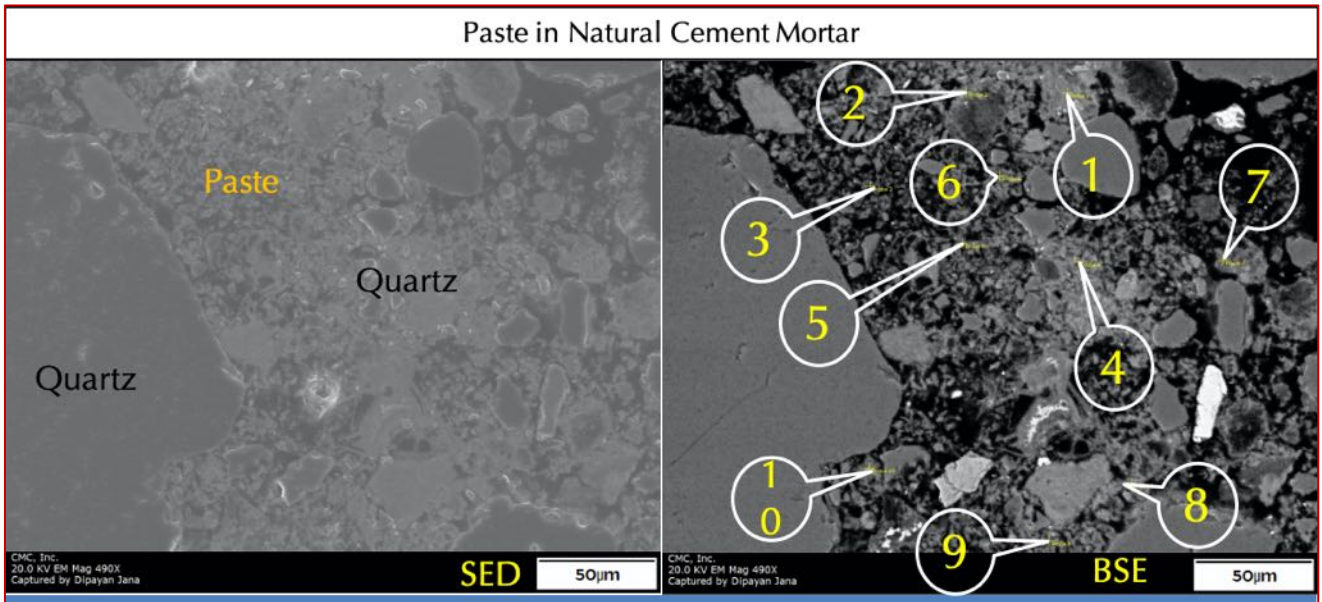

Probe	CaO	SiO2	Al2O3	Na2O	MgO	SO3	K2O	TiO2	FeO	P2O5	CO2	Total	Phase	Paste Cl
1	**49.39**	**20.45**	3.48	0.05	**5.12**	3.68	1.08	0.05	0.93	0.76	15.00	100	Paste	1.09
2	**56.30**	**14.57**	2.92	0.00	**6.14**	1.81	0.63	0.00	1.28	0.65	15.69	100	Paste	0.69
3	12.75	**34.69**	6.07	0.00	7.66	1.84	1.08	0.11	1.63	1.26	**32.90**	100	Leached Paste	-
4	**40.06**	**27.65**	4.93	0.04	**6.31**	2.59	0.53	0.00	1.20	0.56	16.14	100	Paste	1.71
5	**24.78**	**25.77**	8.25	0.17	**10.39**	3.21	0.96	0.54	5.58	1.08	19.27	100	Paste	2.16
6	**37.66**	**17.15**	7.05	0.00	**6.12**	2.89	0.83	0.44	2.78	0.67	24.41	100	Paste	1.25
7	18.28	**50.40**	2.83	0.00	5.09	1.94	0.54	0.01	0.86	1.00	**19.04**	100	Leached Paste	-
8	60.50	16.60	3.49	0.03	**5.28**	1.88	0.62	0.00	0.98	0.85	9.78	100	Paste	0.75
9	24.88	23.37	10.64	0.00	**7.65**	2.42	1.68	1.38	17.80	0.72	9.47	100	Paste	2.52
10	23.17	16.75	6.84	0.21	**3.42**	1.64	1.30	0.04	1.00	0.26	45.37	100	Paste	1.97

Figure C13: Secondary electron image (SED), backscatter electron image (BSE), and X-ray elemental compositions at the tips of callouts shown in the BSE images of paste in the 1950s natural cement mortar M2 showing (i) characteristic enrichment of magnesia in the paste compared to a Portland cement paste, (ii) variable calcium and silica contents of paste depending on degree of hydration of original natural cement, subsequent leaching during service, and lime content along with natural cement, and (iii) variable and higher carbon content in the paste due to variable and higher porosities of paste, respectively.

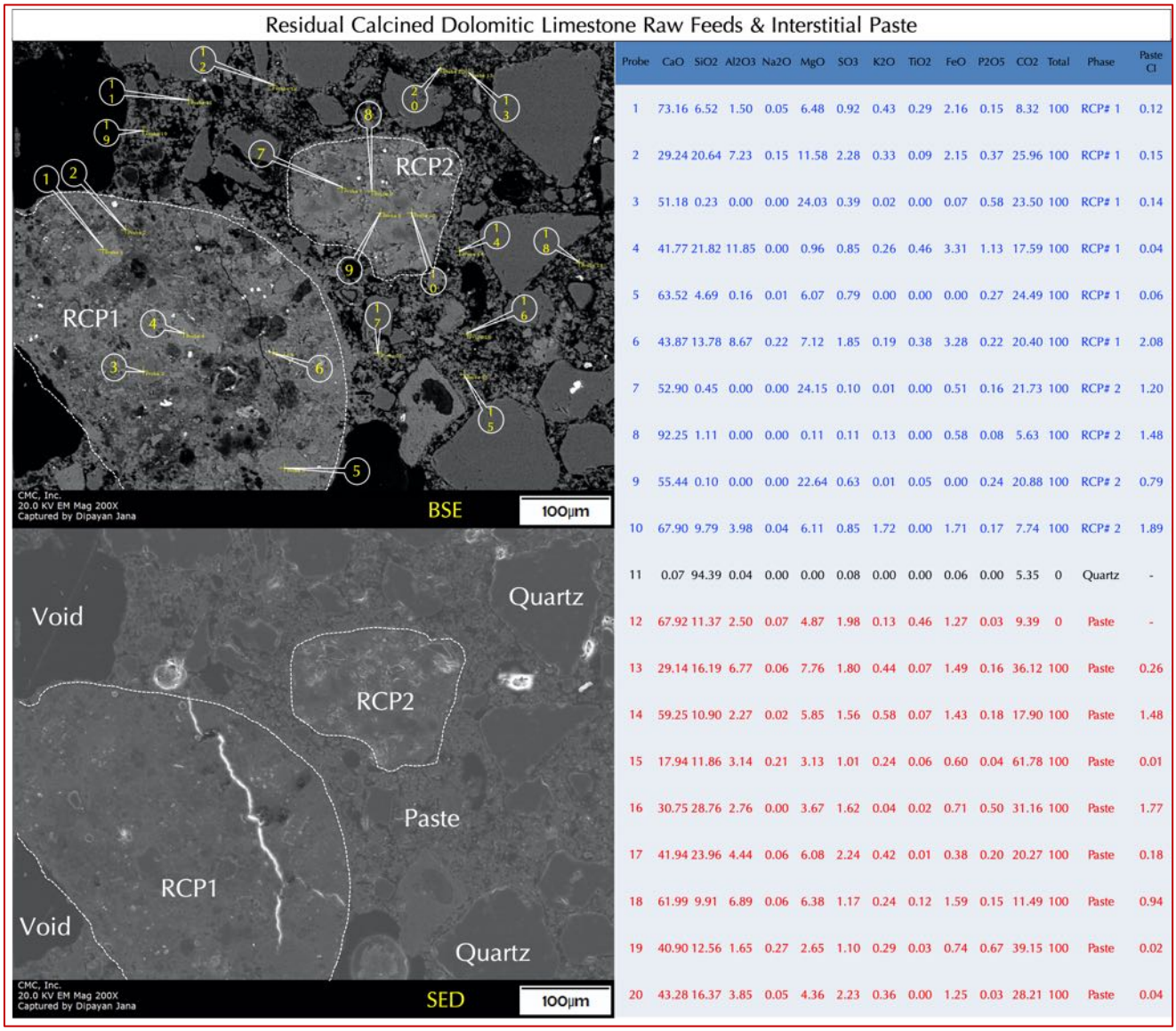

Probe	CaO	SiO2	Al2O3	Na2O	MgO	SO3	K2O	TiO2	FeO	P2O5	CO2	Total	Phase	Paste Cl
1	73.16	6.52	1.50	0.05	6.48	0.92	0.43	0.29	2.16	0.15	8.32	100	RCP# 1	0.12
2	29.24	20.64	7.23	0.15	11.58	2.28	0.33	0.09	2.15	0.37	25.96	100	RCP# 1	0.15
3	51.18	0.23	0.00	0.00	24.03	0.39	0.02	0.00	0.07	0.58	23.50	100	RCP# 1	0.14
4	41.77	21.82	11.85	0.00	0.96	0.85	0.26	0.46	3.31	1.13	17.59	100	RCP# 1	0.04
5	63.52	4.69	0.16	0.01	6.07	0.79	0.00	0.00	0.00	0.27	24.49	100	RCP# 1	0.06
6	43.87	13.78	8.67	0.22	7.12	1.85	0.19	0.38	3.28	0.22	20.40	100	RCP# 1	2.08
7	52.90	0.45	0.00	0.00	24.15	0.10	0.01	0.00	0.51	0.16	21.73	100	RCP# 2	1.20
8	92.25	1.11	0.00	0.00	0.11	0.11	0.13	0.00	0.58	0.08	5.63	100	RCP# 2	1.48
9	55.44	0.10	0.00	0.00	22.64	0.63	0.01	0.05	0.00	0.24	20.88	100	RCP# 2	0.79
10	67.90	9.79	3.98	0.04	6.11	0.85	1.72	0.00	1.71	0.17	7.74	100	RCP# 2	1.89
11	0.07	94.39	0.04	0.00	0.00	0.08	0.00	0.00	0.06	0.00	5.35	0	Quartz	-
12	67.92	11.37	2.50	0.07	4.87	1.98	0.13	0.46	1.27	0.03	9.39	0	Paste	-
13	29.14	16.19	6.77	0.06	7.76	1.80	0.44	0.07	1.49	0.16	36.12	100	Paste	0.26
14	59.25	10.90	2.27	0.02	5.85	1.56	0.58	0.07	1.43	0.18	17.90	100	Paste	1.48
15	17.94	11.86	3.14	0.21	3.13	1.01	0.24	0.06	0.60	0.04	61.78	100	Paste	0.01
16	30.75	28.76	2.76	0.00	3.67	1.62	0.04	0.02	0.71	0.50	31.16	100	Paste	1.77
17	41.94	23.96	4.44	0.06	6.08	2.24	0.42	0.01	0.38	0.20	20.27	100	Paste	0.18
18	61.99	9.91	6.89	0.06	6.38	1.17	0.24	0.12	1.59	0.15	11.49	100	Paste	0.94
19	40.90	12.56	1.65	0.27	2.65	1.10	0.29	0.03	0.74	0.67	39.15	100	Paste	0.02
20	43.28	16.37	3.85	0.05	4.36	2.23	0.36	0.00	1.25	0.03	28.21	100	Paste	0.04

Figure C14: Secondary electron image (SED), backscatter electron image (BSE), and X-ray elemental compositions at the tips of callouts shown in the backscatter electron image of interior of two residual calcined impure dolomitic limestone particles and interstitial paste in the 1950s natural cement mortar M2.

Residual Calcined Dolomitic Limestone Raw Feeds & Interstitial Paste

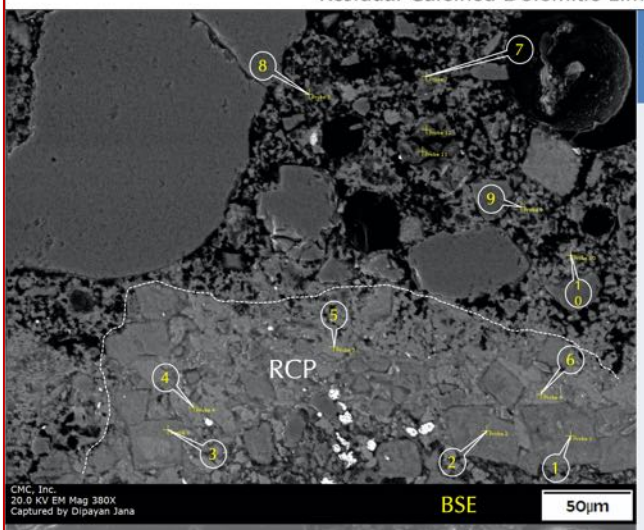

Probe	CaO	SiO2	Al2O3	Na2O	MgO	SO3	K2O	TiO2	FeO	P2O5	CO2	Total	Phase	Paste Cl
1	76.24	3.81	0.33	0.01	10.78	0.15	0.00	0.22	0.33	0.07	8.06	100	Dolomite	-
2	75.24	4.60	0.40	0.02	11.37	0.28	0.00	0.07	0.25	0.30	7.47	100	Dolomite	-
3	79.55	4.14	0.66	0.14	6.65	0.66	0.00	0.06	0.66	0.14	7.35	100	Dolomite	-
4	91.76	1.22	0.03	0.00	0.33	0.23	0.03	0.00	0.08	0.50	5.81	100	Calcite	-
5	92.60	1.75	0.04	0.00	0.21	0.12	0.18	0.01	0.45	0.20	4.44	100	Calcite	-
6	22.53	20.10	3.86	0.01	4.94	1.33	0.11	0.04	1.21	0.31	45.56	100	Paste	2.08
7	41.06	17.46	4.57	0.20	3.66	3.26	0.22	0.81	2.43	0.28	26.03	100	Paste	1.20
8	26.85	17.94	6.21	0.46	8.86	2.11	0.15	0.09	1.66	0.37	35.30	100	Paste	1.48
9	48.27	14.14	4.33	0.02	6.64	2.33	0.13	0.14	1.33	0.32	22.35	100	Paste	0.79
10	38.07	24.70	8.21	0.24	2.68	1.80	0.24	0.00	1.29	0.55	22.20	100	Paste	1.89

Figure C15: Secondary electron image (SED), backscatter electron image (BSE), and X-ray elemental compositions at the tips of callouts shown in the backscatter electron image of interior of a residual calcined impure dolomitic limestone particle (marked by dashed line) and interstitial paste in the 1950s natural cement mortar M2.

Residual Calcined Dolomitic Limestone Raw Feeds & Interstitial Paste

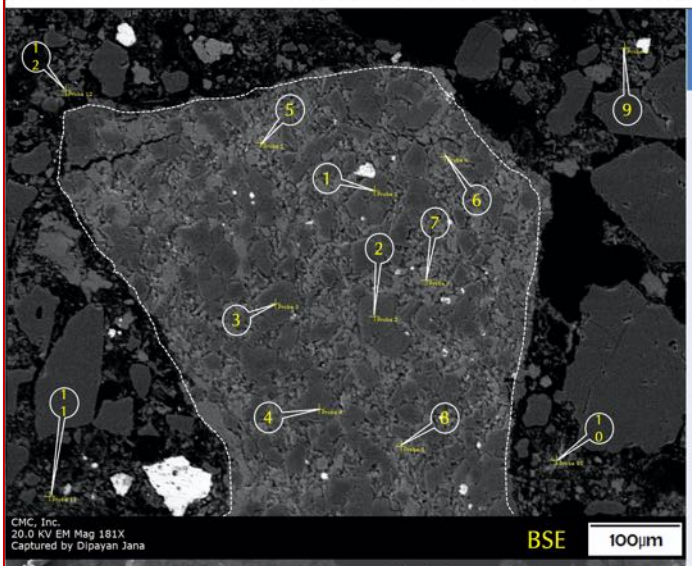

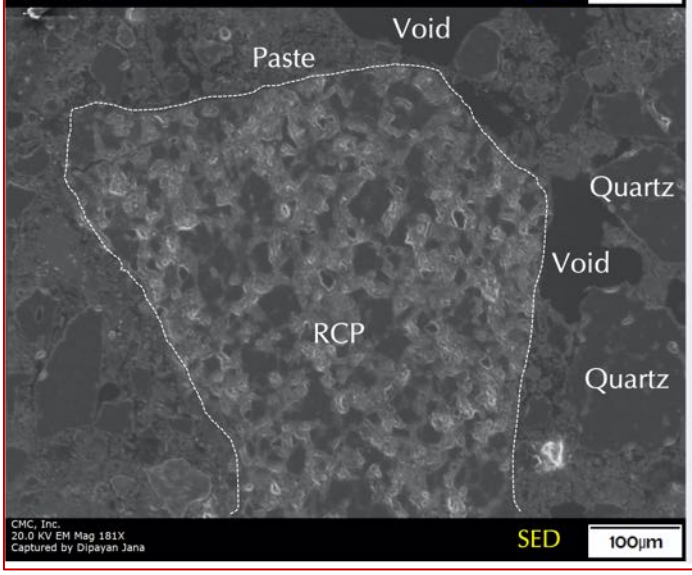

Probe	CaO	SiO2	Al2O3	Na2O	MgO	SO3	K2O	TiO2	FeO	P2O5	CO2	Total	Phase	Paste Cl
1	**47.79**	2.50	0.09	0.00	**21.18**	0.47	0.01	0.04	6.25	0.25	**21.42**	100	Dolomite	-
2	**51.54**	0.03	0.00	0.00	**26.18**	0.00	0.00	0.01	0.19	0.06	**21.98**	100	Dolomite	-
3	**54.71**	0.52	0.00	0.05	**22.97**	0.66	0.00	0.07	0.16	0.90	**19.94**	100	Dolomite	-
4	**58.11**	2.32	0.45	0.00	**22.05**	0.14	0.11	0.05	0.18	0.16	**16.43**	100	Dolomite	-
5	**90.71**	1.08	4.31	0.00	0.00	0.40	0.37	0.00	0.49	0.42	2.21	100	Calcite	-
6	**95.23**	0.69	0.15	0.00	0.13	0.09	0.00	0.00	0.09	0.05	3.57	100	Calcite	-
7	**93.62**	1.05	0.04	0.00	0.00	0.06	0.61	0.00	0.27	0.55	3.80	100	Calcite	-
8	**80.67**	7.71	1.92	0.00	0.63	0.08	0.67	0.08	0.39	0.35	7.51	100	Calcite	-
9	**37.15**	**22.03**	3.60	0.00	8.37	2.54	0.37	0.01	0.98	0.39	**24.55**	100	Paste	1.36
10	**8.19**	**37.17**	9.52	0.39	2.51	1.28	0.08	0.18	0.57	0.79	**39.32**	100	Leached Paste	-
11	0.19	**96.67**	0.20	0.00	0.00	0.15	0.00	0.00	0.11	0.00	2.67	100	Quartz	-
12	**44.01**	**15.91**	4.47	0.00	6.99	2.71	0.33	0.01	2.51	0.24	**22.83**	100	Paste	0.96

Figure C16: Secondary electron image (SED), backscatter electron image (BSE), and X-ray elemental compositions at the tips of callouts shown in the backscatter electron image of interior of a residual calcined impure dolomitic limestone particle (marked by dashed line) and interstitial paste in the 1950s natural cement mortar M2.

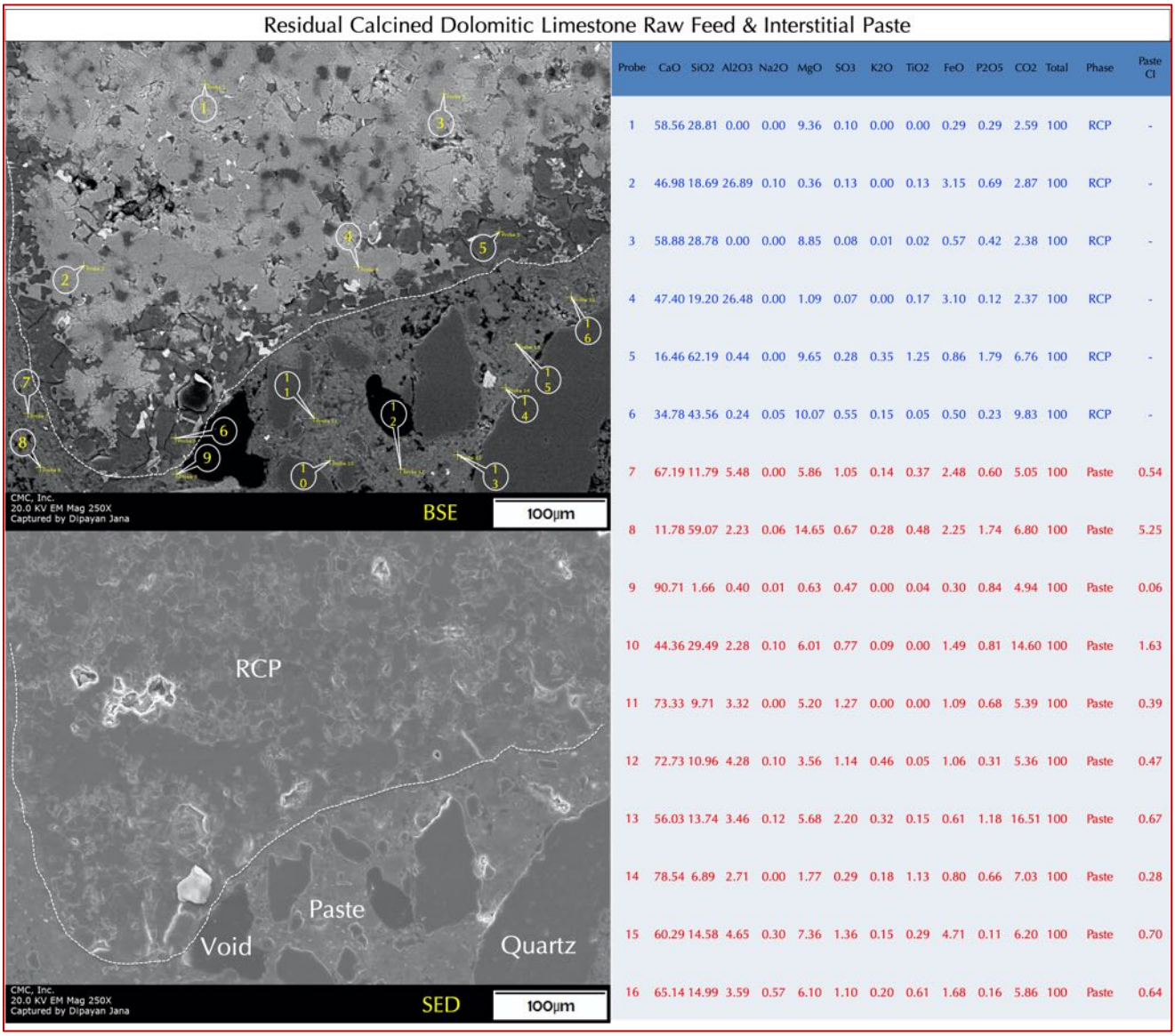

Probe	CaO	SiO2	Al2O3	Na2O	MgO	SO3	K2O	TiO2	FeO	P2O5	CO2	Total	Phase	Paste Cl
1	58.56	28.81	0.00	0.00	9.36	0.10	0.00	0.00	0.29	0.29	2.59	100	RCP	-
2	46.98	18.69	26.89	0.10	0.36	0.13	0.00	0.13	3.15	0.69	2.87	100	RCP	-
3	58.88	28.78	0.00	0.00	8.85	0.08	0.01	0.02	0.57	0.42	2.38	100	RCP	-
4	47.40	19.20	26.48	0.00	1.09	0.07	0.00	0.17	3.10	0.12	2.37	100	RCP	-
5	16.46	62.19	0.44	0.00	9.65	0.28	0.35	1.25	0.86	1.79	6.76	100	RCP	-
6	34.78	43.56	0.24	0.05	10.07	0.55	0.15	0.05	0.50	0.23	9.83	100	RCP	-
7	67.19	11.79	5.48	0.00	5.86	1.05	0.14	0.37	2.48	0.60	5.05	100	Paste	0.54
8	11.78	59.07	2.23	0.06	14.65	0.67	0.28	0.48	2.25	1.74	6.80	100	Paste	5.25
9	90.71	1.66	0.40	0.01	0.63	0.47	0.00	0.04	0.30	0.84	4.94	100	Paste	0.06
10	44.36	29.49	2.28	0.10	6.01	0.77	0.09	0.00	1.49	0.81	14.60	100	Paste	1.63
11	73.33	9.71	3.32	0.00	5.20	1.27	0.00	0.00	1.09	0.68	5.39	100	Paste	0.39
12	72.73	10.96	4.28	0.10	3.56	1.14	0.46	0.05	1.06	0.31	5.36	100	Paste	0.47
13	56.03	13.74	3.46	0.12	5.68	2.20	0.32	0.15	0.61	1.18	16.51	100	Paste	0.67
14	78.54	6.89	2.71	0.00	1.77	0.29	0.18	1.13	0.80	0.66	7.03	100	Paste	0.28
15	60.29	14.58	4.65	0.30	7.36	1.36	0.15	0.29	4.71	0.11	6.20	100	Paste	0.70
16	65.14	14.99	3.59	0.57	6.10	1.10	0.20	0.61	1.68	0.16	5.86	100	Paste	0.64

Figure C17: Secondary electron image (SED), backscatter electron image (BSE), and X-ray elemental compositions at the tips of callouts shown in the backscatter electron image of interior of a residual calcined impure dolomitic limestone particle (marked by dashed line) and interstitial paste in the 1950s natural cement mortar M2.

Paste in Natural Cement Mortar														
Probe	CaO	SiO2	Al2O3	Na2O	MgO	SO3	K2O	TiO2	FeO	P2O5	CO2	Total	Phase	Paste Cl
1	**46.27**	**21.27**	4.94	0.01	**3.42**	2.54	0.19	0.16	1.58	0.16	19.47	100	Paste	1.29
2	**25.71**	**24.88**	8.00	0.06	**12.36**	1.44	0.82	0.04	1.10	0.76	24.83	100	Paste	1.84
3	**4.17**	**19.78**	19.83	0.11	**36.63**	1.62	0.13	0.02	1.47	0.28	15.96	100	Leached Paste	1.41
4	**51.34**	**16.21**	4.68	0.28	**2.59**	2.40	0.42	0.15	0.81	0.26	20.89	100	Paste	0.93
5	**63.28**	**16.18**	4.47	0.05	**4.18**	2.01	0.67	0.05	2.23	0.46	6.40	100	Paste	0.75
6	**84.34**	**4.88**	0.33	0.00	**2.83**	1.53	0.06	0.00	0.00	0.50	5.51	100	Paste	0.16
7	**51.01**	**14.15**	3.36	0.08	**7.00**	3.15	0.36	0.47	0.71	0.96	18.75	100	Paste	0.72
8	**6.60**	**28.94**	17.02	0.00	**22.44**	1.31	0.29	0.00	1.24	0.41	21.74	100	Leached Paste	2.65
9	**76.48**	**7.94**	2.72	0.02	**1.92**	1.20	0.74	0.09	0.83	0.06	8.01	100	Paste	0.33
10	**45.75**	**18.41**	1.12	0.31	**6.41**	2.10	0.45	0.02	0.70	0.25	24.47	100	Paste	0.97
11	**57.99**	**10.45**	3.88	0.09	**6.38**	1.65	0.46	0.01	0.60	0.46	18.04	100	Paste	0.51

Figure C18: X-ray elemental compositions of paste in the 1950s natural cement mortar M2.

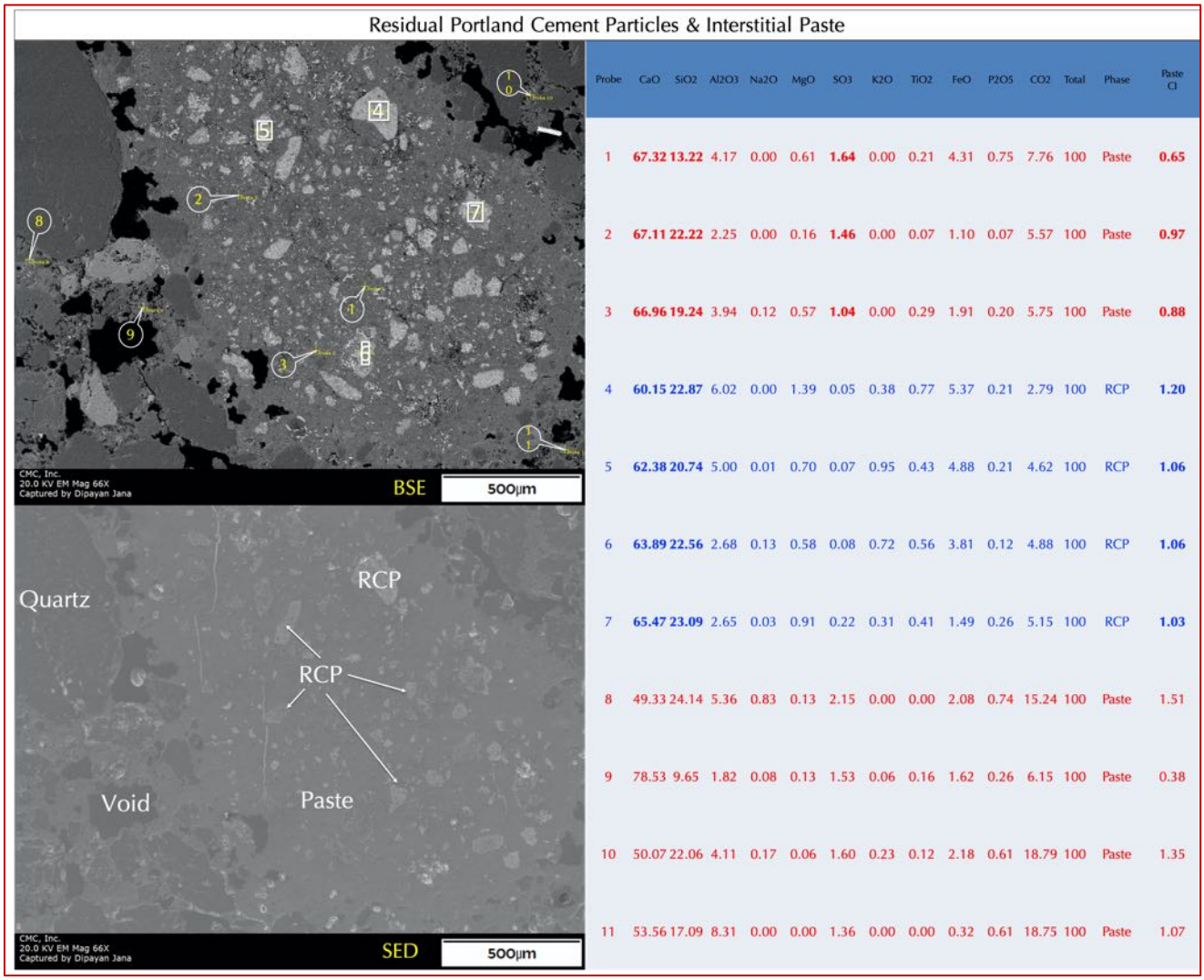

Probe	CaO	SiO2	Al2O3	Na2O	MgO	SO3	K2O	TiO2	FeO	P2O5	CO2	Total	Phase	Paste Cl
1	**67.32**	**13.22**	4.17	0.00	0.61	**1.64**	0.00	0.21	4.31	0.75	7.76	100	Paste	**0.65**
2	**67.11**	**22.22**	2.25	0.00	0.16	**1.46**	0.00	0.07	1.10	0.07	5.57	100	Paste	**0.97**
3	**66.96**	**19.24**	3.94	0.12	0.57	**1.04**	0.00	0.29	1.91	0.20	5.75	100	Paste	**0.88**
4	**60.15**	**22.87**	6.02	0.00	1.39	0.05	0.38	0.77	5.37	0.21	2.79	100	RCP	**1.20**
5	**62.38**	**20.74**	5.00	0.01	0.70	0.07	0.95	0.43	4.88	0.21	4.62	100	RCP	**1.06**
6	**63.89**	**22.56**	2.68	0.13	0.58	0.08	0.72	0.56	3.81	0.12	4.88	100	RCP	**1.06**
7	**65.47**	**23.09**	2.65	0.03	0.91	0.22	0.31	0.41	1.49	0.26	5.15	100	RCP	**1.03**
8	49.33	24.14	5.36	0.83	0.13	2.15	0.00	0.00	2.08	0.74	15.24	100	Paste	1.51
9	78.53	9.65	1.82	0.08	0.13	1.53	0.06	0.16	1.62	0.26	6.15	100	Paste	0.38
10	50.07	22.06	4.11	0.17	0.06	1.60	0.23	0.12	2.18	0.61	18.79	100	Paste	1.35
11	53.56	17.09	8.31	0.00	0.00	1.36	0.00	0.00	0.32	0.61	18.75	100	Paste	1.07

Figure C19: Secondary electron image (SED), backscatter electron image (BSE), and X-ray elemental compositions in the boxed areas and at the tips of callouts shown in the backscatter electron image of interior of a residual Portland cement particle and interstitial paste in the 1916 cement-lime mortar M3. Portland cement paste shows typical characteristic enrichment in calcium and subordinate silica from calcium-silicate hydrate composition of cement-lime paste.

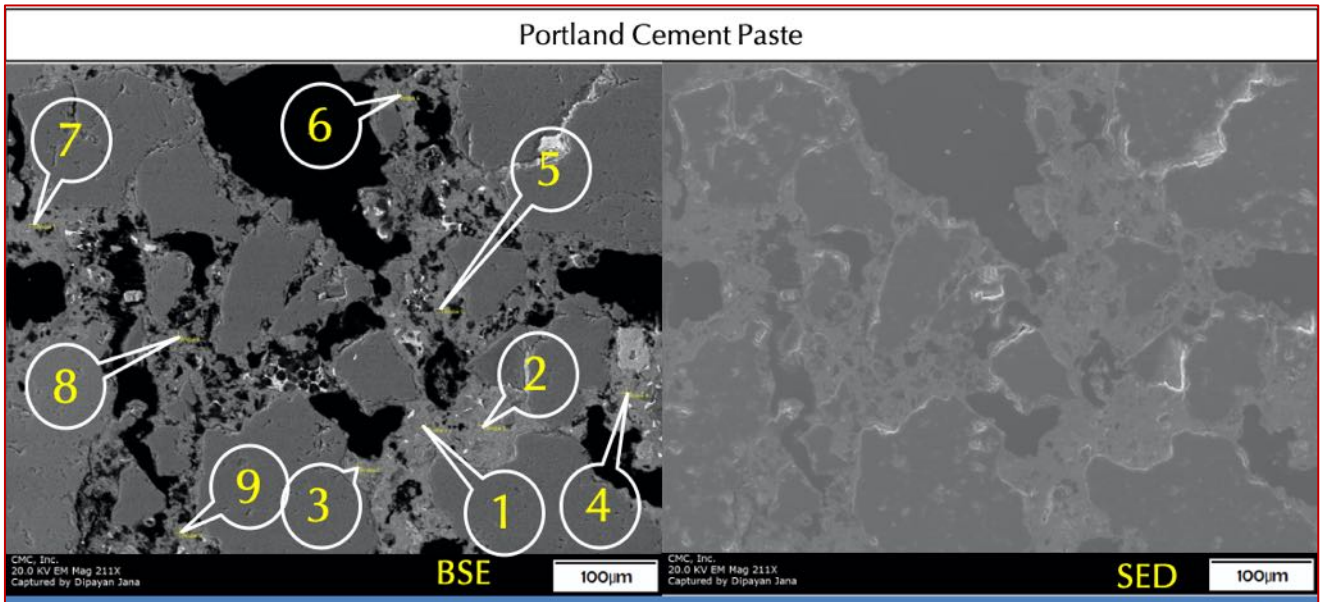

Probe	CaO	SiO2	Al2O3	Na2O	MgO	SO3	K2O	TiO2	FeO	P2O5	CO2	Total	Phase	Paste Cl
1	38.14	34.49	7.80	0.11	0.07	0.69	0.88	0.09	2.23	0.48	15.02	100	Paste	2.79
2	73.24	14.13	2.82	0.00	0.38	0.71	0.20	0.30	1.48	0.27	6.46	100	Paste	0.59
3	56.31	14.42	5.82	0.05	0.35	2.10	0.08	0.42	4.34	0.21	15.90	100	Paste	0.88
4	82.12	4.13	1.31	0.00	0.00	1.75	0.04	0.32	2.20	0.25	7.86	100	Paste	0.18
5	36.23	43.85	3.77	0.01	0.16	1.13	0.38	0.01	1.60	0.36	12.51	100	Paste	3.51
6	29.07	40.40	11.94	2.11	0.26	0.14	0.98	0.00	1.55	0.70	12.85	100	Paste	4.33
7	51.96	23.17	5.71	0.07	0.06	2.15	0.37	0.43	1.47	0.82	13.80	100	Paste	1.39
8	45.31	23.41	6.15	0.23	0.09	1.40	1.29	1.23	2.31	0.54	18.04	100	Paste	1.63
9	0.11	**94.50**	0.00	0.00	0.00	0.32	0.06	0.09	0.02	0.03	4.86	100	Quartz	-

Figure C20: Secondary electron image (SED), backscatter electron image (BSE), and X-ray elemental compositions at the tips of callouts shown in the backscatter electron image of paste in the 1916 cement-lime mortar M3. Portland cement paste shows typical characteristic enrichment in calcium and subordinate silica from calcium-silicate-hydrate composition of cement-lime paste.

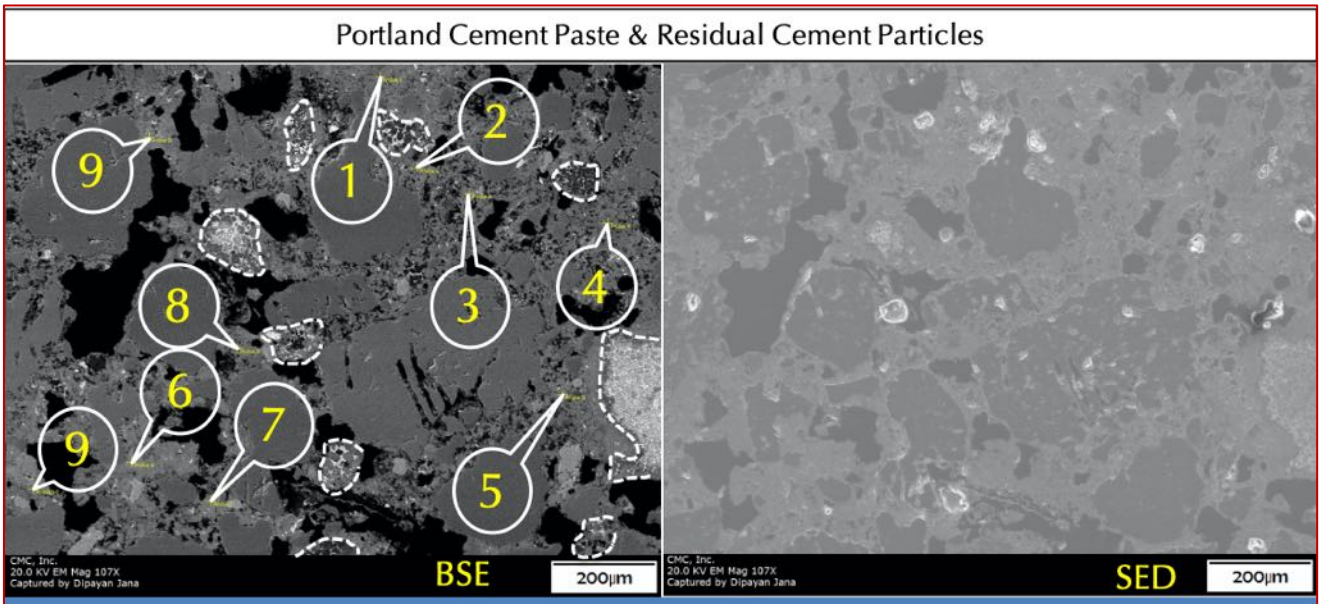

Probe	CaO	SiO2	Al2O3	Na2O	MgO	SO3	K2O	TiO2	FeO	P2O5	CO2	Total	Phase	Paste Cl
1	43.15	33.62	3.80	0.02	0.07	2.37	0.98	0.00	0.68	0.49	14.82	100	Paste	2.28
2	69.16	14.65	3.28	0.12	0.86	1.88	1.00	0.22	2.26	0.52	6.05	100	Paste	0.66
3	84.02	6.43	0.10	0.00	0.17	1.89	0.43	0.00	0.00	0.15	6.81	100	Paste	0.21
4	43.26	25.62	4.90	0.01	0.14	2.82	0.73	0.42	4.79	1.04	16.26	100	Paste	1.85
5	70.54	8.34	4.03	0.00	2.12	1.25	0.19	0.34	5.27	0.24	7.68	100	Paste	0.43
6	12.19	53.23	6.07	0.39	12.09	0.08	0.01	0.07	10.71	0.37	4.78	100	Paste+	-
7	85.25	4.45	1.66	0.00	0.10	0.61	0.17	0.03	1.35	0.07	6.31	100	Paste	0.18
8	53.27	22.38	3.57	0.08	0.27	0.80	0.53	0.37	1.42	0.02	17.29	100	Paste	1.26
9	16.93	35.90	13.17	0.10	6.98	0.68	3.29	0.00	12.28	0.38	10.29	100	Paste+	-
10	66.84	16.51	3.17	0.00	0.00	1.59	0.86	1.23	2.10	0.86	6.82	100	Paste	0.77

Figure C21: Secondary electron image (SED), backscatter electron image (BSE), and X-ray elemental compositions at the tips of callouts shown in the backscatter electron image of paste in the 1916 cement-lime mortar M3. Outlines of a few residual Portland cement particles are shown by dashed lines in BSE image. Portland cement paste shows typical characteristic enrichment in calcium and subordinate silica from calcium-silicate-hydrate composition of cement-lime paste.

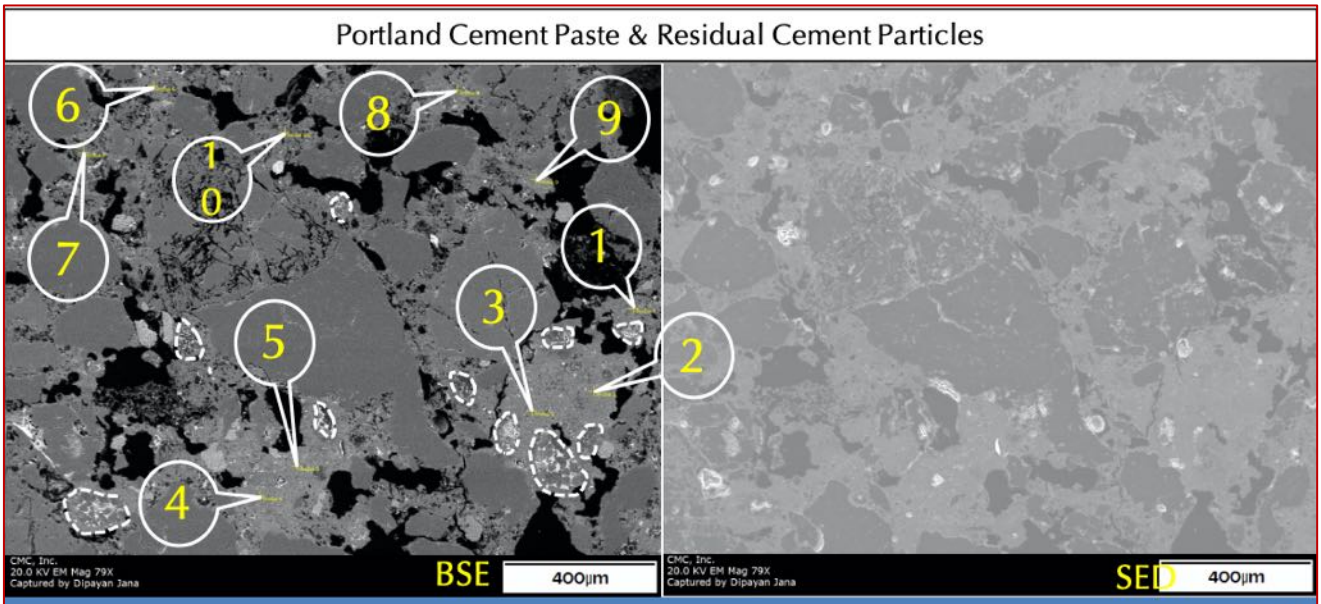

Probe	CaO	SiO2	Al2O3	Na2O	MgO	SO3	K2O	TiO2	FeO	P2O5	CO2	Total	Phase	Paste Cl
1	58.89	20.97	4.94	0.04	0.00	1.32	0.56	0.10	6.30	0.81	6.08	100	Paste	1.16
2	67.79	18.47	3.58	0.00	0.23	1.39	0.35	0.12	2.17	0.37	5.52	100	Paste	0.84
3	58.41	18.48	5.00	0.00	1.15	1.17	0.16	0.40	9.03	0.83	5.38	100	Paste	1.06
4	39.45	26.38	11.43	0.50	0.03	2.57	0.09	0.17	3.92	0.88	14.58	100	Paste	2.26
5	0.00	95.24	0.00	0.00	0.00	0.64	0.00	0.20	0.00	1.23	2.69	100	Quartz	-
6	61.18	21.30	5.27	0.00	0.46	1.43	0.73	0.00	2.62	1.09	5.93	100	Paste	1.09
7	65.19	15.93	4.91	0.06	0.32	1.38	0.92	0.71	4.82	0.88	4.87	100	Paste	0.81
8	56.54	24.01	5.13	0.12	0.05	1.65	1.23	0.55	3.52	0.52	6.67	100	Paste	1.33
9	23.97	42.42	9.72	1.31	0.00	0.94	4.70	0.28	1.95	1.39	13.31	100	Paste+	-
10	5.23	62.12	21.19	4.65	0.00	0.48	0.00	0.06	0.09	0.92	5.27	100	Feldspar	-

Figure C22: Secondary electron image (SED), backscatter electron image (BSE), and X-ray elemental compositions at the tips of callouts shown in the backscatter electron image of paste in the 1916 cement-lime mortar M3. Outlines of a few residual Portland cement particles are shown by dashed lines in BSE image. Portland cement paste shows typical characteristic enrichment in calcium and subordinate silica from calcium-silicate-hydrate composition of cement-lime paste.

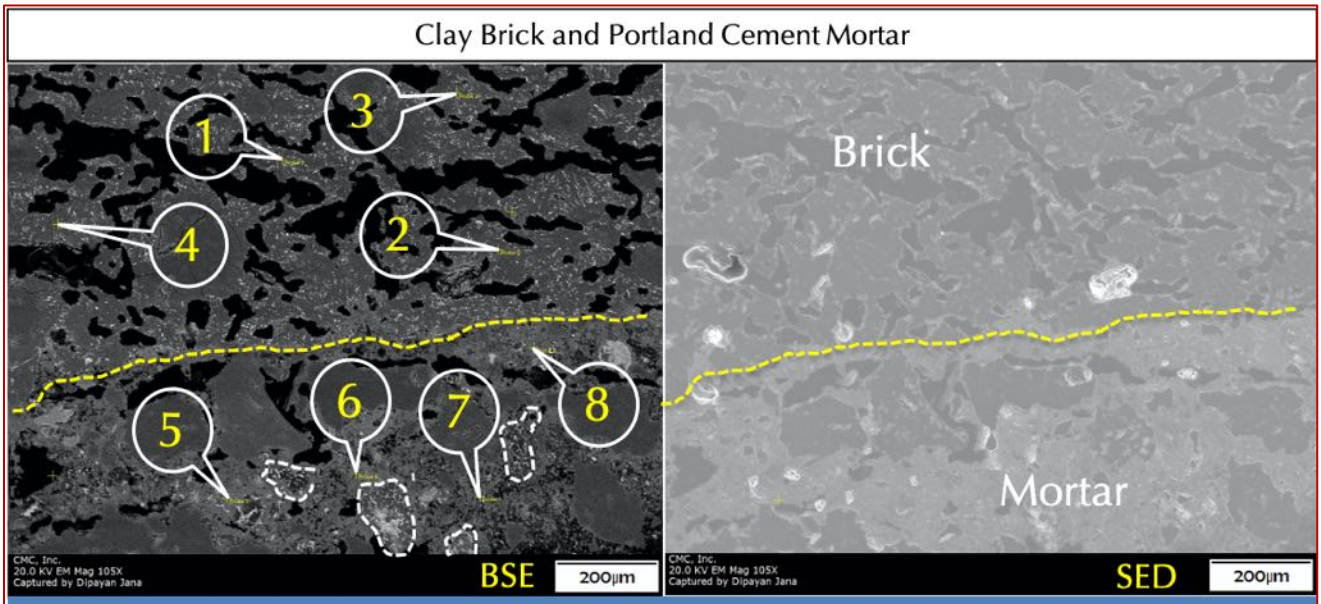

Probe	CaO	SiO2	Al2O3	Na2O	MgO	SO3	K2O	TiO2	FeO	P2O5	CO2	Total	Phase	Paste Cl
1	0.03	**84.35**	**6.85**	0.03	0.00	0.00	0.00	0.77	**1.92**	1.63	4.40	100	Brick	-
2	0.08	**67.94**	**22.49**	0.00	0.00	0.00	0.01	0.88	**5.16**	0.68	2.75	100	Brick	-
3	0.07	**55.16**	**9.35**	0.03	0.00	0.47	0.00	3.70	**23.01**	1.01	7.19	100	Brick	-
4	0.03	**48.34**	**36.54**	0.00	0.00	0.28	0.00	0.83	**7.22**	1.89	4.87	100	Brick	-
5	61.64	20.15	2.50	0.48	1.12	2.53	1.34	0.66	3.07	1.03	5.48	100	Paste	0.97
6	19.69	70.88	0.79	0.00	0.00	0.49	0.26	0.00	0.00	1.74	6.14	100	Paste+	-
7	60.40	15.76	2.32	0.00	1.18	1.73	0.57	0.49	10.44	1.36	5.75	100	Paste	0.87
8	0.03	55.52	30.16	0.00	0.00	0.10	0.02	0.67	4.46	1.55	7.50	100	Paste+	-

Figure C23: Secondary electron image (SED), backscatter electron image (BSE), and X-ray elemental compositions at the tips of callouts shown in the backscatter electron image of paste in the 1916 cement-lime mortar M3. Outlines of a few residual Portland cement particles are shown by dashed lines in BSE image.

Also shown is the adhered remains of clay brick in the mortar showing the typical aluminosilicate glassy matrix of brick as evidenced by high silica and alumina in the brick compositions highlighted in bold in the composition Table. Portland cement paste shows typical characteristic enrichment in calcium and subordinate silica from calcium-silicate-hydrate composition of cement-lime paste.

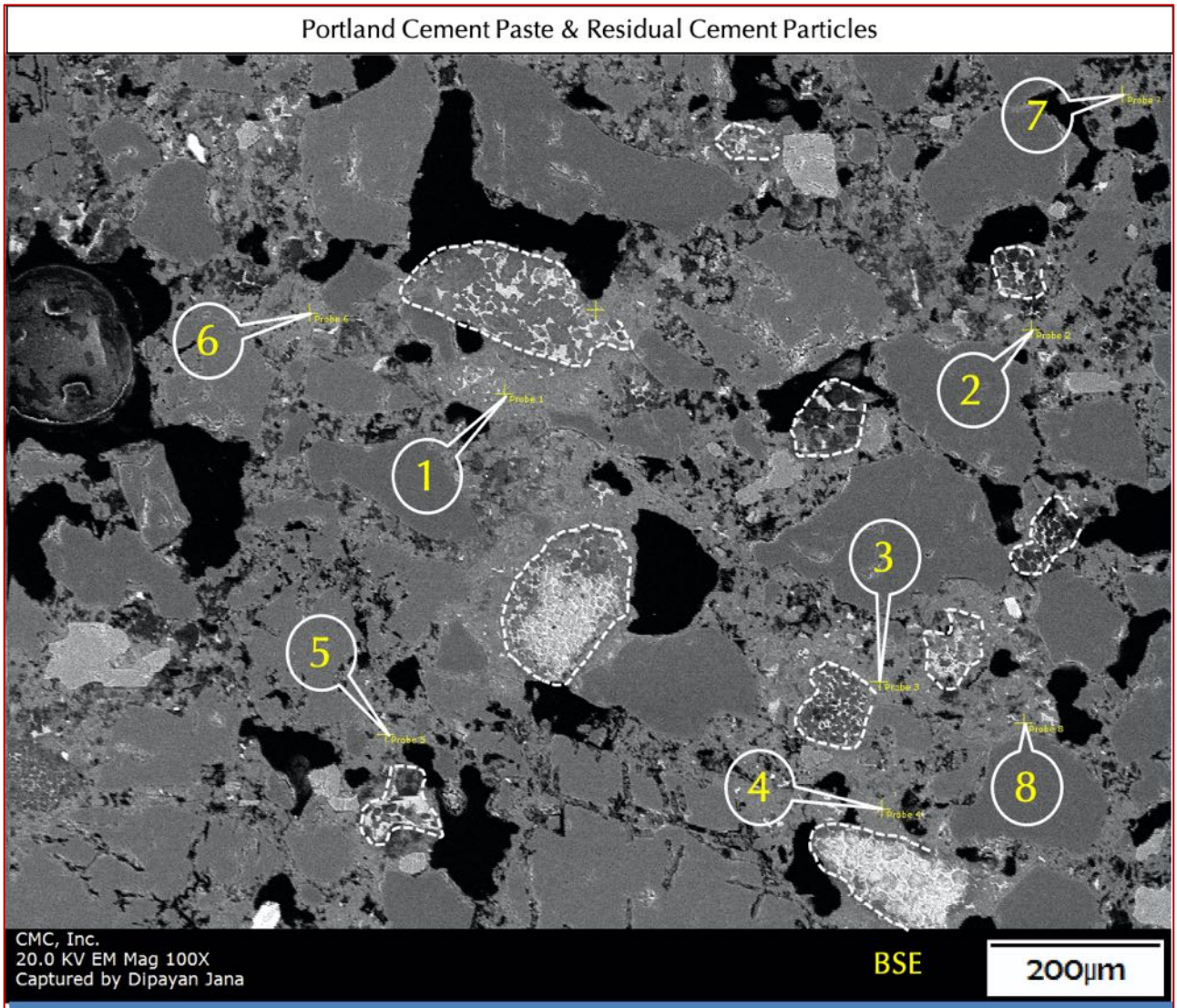

Probe	CaO	SiO2	Al2O3	Na2O	MgO	SO3	K2O	TiO2	FeO	P2O5	CO2	Total	Phase	Paste Cl
1	**60.08**	**20.14**	4.54	0.01	2.95	0.67	0.52	0.49	4.33	1.41	4.88	100	Paste	1.00
2	**70.51**	**16.16**	2.82	0.00	0.00	0.76	0.85	0.00	2.63	0.48	5.79	100	Paste	0.71
3	**72.73**	**14.02**	3.45	0.38	0.02	1.17	0.48	0.11	1.21	1.24	5.19	100	Paste	0.60
4	**41.59**	**22.80**	9.17	0.39	0.64	1.72	0.14	0.94	10.99	1.79	9.83	100	Paste	1.92
5	21.41	54.42	10.77	1.54	0.00	0.87	0.64	0.79	4.21	1.46	3.88	100	Paste+	-
6	**78.54**	**7.09**	3.07	0.00	0.77	1.82	0.05	0.05	2.36	1.32	4.93	100	Paste	0.31
7	**75.66**	**9.05**	2.65	0.24	0.26	2.03	0.35	0.00	3.00	1.17	5.59	100	Paste	0.40
8	8.53	**81.41**	0.90	0.00	0.00	0.74	0.32	0.00	1.19	1.58	5.32	100	Quartz	-

Figure C24: Backscatter electron image (BSE), and X-ray elemental compositions at the tips of callouts shown in the backscatter electron image of paste in the 1916 cement-lime mortar M3. Outlines of a few residual Portland cement particles are shown by dashed lines in BSE image. Portland cement paste shows typical characteristic enrichment in calcium and subordinate silica from calcium-silicate-hydrate composition of cement-lime paste.

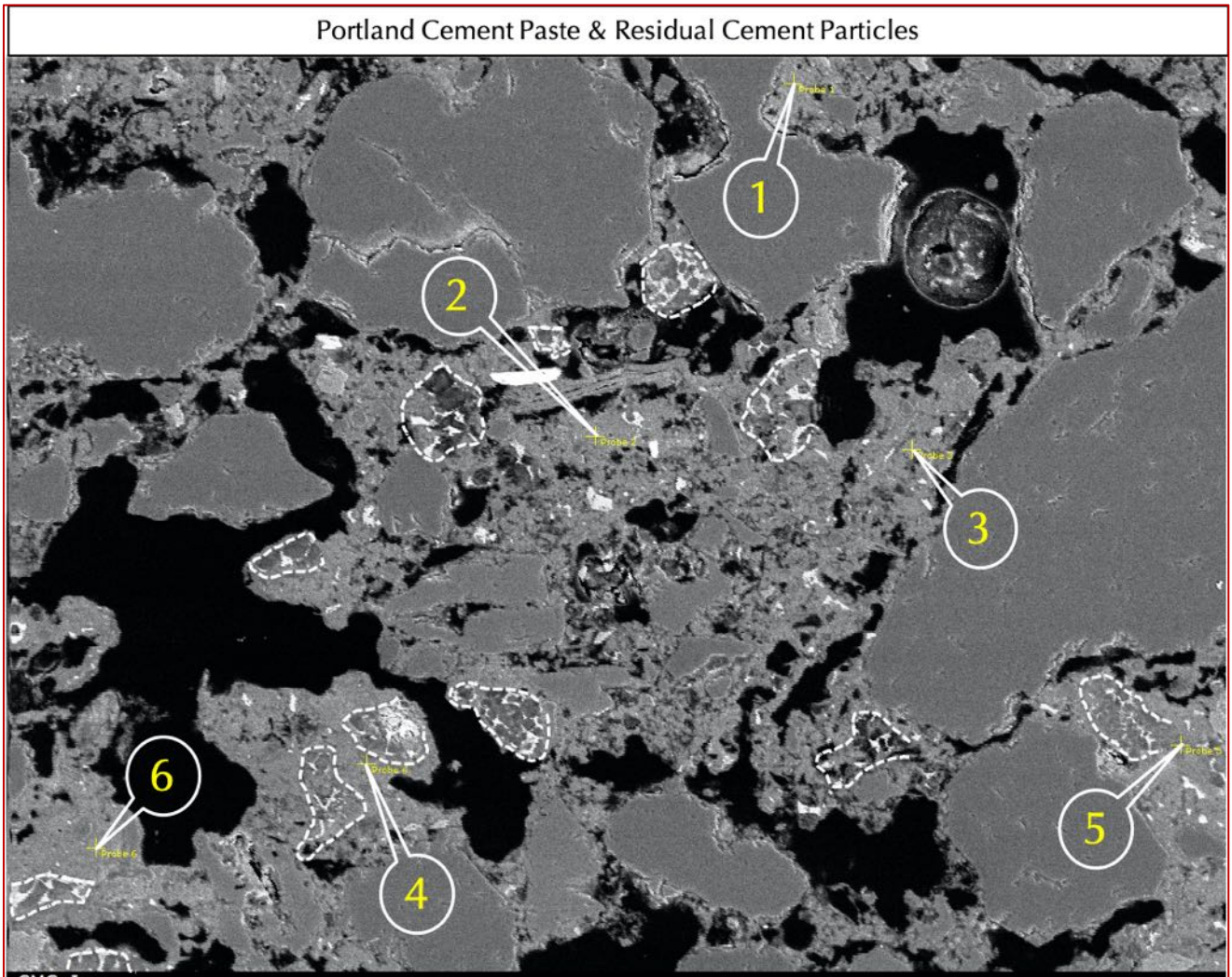

Probe	CaO	SiO2	Al2O3	Na2O	MgO	SO3	K2O	TiO2	FeO	P2O5	CO2	Total	Phase	Paste CI
1	**54.11**	**24.38**	7.24	1.66	0.00	1.55	0.96	0.10	2.74	1.11	6.16	100	Paste	1.44
2	**46.18**	**13.80**	10.14	0.76	2.40	1.69	1.55	0.64	17.25	0.98	4.62	100	Paste	1.25
3	**70.34**	**14.40**	1.15	0.90	0.04	2.46	1.21	0.36	2.51	1.06	5.56	100	Paste	0.62
4	**60.71**	**18.07**	4.80	0.78	0.00	1.40	1.19	0.00	6.19	1.28	5.58	100	Paste	0.99
5	**55.39**	**26.35**	3.78	0.47	0.75	2.37	0.93	0.10	3.17	0.77	5.92	100	Paste	1.42
6	**71.12**	**16.29**	1.88	0.02	0.17	2.00	0.51	0.40	1.96	0.77	4.89	100	Paste	0.69

Figure C25: Backscatter electron image (BSE), and X-ray elemental compositions at the tips of callouts shown in the backscatter electron image of paste in the 1916 cement-lime mortar M3. Outlines of a few residual Portland cement particles are shown by dashed lines in BSE image. Portland cement paste shows typical characteristic enrichment in calcium and subordinate silica from calcium-silicate-hydrate composition of cement-lime paste.

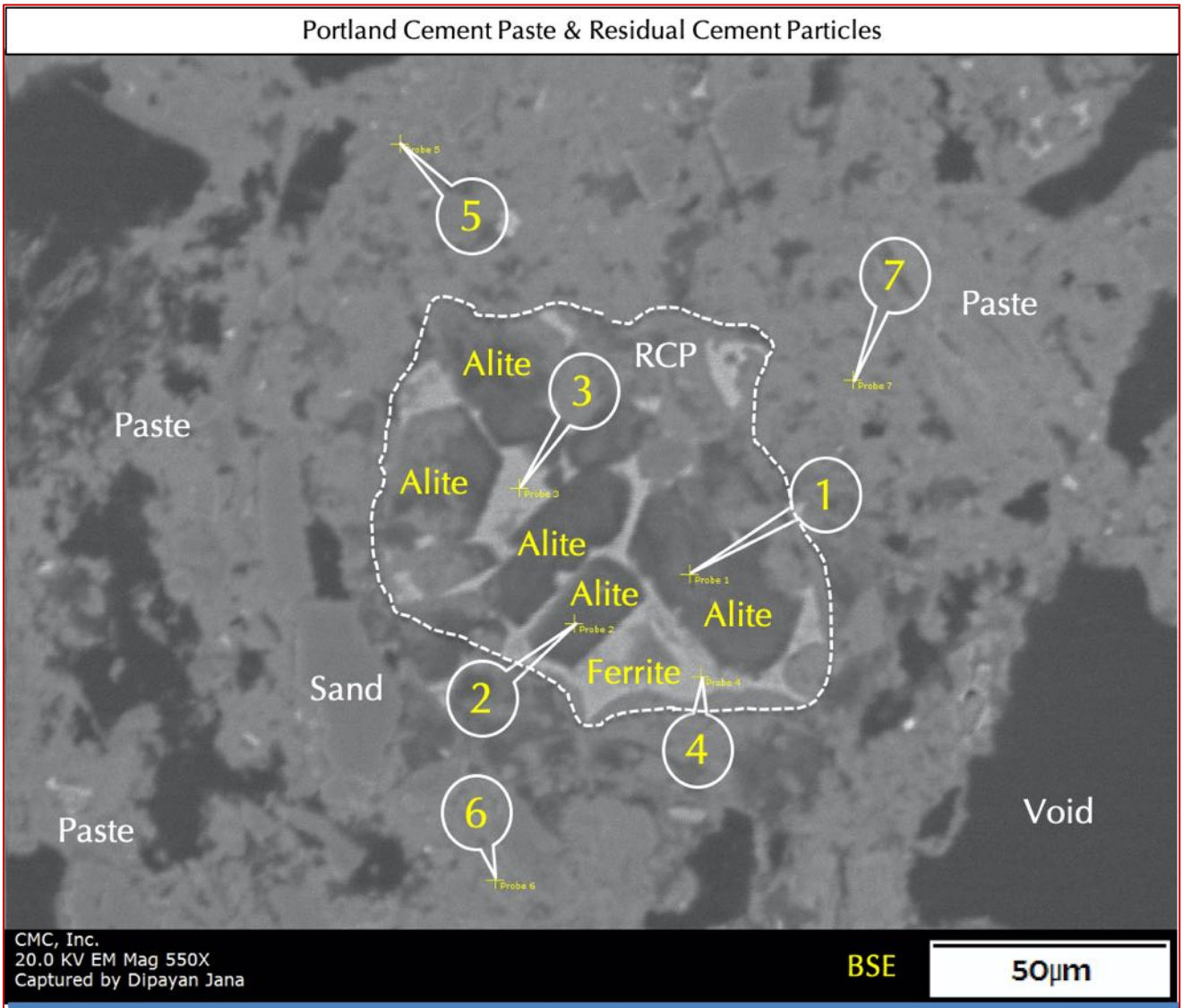

Probe	CaO	SiO2	Al2O3	Na2O	MgO	SO3	K2O	TiO2	FeO	P2O5	CO2	Total	Phase	Paste Cl
1	**4.77**	**51.38**	**11.46**	0.11	1.15	1.28	0.83	0.00	**6.75**	2.30	19.98	100	Alite	-
2	**29.72**	**19.94**	**15.00**	0.28	2.76	2.88	0.62	0.85	**15.65**	1.86	10.43	100	Alite	-
3	**47.43**	5.07	**18.19**	0.67	3.67	0.25	1.76	0.69	**19.72**	0.81	1.73	100	Ferrite	-
4	**47.57**	5.19	**18.01**	0.54	4.35	0.00	1.76	0.87	**19.59**	0.88	1.25	100	Ferrite	-
5	14.19	52.74	15.09	4.17	0.02	1.89	0.20	0.03	0.30	2.13	9.23	100	Paste	-
6	51.55	17.89	7.01	0.40	2.60	2.65	0.91	0.59	10.24	1.38	4.78	100	Paste	1.18
7	62.99	18.66	3.88	0.31	0.46	2.85	0.94	0.66	2.13	1.41	5.70	100	Paste	0.91

Figure C26: Characteristic microstructure of a residual Portland cement particle (outline marked by dashed line) in the 1916 cement-lime mortar M3 showing euhedral alite and interstitial ferrite phase in the residual cement. Table shows compositions of residual cement phases, along with paste around the cement.

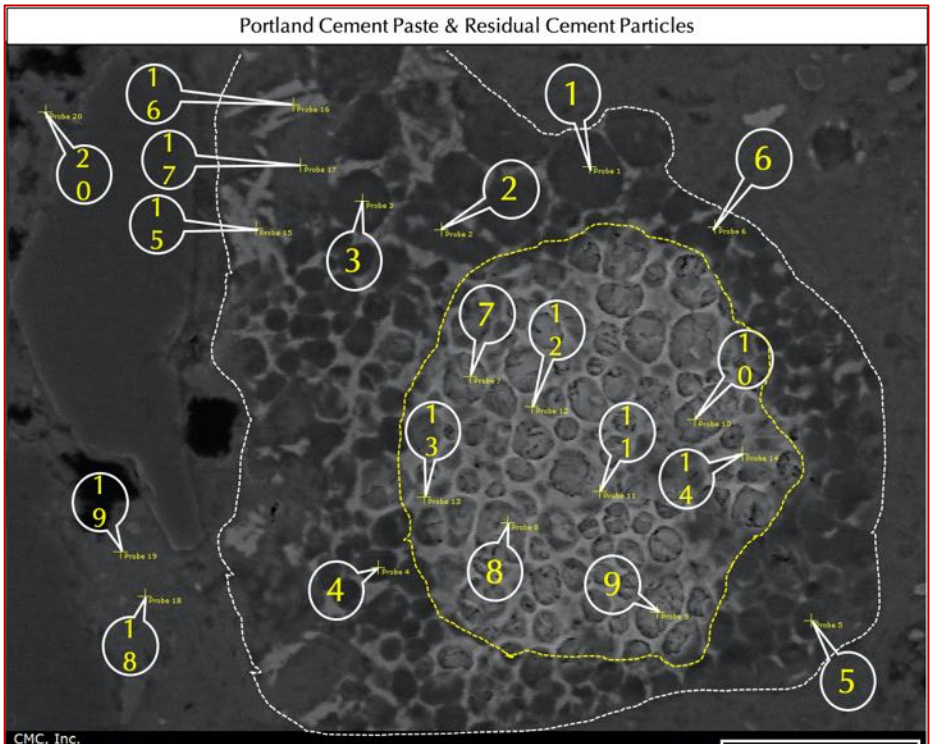

Probe	CaO	SiO2	Al2O3	Na2O	MgO	SO3	K2O	TiO2	FeO	P2O5	CO2	Total	Phase	Paste Cl
1	12.88	67.39	3.41	0.41	0.07	0.43	0.37	1.36	6.05	2.78	4.86	100	RCP	-
2	17.70	54.23	6.73	0.33	0.60	1.49	0.06	0.86	8.27	1.97	7.77	100	RCP	-
3	17.11	63.21	4.81	0.54	0.01	0.69	0.37	1.24	5.65	2.56	3.81	100	RCP	-
4	18.66	61.65	3.29	0.35	0.71	0.45	0.21	0.61	7.81	0.58	5.66	100	RCP	-
5	20.35	50.36	4.53	0.20	3.74	1.27	0.29	0.72	3.37	2.51	12.65	100	RCP	-
6	24.61	55.95	1.85	0.15	3.27	1.34	0.37	0.49	3.35	2.59	6.04	100	RCP	-
7	66.40	23.81	1.94	0.11	0.30	0.25	0.71	0.39	1.82	1.18	3.09	100	RCP	-
8	66.12	24.93	1.11	0.00	0.38	0.18	0.79	0.24	1.70	1.34	3.21	100	RCP	-
9	52.63	13.40	13.36	0.52	2.28	0.11	1.01	0.94	12.14	1.40	2.22	100	RCP	-
10	64.61	15.98	6.03	0.01	0.39	0.18	1.07	0.49	8.78	0.76	1.71	100	RCP	-
11	48.63	13.94	11.13	0.20	1.74	0.56	0.06	1.12	17.72	1.22	3.67	100	RCP	-
12	53.73	13.97	13.99	0.11	2.81	0.04	0.22	0.37	11.94	0.67	2.14	100	RCP	-
13	29.97	36.26	11.24	0.00	1.37	0.25	0.02	0.71	16.04	1.40	2.75	100	RCP	-
14	59.25	16.06	9.33	0.00	1.59	0.23	0.62	0.29	9.68	0.79	2.17	100	RCP	-
15	39.57	5.70	23.60	0.30	5.38	0.84	0.00	0.19	21.49	0.84	2.09	100	RCP	-
16	42.79	7.36	16.62	0.65	3.47	0.70	0.08	1.02	23.84	0.99	2.47	100	RCP	-
17	61.68	23.06	1.86	0.78	0.51	0.69	0.08	0.43	3.97	1.60	5.35	100	RCP	-
18	66.96	15.47	4.98	0.08	0.72	1.71	0.21	0.00	3.11	1.69	5.08	100	Paste	0.75
19	72.44	14.25	2.78	0.26	0.05	1.34	0.09	0.26	1.81	1.40	5.32	100	Paste	0.61
20	30.27	34.48	14.00	0.09	0.43	2.15	0.56	0.00	2.80	2.28	12.93	100	Paste+	3.69

Figure C27: Characteristic microstructure of a residual Portland cement particle (outline marked by dashed line) in the 1916 cement-lime mortar M3 showing euhedral alite anhedral spherical clusters of belite, and interstitial ferrite phase in the residual cement. Table shows compositions of residual cement phases, along with paste around the cement.

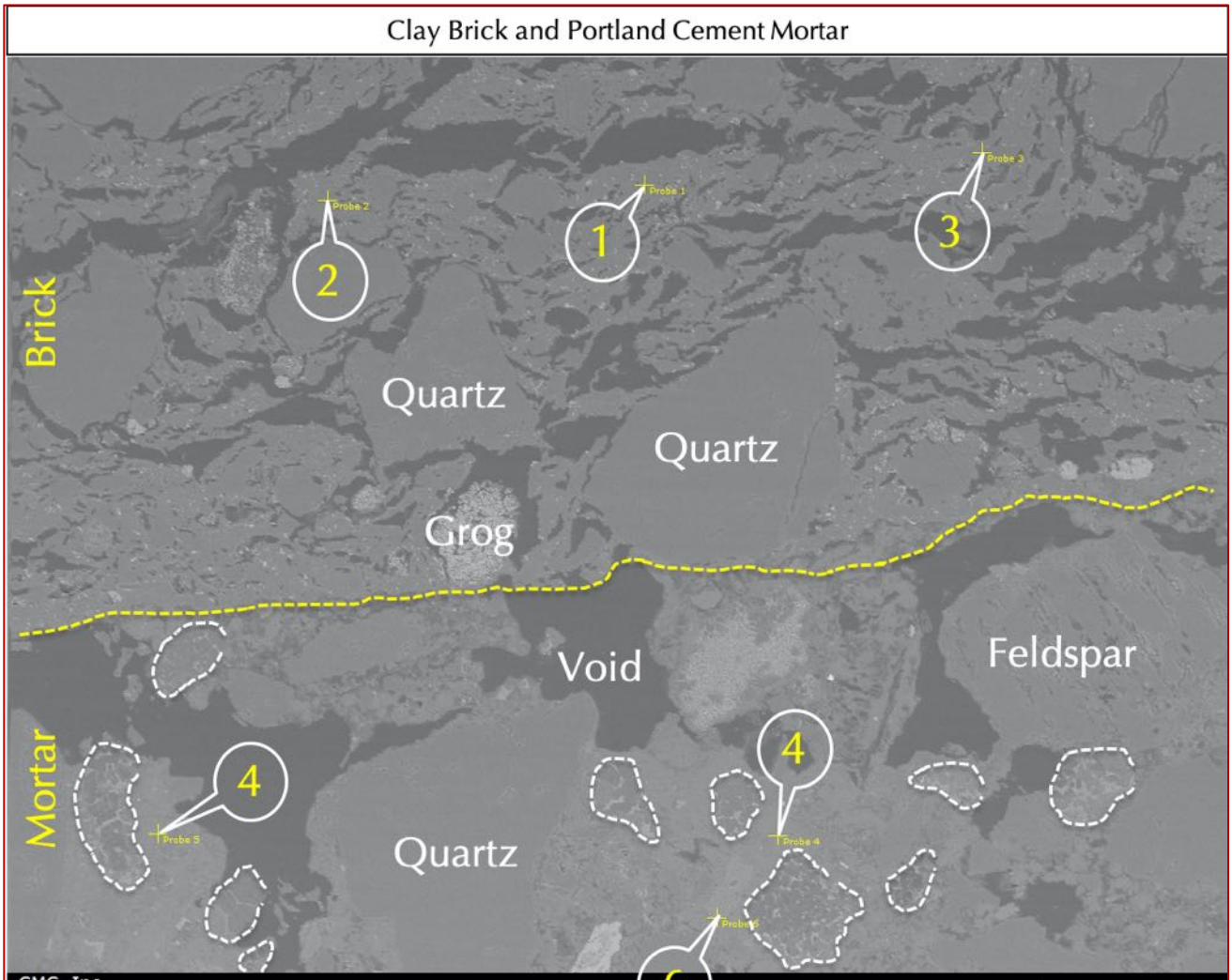

Probe	CaO	SiO2	Al2O3	Na2O	MgO	SO3	K2O	TiO2	FeO	P2O5	CO2	Total	Phase	Paste Cl
1	0.30	**62.61**	**22.18**	0.00	0.00	0.05	0.02	0.55	**5.78**	1.01	7.51	100	Brick	-
2	0.31	**57.87**	**25.44**	0.00	0.02	0.07	0.00	0.93	**8.92**	1.45	4.99	100	Brick	-
3	0.04	**93.37**	**0.47**	0.00	0.00	0.48	0.01	0.12	**0.71**	0.68	4.13	100	Brick	-
4	58.23	14.19	7.10	0.43	0.28	0.89	0.47	1.13	12.28	1.06	3.94	100	Paste	0.96
5	33.25	36.82	13.48	2.85	0.00	0.91	0.15	0.10	1.14	1.50	9.81	100	Paste+	3.57
6	60.49	16.24	8.94	0.00	0.00	1.42	0.77	0.68	7.08	0.90	3.46	100	Paste	1.00

Figure C28: Backscatter electron image (BSE), and X-ray elemental compositions at the tips of callouts shown in the backscatter electron image of paste in the 1916 cement-lime mortar M4. Outlines of a few residual Portland cement particles are shown by dashed lines in BSE image. Also shown is the adhered remains of clay brick on the mortar showing the typical aluminosilicate glassy matrix of brick as evidenced by high silica and alumina in the brick compositions highlighted in bold in the composition Table. Portland cement paste shows typical characteristic enrichment in calcium and subordinate silica from calcium-silicate-hydrate composition of cement-lime paste.

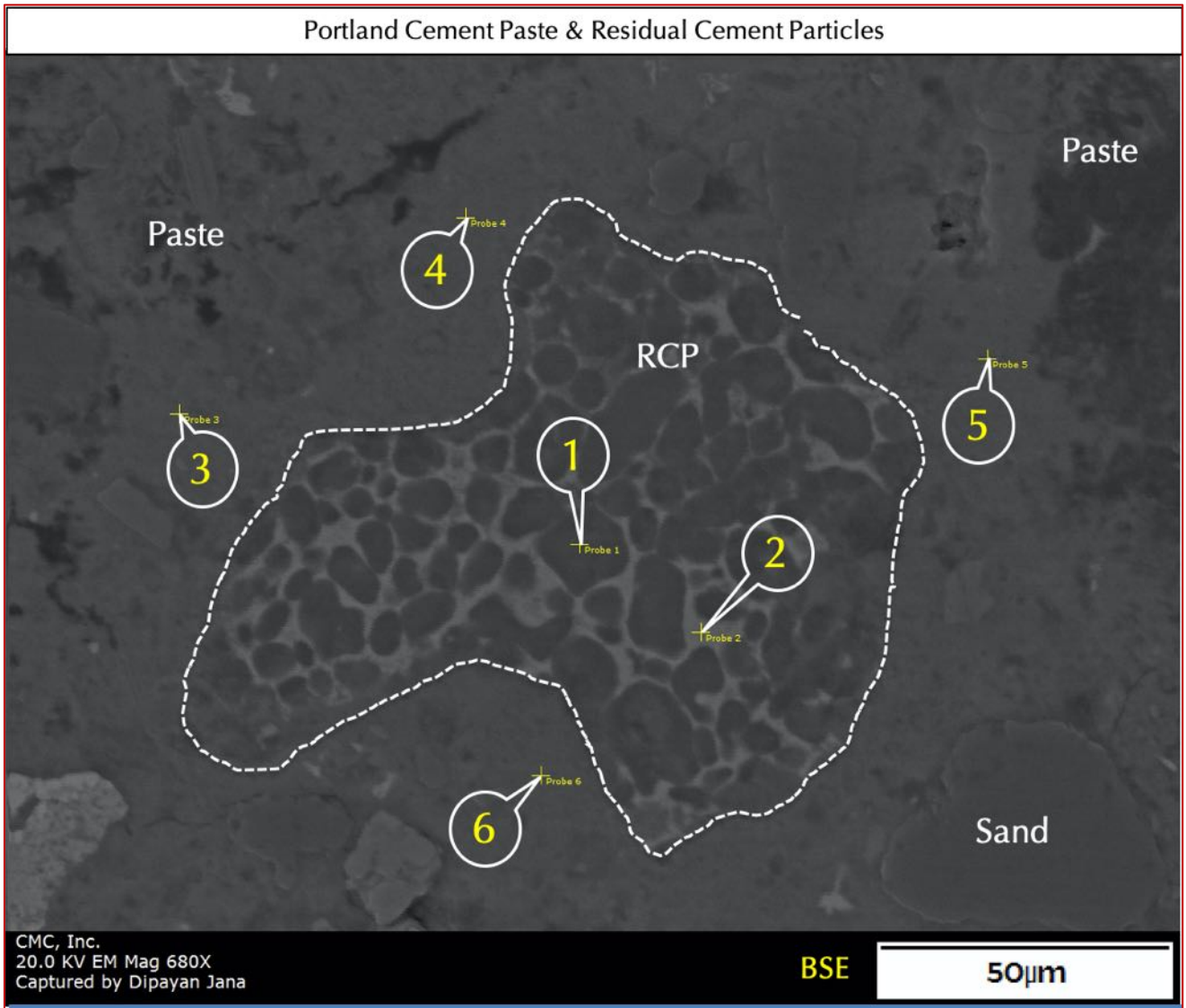

Probe	CaO	SiO2	Al2O3	Na2O	MgO	SO3	K2O	TiO2	FeO	P2O5	CO2	Total	Phase	Paste CI
1	4.64	74.72	2.78	0.33	0.64	0.40	0.56	0.32	2.75	0.93	11.92	100	RCP	-
2	15.61	45.52	13.48	0.12	1.49	1.11	0.32	0.55	11.59	0.27	9.95	100	RCP	-
3	**68.92**	**16.54**	3.08	0.08	0.46	1.58	0.22	0.29	1.60	0.79	6.43	100	Paste	0.73
4	**63.91**	**19.78**	3.47	0.24	0.34	1.91	0.51	0.00	3.15	0.92	5.77	100	Paste	0.95
5	**59.94**	**25.72**	3.01	0.06	0.26	2.52	0.60	0.06	2.00	0.64	5.17	100	Paste	1.27
6	**63.00**	**22.59**	2.66	0.14	0.19	1.96	0.55	0.10	2.42	0.25	6.15	100	Paste	1.07

Figure C29: Characteristic microstructure of a residual Portland cement particle (outline marked by dashed line) in the 1916 cement-lime mortar M4 showing euhedral alite, anhedral spherical clusters of belite, and interstitial ferrite phase in the residual cement. Table shows compositions of residual cement phases, along with paste around the cement.

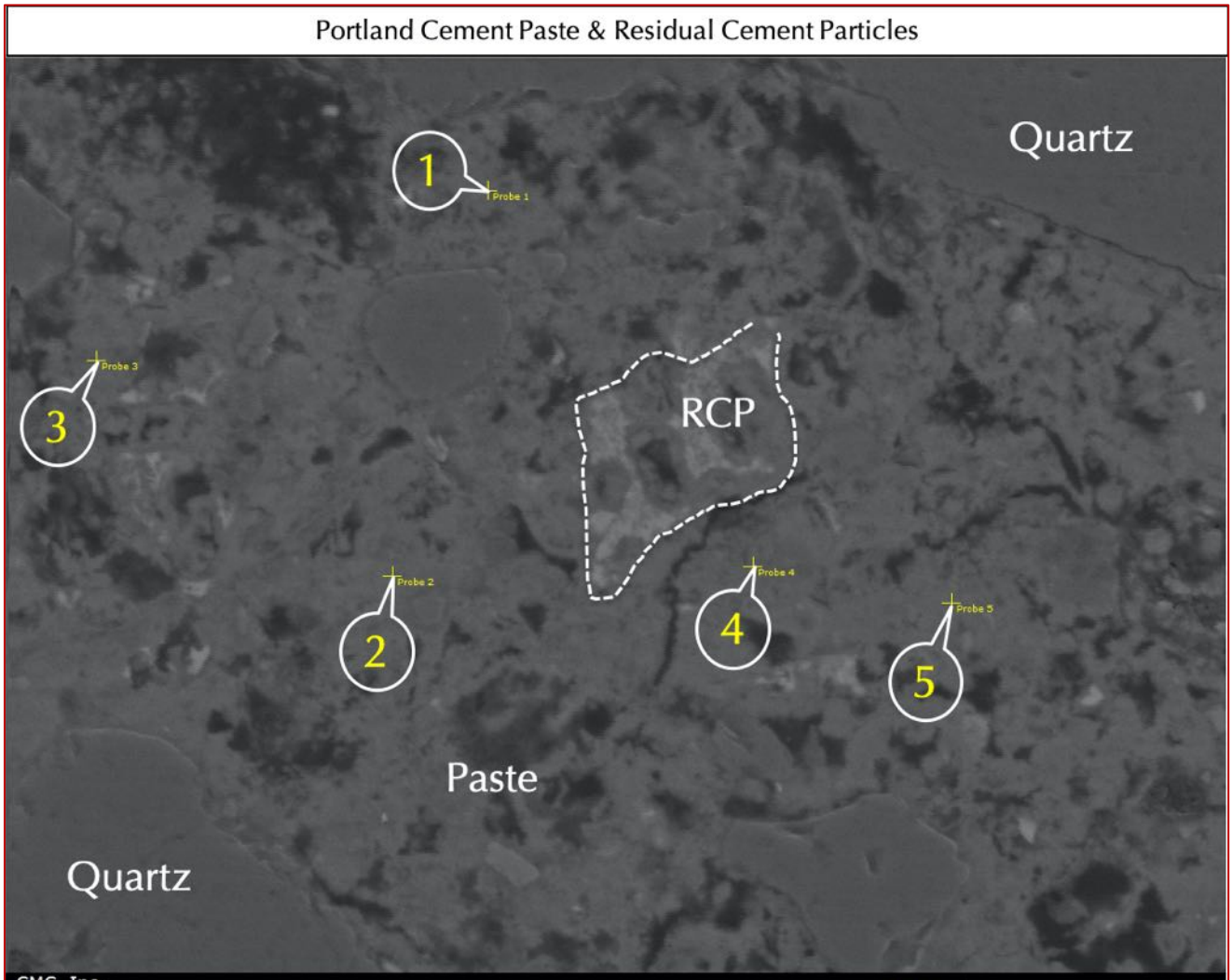

Probe	CaO	SiO2	Al2O3	Na2O	MgO	SO3	K2O	TiO2	FeO	P2O5	CO2	Total	Phase	Paste CI
1	74.68	11.55	1.86	0.02	0.00	1.51	0.57	0.00	1.28	0.43	8.10	100	Paste	0.47
2	66.63	18.00	2.99	0.06	0.05	1.41	0.92	0.03	2.26	0.25	7.40	100	Paste	0.83
3	66.43	20.52	1.93	0.05	0.02	1.60	0.91	0.00	1.26	0.17	7.11	100	Paste	0.91
4	37.20	34.91	6.38	0.35	0.00	1.54	0.53	0.00	0.97	0.45	17.67	100	Paste+	2.83
5	70.42	16.79	2.25	0.12	0.08	1.54	0.56	0.05	1.73	0.27	6.19	100	Paste	0.72

Figure C30: Backscatter electron image (BSE), and X-ray elemental compositions at the tips of callouts shown in the backscatter electron image of paste in the 1916 cement-lime mortar M4. Outline of a residual Portland cement particle is shown by dashed line. Portland cement paste shows typical characteristic enrichment in calcium and subordinate silica from calcium-silicate-hydrate composition of cement-lime paste.

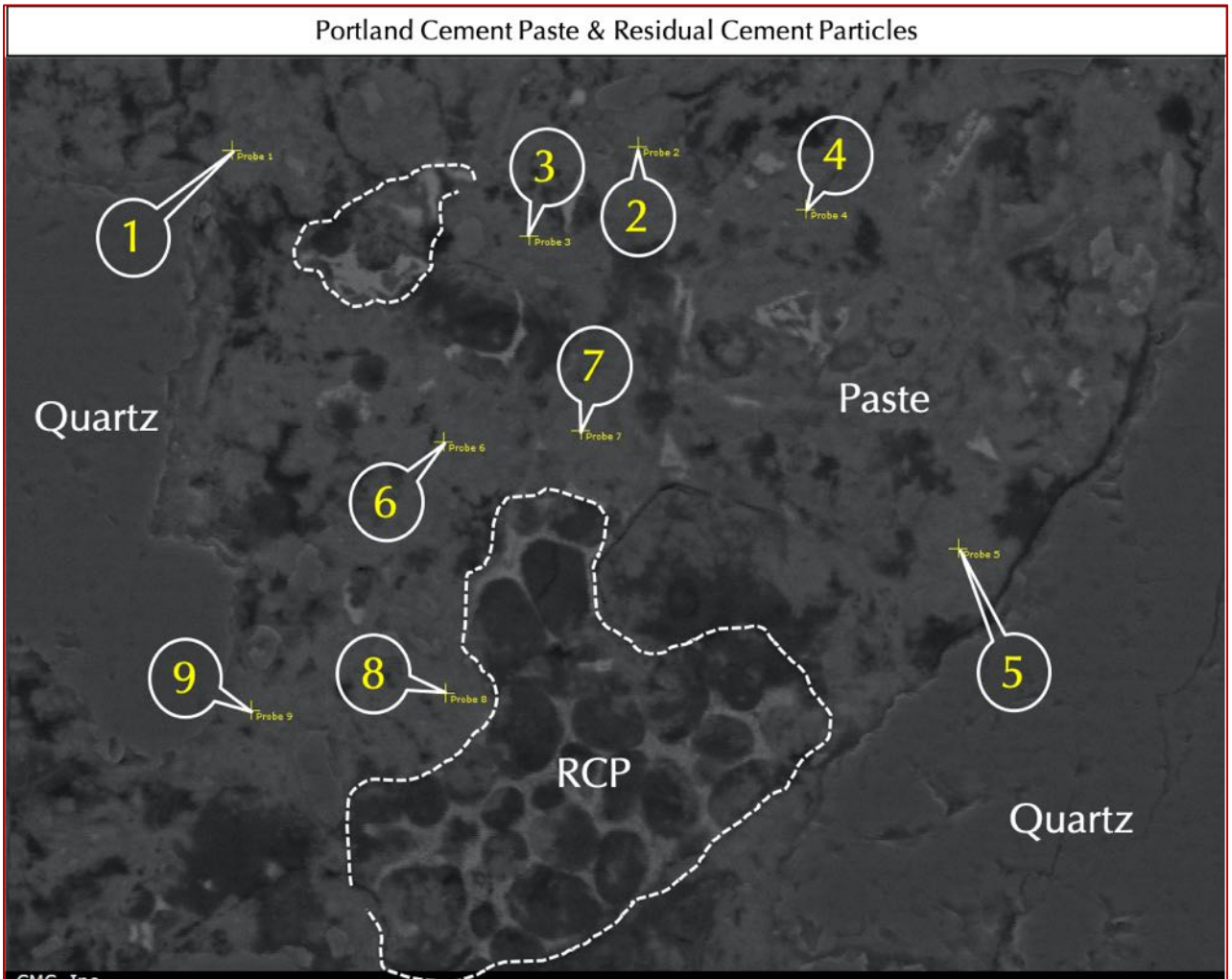

Probe	CaO	SiO2	Al2O3	Na2O	MgO	SO3	K2O	TiO2	FeO	P2O5	CO2	Total	Phase	Paste Cl
1	**65.51**	**20.93**	2.40	0.37	0.07	1.22	0.99	0.01	2.15	0.40	5.94	100	Paste	0.96
2	**68.92**	**14.46**	4.11	0.05	0.03	1.17	1.28	0.56	4.26	0.80	4.36	100	Paste	0.70
3	**68.89**	**16.92**	3.71	0.00	0.00	0.76	0.49	0.47	2.09	0.45	6.21	100	Paste	0.77
4	**48.36**	**26.93**	4.64	0.05	0.07	2.06	0.66	0.07	1.91	1.18	14.05	100	Paste	1.69
5	**38.69**	**26.93**	11.38	0.04	0.92	1.62	0.36	0.69	11.41	0.43	7.53	100	Paste	2.40
6	**75.00**	**12.34**	2.69	0.00	0.08	1.12	0.47	0.14	0.94	0.20	7.03	100	Paste	0.51
7	**68.62**	**16.64**	3.46	0.20	0.08	1.09	0.85	0.00	2.71	0.18	6.17	100	Paste	0.76
8	**62.12**	**21.05**	5.72	0.03	0.08	0.44	0.93	0.00	3.45	0.48	5.69	100	Paste	1.09
9	**63.20**	**20.79**	4.49	0.19	0.00	1.23	1.08	0.33	2.30	0.81	5.58	100	Paste	1.02

Figure C31: Characteristic microstructure of residual Portland cement particles (outlines marked by dashed line) in the 1916 cement-lime mortar M4 showing anhedral spherical clusters of belite, and interstitial ferrite phase in the residual cement. Table shows compositions of with paste around the residual cement particles.

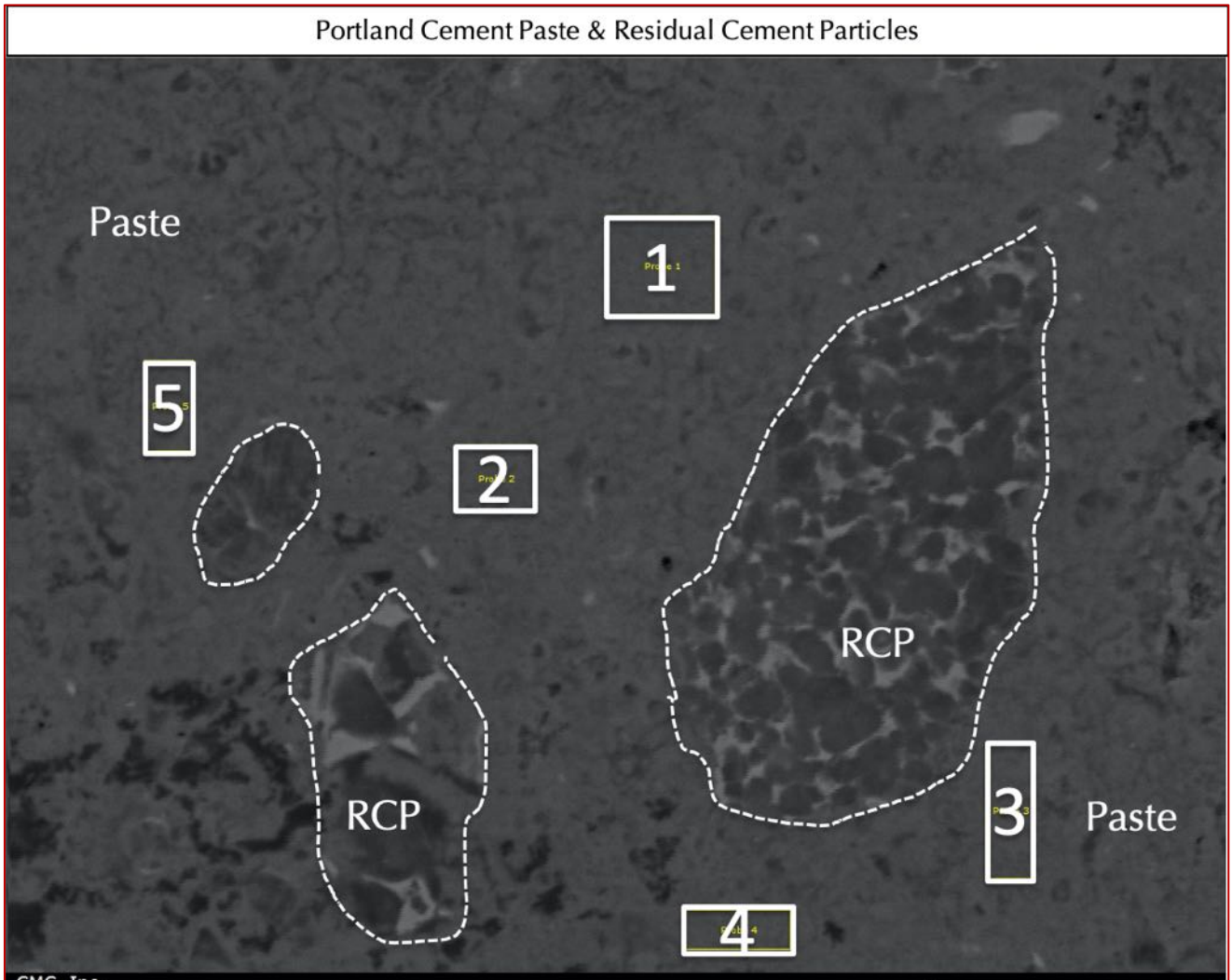

Probe	CaO	SiO2	Al2O3	Na2O	MgO	SO3	K2O	TiO2	FeO	P2O5	CO2	Total	Phase	Paste CI
1	**57.83**	**18.21**	2.16	0.10	0.33	2.53	0.45	0.05	1.08	0.26	16.98	100	Paste	0.93
2	**54.04**	**17.04**	4.01	0.10	0.80	2.16	0.41	0.00	1.86	0.51	19.08	100	Paste	0.97
3	**55.56**	**17.08**	3.15	0.02	0.51	2.06	0.36	0.16	3.01	0.42	17.67	100	Paste	0.95
4	**56.89**	**17.64**	3.34	0.08	0.03	2.38	0.00	0.17	1.91	0.21	17.34	100	Paste	0.96
5	**50.94**	**18.91**	4.79	0.37	0.72	2.04	0.40	0.10	4.50	0.25	16.98	100	Paste	1.18

Figure C32: Characteristic microstructure of residual Portland cement particles (outlines marked by dashed line) in the 1916 cement-lime mortar M4 showing anhedral spherical clusters of belite, and interstitial ferrite phase in the residual cement. Table shows compositions of with paste around the residual cement particles.

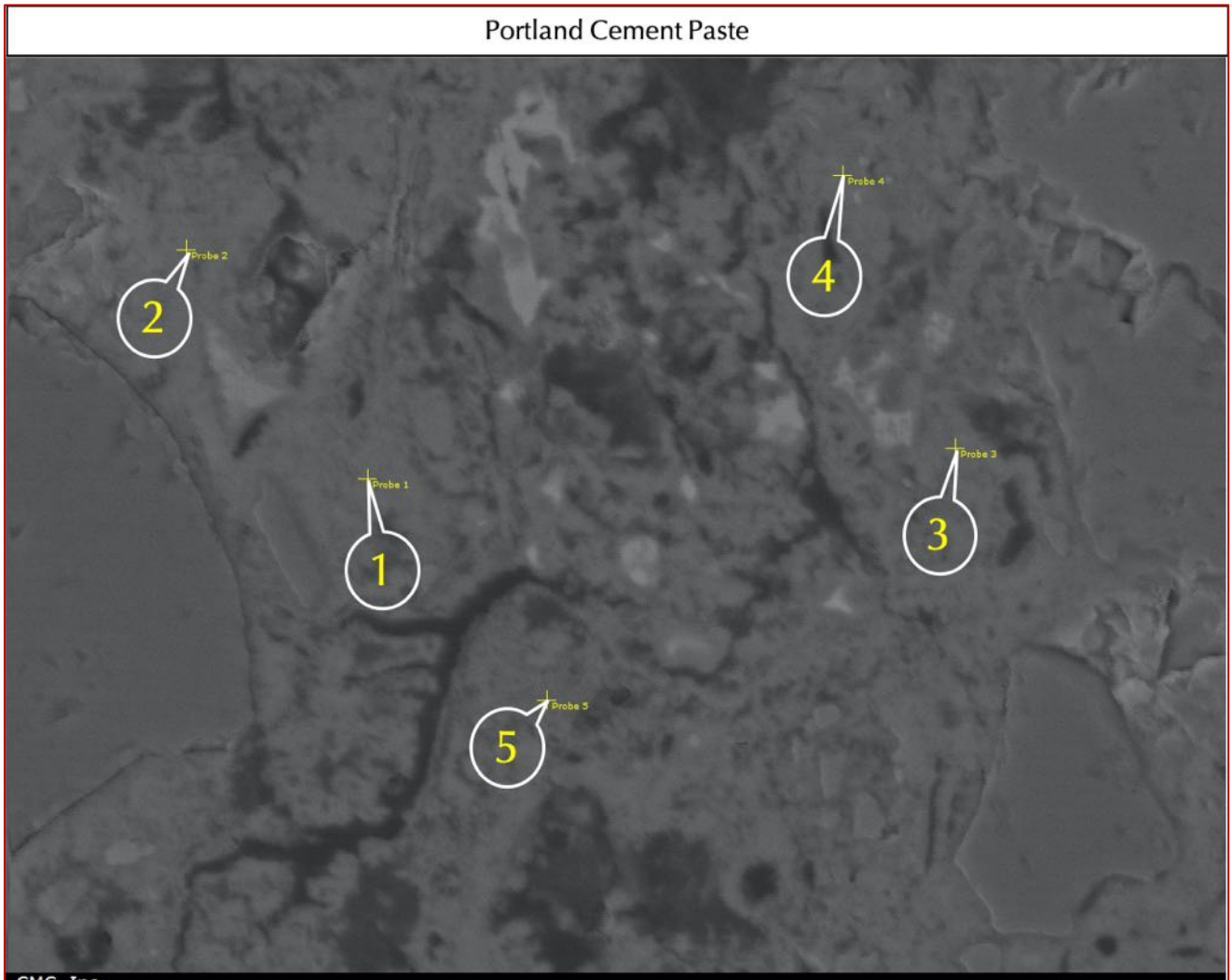

Probe	CaO	SiO2	Al2O3	Na2O	MgO	SO3	K2O	TiO2	FeO	P2O5	CO2	Total	Phase	Paste CI
1	**75.34**	**10.57**	2.67	0.00	0.62	1.75	0.26	0.34	1.39	0.17	6.89	100	Paste	0.44
2	**71.26**	**15.50**	2.19	0.00	0.09	1.63	0.49	0.00	2.07	0.36	6.43	100	Paste	0.66
3	**70.14**	**15.82**	3.08	0.07	0.04	1.32	0.43	0.00	1.60	0.17	7.33	100	Paste	0.70
4	**72.76**	**12.90**	1.85	0.14	0.00	1.25	0.34	0.30	4.34	0.51	5.60	100	Paste	0.57
5	**51.07**	**22.21**	3.97	0.00	0.02	1.72	0.23	0.11	1.72	0.63	18.33	100	Paste	1.33

Figure C33:Backscatter electron image (BSE), and X-ray elemental compositions at the tips of callouts shown in the backscatter electron image of paste in the 1916 cement-lime mortar M4. Portland cement paste shows typical characteristic enrichment in calcium and subordinate silica from calcium-silicate-hydrate composition of cement-lime paste.

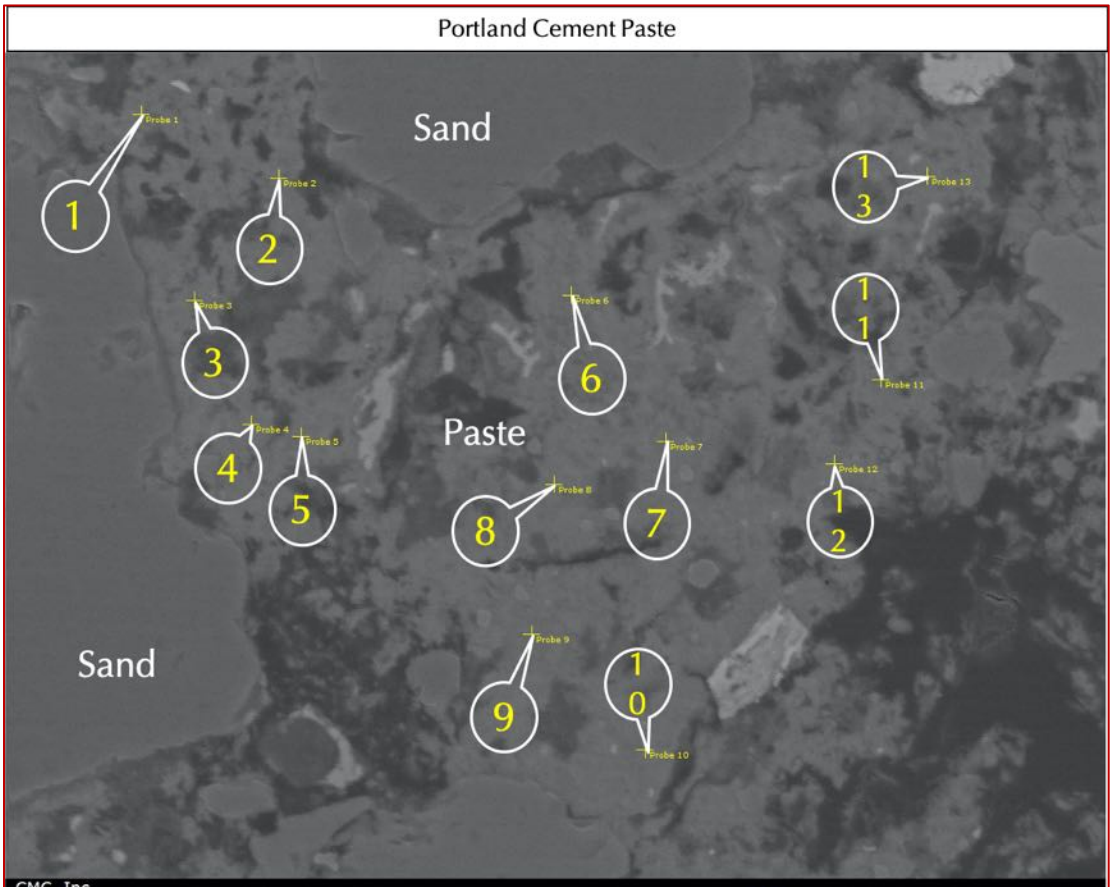

Probe	CaO	SiO2	Al2O3	Na2O	MgO	SO3	K2O	TiO2	FeO	P2O5	CO2	Total	Phase	Paste Cl
1	**74.78**	**10.21**	2.62	0.01	0.07	1.85	0.08	0.27	2.41	0.41	7.29	100	Paste	0.54
2	**68.57**	**17.13**	2.77	0.09	0.00	1.65	0.69	0.21	1.98	0.86	6.06	100	Paste	0.76
3	**74.33**	**13.39**	1.62	0.04	0.00	2.03	0.21	0.02	1.73	0.86	5.77	100	Paste	0.54
4	**72.61**	**14.66**	3.48	0.00	0.10	1.70	0.00	0.25	1.62	0.89	4.69	100	Paste	0.77
5	48.14	37.04	1.88	0.12	0.00	1.62	0.49	0.84	1.31	1.45	7.11	100	Paste+	2.22
6	59.09	20.03	4.19	0.18	1.09	1.99	0.92	0.21	6.94	1.10	4.25	100	Paste+	2.64
7	63.84	17.96	5.95	0.10	0.67	1.79	0.97	0.25	2.17	1.08	5.22	100	Paste+	1.85
8	**68.63**	**18.32**	2.33	0.19	0.00	1.27	0.88	0.03	2.03	0.60	5.73	100	Paste	0.81
9	**64.70**	**20.08**	3.79	0.26	0.04	1.84	0.82	0.20	1.80	1.05	5.41	100	Paste	1.01
10	**64.85**	**18.46**	3.40	0.52	0.09	1.51	0.89	0.45	3.25	1.24	5.34	100	Paste	1.02
11	40.64	30.40	7.50	0.08	0.34	2.14	0.62	0.49	4.45	1.64	11.70	100	Paste+	2.85
12	23.70	36.00	17.49	0.00	0.36	1.36	1.46	0.57	9.29	1.60	8.18	100	Paste+	5.84
13	68.07	10.22	5.17	0.65	1.13	1.86	0.06	0.48	7.51	0.89	3.94	100	Paste+	2.16

Figure C34: Backscatter electron image (BSE), and X-ray elemental compositions at the tips of callouts shown in the backscatter electron image of paste in the 1916 cement-lime mortar M4. Portland cement paste shows typical characteristic enrichment in calcium and subordinate silica from calcium-silicate-hydrate composition of cement-lime paste.

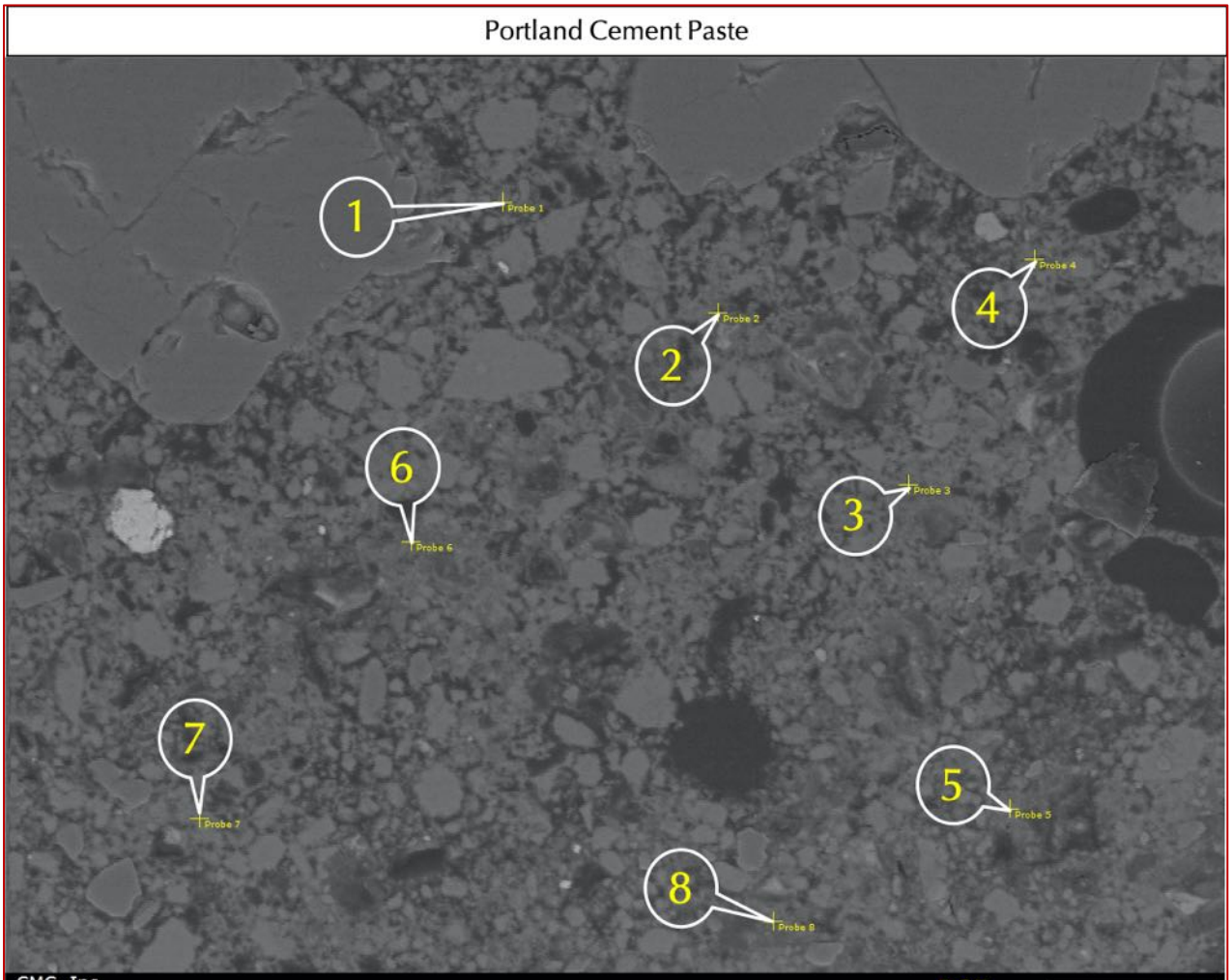

Probe	CaO	SiO2	Al2O3	Na2O	MgO	SO3	K2O	TiO2	FeO	P2O5	CO2	Total	Phase	Paste Cl
1	64.31	9.20	3.11	0.07	8.94	0.85	0.06	0.00	1.49	0.83	11.15	100	Paste	0.39
2	40.93	16.06	6.94	0.07	1.26	1.57	0.20	0.00	1.23	0.83	30.90	100	Paste	1.25
3	66.85	10.64	4.97	0.34	1.43	1.60	0.05	0.00	1.18	0.32	12.62	100	Paste	0.52
4	47.39	14.38	4.72	0.00	0.25	1.16	0.09	0.09	1.72	0.94	29.26	100	Paste	0.98
5	18.25	5.91	1.13	0.04	0.48	1.10	0.34	0.00	0.82	0.50	71.42	100	Paste	0.97
6	63.19	10.98	5.41	0.00	0.88	1.38	0.94	0.12	1.35	0.17	15.57	100	Paste	0.58
7	23.84	31.28	7.92	0.00	0.20	1.22	6.31	0.22	0.67	0.79	27.55	100	Paste+	4.01
8	71.33	8.00	2.39	0.21	0.53	0.50	0.08	0.15	1.19	0.24	15.38	100	Paste	0.36

Figure C35: Backscatter electron image (BSE) and X-ray elemental compositions at the tips of callouts shown in the backscatter electron image of paste in the late 1960s masonry cement mortar M5. Paste shows a granular appearance due to the presence of lime and limestone fine particles. Paste compositions show enrichment in calcium and subordinate silica from carbonated lime and calcium-silicate-hydrate composition of masonry cement paste. High carbon content is a testament of high lime, and limestone fine content of cement.

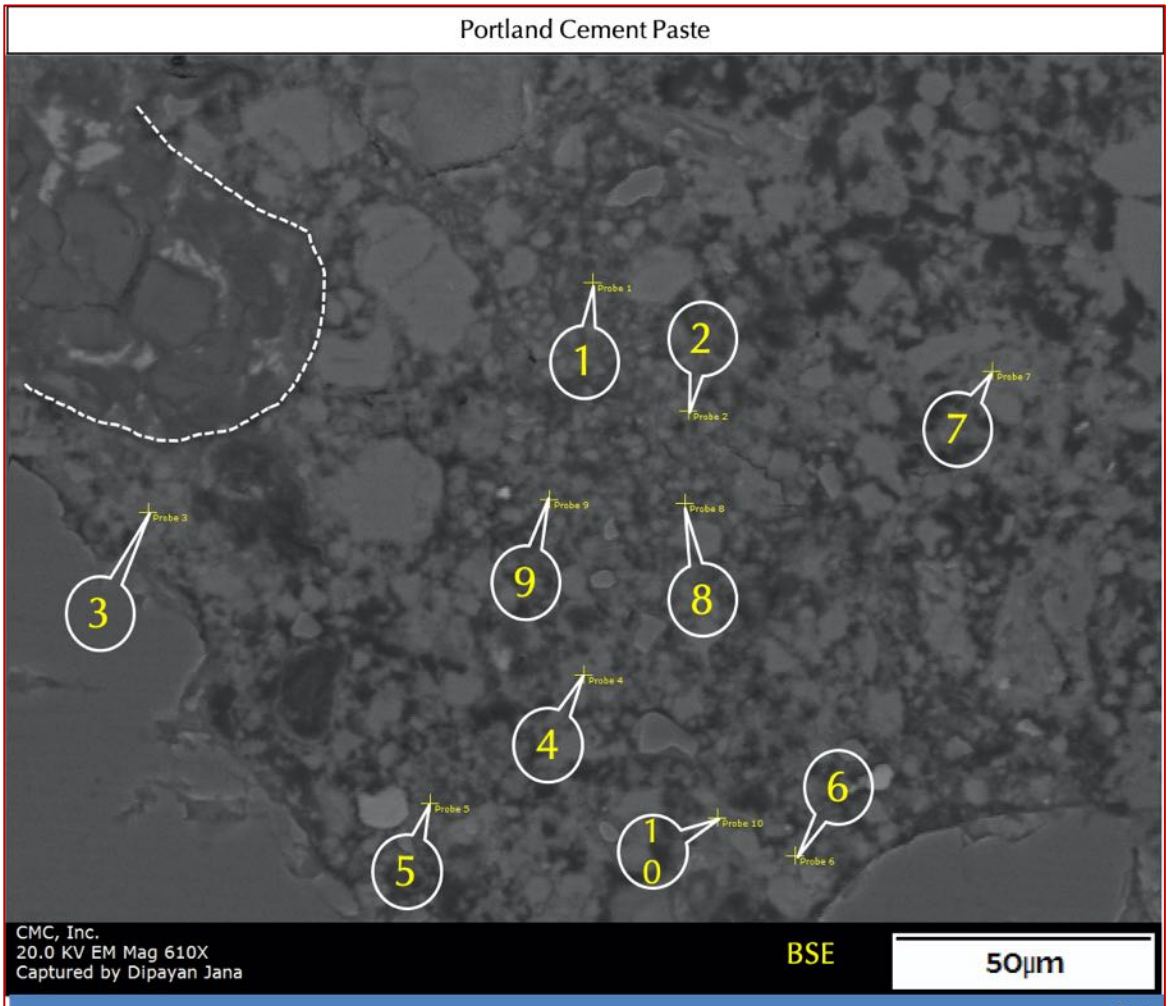

Probe	CaO	SiO2	Al2O3	Na2O	MgO	SO3	K2O	TiO2	FeO	P2O5	CO2	Total	Phase	Paste Cl
1	39.07	14.93	6.78	0.65	0.36	1.75	0.21	0.00	2.94	0.58	32.72	100	Paste	1.30
2	57.03	13.95	5.89	0.29	1.23	1.66	1.45	0.10	1.56	0.59	16.24	100	Paste	0.79
3	50.79	15.12	5.23	0.30	2.19	2.32	0.13	0.02	1.16	0.59	22.15	100	Paste	0.91
4	64.94	10.36	2.88	0.13	0.35	1.73	0.54	7.55	3.13	0.20	8.18	100	Paste	0.53
5	58.38	10.66	4.12	0.09	0.79	1.16	0.21	0.47	2.47	0.27	21.40	100	Paste	0.61
6	60.99	13.08	5.32	0.62	1.70	1.21	0.88	0.12	1.55	0.21	14.33	100	Paste	0.69
7	76.76	7.73	2.00	0.35	0.55	1.90	0.34	0.01	0.19	0.44	9.73	100	Paste	0.31
8	34.52	15.05	5.30	0.50	0.36	2.13	0.00	0.05	1.10	0.84	40.14	100	Paste	1.39
9	70.91	6.70	1.43	0.51	0.28	2.04	0.58	0.21	0.37	0.95	16.02	100	Paste	0.29
10	70.74	10.60	3.31	0.08	0.90	2.05	0.78	0.02	0.69	0.19	10.65	100	Paste	0.47

Figure C36: Backscatter electron image (BSE) and X-ray elemental compositions at the tips of callouts shown in the backscatter electron image of paste in the late 1960s masonry cement mortar M5. Paste shows a granular appearance due to the presence of lime and limestone fine particles. Paste compositions show enrichment in calcium and subordinate silica from carbonated lime and calcium-silicate-hydrate composition of masonry cement paste. A residual Portland cement particle is marked by dashed line at the top left corner. High carbon content is a testament of high lime, and limestone fine content of cement.

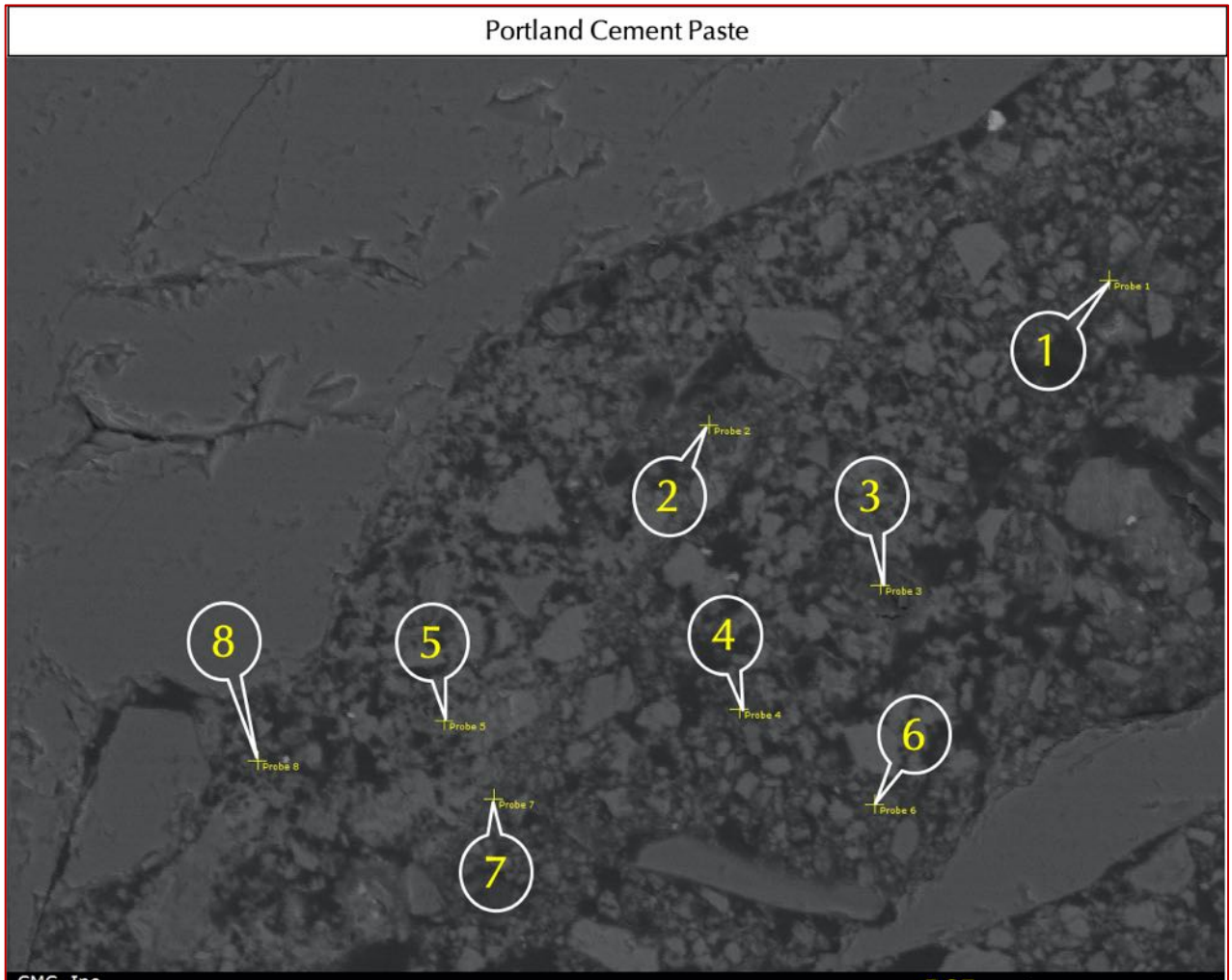

Probe	CaO	SiO2	Al2O3	Na2O	MgO	SO3	K2O	TiO2	FeO	P2O5	CO2	Total	Phase	Paste Cl
1	23.52	8.58	4.55	0.38	0.65	1.02	0.05	0.00	0.78	0.10	60.37	100	Paste	1.21
2	23.10	17.23	6.81	0.67	1.51	1.32	0.25	0.35	0.81	0.40	47.54	100	Paste+	2.23
3	28.28	10.23	3.79	0.07	0.87	1.28	0.07	0.08	0.82	0.13	54.40	100	Paste	1.13
4	24.38	16.66	2.94	0.00	0.64	1.44	0.16	0.35	1.30	0.16	51.98	100	Paste+	2.01
5	21.54	30.94	13.73	0.06	0.78	0.47	3.74	0.09	1.58	0.59	26.49	100	Paste+	4.54
6	21.93	23.15	9.41	0.49	4.38	1.27	0.21	0.77	10.17	0.25	27.97	100	Paste+	2.93
7	61.61	10.68	1.39	0.00	0.04	0.17	0.19	0.00	0.53	0.04	25.34	100	Paste	0.52
8	28.46	12.52	4.75	0.60	0.67	0.36	0.07	0.27	0.31	0.09	51.90	100	Paste	1.38

Figure C37: Backscatter electron image (BSE) and X-ray elemental compositions at the tips of callouts shown in the backscatter electron image of paste in the late 1960s masonry cement mortar M5. Paste shows a granular appearance due to the presence of lime and limestone fine particles. Paste compositions show enrichment in calcium and subordinate silica from carbonated lime and calcium-silicate-hydrate composition of masonry cement paste. High carbon content is a testament of high lime, and limestone fine content of cement.

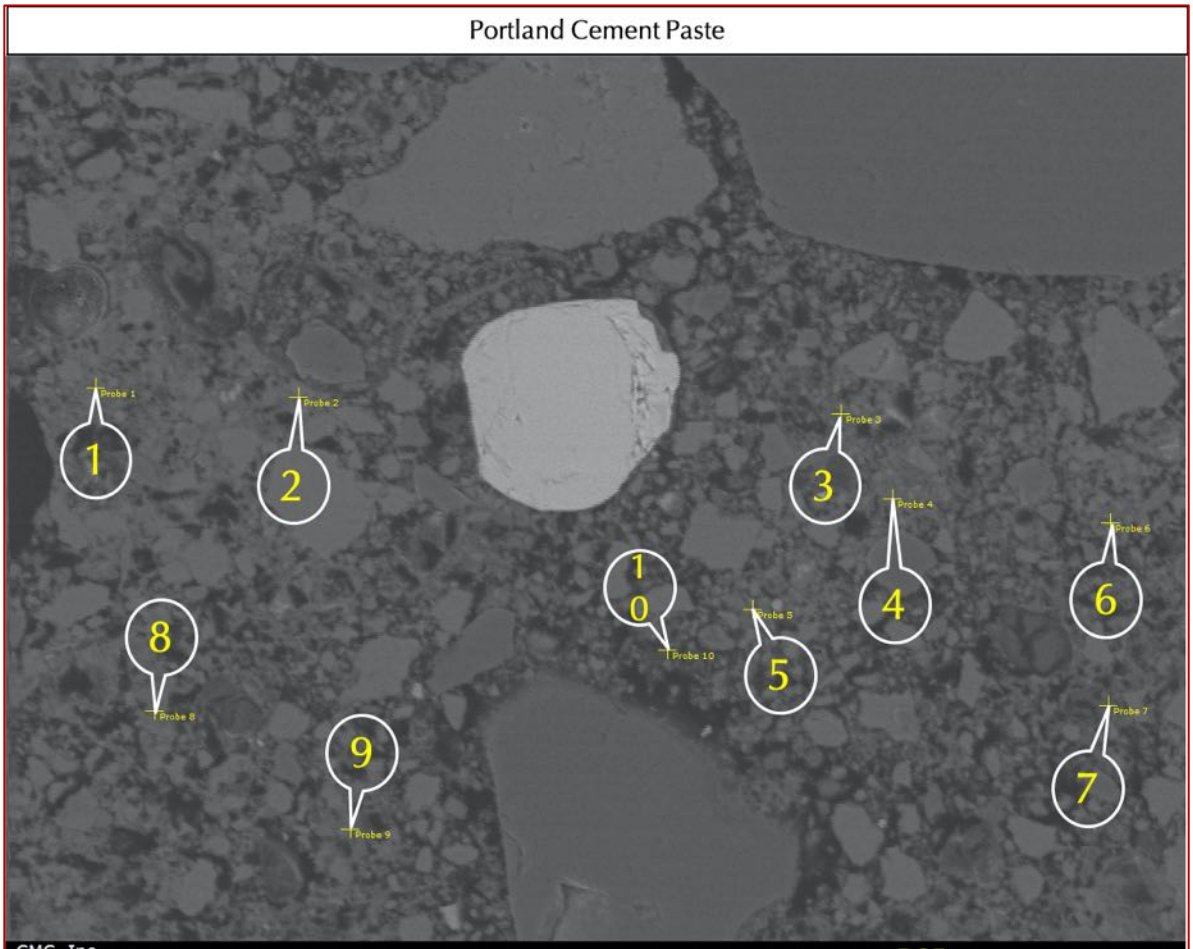

Probe	CaO	SiO2	Al2O3	Na2O	MgO	SO3	K2O	TiO2	FeO	P2O5	CO2	Total	Phase	Paste Cl
1	65.06	14.09	2.57	0.00	0.69	0.91	0.55	0.14	1.20	0.81	13.97	100	Paste	0.65
2	77.41	7.52	1.40	0.00	2.80	0.88	0.23	0.08	0.23	0.85	8.61	100	Paste	0.28
3	72.13	10.84	2.51	0.03	0.17	0.85	1.04	0.12	0.98	0.75	10.58	100	Paste	0.47
4	37.01	23.11	7.80	0.16	1.71	2.02	0.53	0.08	6.18	0.99	20.41	100	Paste+	1.97
5	63.19	19.17	3.73	0.13	0.49	0.71	0.22	0.00	0.35	0.53	11.47	100	Paste	0.91
6	20.05	45.76	1.87	0.00	0.10	0.71	0.17	0.08	0.78	0.97	29.51	100	Paste+	6.48
7	27.12	27.80	11.87	0.01	0.92	0.61	2.18	0.01	1.24	1.19	27.05	100	Paste+	3.23
8	65.40	10.18	3.04	0.14	2.08	1.26	0.38	0.07	1.37	0.25	15.82	100	Paste	0.48
9	94.86	0.04	0.00	0.00	0.38	0.07	0.08	0.09	0.00	0.41	4.06	100	Paste	0.00
10	50.07	8.02	2.57	0.00	0.05	0.81	0.06	0.11	1.08	0.84	36.40	100	Paste	0.52

Figure C38: Backscatter electron image (BSE) and X-ray elemental compositions at the tips of callouts shown in the backscatter electron image of paste in the late 1960s masonry cement mortar M5. Paste shows a granular appearance due to the presence of lime and limestone fine particles. Paste compositions show enrichment in calcium and subordinate silica from carbonated lime and calcium-silicate-hydrate composition of masonry cement paste. High carbon content is a testament of high lime, and limestone fine content of cement.

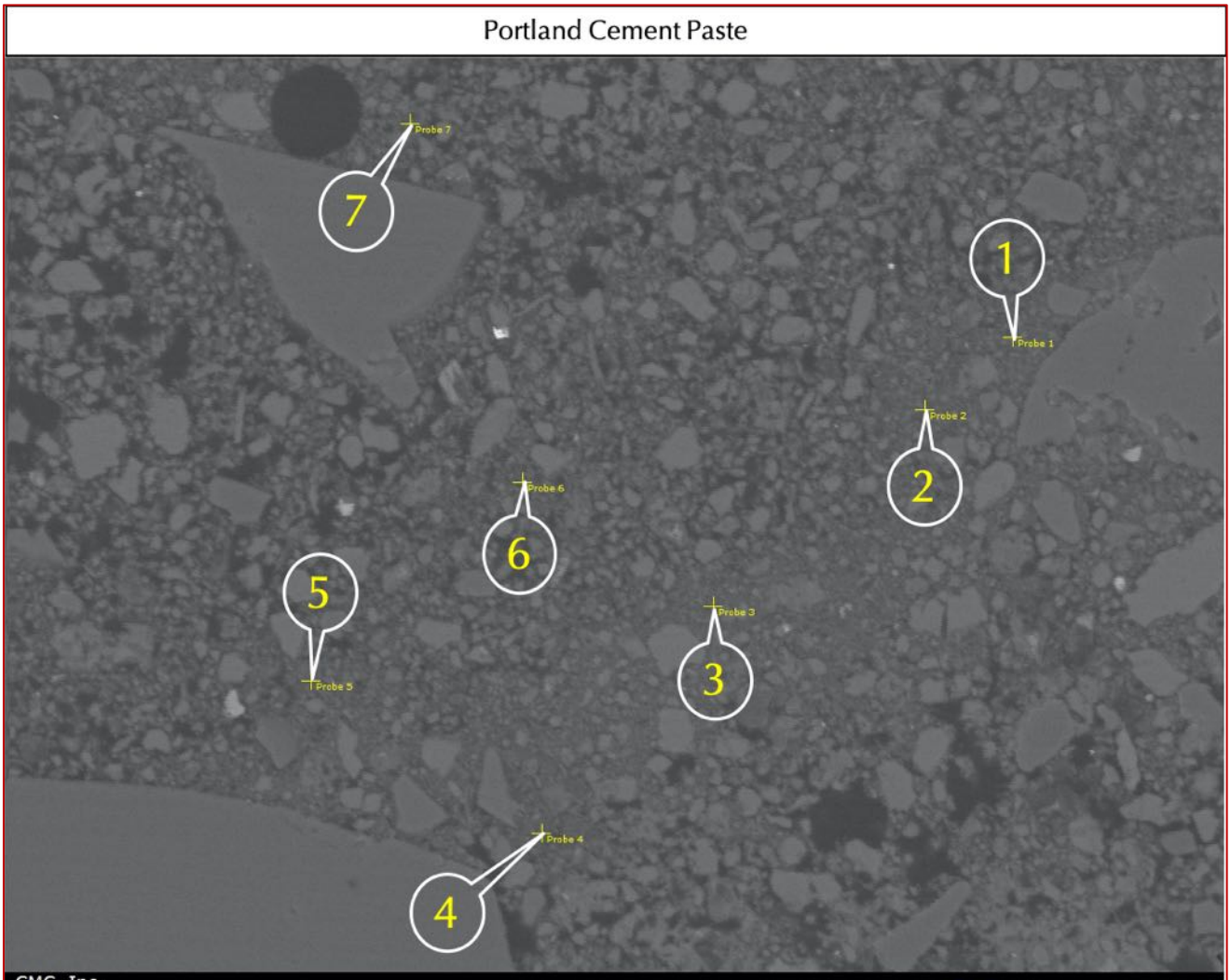

Probe	CaO	SiO2	Al2O3	Na2O	MgO	SO3	K2O	TiO2	FeO	P2O5	CO2	Total	Phase	Paste Cl
1	30.91	24.01	2.73	0.11	0.28	1.38	0.23	2.49	3.08	0.30	34.49	100	Paste+	2.31
2	31.09	16.47	3.61	0.08	1.76	1.49	0.17	0.07	0.87	0.57	43.82	100	Paste	1.51
3	56.85	14.64	4.64	0.23	0.88	1.33	0.53	0.17	1.41	0.81	18.52	100	Paste	0.81
4	55.35	12.10	2.82	0.00	1.25	1.42	0.43	0.00	1.86	1.12	23.64	100	Paste	0.67
5	55.02	14.10	4.39	0.73	1.14	0.40	0.39	0.00	1.83	0.88	21.11	100	Paste	0.81
6	33.94	17.37	9.09	0.09	0.47	0.19	0.60	0.46	1.57	0.71	35.52	100	Paste+	1.73
7	53.88	15.07	4.89	0.00	1.51	0.67	0.09	0.21	2.08	0.34	21.26	100	Paste	0.88

Figure C39: Backscatter electron image (BSE) and X-ray elemental compositions at the tips of callouts shown in the backscatter electron image of paste in the late 1960s masonry cement mortar M5. Paste shows a granular appearance due to the presence of lime and limestone fine particles. Paste compositions show enrichment in calcium and subordinate silica from carbonated lime and calcium-silicate-hydrate composition of masonry cement paste. High carbon content is a testament of high lime, and limestone fine content of cement.

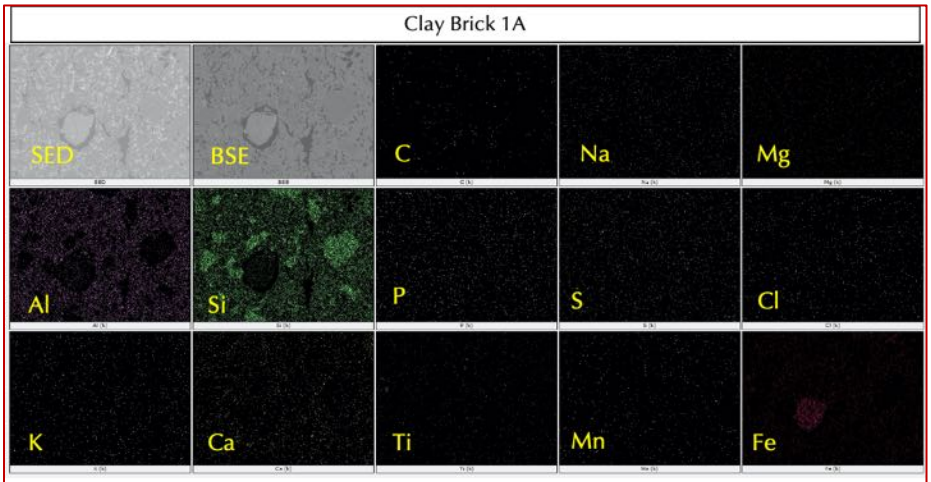

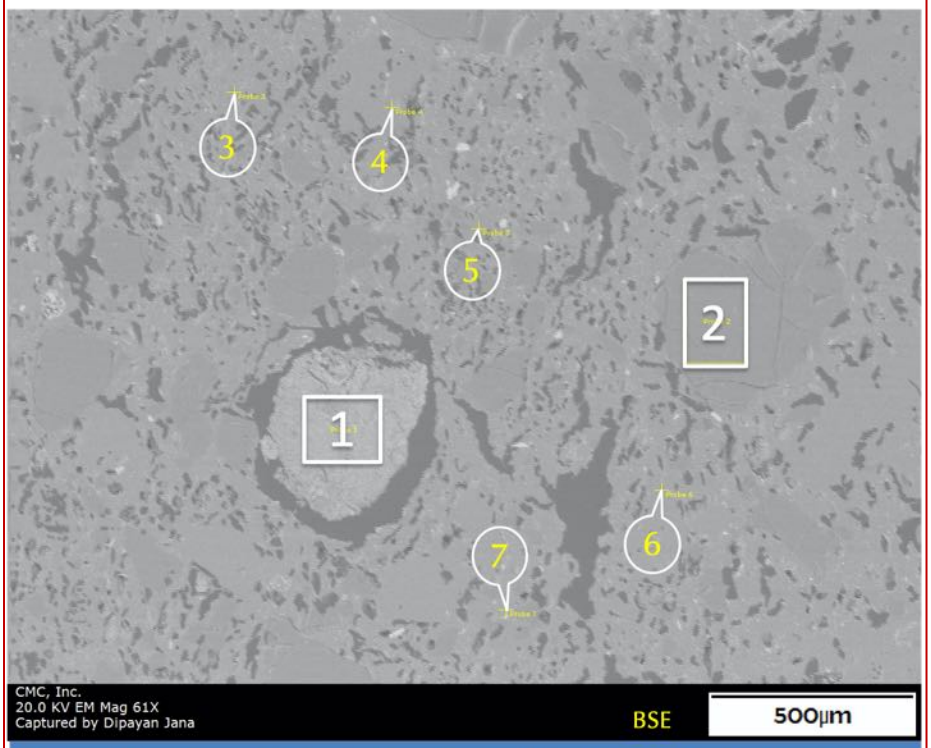

Probe	CaO	SiO2	Al2O3	Na2O	MgO	SO3	K2O	TiO2	FeO	P2O5	CO2	Total
1	0.08	19.35	11.40	0.18	0.00	0.21	0.00	0.00	45.62	0.20	22.97	100.01
2	0.00	94.35	0.36	0.00	0.00	0.04	0.02	0.06	0.06	0.27	4.85	100.01
3	0.33	79.69	9.75	0.17	0.01	0.02	0.04	0.13	5.51	0.35	3.99	99.99
4	0.38	86.99	4.47	0.64	0.02	0.02	0.02	0.13	0.36	0.60	6.36	99.99
5	1.36	52.87	34.89	0.72	0.46	0.03	0.13	0.35	4.88	0.93	3.39	100.01
6	1.61	61.70	26.40	1.36	0.34	0.00	0.46	0.36	4.07	0.07	3.62	99.99
7	2.62	67.87	19.14	1.86	0.30	0.10	0.30	0.61	2.25	0.27	4.69	100.01

Figure C40: X-ray elemental maps (top), backscatter electron image (BSE, middle), and X-ray elemental compositions at the boxes and tips of callouts shown in the backscatter electron image of fired clay brick 1A from 1950s vintage showing typical aluminosilicate composition of glassy matrix of brick as seen in silica and alumina contents.

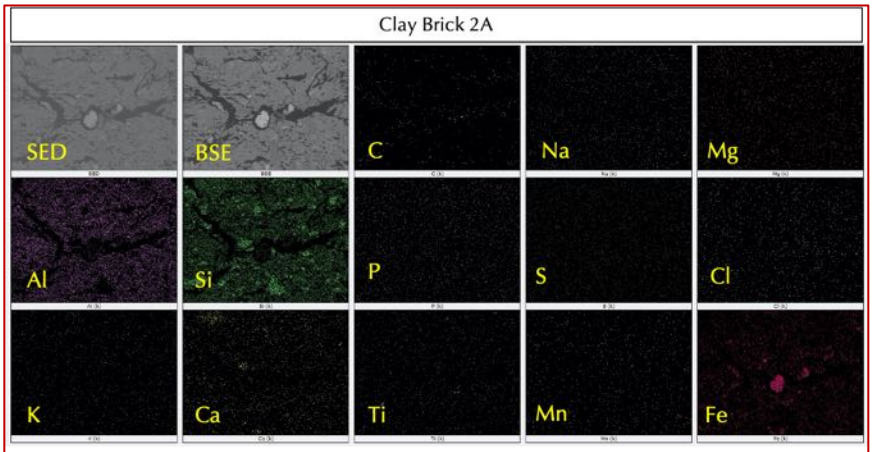

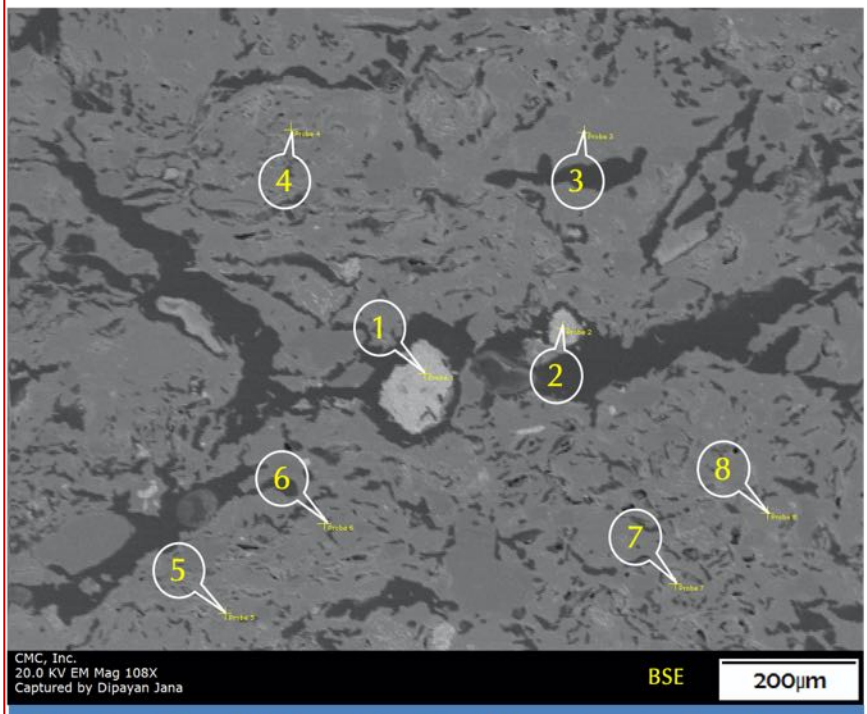

Probe	CaO	SiO2	Al2O3	Na2O	MgO	SO3	K2O	TiO2	FeO	P2O5	CO2	Total
1	0.03	16.90	11.11	0.50	0.00	0.01	0.00	0.35	68.06	0.77	2.26	100.01
2	0.04	16.19	12.37	0.86	0.00	0.00	0.00	0.57	66.85	0.48	2.63	100.01
3	1.27	59.04	26.81	1.33	0.22	0.10	0.23	0.51	4.23	1.02	5.23	100.01
4	0.79	53.89	32.15	1.16	0.40	0.13	0.04	0.61	4.53	1.42	4.87	100.01
5	1.19	59.41	26.51	1.02	0.48	0.08	0.06	0.44	4.97	1.19	4.66	100.01
6	0.63	47.37	35.49	0.69	0.23	0.19	0.09	0.21	5.53	0.96	8.61	100.01
7	0.79	50.49	36.38	1.10	0.38	0.11	0.23	0.50	5.21	0.99	3.83	100.01
8	1.25	60.97	22.69	1.49	0.32	0.02	0.26	0.38	6.89	0.89	4.83	100.01

Figure C41: X-ray elemental maps (top), backscatter electron image (BSE, middle), and X-ray elemental compositions at the boxes and tips of callouts shown in the backscatter electron image of fired clay brick 2A from 1950s vintage showing typical aluminosilicate composition of glassy matrix of brick as seen in silica and alumina contents. Probe #1 and 2 are from two iron oxide grains in the brick that are responsible for imparting the typical reddish-brown color tone of brick.

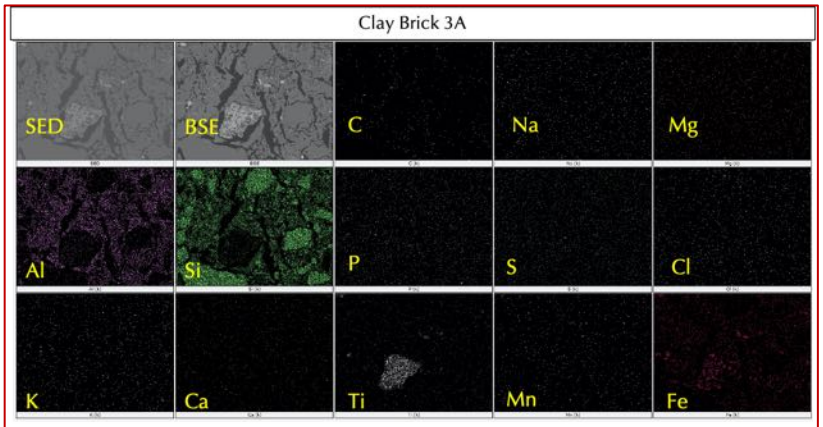

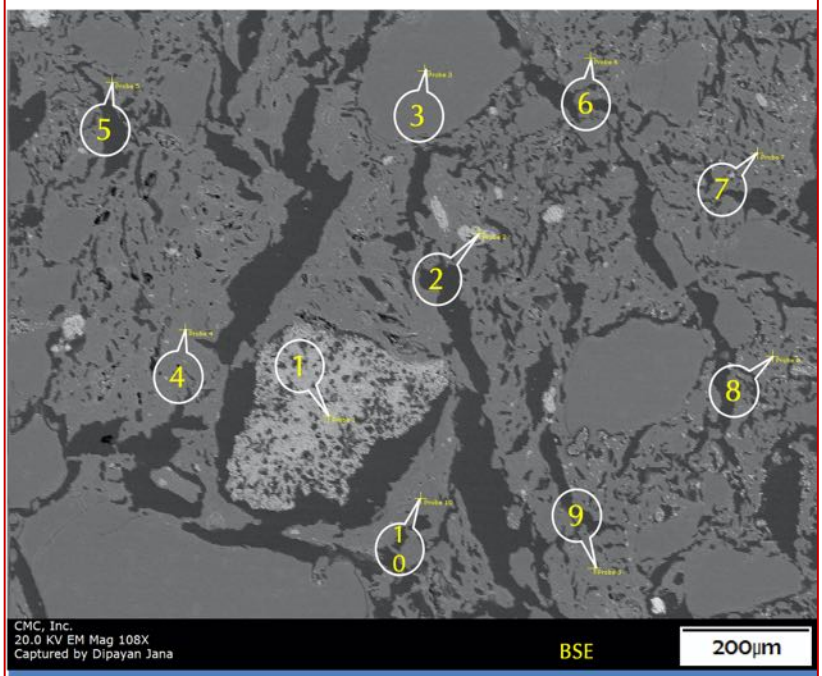

Probe	CaO	SiO2	Al2O3	Na2O	MgO	SO3	K2O	TiO2	FeO	P2O5	CO2	Total
1	0.03	0.59	9.56	0.00	0.12	0.05	0.00	50.71	37.58	0.39	0.97	100.00
2	0.00	0.97	12.05	0.10	0.38	0.09	0.01	34.73	48.16	1.19	2.31	99.99
3	0.00	95.12	0.06	0.00	0.00	0.17	0.02	0.05	0.10	1.18	3.29	99.99
4	0.02	71.29	17.46	0.00	0.00	0.55	0.03	0.81	3.43	1.51	4.90	100.00
5	0.06	84.85	8.21	0.02	0.00	0.16	0.02	0.31	2.20	1.14	3.04	100.01
6	0.28	91.23	2.48	0.00	0.00	0.76	0.22	1.02	0.08	0.84	3.10	100.01
7	0.04	54.72	29.81	0.00	0.00	0.07	0.00	0.21	5.63	0.89	8.63	100.00
8	0.07	62.40	26.21	0.04	0.00	0.21	0.05	0.52	4.78	1.55	4.16	99.99
9	0.09	60.18	21.72	0.00	0.05	0.06	0.02	3.21	8.34	1.45	4.88	100.00
10	0.08	95.62	0.09	0.00	0.01	0.25	0.00	0.23	0.39	1.46	1.85	99.98

Figure C42: X-ray elemental maps (top), backscatter electron image (BSE, middle), and X-ray elemental compositions at the boxes and tips of callouts shown in the backscatter electron image of fired clay brick 3A from 1916 vintage showing typical aluminosilicate composition of glassy matrix of brick as seen in silica and alumina contents. Probe #1 and 2 are from two iron oxide grains in bricks that are responsible for imparting the typical reddish-brown color tone of brick.

END OF REPORT[2]

[2] The CMC logo is made using a lapped polished section of a 1930's concrete from an underground tunnel in the U.S. Capitol.